Adaptive strategies of carbon transformation amongst coral symbionts (Symbiodiniaceae)

Mickael Ros

PhD by Research

Submitted in fulfilment of the requirements for

The degree of Doctor of Philosophy

Climate Change Cluster

School of Life Sciences

University of Technology Sydney

July 2020

Certificate of original authorship

I, Mickael Ros declare that this thesis is submitted in fulfilment of the requirements for the award of Doctor of Philosophy, in the Faculty of Science at the University of Technology Sydney.

This thesis is wholly my own work unless otherwise reference or acknowledged.

In addition, I certify that all information sources and literature used are indicated in the thesis.

This document has not been submitted for qualifications at any other academic institution.

This research is supported by the Australian Government Research Training Program.

Signature:

Production Note:
Signature removed prior to publication.

Mickael Ros

Date: 10th of July 2020

Acknowledgements

First and foremost, I would like to express my sincerest thanks and gratitude to my supervisor David Suggett, who with my co-supervisor Emma Camp agreed to accept me in his team for my PhD journey. I still remember our Skype interview! Thank you for your patience and your unfailing availability in preparing my arrival at UTS and overcome the multiple challenges inherent in moving to another country. Thanks to both of you for your support in all our weekly meetings to check if I was on track and continuously provide feedback on my progress.

I would then like to thank David Hughes, who was always patient and available in helping me lifting the veil on the arcane processes of photochemistry. You helped me go beyond my PhD duties and taught me how to be a (hopefully good!) aquarist, an activity that I truly enjoy and served as a means to get my mind off things when experiments or writing did not go according to the plan. Thank you for your support and your open-mindedness that are characteristic of a genuine friend.

Thank you to the past and present Future Reefs group members: Risa, Sam, Caitlin, Nerissa, Jen, Trent, Rachel, Sage, Amanda and Isabel in providing thoughtful insights regarding the questions I had and their help in the lab, and in organising well sought after lab dinners to get everyone together.

I want to address special thanks to the C3 technical staff, Paul Brooks who was always here to provide his assistance when everything was going wrong in the lab and helped me set my experiments up; and Susan Fenech for her patience and involvement in teaching me how to use and optimise the automated microscope and the TCN analyser.

Special thanks to my parents and family – for which it has been probably harder than for me to move overseas for these three and half years – for their emotional support and for being strong at all times and believing in me no matter what. I hope this document will make you proud!

Last but not least, I would like to thank Princes, my wife, who always has been there for the whole duration of this journey, who did her best to understand what it takes to do a PhD, and always cheered me up day after day. After this, a page will be turned, and I really look forward to starting the next one – our life together!

Table of contents

List of Figures

Chapter 1

Figure 1.6. Outline of the production and fate of reactive oxygen species (ROS) in a Symbiodiniaceae cell under ambient (**a**), and stressful (**b**) temperature and light conditions. Photosystem I (PSI), photosystem II (PSII), Calvin-Benson cycle (CBC), protein D1 (D1), superoxide dismutase (SOD), ascorbate peroxidase (APX), singlet oxygen ($^1O_2$), superoxide radical (O_2^-), hydroxyl radical (•OH), hydrogen peroxide (H_2O_2), ferrous ion (Fe^{2+}). Yellow flashes represent photoinhibition and damages to cellular pathways. They occur on D1 protein activity (Warner et al. 1999), thylakoid membranes (Tchernov et al. 2004), and RuBisCO (Venn et al. 2008). Modified from Weis et al. (2008).

Chapter 2

Figure 2.1. Schematic summarising carbon transfers and mechanisms occurring between the Symbiodiniaceae algae and their surrounding environment (here as free-living in culture). **(1)** Uptake. **(2)** Carboxylation. **(3)** Recycling of internal pools. **(4)** Respiration. **(5)** Active excretion or passive leakiness. **(6)** Heterotrophy. **(a)** Long-term storage for growth net carbon production (NPC) as the product of particulate organic carbon (POC) and growth rate (μ × POC). **(b)** Short-term storage for maintenance as gross carbon production (GPC, as ^{14}C fixed). POC: Particulate organic carbon. iDOC: Internal dissolved organic carbon. eDOC: External dissolved organic carbon. Red frames show the parameters measured in the study. Solid lines represent established pathways, and dashed lines represent hypothesised pathways.

Figure 2.2. Carbon fluxes (as ^{14}C) occurring within the 23 Symbiodiniaceae isolates after 1h of photosynthesis at 26°C. Data shown is the mean (n = 3) ± standard deviation for each Symbiodiniaceae isolate. Isolates are grouped by genus; *Symbiodinium* (blue), *Breviolum* (orange), *Cladocopium* (grey), *Durusdinium* (yellow), *Effrenium* (red), and *Fugacium* (green). **(a)** The gross carbon production (GPC) rates (pg C [cell h]$^{-1}$), where the upper bar is the rate of inorganic carbon fixation (C_{fix}) and the lower bar is the rate of organic carbon excretion in the media (as eDOC, C_{exc}). Relationships between the cell volume (μm^3) and **(b)** the percentage ($\%C_{fix}$) of GPC retained in the cell (i.e. C_{fix}/GPC × 100); and **(c)** the percentage ($\%C_{exc}$) of GPC excreted in the media (i.e. C_{exc}/GPC × 100).

Figure 2.3. Carbon productivity of the 23 Symbiodiniaceae isolates grown at 26°C. Data shown is the mean (n = 3) ± standard deviation for each Symbiodiniaceae isolate. Isolates are grouped by genus; *Symbiodinium* (blue), *Breviolum* (orange), *Cladocopium* (grey), *Durusdinium* (yellow), *Effrenium* (red), and *Fugacium* (green). **(a)** The net carbon production (NPC), as the product of particulate organic carbon (POC) and growth rate, normalised per illumination time (12h). **(b)** Relationship between gross carbon production (GPC) and NPC, where the black line represents the 1:1 ratio between the two variables. Each dot represents the mean (n = 3) data of one isolate. Error bars were not shown for clarity of the representation but can be found in the Supplementary Table S2.3.

Figure 2.4. Functional groupings based on measured factors associated with inorganic carbon uptake and utilisation (cell volume, C_{fix}, C_{exc} and NPC) across all 23 Symbiodiniaceae isolates grown at 26°C. Cluster analysis and principal component analysis (PCA) were performed on the average of each variable (n = 3) per isolate. Axes X and Y represent the first and second component of the PCA, respectively. Similarity at 95% level is shown at the 1.5 (red line) and 2 (dashed blue line) Euclidean distance levels, and vectors driving the clustering are shown in black. Isolates are grouped by genus for clarity; *Symbiodinium* (blue), *Breviolum* (orange), *Cladocopium* (grey), *Durusdinium* (yellow), *Effrenium* (red), and *Fugacium* (green).

Figure 2.5. Physiological parameters of the Symbiodiniaceae *Cladocopium* (C1-SCF124), *Durusdinium* (amur-D-MI) and *Effrenium* (E-421) isolates grown at 20°C, 26°C and 30°C. Data shown is the mean (n = 3) ± standard deviation for each Symbiodiniaceae isolate. Isolates and temperatures of growth are represented as: C1-SCF124 (grey), amur-D-MI (yellow), E-421 (red), 20°C (vertical hatches), 26°C (plain bars), and 30°C (dotted bars). **(a)** Growth rates (d^{-1}) of the three isolates. **(b)** Cell volumes (μm^3) of the three isolates. **(c)** Gross carbon production (GPC) rates (pg C [cell h]$^{-1}$), where the upper bar is the rate of inorganic carbon fixation (C_{fix}) and the lower bar is the rate of organic carbon excretion in the media (as eDOC, C_{exc}). **(d)** Percentage (%C_{exc}) of GPC excreted in the media (i.e. C_{exc}/GPC × 100). **(e)** Relationship between gross and net carbon production (respectively GPC and NPC; pg C [cell h]$^{-1}$), where the black line represents the 1:1 ratio between GPC and NPC. Each dot represents the mean (n = 3) data of one isolate grown at one temperature: 20°C (white-centre shapes), 26°C (regular shapes), and 30°C (black-bordered shapes). Error bars are not shown for clarity but are provided in Supplementary Table S2.10.

Figure 2.6. Functional groupings based on measured factors associated with inorganic carbon uptake and utilisation (cell volume, C_{fix}, C_{exc} and NPC) of the Symbiodiniaceae *Cladocopium* (C1-SCF124), *Durusdinium* (amur-D-MI) and *Effrenium* (E-421) isolates grown at 20°C, 26°C and 30°C. Cluster analysis and principal component analysis (PCA) were performed on the average of each variable (n = 3) per isolate. Axes X and Y represent the first and second components of the PCA, respectively. Similarity at 95% level is shown at the 1.5 (red line) and 2 (dashed blue line) Euclidean distance levels, and vectors driving the clustering are shown in black. Isolates and temperatures of growth are represented as: C1-SCF124 (grey), amur-D-MI (yellow), E-421 (red), 20°C (white-centre shapes), 26°C (regular shapes), and 30°C (black-bordered shapes).

Figure 2.7. Relationship between gross carbon production and net carbon production ratios (GPC:NPC) and O_2 consumption rates (fmol O_2 [cell h]$^{-1}$) for the Symbiodiniaceae *Symbiodinium* (A1-61 and A13-80) and *Breviolum* (B1-2) isolates grown at 26°C. Data shown is the mean (n = 3) ± standard deviation for each Symbiodiniaceae isolate. GPC:NPC ratios are calculated from the present study, whilst O_2 consumption rates are retrieved from Brading et al. (2011). The linear relationship between the two sets of variables is described by the equation GPC:NPC = (- 0.000461 × O_2 consumption rate) + 0.347. $R^2 = 0.996$, $P = 0.039$ (see Supplementary Table S2.14).

Chapter 3

Figure 3.1. Inorganic **c**arbon (Ci) uptake (bars; pg C [cell.h]$^{-1}$) of the three studied Symbiodiniaceae isolates (**a**) B1-UTS-B: *Breviolum minutum*, (**b**) C1-SCF124: *Cladocopium goreaui*, and (**c**) amur-D-MI: *Durusdinium trenchii* as labelled ^{14}C after 20 min of photosynthesis, matched with the photochemical efficiency of their PSII (lines; F_v/F_m) the day of the incubation. Control (white bars and dots ○) stayed at 26°C for the duration of the experiment. Treatment (grey bars and black dots ●) consisted of acclimation phase at 26°C (T0), ramping phase from 26°C to 32°C in two days (TI), and stress phase at 32°C for seven days (TE).

Figure 3.2. Venn diagrams illustrating the outcome of the analysis targeting 156 functional proteins of interest, returning **(a)** 76 total functions found in the extracted transcripts and **(b)** 54 functions encoded by differentially expressed genes (DEGs; log2 FC ≥1; FDR ≤ 0.05) of the three studied Symbiodiniaceae species (*Breviolum minutum*, *Cladocopium goreaui*, and *Durusdinium trenchii*) between the control (26°C) and treatment at the end of the experiment (TE, after seven days at 32°C). For both **(a)** and **(b)**, the number of gene isoforms is indicated between brackets (number of functions can be found in Table 3.1, list in Supplementary Table S3.1). Numbers over superposed circles correspond to the number of the conserved functions (and similar isoforms) expressed between the species that were allocated to the said circles. The list of commonly expressed transcripts associated to their functional groups can be found in Supplementary Table S3.9.

Figure 3.3. Number of functional gene isoforms of interest found to be differentially down- (purple) or up-regulated (yellow) in the three studied Symbiodiniaceae isolates (**a**) B1-UTS-B: *Breviolum minutum*, (**b**) C1-SCF124: *Cladocopium goreaui*, and (**c**) amur-D-MI: *Durusdinium trenchii* at the end of the experiment (TE, after seven days at 32°C), relative to their control (26°C). Transcripts are grouped by function, and the full list of genes can be found in Supplementary Table S3.10).

Chapter 4

Figure 4.1. Physiology of *Pocillopora acuta* (n = 5; mean ± SE) in the Low Isles reef site (blue) and Woody Isles mangrove lagoon (red). (**a**) respiration and gross photosynthesis (P_G) (as the sum of net photosynthesis and respiration) normalised per surface area, and (**b**) per endosymbiont cell , (**c**) photochemical quenching (1 – C) *versus* non-photochemical quenching (1 – Q).

Figure 4.2. Carbon enrichments at the bulk and single-cell levels. (**a**) Bulk (n = 4) $\delta^{13}C$ enrichment levels (normalised to natural abundances) for the different incubated fractions of the coral: ("Coral" and "In hosp. Sym." refer to the incubated holobiont, later separated between animal and algae fractions, respectively; "FIS" refer to freshly isolated Symbiodiniaceae). (**b**) Single cell $\delta^{13}C$ enrichment levels with NanoSIMS. The errors bars represent the standard error, the asterisk symbols denote statistical differences ($p < 0.05$) between (**c-d**; **g-h**) and mangrove (**e-f**; **i-j**) sites. Representative NanoSIMS images showing (**c-f**) the distribution of $^{12}C^{14}N^-$, indicative of the biological structure of the sample, and (**g-j**) the isotope ratio of $^{13}C/^{12}C^-$, with natural abundance in blue, changing to pink with increasing ^{13}C levels. Number of cells analysed: FIS (n = 18); in hospite Symbiodiniaceae (n = 19); and enriched areas in host tissue (n = 5).

Figure 4.3. Relative abundances (%) of recovered ITS2 sequences (upper section) and predicted major ITS type profiles (lower section) for *Pocillopora acuta* across the Low Isles reef and Woody Isles mangrove habitats on the Great Barrier Reef. Each stacked bar corresponds to a biological replicate of a different colony, and each replicate is plotted relative to each other between the upper and lower sections of the figure. Sequences with designated names (e.g. C1b, D4c, or D6) refer to sequences frequently found in the literature or already characterising ITS2 profiles previously ran through the SymPortal analytical framework (Hume et al. 2019). Other sequences designated by a unique database ID and their associated genus (e.g. 70776_D) refer to sequences that are less common and not previously used to characterise ITS type profiles.

Figure 4.4. Comparisons of (**a**) mean (± SE) gross photosynthesis (P_G, as the sum of net photosynthesis and respiration R) and respiration rates between reef (blue dots) and mangrove (red squares) sites. Species-specific metabolic shifts are represented by lines (black), and the dashed line indicates the 1:1 ratio. The table summarises the mean (± SE) P_G:R ratios for reef and mangrove sites. (**b**) Summary of key metrics shifts from reef and mangrove sites. Data for *Acropora millepora* and *Porites lutea* are retrieved from Camp et al. (2019) and for *Pocillopora acuta* come from the present study.

Figure 4.5. Comparisons of light-dependant dynamic quenching patterns between (**a**) *Pocillopora acuta* (present study) and (**b**) *Acropora millepora* (Camp et al. 2019) in the Low Isles reef (blue dashed

lines) and Woody Isles mangrove lagoon (red dashed lines). Values of [1 – C] stand for photochemical quenching (qP) and [1 – Q] for non-photochemical quenching (NPQ) (see Methods).

Chapter 5

Figure 5.1. Summary of the interplay between light reactions and dark reactions of photosynthesis and how strategies promoting survival affects Ci fixation. LR: light reactions, DR: dark reactions, PG: gross photosynthesis, qP: photochemical quenching, AEF: alternative electron flows, Ci fix: inorganic carbon fixation. Question marks stand for pathways that have been suggested to play a role in coral-Symbiodiniaceae fitness but are to be quantified.

Figure 5.2. Proposed roadmap of future studies over the short and mid-terms leading on the long term to a better understanding of the Symbiodiniaceae and their holobiont physiologies.

List of Tables

Chapter 1

Chapter 2

Chapter 3

Supplementary Table S3.1 (Abbreviations: CBC: Calvin-Benson cycle; PPP: pentose phosphate pathway; TCA: tricarboxylic acid – Krebs cycle).

Table 3.2. Summary of trends found across the studied Symbiodiniaceae isolates. Numbers between brackets represent the number of differentially expressed genes (DEGs) in a sequential order of isolate appearance in the table (*Breviolum minutum*, *Cladocopium goreaui*, *Durusdinium trenchii*). The percent of change of all DEGs indicate how are allocated the DEGs between down- and up-regulated genes. Arrows thickness represent the number of DEGs found in each functional group.

Chapter 4

Table 4.1. Summary of abiotic conditions characterising Woody Isles mangrove lagoon and the adjacent Low Isles reef in June 2017 and February-April 2018. Data were retrieved from Camp et al. (2019) and collected with a SeapHOx sensor set at 1 minute sampling frequency over 48 hours (2017 dataset) and at 5 minutes sampling frequency over 50 days (2018 dataset). Mean is provided with standard error (SE) and diel range of measurements with coefficient of variance (CV). Data for the reef in February-April 2018 is not available.

Chapter 5

Table 5.1. Summary of advantages and disadvantages of using Symbiodiniaceae in culture and in symbiosis with the holobiont. References: (**1**) Chapter 2; (**2**) Chapter 3; (**3**) Chapter 4; (**4**) Camp et al. 2019; (**5**) Hughes et al. 2018; (**6**) Gorbunov et al. 2001.

List of Supplementary Figures

Chapter 2

Supplementary Figure S2.1. Relative ^{14}C fixation (DPM) as (**a**) C_{fix} and (**b**) C_{exc} over time (5, 10, 20, 60, 120 and 360 minutes) of F1-156 and amur-D-MI, characterised as fastest and slowest growing isolates at the time of the assay, respectively.

Supplementary Figure S2.2. Carbon fluxes as (**a**) C_{fix} and (**b**) C_{exc} occurring within the 23 Symbiodiniaceae isolates grouped per genus after 1h of photosynthesis, as a function of their respective cell volumes.

Supplementary Figure S2.3. Summary of (**a**) C:N and (**b**) C:Chl*a* ratios for each of the 23 studied Symbiodiniaceae isolates.

Chapter 4

Supplementary Figure S4.1. Localisation of Low Isles on a map of Australia (**a**, denoted by a red rectangle) and relatively to Cairns (**b**, denoted by a red circle). Low Island reef (**c**) and Woody Island mangrove lagoon (**c**, **d**) were the collection sites of *Pocillopora acuta* colonies (**e**, in the mangrove).

Supplementary Figure S4.2. Mean (± SE) relative electron transport rates (rETR, mol e^{-} μm^{-3} s^{-1}) obtained using rapid light curves (see Methods) for *Pocillopora acuta* (n = 4) across the Woody Isles mangrove lagoon (red) and Low Isles reef (blue).

Supplementary Figure S4.3. Image of the stable isotope incubations set-up, where FIS are incubated (small vials) close to their respective holobiont fraction (large vessels).

Supplementary Figure S4.4. Mean (± SE) Symbiodiniaceae cell density (cells cm^{-2}) for *Pocillopora acuta* (n = 4) across the Woody Isles mangrove lagoon (red) and Low Isles reef (blue).

List of Supplementary Tables

Chapter 2

Supplementary Table S2.9. Summary of the regression analyses carried out between the mean (±SD) of cell volume (μm^3) and growth rate (μ, d^{-1}) of the three Symbiodiniaceae isolates grown at 20°C, 26°C and 30°C.

Supplementary Table S2.10. Carbon fluxes and productivity characteristics of the three studied Symbiodiniaceae isolates grown at 20°C, 26°C and 30°C: mean (±SD) (n = 3) of GPC (pg C [cell h]$^{-1}$), the detail of C_{fix} (pg C [cell h]$^{-1}$) and C_{exc} (pg C [cell h]$^{-1}$), and NPC (pg C [cell h]$^{-1}$).

Supplementary Table S2.11. Contribution of variables (in %) to each component of the PCA carried out on the dataset of isolates grown at sub-optimal temperatures.

Supplementary Table S2.12. Summary of significant non-parametric ANOVA (Kruskal-Wallis) with discrimination of the isolates specifically grown at the mentioned temperature, significantly apart from each other using Dunn-Bonferroni post-hoc tests, carried out on each dimension of the PCA carried out on the dataset of isolates grown at sub-optimal temperatures.

Supplementary Table S2.13. Mean (±SD) GPC:NPC ratios (present study) of specific isolates used in Brading et al. (2011) and their retrieved O_2 production rates (fmol O_2 [cell h]$^{-1}$). GPC:NPC ratios averaged per genus are from the present study.

Supplementary Table S2.14. Summary of the regression analyses carried out between the mean (±SD) GPC:NPC and O_2 production rates (fmol O_2 [cell h]$^{-1}$) of the three Symbiodiniaceae isolates retrieved from Brading et al. (2011), in light and dark conditions.

Supplementary Table S2.15. Photobiology characteristics of studied Symbiodiniaceae isolates: mean ± SD (n = 3) of photosystem II (PSII) maximum photochemical efficiency (F_v/F_m, dimensionless) and PSII absorption cross-section (σ_{PSII}, nm^2).

Supplementary Table S2.16. Photobiology characteristics of the three studied Symbiodiniaceae isolates grown at 20°C, 26°C and 30°C: mean ± SD (n = 3) of photosystem II (PSII) maximum photochemical efficiency (F_v/F_m, dimensionless) and PSII absorption cross-section (σ_{PSII}, nm^2).

Chapter 3

Supplementary Table S3.1 Full list of proteins and their associated genes and cellular functions used to target and refine the transcripts analysis in all the studied Symbiodiniaceae (*Breviolum minutum*, *Cladocopium goreaui,* and *Durusdinium trenchii*). Colours of cells represent the functional grouping proteins were associated with green: light reactions; blue: dark reactions; yellow: metabolism; orange: stress response; grey: transport. Information of protein function was retrieved from the UniProt knowledgebase (UniProtKB). "N/A" denotes a protein for which a gene name has not been identified.

Supplementary Table S3.2. Summary of DEGs for *Breviolum minutum* at the TI of the experiment (post-temperature ramping).

Supplementary Table S3.3. Summary of DEGs for *Cladocopium goreaui* at the TI of the experiment (post-temperature ramping).

Supplementary Table S3.4. Summary of DEGs for *Durusdinium trenchii* at the TI of the experiment (post-temperature ramping).

Supplementary Table S3.5. Summary of DEGs for *Breviolum minutum* at the TE of the experiment (after seven days at 32°C).

Supplementary Table S3.6. Summary of DEGs for *Cladocopium goreaui* at the TE of the experiment (after seven days at 32°C).

Supplementary Table S3.7. Summary of DEGs for *Durusdinium trenchii* at the TE of the experiment (after seven days at 32°C).

Supplementary Table S3.8. Summary of one-way ANOVAs carried out on the ^{14}C uptake data. Differences are between control and treatment for each time point. The star symbol denotes a significant difference at alpha = 0.05

Supplementary Table S3.9. Summary of genes (functional proteins between brackets) sharing a difference in expression between the studied Symbiodiniaceae isolates (B1: *Breviolum minutum*; C1: *C. goreaui*; D1a: *D. trenchii*) after seven days of thermal stress (32°C)

Supplementary Table S3.10. Heat-map summarising the differential gene expression at the end of the temperature ramping (TI) and after seven days of thermal stress at 32°C (TE) in our three Symbiodiniaceae isolates (B1: *B. minutum*; C1: *C. goreaui*; D1a: *D. trenchii*). Heat-map was populated first for the DEGs conforming to our threshold cut-off (log2 fold change [FC] ≥1 and false discovery rate [FDR] ≤ 0.05) for either TI and TE, and then the corresponding DEG for the same gene at the other time point was reported regardless of significance and log2 fold change. Blank cells denote the lack of DEGs according to our set cut-off for both TI and TE. The presence of a star in the column "Sig" denotes a FDR < 0.05. Shade of “Protein” column represent the functional grouping proteins were associated with green: light reactions; blue: dark reactions; yellow: metabolism; orange: stress response. Colour scale of heat-map varies from a gradient of purple (most down-regulated) to gold (most up-regulated).

Chapter 4

Supplementary Table S4.1. Summary of the *Pocillopora acuta* samples taken from both Low Isles reef and Woody Isles mangrove and their subsamples (for stable isotope incubations and genomic analyses). Abbreviations: HB, holobiont; FIS, freshly isolated symbionts; H, host; S, symbiont; EA, enrichment analysis; NA, natural abundance; NS, NanoSIMS; CC, cell counts; PAM, pulse-amplified fluorometry.

List of abbreviations

ADP	Adenosine diphosphate
AEF	Alternative electron flow
ANOVA	Analysis of variance
APX	Ascorbate peroxidase
ASW	Artificial seawater
ATP	Adenosine triphosphate
C	Carbon
CA	Carbonic anhydrase
$CaCl_2$	Calcium chloride
CAM	Crassulacean acid metabolism
CBC	Calvin-Benson-Bassham cycle
CCM	Carbon concentrating mechanism
CEF-PSI	Circular electron flow around PSI
C_{exc}	Rate of organic carbon excretion
$\%C_{exc}$	Fraction of GPC excreted in the media
C_{fix}	Rate of Ci fixation
$\%C_{fix}$	Fraction of GPC retained in the cell
$(CH_2O)_n$	Carbohydrate
Chl*a*	Chlorophyll-*a*
Ci	Inorganic carbon
CO_2	Carbon dioxide
COP	Conference of the Parties
CV	Coefficient of variance
Cyt b6f	Cytochrome b6f
DEG	Differentially expressed gene
DIC	Dissolved inorganic carbon
DIN	Dissolved inorganic nitrogen
DMSP	Dimethylsulfoniopropionate
DOC	Dissolved organic carbon
DOM	Dissolved organic matter

DPM	Disintegrations per minute
DR	Dark reactions
EA	Enrichment analysis
eDOC	External dissolved organic carbon
EDTA	Ethylenediaminetetraacetic acid
ENSO	El Niño-Southern Oscillation
FC	Fold change
Fd	Ferredoxin
FBP	Fructose-1,6-biphosphate
FDR	False discovery rate
Fe^{2+}	Ferrous ion
FIS	Freshly isolated symbionts
FNR	Ferredoxin-NADP reductase
FRRf	Fast repetition rate fluorometry
GAP	Glyceraldehyde-3-phosphate
GAPDH	Glyceraldehyde-3-phosphate dehydrogenase
GBR	Great Barrier Reef
GBRMPA	Great Barrier Reef Marine Park Authority
GEB	Gene expression biomarker
GHG	Greenhouse gases
GPC	Gross carbon production
H_2O_2	Hydrogen peroxide
HB	Holobiont
HCl	Hydrochloric acid
HCO_3^-	Bicarbonate ion
$HgCl_2$	Mercuric chloride
HSI	Hue saturation intensity
HSP	Heat-shock protein
iDOC	Internal dissolved organic carbon
IPCC	Intergovernmental Panel on Climate Change
ITS2	Internal transcribed spacer 2
LED	Light-emitting diode

LEF	Linear electron flow
LHC	Light-harvesting complex
LIFT	Light-induced fluorescence transient
LR	Light reactions
MDS	Multidimensional scaling
MIMS	Membrane inlet mass spectrometry
MPP	Marine primary productivity
N	Nitrogen
N_2	Atmospheric nitrogen
NA	Natural abundance
NaCl	Sodium chloride
NADP(H)	Nicotinamide adenine dinucleotide phosphate
$NaH^{13/14}CO_3$	$^{13/14}$C-labelled sodium bicarbonate
NanoSIMS	Nanoscale secondary ion mass spectrometry
NH_4^+	Ammonium ion
NO_3^-	Nitrate ion
NPC	Net carbon production
NPQ	Nonphotochemical quenching
O2	Dioxygen
$^1O_2$	Singlet oxygen
O_2^-	Superoxide radical
OA	Ocean acidification
OAA	Oxaloacetic acid
•OH	Hydroxyl radical
ORF	Open reading frame
OsO_4	Osmium tetroxide
P	Phosphorus
PAM	Pulse amplitude modulation
PAR	Photosynthetically active radiation
PBS	Phosphate-buffered saline
PC	Plastocyanin
PCA	Principal components analysis

pCO_2	Partial pressure of CO_2
PCR	Polymerase chain reaction
PG	Gross photosynthesis
PGA	3-phosphoglyceric acid
Pi	Inorganic phosphorus
P-I	Photosynthesis response to irradiance
PN	Net photosynthesis
PO_4^{3-}	Phosphate ion
POC	Particulate organic carbon
POM	Particulate organic matter
PPP	Pentose phosphate pathway
PQ	Plastoquinone
PSI	Photosystem I
PSII	Photosystem II
Q_A	Electron transport chain
qP	Photochemical quenching
R	Respiration
RCF	Relative centrifuge force
RCII	Functional PSII reaction centre
RLC	Rapid light curve
ROS	Reactive oxygen species
RuBisCO	Ribulose-1,5-biphosphate carboxylase/oxygenase
SD	Standard deviation
SE	Standard error
SOD	Superoxide dismutase
SST	Sea surface temperature
TCA	Tricarboxylic acid
TEM	Transmission electron microscopy
TN	Total nitrogen
UNESCO	United Nations Educational, Scientific and Cultural Organization

List of symbols

[1 - C]	Photochemical quenching
[1 - Q]	Non photochemical quenching
$\delta^{13}C$	Difference in enrichment of ^{13}C from natural isotope abundance
E_k	Light saturation parameter
ETRmax	Maximal electron transport rate
ETR_{PSII}	Electron transport rate through PSII
F'	Fluorescence yield under actinic light
F_0	Minimum PSII fluorescence yield (dark acclimated state, RCII open)
F_0'	Minimum PSII fluorescence yield (light-acclimated state, RCII open)
F_m	Maximum PSII fluorescence yield (dark-acclimated state, RCII closed)
F_m'	Maximum PSII fluorescence yield (light-acclimated state, RCII closed)
F_v	Maximum variable PSII fluorescence yield (dark-acclimated state)
F_v/F_m	Maximum photochemical efficiency (dark-acclimated state)
μ	Growth rate
σ_{PSII}	Functional absorption cross-section of PSII
rETR	relative electron transport rate

Thesis abstract

Algal endosymbionts (family Symbiodiniaceae) fuel the metabolism of reef-forming corals through uptake and utilisation of inorganic carbon (Ci) from photosynthesis. Changes in photosynthetic performance both within, and between endosymbiont taxa influence the extent of organic carbon ultimately translocated to the host coral. However, how such changes are regulated by plasticity in light harvesting, *versus* Ci assimilation processes remains unknown. In this thesis, I therefore built on novel approaches to assess functional diversity of fitness traits across Symbiodiniaceae to identify the extent with which Ci-uptake and incorporation differed amongst taxa and the extent with which differences could be reconciled against evolutionary adaptation across the family to sustain reef functioning in response to climate change.

This thesis focused on direct assessment of Ci-uptake, and how it is linked to light harvesting and utilisation by Symbiodiniaceae both *ex hospite* (in culture) and *in hospite* (in symbiosis with their host). I first cultured a broad range of Symbiodiniaceae taxa to assess how Ci was invested into cellular uptake, excretion, and growth; and how these metrics changed when three isolates of different thermal tolerances were subjected to sub-optimal conditions of growth. I further examined how these different thermo-tolerant Symbiodiniaceae coped with a stress-inducing increase of temperature. In parallel with photophysiology and Ci-uptake rate measurements, transcriptomics were carried out to resolve the underlying molecular network driving physiological response to heat stress. Finally, I extended this laboratory-based approach to examine Ci-uptake performance of natural coral communities across complex environmental gradients (mangrove *vs*. reef corals) on the Great Barrier Reef to resolve the adaptations of symbionts linked to their survival to extreme environments.

My results revealed that environmental regulation outweighed evolutionary adaptation of Symbiodiniaceae in their capacity for Ci-uptake, suggesting that their ecological success

predominantly relies on plasticity of upstream photosynthetic processes (efficiency of light-harvesting and non-photochemical energy quenching) rather than those downstream (Ci-uptake, assimilation, and excretion). Despite exhibiting similar trends in functional gene expression, each studied Symbiodiniaceae isolate exhibited different photophysiology and Ci-uptake rates in response to thermal stress for both (previously well studied) light reactions and dark reactions of photosynthesis. When in symbiosis, flexibility in the major Symbiodiniaceae taxa between reef and mangrove corals was associated with a reduced Ci incorporation in mangrove corals compared to reef corals. Together, these results will serve as a stepping stone to future research on the long term, aiming to improve worldwide reef health in response to global climate change.

Declaration of the contribution to each Chapter

Chapter 2

This thesis is presented as the accepted final version for publication with Limnology & Oceanography following peer-review.

Ros M., Camp E.F., Hughes D.J., Crosswell J.R., Warner M.E., Leggat W.P., Suggett D.J. 2020. Unlocking the black-box of inorganic carbon-uptake and utilisation strategies amongst coral endosymbionts (Symbiodiniaceae). Limnol. Oceanogr. doi: 10.1002/lno.11416

MR, DJS and EFC designed, and MR conducted experiments at University of Technology Sydney; MR performed dissolved inorganic carbon measurements and analysis with the help of JRC at CSIRO; MR and DJH analysed the data and generated manuscript figures. MR wrote the manuscript with substantial critical contributions from DJS, EFC, DJH, MEW, JRC and WPL.

Chapter 3

MR, DJS and EFC designed the heat-stress experiment. MR, EFC, NF, LF, SG, and CAL oversaw culture maintenance and monitoring. MR, EFC, NF, LF, SG, DJS, and CAL were involved in sample collection. DV undertook the DNA extractions and photophysiology measurements. MR and DJH performed the ^{14}C incubations and DIC measurements. EFC performed the transcripts extractions, TK and DV oversaw the transcript analysis. MR created the figures. MR led the writing of the manuscript, with EFC, DJH and DJS providing significant editorials.

Chapter 4

MR, DJS, EFC and JE designed and conducted all fieldwork and MR conducted experiments; MR and DJH designed the dual fractions incubation chambers, EFC performed respirometry measurements and symbiont identity analysis; MR, DJS, EFC collected the coral samples; MR performed stable isotope incubations, cell density measurements, prepared samples for stable isotope analysis and analysed NanoSIMS images; TH performed host and symbiont DNA extraction for identity analysis; MK, JBR and MP prepared the samples for NanoSIMS analysis; PG and MRK performed the NanoSIMS image acquisition. MR led writing of the manuscript with substantial critical contributions from DJS, DJH and EFC.

Chapter 1

General Introduction and Thesis Outline

1.1. Coral reefs

1.1.1. Environmental and societal significance

Coral reef ecosystems create unique environmental habitats that sustain numerous marine species over 150 ecoregions worldwide (Veron et al. 2015). These habitats include shallow water flats and low light deep reefs, but also inherently encompass connected neighbouring seagrass beds and mangroves (Camp et al. 2018) that together house incredible coral diversity encompassing 700 species of scleractinian corals. Tropical reef-building corals (i.e. hermatypic) are found across intertropical latitudes with an average water temperature of 26-28ºC, as deep as 70m depending on light availability (Muir et al. 2015), and in relatively oligotrophic waters, i.e. offering very low levels of nutrients (PO_4^{3-} < 0.2 μmol.L^{-1}; NO_3^- < 2 μmol.L^{-1}) (Wall et al. 2020). Coral growth within these environments provides the physical structure that underpins the entire biological diversity and productivity of coral reef ecosystems (Darling et al. 2017). Whilst coral reefs only cover <0.2% of the total ocean surface (Crossland et al. 1991; Birkeland 1997), it is estimated that their high productivity sustains 30% of the total oceanic biomass (Erez 1990), across diverse invertebrate and vertebrate taxa, notably fishes. Such diversity is fuelled by an array of functional groups across complex trophic relationships (Harborne et al. 2017; Darling et al. 2017).

Coral reef productivity and biodiversity ultimately sustain numerous "ecosystem services" that fuel human populations and economies (Elliff and Kikuchi 2017). Millions of reef fishers across hundreds of countries worldwide rely on small-scale subsistence reef fishing (Teh et al. 2013; Martin et al. 2017). Australia has a particularly valuable reef-based industry generating $6.4 billion (AUD) annually, where tourism-based industries represents over 90% of this value (Deloitte 2017; Spalding et al. 2017; Suggett et al. 2019). Much of this value is potentially untapped, where coral reefs likely contain a broad range of pharmacological

compounds that are yet to be discovered (Simmons et al. 2005). For instance, secondary metabolites extracted from the soft coral *Sarcophyton* sp. (Januar et al. 2017) or from algal species such as *Udotea orientalis* that express cytotoxic activity against human cancer cell lines (Sabry et al. 2017). Coral reef ecosystems are fundamentally protecting shorelines against strong waves (Elliff and Silva 2017) and storms (Vila-Concejo and Kench 2017), and bringing minerals to coasts (e.g. sands) that draw further tourism economies (Hoegh-Guldberg 1999). Finally, many reefs – including the Great Barrier Reef (GBR) and Ningaloo Reef in Australia – have cultural and historical importance that is virtually impossible to value economically. Such diversity of ecosystem services has led many reef systems to be considered under UNESCO World Heritage Listings, for example, the GBR in 1981, as a result of "an exceptional natural beauty and aesthetic importance; an outstanding example of an ecosystem that has evolved over millennia; ongoing geomorphic, oceanographic and environmental processes; and one of the richest and most complex natural ecosystems on earth" (GBRMPA 1981).

1.1.2. Ever-growing anthropogenic impacts on coral reefs

Coral reef ecosystems have been significantly impacted since entering the current "Anthropocene epoch", a globalized phenomenon of climate change from human activity based greenhouse gases (GHG) emissions, principally carbon dioxide (CO_2) (De Klein et al. 2008). Increasing CO_2 emissions since the Industrial Revolution have globally led to a rise of sea surface temperature (SST) of 1.5°C (IPCC 2018; Hoegh-Guldberg et al. 2018) with a predicted increase by up to 0.5ºC per decade (Alexander et al. 2018). El Niño-Southern Oscillation (ENSO) marine heatwave events that periodically increase SSTs by up to 2ºC above the seasonal average are also increasing in frequency and intensity (Ainsworth et al. 2016; Wang et al. 2017). In parallel to warming, the absorption of CO_2 by the oceans has decreased global

pH by 0.1 units since the pre-industrial period (IPCC 2018). Such "ocean acidification" (OA) leads to changes in the availability of carbonates required for corals to calcify and grow (Hoegh-Guldberg et al. 2007; Pelejero et al. 2010; D'Olivo et al. 2019). Simultaneously, this increase in dissolved CO_2 leads to simultaneous oceanic deoxygenation reaching critical thresholds of less than 2 mg O_2 L^{-1} (Diaz and Rosenberg 2008), creating hypoxic "dead-zones" in the oceans unable to support oxygen-dependent life (Hansson et al. 2019).

Localised impacts further compound global- to regional-scale changes in climate. Fishing and tourism activities are increasingly unsustainable as population pressures grow (Darling and D'Agata 2017); for example, shoreline construction (Benham 2017), land clearing (Reside et al. 2017), deforestation (Hamilton et al. 2017) and dredging (Bessell-Browne et al. 2017). Release of untreated sewage fuels reefs with heavy metals (Armid et al. 2017) and nutrients (Mwaura et al. 2017), which in the latter case leads to eutrophication-induced algal blooms (Fabricius 2005; Haas et al. 2016). Recently, the controversy of new coal mining operations along the coasts of Queensland, Australia has triggered political and societal uncertainty in the scale of future localised impacts (McCall 2017; Shumway et al. 2017). Not only do coal mines inherently contribute to the GHG emissions, but mining itself decreases water quality and drives hyper sedimentation surrounding coral reef ecosystems (Hughes et al. 2015). Enhanced predation pressure from the crown-of-thorns starfish, *Acanthaster planci*, has notably driven mass coral mortality on the GBR (De'ath et al. 2012). However, whether outbreaks are related to poor water quality remains unresolved (Wooldridge and Brodie 2015; Wolfe et al. 2017).

The rapidity and the intensity of interacting anthropogenic impacts are leading to reef deterioration and loss globally (Eakin et al. 2019), including the GBR (Hughes et al. 2017, 2018). Heavily stressed corals by pollution, eutrophication and elevated water temperatures are increasing the susceptibility of corals to diseases and pathogens (Bourne et al. 2009; van

Woesik and Randall 2017). However, of all stressors, marine heatwaves (SST anomalies) that drive coral bleaching and mortality are considered the most significant threat. In 2016, 30% of all corals died on the GBR alone from extreme SST anomalies (Hughes et al. 2017); this number is closer to 50% (Hughes et al. 2018, 2019) following back-to-back events and poor recovery trajectories. Corals that survive a single heat stress event not only remain susceptible to subsequent events (Grottoli et al. 2006), but also to pathogens (Ben-Haim et al. 2003). The Paris Agreement signed by 195 countries during the Conference of the Parties in Paris, 2015 (COP21) aimed to reduce GHG emissions to hold the increase in global average temperature below 2ºC above pre-industrial levels (COP21, 2015). However, the last IPCC report showed that we are now drawing closer to these levels, and the latest COP in Madrid (COP24, 2019) highlighted the critical need of lifestyle changes worldwide to meet the 2015 agreement. Moreover, with retention times of GHG peaking up to 50 years in the atmosphere, coral reefs remain threatened even if the signatories meet the requirements of the document (van Hooidonk et al. 2013, 2016). As such, we have a desperate need to improve coral reef management, in terms of policy but also its applicability on-ground (Fraser et al. 2017). Downgrading policies to the local scale will help to enhance the efficiency of reef management (van Hoodoink et al. 2016), but only if novel tools can be developed to diagnose resistance and resilience to key stressors, that enables targeted local action.

1.2. Coral algal endosymbionts (Symbiodiniaceae): the "make-or-break" of coral resilience?

1.2.1. Definition and influence

Symbiodiniaceae is a family of marine unicellular microalgae belonging to the phylum Dinoflagellata, (class: Dynophycae, order: Suessiales, and family: Symbiodiniaceae; LaJeunesse et al. 2018). This dinoflagellate forms an endosymbiotic relationship with reef forming corals by living within the host coral's gastrodermal cells, in differentiated compartments called symbiosomes (*sensu* Roth et al. 1988; Davy et al. 2012). Symbiodiniaceae cells are also found in symbiosis with other cnidarian hosts such as sea anemones, giant clams, and jellyfish, as well as in other diverse taxa spanning the phyla Mollusca and Foraminifera (LaJeunesse et al. 2018). Association of Symbiodiniaceae with their coral host begins either from vertical transmission (i.e. *via* heredity) or horizontal acquisition (i.e. *via* phagocytosis from the surrounding environment) depending on the life history of the host (del Gomez-Cabrera et al. 2008; Fransolet et al. 2012; Davy et al. 2012). In the latter case, free-living state of Symbiodiniaceae cells have an important role in sustaining symbiosis across life stages and generations of corals (Nitschke et al. 2016; Quigley et al. 2017). Algal-glycan/host-lectin interactions may trigger host recognition (Wood-Charlson et al. 2006; Vidal-Dupiol et al. 2009), suggesting a diversity of the surface proteins amongst Symbiodiniaceae (Logan et al. 2010; Tivey et al. 2019).

Symbiosis governing Symbiodiniaceae-coral associations is fuelled through resource exchange: the coral host relies on Symbiodiniaceae to acquire carbon compounds via translocation of photosynthates (Muscatine 1990; Sproles et al. 2019) (Figure 1.1) and appears to control this process through the release of inorganic nutrients from host to Symbiodiniaceae (Morris et al. 2019). This exchange enables corals to grow in otherwise nutrient-poor waters.

Host corals not only provide inorganic macronutrients (N, P), but through metabolic activity also locally increase pH to promote photosynthesis (Venn et al. 2009; Barott et al. 2015). Indeed, Tansik et al. (2017) have recently shown that Symbiodiniaceae photosynthesis is frequently inorganic carbon limited *in hospite* when host metabolism is depressed (see also Suggett et al. 2012). In turn, photosynthesis acts to drive increased internal pH of host tissue during the day and therefore "light-enhanced calcification" (Gattuso et al. 1999). Importantly, the photosynthates are considered "junk food" due to their high quantity, but poor "quality" (Falkowski et al. 1984), and thus coral polyps must also feed on phytoplankton and zooplankton to sustain N and P (heterotrophy; Houlbrèque and Ferrier-Pagès 2009; Jeong et al. 2012; Wall et al 2020). Several other microorganisms, such as bacteria are also present in the surroundings of corals (Blackall et al. 2015). Studies focusing on these less well understood constituents of corals are starting to emerge, especially on determining their role in coral response to climate change (Bourne et al. 2009; Diaz et al. 2016; Ziegler et al. 2017) and their community complexity (Rohwer et al. 2001; Lawson et al. 2018; Matthews et al. 2020). Altogether, corals, endosymbionts and bacteria are termed "holobiont" (*sensu* Rohwer et al. 2002) to design this complex network of organisms interacting with each other.

Given the crucial role of Symbiodiniaceae photosynthesis in fuelling coral metabolism and growth, how it alters over space and time and is influenced by resource availably for cells both *in* and *ex hospite*, has remained a core focus for research over the past 50 years. Importantly, Symbiodiniaceae photosynthetic performance can be directly related to the metabolic performance (Leal et al. 2015) and fitness (Suggett et al. 2012) of their hosts. However, research has increasingly demonstrated that the benefits of housing Symbiodiniaceae also come at a cost: when corals experience anthropogenic-induced stressors, the coral-Symbiodiniaceae associations rapidly destabilise as Symbiodiniaceae photosynthesis and metabolism become "toxic" (Downs et al. 2002; Tchernov et al. 2004; Suggett and Smith

2020). In order to understand how, when and why Symbiodiniaceae become a problem for its host, it is first essential to consider the core process of (Symbiodiniaceae) photosynthesis (Warner and Suggett 2016; Suggett et al. 2017).

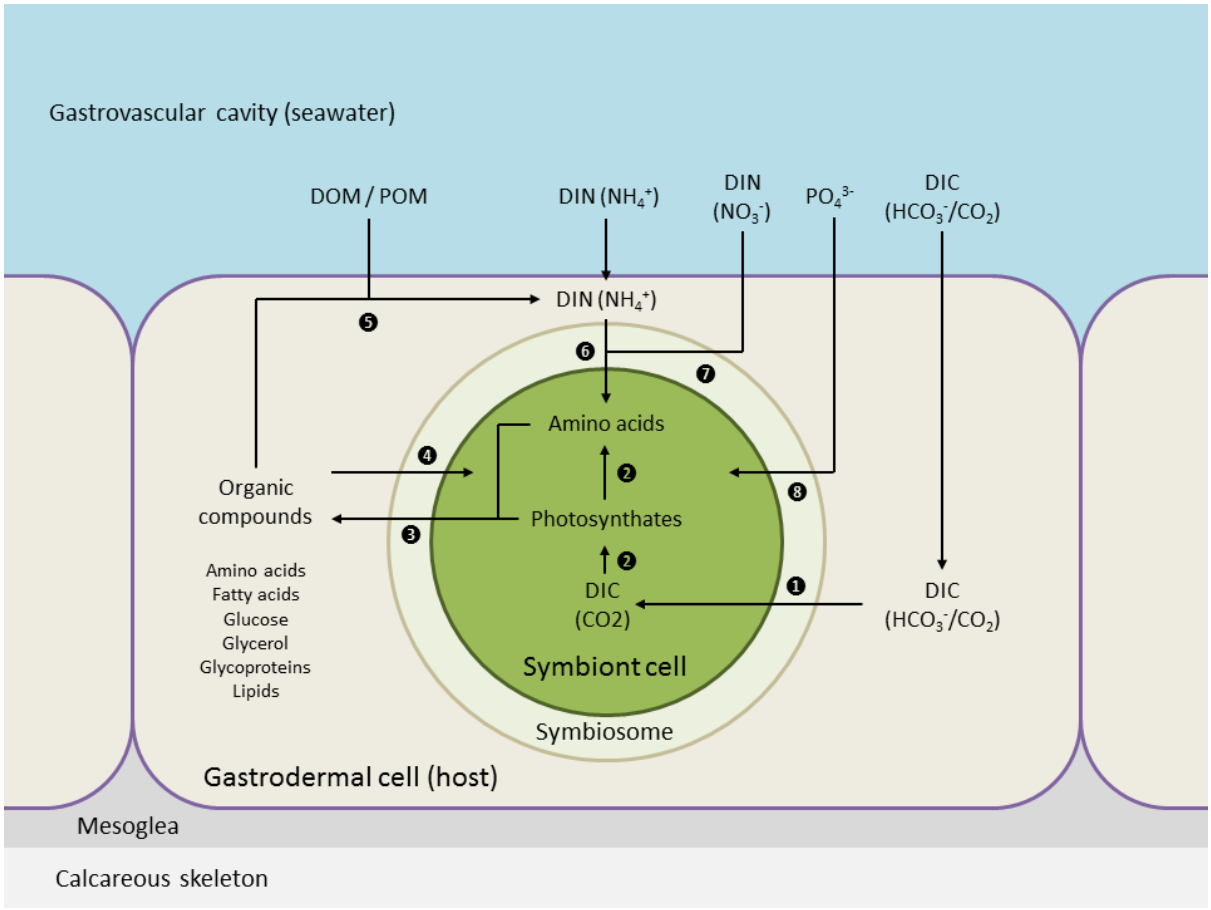

Figure 1.1. Outline of the nutrient and metabolite transfers between the coral host, a symbiont cell, and their surrounding environment. (**1**) Dissolved inorganic carbon (DIC) uptake from seawater under the form of either carbon dioxide (CO_2) or bicarbonate (HCO_3^-). (**2**) Photosynthesis. (**3**) Translocation of organic compounds by the symbiont to the host. (**4**) Translocation of organic compounds by the host to the symbiont. (**5**) Host metabolism underlining the uptake of dissolved and particulate organic matter (DOM/POM) generating ammonium (NH_4^+) waste. (**6**) Dissolved inorganic nitrogen (DIN) assimilation by the symbiont. (**7**) Nitrate (NO_3^-) uptake from seawater by the symbiont. (**8**) Phosphate (PO_4^{3-}) uptake from seawater by the symbiont. Figure modified from Davy et al. (2012).

1.2.2. Symbiodiniaceae – Photosynthesis and Respiration

Marine primary production (MPP) by plants and algae is driven by photosynthesis (Field et al. 1998). Dissolved inorganic carbon (DIC) present in seawater (under the form of CO_2 and HCO_3^-) is transformed into organic carbon skeletons (*sensu* MacIntyre et al. 2002; carbohydrates and ultimately proteins and lipids) (Figure 1.1) through light energy (Beardall and Raven 2016). The metabolic rate of a photosynthetic organism is defined by the rate at which it acquires energy and materials from the environment and converts them into products for maintenance, growth, and reproduction, with any carbon loss in respiration and excreted materials (organic and inorganic, i.e. wastes) (Raven, 1984). In the case of photosynthesis, such rates are considered to be light-dependent reactions – or light reactions (LR) – under relatively low irradiance *versus* light-independent reactions – or dark reactions (DR) – under higher irradiance (Figure 1.2) (Bassham and Calvin 1960). Since these reactions operate at the same time within cell chloroplasts, the reaction with the slowest rate inevitably dictates the overall photosynthesis rates achievable (Larkum 2016) to constitute the integrated cellular metabolic rate.

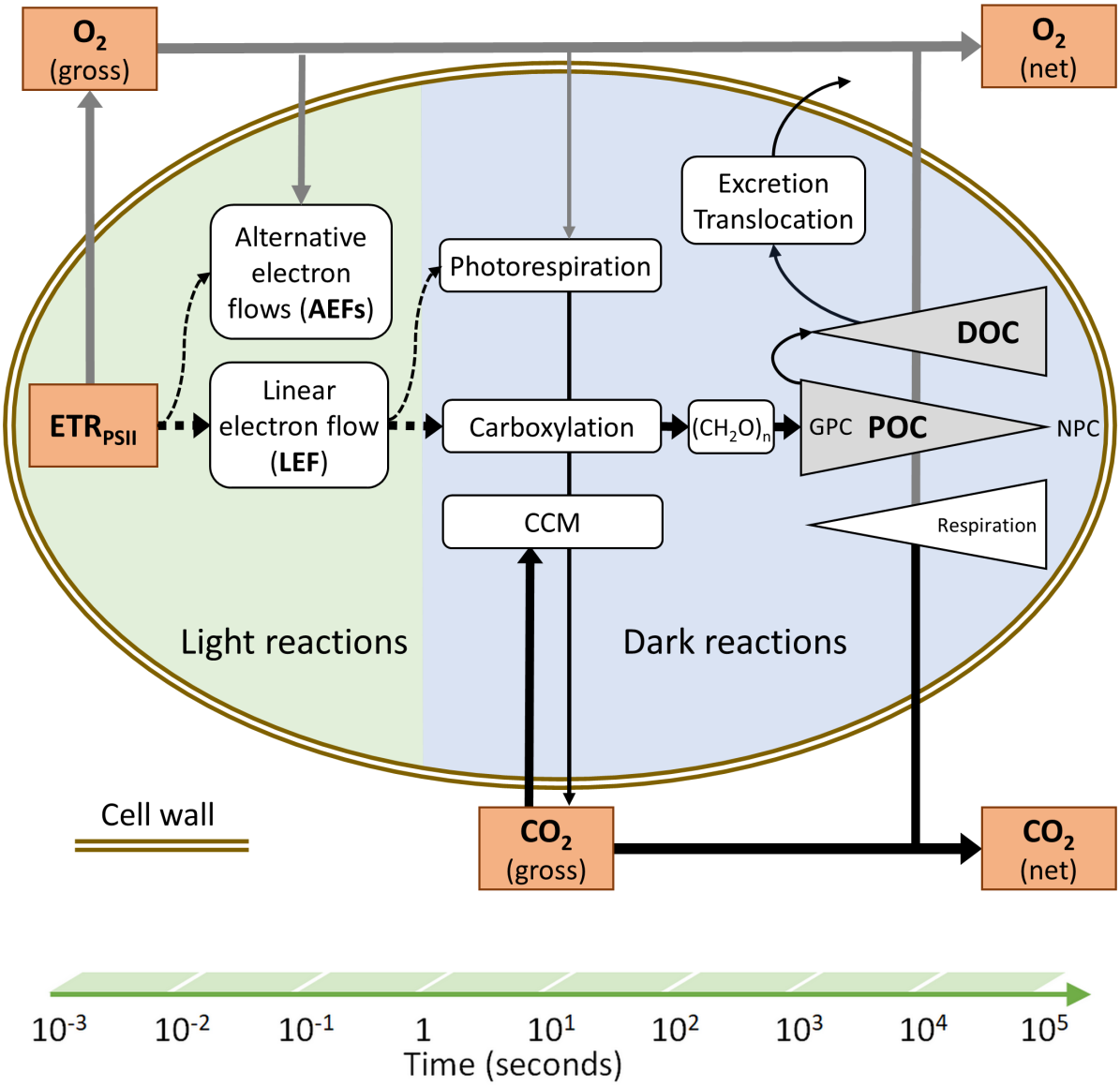

Figure 1.2. Summary of light and dark reactions of photosynthesis in plants, highlighting the fluxes of the three major photosynthetic currencies (orange boxes): electrons (ETR_{PSII} – dashed arrows), oxygen (grey arrows), and carbon (black arrows) over a time scale from milliseconds to hours and days, with the direction of arrows indicating production (arrowhead: sink) and consumption (arrow tail: source). Major and minor pathways are indicated by thick and thin lines, respectively. Grey triangles indicate particulate (POC) and dissolved organic carbon (DOC). The direction of the triangles reflects that the fraction of POC measured by ^{14}C-incorporation retained decreases over time due to respiration and/or extracellular release of DOC, as the photosynthetic rate captured transitions from gross to net carbon production (GPC and NPC) with increasing incubation length (e.g., from minutes to hours). Modified from Hughes et al. (2018).

Whilst photosynthesis in Symbiodiniaceae clearly plays a significant role in determining metabolism, mitochondrial respiration is a key facilitator (Oakley et al. 2014a). Mitochondrial respiration rates in darkness are typically between 26 and 43% (Brading et al. 2011) and can reach up to 50% (Roberty et al. 2014) of the photosynthesis rates measured during daylight for Symbiodiniaceae, but can shift under particular circumstances (e.g. elevated partial pressure of CO_2). Furthermore, it has been shown that Symbiodiniaceae can feed on bacteria in culture (Jeong et al. 2014) but also can be grown in the dark with glucose (Xiang et al. 2013). Such "mixotrophy" therefore enables photosynthetic metabolism to be supplemented and overcomes some of the conventional limitations of LR and DR in governing the rates of metabolism. However, very little is known about the balance of these processes in regulating Symbiodiniaceae fitness.

1.2.3. Symbiodiniaceae – Light-dependant reactions (LR)

Also referred to as the "light reactions", LR describe the processes of light-harvesting and utilisation. These reactions have been intensively studied for the past two decades on Symbiodiniaceae, mainly through the growing wealth of bio-optical instrumentation able to assay routinely and non-invasively photochemical pathways (Suggett et al. 2015; Warner and Suggett 2016). The capacity for photoacclimation defines light-harvesting capability by Symbiodiniaceae, and several vital studies have probed photoacclimation "strategies" amongst different Symbiodiniaceae culture isolates (Iglesias-Prieto and Trench 1994; Hennige et al. 2009) and *in hospite* (e.g. Hennige et al. 2008; Frade et al. 2008). Light-harvesting is governed by an array of pigments and pigment-proteins complexes (the light-harvesting complex, LHC) that absorbs and channel light to the photosynthetic reaction centres. Symbiodiniaceae pigmentation is characterised by chlorophyll-*a*, c2, peridinin and an array of carotenoids (Venn et al. 2006) that preferentially targets blue-green light absorption of photosynthetically active

radiation (PAR). Importantly, photoacclimation can be achieved through altering either the amount of pigments (the size of the LHC) or the number of reaction centres (Falkowski and LaRoche 1991). Whilst Symbiodiniaceae appear to preferentially adopt the latter strategy (Hennige et al. 2009), which is a strategy more associated with dynamic environments, recent research suggests that different Symbiodiniaceae isolates may employ either (or a mix) of these strategies (Suggett et al. 2015). In part, this complex mix of photoacclimation is likely facilitated through capacity for Symbiodiniaceae to initiate complex photoprotection properties under dynamic light fields (Warner and Suggett 2016). Notably, a high capacity to "quench" excess absorbed energy by cycling their xanthophyll pigments (e.g. Warner and Berry-Lowe 2006), as well as membrane antenna complexes associated with acpCP (the integral Chla-ChlaC2-peridinin protein complex) and reaction centres (Reynolds et al. 2008; Kanazawa et al. 2014). Besides, Symbiodiniaceae appear to exhibit substantial reaction centre "repair rates" (Takahashi et al. 2009; Hill et al. 2011; Ragni et al. 2010)

Pigments contained in coupled antennae of photosystem II (PSII) (σ_{PSII},) also emit fluorescence (i.e. 685 nm from chlorophyll-*a* [Chl*a*]) at room temperature when stimulated by light. Chlorophyll-induction fluorometers have thus been designed to exploit this signature and for the past decade have revealed major features of light-harvesting and utilisation in Symbiodiniaceae (e.g. Warner et al. 2002). Energetic photons absorbed by PSII catalyse photolysis with D1 protein and produce electrons from water by the PSII reaction centre complex (RCII), which are then transferred to photosystem I (PSI) via a series of intermediate molecules, including plastoquinone (PQ) and cytochrome b6f complex (Cyt b6f). Electrons passing through PSII drive a proton gradient that is required to convert ADP into ATP (adenosine triphosphate), and when passed to PSI complete the reduction of NADP into NADPH (Figure 1.3) (Madoz et al. 1998; Hald et al. 2008); this energy (ATP) and reductant (NADPH) are the currency used by all cellular metabolic reactions (Bertucci et al. 2009). The

linear electron flow (LEF) throughout PSII and PSI is referred to as the electron transport chain (Q_A), and the rate of electrons generation by PSII (ETR_{PSII}) provides a key metric of the photosynthetic of the LR (Figure 1.2; Genty et al. 1989; Hughes et al. 2018).

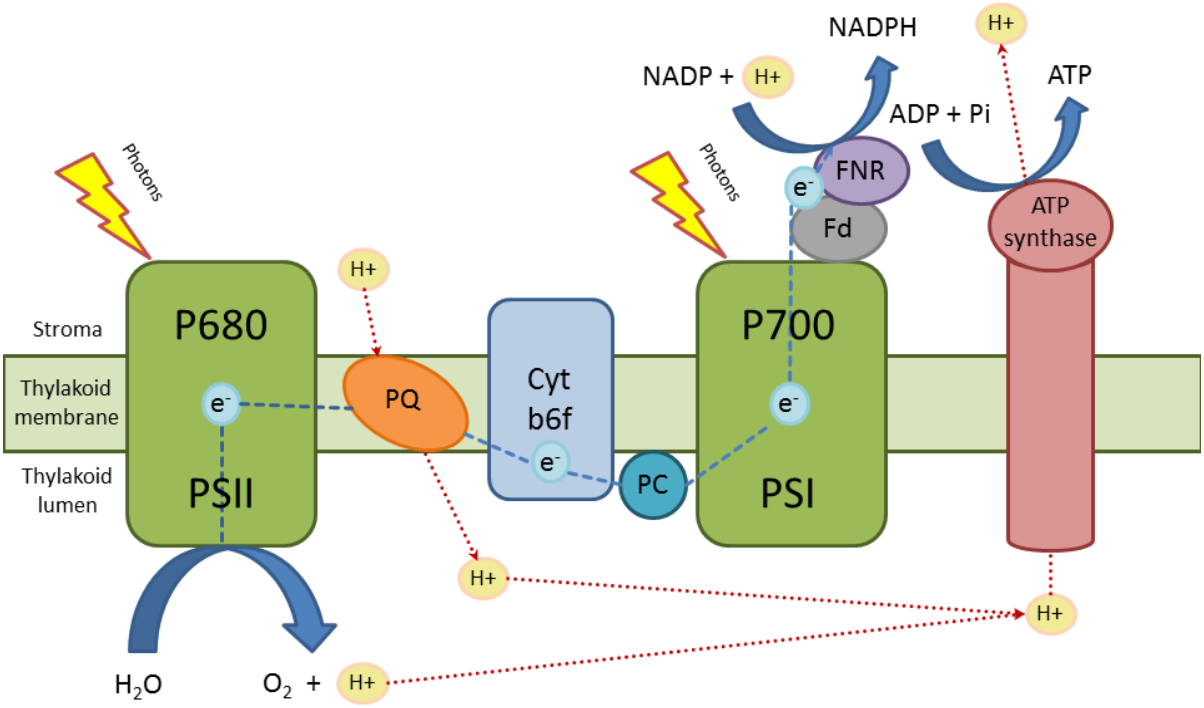

Figure 1.3. Schematic representation of the light-dependant reactions of photosynthesis occurring at the thylakoid membrane. The bright blue line represents the linear electron (e^-) flow (LEF). Photosystem I (PSI), photosystem II (PSII), plastoquinone (PQ), cytochrome b6f (Cyt b6f), plastocyanin (PC), ferredoxin (Fd), ferredoxin-NADP reductase (FNR), inorganic phosphate (Pi).

Whilst electron flow by Q_A via PSII and PSI fuels cellular metabolism, Symbiodiniaceae appear to have acquired several additional pathways to cope with excessive excitation when photoprotection by the LHC is insufficient. Mehler ascorbate peroxidase pathway (MAP) is the main alternative electron flow (AEF) in Symbiodiniaceae (Figure 1.2; Suggett et al. 2008; Cardol et al. 2011; Roberty et al. 2014), providing means for PSI to transfer electrons in excess to O_2, producing a superoxide ion ($O_2^{\bullet-}$) which can be converted back to H_2O. This key photoprotection mechanism comes at the cost of exposing the cell to additional reactive oxygen species (ROS), and therefore, requires fine-tuning between this process and

synthesis of ROS quenching components (Levin et al. 2016). Recent work has similarly shown that cyclic flow around PSI (CEF-PSI) may alleviate excess energy in response to an elevation of temperature (Aihara et al. 2016). Symbiodiniaceae appear to have an active reduction of the PQ pool in the dark (Hill and Ralph 2008) through "chlororespiration"; allowing the transfer of electrons from produced NADPH to O_2; whether this also extends into the light to act to consume excess electrons has not yet been demonstrated. Overall, the capacity to "consume" electrons in the light is an active area of research highlighting the complexity of Symbiodiniaceae cellular functioning, and their evolution within this family.

1.2.4. Symbiodiniaceae – Light-independent reactions (DR)

Also called the "dark reactions", DR are predominantly characterised through the Calvin-Benson cycle (CBC; Figure 1.4). Alternate modes of photosynthesis (termed C3 and C4) depend on the site of the CBC and the enzyme involved in the assimilation of CO_2. More precisely, CO_2 is incorporated into a three-carbon (C3) compound (3-phosphoglyceric acid or PGA) inside the cell (Moore et al. 1995). Alternatively, for C4 photosynthesis, CO_2 is incorporated into a four-carbon (C4) compound (oxaloacetic acid or OAA) by PEP-carboxylase. The difference between these two strategies is that C3-photosynthesis requires fewer enzymes to perform than C4, but CO_2 uptake is faster in C4- than in C3- photosynthesis, primarily due to a spatial separation in the use of CO_2. Symbiodiniaceae have conventionally been thought to mostly operate C3-based photosynthesis (Descolas-Gros and Fontugne 1985); however, recent genome assembly of the Symbiodiniaceae species *Fugacium kawagutii* suggests that the chloroplastic CBC, C4 cycle, crassulacean acid metabolism (CAM), and associated biosynthesis pathways are all present (Lin et al. 2015). As such, it is entirely unclear whether Symbiodiniaceae always exclusively conform to C3, C4 or somewhere intermediate, and is a central area to resolve, especially by determining which carbon compound is used by

Symbiodiniaceae to initiate the CBC (Beardall and Raven 2016). Such a major gap in knowledge fundamentally highlights that studies focussing on the DR are fewer for Symbiodiniaceae compared to the LR, but has recently emerged with renewed interest due to ocean acidification, and how Symbiodiniaceae photosynthesis is controlled by CO_2 availability (Brading et al. 2011). In either case, the carbonated products of photosynthesis will be allocated to different pools (Figure 1.2): they could be used by the cell (Halsey and Jones 2015), either on the short term to sustain its maintenance (gross carbon production, GPC) or on the long term to ensure cell growth (net carbon production, NPC). Finally, the remaining organic carbon not used by the symbiotic cell can be excreted either passively or actively to their surroundings to sustain symbiosis with their host.

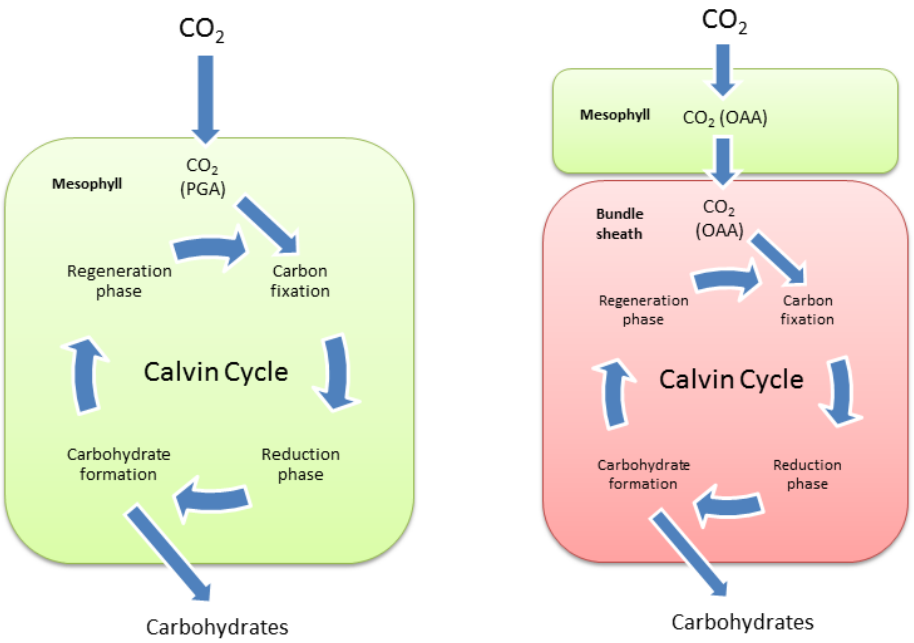

	C3 photosynthesis	C4 photosynthesis
Costs	Photorespiration	ATP cost associated with fixing carbon twice Less efficient under cold conditions
Benefits	Carbon fixation without using ATP	Reduced photorespiration and ability to fix carbon under high temperature and reduced water loss
Separation	None	Spatial

Figure 1.4. Representation of carbon assimilation in C3- and C4-photosynthesis in plants, with their associated costs and benefits.

Symbiodiniaceae cells living *in hospite* are limited by the ability of the host to provide them with dissolved inorganic carbon (DIC) (Tansik et al. 2017). Similarly, some Symbiodiniaceae taxa *ex hospite* (Brading et al. 2011) or *in hospite* (e.g. Suggett et al. 2012) appear to be CO_2-limited under present-day CO_2 concentrations in the oceans. In C3-photosynthesis, the enzyme ribulose-1,5-biphosphate carboxylase oxygenase (RuBisCO) (Dhingra et al. 2004) is involved in the assimilation of CO_2. RuBisCO catalyses two important activities depending on the ratio of O_2 and CO_2 at the active site of the enzyme: carboxylase reaction occurs when CO_2:O_2 is higher than 0.5, and oxygenase reaction happens when CO_2:O_2 is lower than 0.5 (Beardall and Raven 2016). Amongst all the different existing forms of RuBisCO, the form II RuBisCO is present in Symbiodiniaceae (Rowan et al. 1996), and it is known to have a very low CO_2:O_2 selectivity, but are poorly characterised given their poor stability *in vitro* (John Raven, personal communication). Even so, oxygenation of RuBisCO provides a purpose – as with the LR, consumption of O_2 may provide a means to limit O_2 build-up that acts as a precursor to toxic ROS generation. This process, called photorespiration, results in the production of "simple" carbohydrates and thought to be the primary process by which Symbiodiniaceae when in symbiosis generates "junk food" to the host (Falkowski et al. 1984; Crawley et al. 2010). That said, photorespiration has not yet been commonly observed in free-living Symbiodiniaceae (compared to other O_2 consuming pathways, such as the Mehler reaction; Roberty et al. 2014) and may be restricted to the coupled dynamics of life *in hospite* (Crawley et al. 2010; see also Warner and Suggett 2016).

Interestingly, RuBisCO cellular content appears to vary across different Symbiodiniaceae isolates, perhaps to overcome different constraints on CO_2 availability (Brading et al. 2013). However, more importantly, Symbiodiniaceae appear to employ a complex mix of carbon concentrating mechanisms (CCMs) to overcome fundamental CO_2 limitation at the site of RuBisCO (Leggat et al. 1999). Coral symbionts do not rely on passive

diffusion of CO_2 because of the RuBisCO properties for CO_2 and its low selectivity towards O_2 (Leggat et al. 1999; Brading et al. 2013). Symbiodiniaceae use both CO_2 and HCO_3^- ion as sources of carbon for photosynthesis, with a predominant use of the latter (Goiran et al. 1996). Two mechanisms of HCO_3^- utilisation are possible. Firstly, HCO_3^- may be actively converted to CO_2 according to its equilibrium constant, temperature and pH to diffuse through the cell membrane by the action of a membrane-associated enzyme, the carbonic anhydrase (CA). Secondly, HCO_3^- can diffuse through the cell membrane to be converted into CO_2 in the cytosol to be brought inside of the chloroplast (Giordano et al. 2005). However, these processes remain poorly studied in the model Symbiodiniaceae, and the diversity in the CA activity might explain the differences between isolates in the capacity of assimilating carbon (Brading et al. 2013).

Fundamentally DR are more complex to study than LR because they involve the study of enzymes (i.e. RuBisCO), many of which are metabolic intermediates in rapid cycling processes, and therefore cannot be assessed by rapid and non-invasive techniques such as optics and fluorometry. As a result, DR mechanisms constitute a substantial gap in the knowledge of Symbiodiniaceae function and governance of their competitive success in nature. Clearly, the studies to date suggest immense complexity and possibly diversity in how DR have evolved to operate amongst the genus Symbiodiniaceae, and it may only be that we can understand this through the use of more advanced "omics"-based platforms (Leggat et al. 2011; Levin et al. 2016; Matthews et al. 2017).

1.3. Symbiodiniaceae diversity

1.3.1. Genus diversity

A key challenge in trying to reconcile "universal" models by which photosynthesis operates in Symbiodiniaceae reflects that the genus is comprised of immense diversity. Analysis across numerous isolates frequently demonstrates that a "universal" model may, in

fact, never hold (Warner and Suggett 2016; Goyen et al. 2017; Lawson et al. 2019). Continued advances in the development of genomic tools using high definition molecular markers allowed unravelling the vast phylogenetic diversity of the family Symbiodiniaceae (LaJeunesse et al. 2018). Ribosomal (18S/28S-rDNA; Baker and Rowan 1997; Figure 1.5) or chloroplastic (cp23S-rDNA; Santos et al. 2004) genes are markers used to determine the genus diversity, ranging from A to I (Pochon et al. 2004; Pochon and Gates 2010; see LaJeunesse et al. 2018). These genus-level descriptions are thought to be analogous to genus-level separation (LaJeunesse et al. 2012), and convergence of symbionts and hosts taxonomic diversity at this level appears to explain the coevolution processes (van Oppen et al. 2001) that lead to the current host-symbiont specific relationships (Figure 1.5). LaJeunesse et al. (2012) also proposed improved approaches to resolve species identity, based in integrating molecular and conventional taxonomic tools and providing a more rigorous and standardised framework to close complex taxonomy that was variable across markers; and they later reclassified the whole Symbiodiniaceae taxonomy (LaJeunesse et al. 2018). Symbiodiniaceae of the genus *Symbiodinium sensu stricto* (formerly clade A), prevail in western Atlantic (Baker and Rowan 1997) and the Red Sea (Karako-Lampert et al. 2004). *Breviolum* (formerly clade B) prevail in the Caribbean (Santos et al. 2004), *Cladocopium* and *Durusdinium* (formerly clades C and D) dominate the coral host assemblages as a symbiont due to their genetic diversity over the GBR (LaJeunesse et al. 2004) and the Indian Ocean (LaJeunesse et al. 2010).

Such genus diversity becomes even more complex at the "sub-genus" level: the internal transcribed spacer (ITS2-rDNA; LaJeunesse 2001) has been particularly popular to describe Symbiodiniaceae phylogenetic diversity (commonly assigned alpha-numerically; e.g. Type C1, where "C" refer to the genus *Cladocopium*) and how this compared to ecological fitness over space and time (Mieog et al. 2009). Intriguingly, the use of "multi-locus" descriptions (more than one "amplicon", e.g. ITS2 alongside *psbA*) alongside conventional taxonomic platforms

have now enabled species level descriptions of Symbiodiniaceae (LaJeunesse et al. 2012). Even more sophisticated approaches such as microsatellites (Santos et al. 2004), DNA fingerprints (Goulet and Coffroth 2003) and RAPDs (Baillie et al. 2000) have been used for determining the clonal diversity level, which has become increasingly popular to understand how Symbiodiniaceae populations are connected over space and time (Thornhill et al. 2017), as well as evolutionary time scales of adaptation (e.g. Thornhill et al. 2013).

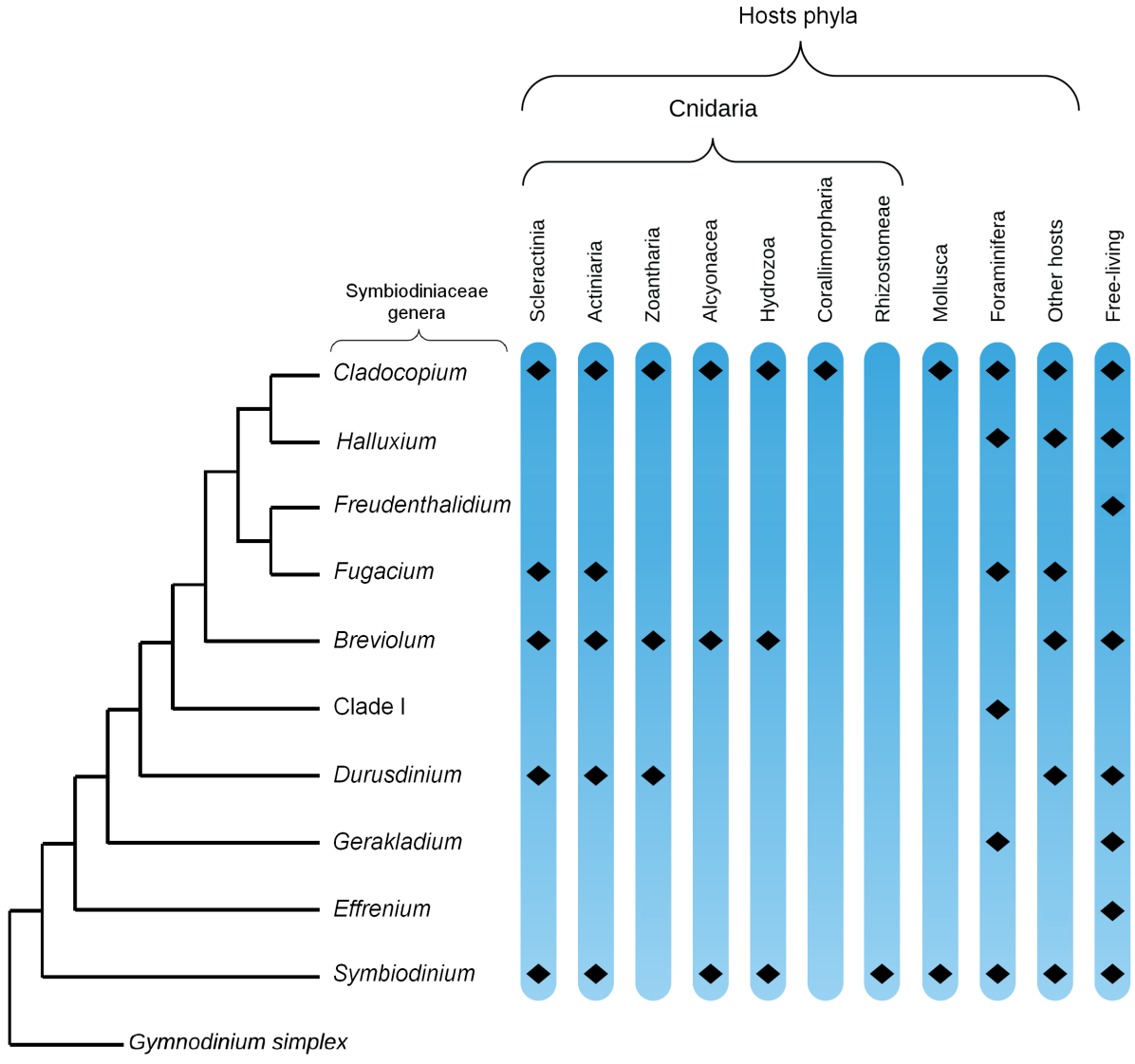

Figure 1.5. Topology of Symbiodiniaceae genera based on nr28S-rDNA datasets, and their host occupancy. Modified from Pochon and Gates (2010); Fournier (2013); Nitschke (2015); Baker et al. (2017), LaJeunesse et al. (2018) and Nitschke et al. (2020)

Whilst genus diversity has been commonly used to assign niche separation (Sampayo et al. 2007; Cooper et al. 2011) and differences in ecological successes and fitness of host-Symbiodiniaceae, this has resulted in some fundamental problems; for example, on the GBR *Cladocopium* (ITS2 type C1) can express both thermo-tolerant populations *vs*. thermo-sensitive populations (Levin et al. 2016). Diaz-Almeyda et al. (2017) also compared the wide genotypic variation in heat tolerance of the genus *Symbiodinium*, further suggesting that genus diversity does not account for local environmental pressures selected for emergent functional properties. Consequently, diversity of physiological properties characterising function amongst Symbiodiniaceae isolates has been suggested to be a more appropriate means to classify Symbiodiniaceae (Suggett et al. 2015; Warner and Suggett 2016), at least in terms of defining functional fitness trends over space and time.

1.3.2. Functional diversity

Oceanographers began using "functional diversity" as a means to describe complex microbial communities over fifteen years ago (Azam and Worden 2004). For example, calcification and nitrogen fixation are critical processes regulating biogeochemical cycles (Church et al. 2008), and therefore knowing how indicators of these processes change independently of taxonomic shifts overcome limitations in how taxonomy is resolved. However, such a concept has only recently been suggested for Symbiodiniaceae (Suggett et al. 2015) – but is only possible by "screening" a large number of isolates that sufficiently captures isolate diversity and distribution. Few physiological characteristics have yet been investigated (light-harvesting, Suggett et al. 2015; ROS emissions, Goyen et al. 2017; volatile metabolites, Lawson et al. 2019), and the level of complexity required to describe functional diversity is not yet resolved.

Firstly, physiological processes can be related to an organism size and growth rate, such as the metabolic rate, the maximum nutrient uptake rate and the cellular composition (Finkel et al. 2010). Cell size governs the functional diversity of photobiological traits (Suggett et al. 2015), but whether this extends to nutrient uptake properties is not yet explored. The rate of infectivity by Symbiodiniaceae into hosts is also dependant on the cell size of the symbiont (Biquand et al. 2017). The size of Symbiodiniaceae cells might then constitute a pivotal feature to explain the diversity of symbionts amongst hosts and the selectivity of the host amongst the vast diversity of symbionts. Secondly, given the importance of photosynthesis in the Symbiodiniaceae-host symbiosis, critical parameters defining Symbiodiniaceae photobiology are good candidates (Suggett et al. 2015) but whether plasticity of physiological characteristics defining photoacclimation of light-harvesting (Hennige et al. 2009; Suggett et al. 2015) comes at a cost of other key processes, such as uptake of carbon (and other nutrients), to result in different functional groupings is unknown. Finally, the ratio of carbon assimilated that is utilised (growth and maintenance or NPC and GPC, respectively) *vs.* carbon translocated to the host are pivotal for answering the question of what makes a "good" symbiont. However, how functional diversity further extends to the mechanisms underlying carbon translocation (and how critical this is to coral survival) similarly remains largely untested (Davy et al. 2012; Sproles et al. 2019). These various complexities in biology and fundamental knowledge gaps suggest again that high throughput approaches that retrieve multiple characteristics and can simultaneously screen multiple types may be our best platform to resolve functional diversity.

1.4. Environmental stress – when Symbiodiniaceae become toxic

Under ambient conditions of temperature and light, photosynthesis reactions produce oxygen that is the precursor for reactive oxygen species (ROS), also called "free radicals". They include superoxide radicals, singlet oxygen, hydroxyl radicals and hydrogen peroxide

(Downs et al. 2002). These natural by-products of photosynthesis are essential signalling molecules (e.g. Smith et al. 2005) and are degraded by protective enzymatic antioxidants (e.g. superoxide dismutase, catalase, and peroxidase) and non-enzymatic antioxidants (e.g. ascorbic acid, glutathione; Lesser 2006) to sustain cellular homeostasis (Figure 1.6). ROS production appears to be an important component in determining stress tolerance amongst Symbiodiniaceae isolates (Downs et al. 2002; McGinty et al. 2012; Goyen et al. 2017; Suggett and Smith 2020). When Symbiodiniaceae encounter a dose (i.e. intensity, duration, or both) of light beyond their capacity for photoacclimation and photoprotection, more ROS are produced (i.e. photoinhibition, Venn et al. 2008; Weis 2008), which ultimately targets the deactivation of RCIIs (Warner et al. 1999). Whilst photoprotection pathways are diverse amongst Symbiodiniaceae (see section 2.2.3), differences in ROS-quenching *vs.* production capability clearly separate Symbiodiniaceae functional diversity (Goyen et al. 2017). Considerable interest has focused on other secondary metabolites of interest that may be important ROS quenchers in Symbiodiniaceae (e.g. DMSP, Sunda et al. 2002; Yost and Mitchelmore 2009; Deschaseaux et al. 2014; other volatile gases, Lawson et al. 2019) to understand better how all physiological pathways need to co-operate to maintain homeostasis under stress.

Most studies examining Symbiodiniaceae "stress" responses to date have examined (sub) lethal temperatures. Importantly, temperature drives the conspicuous decoupling of the Symbiodiniaceae-host associations (coral bleaching; Smith et al. 2005; Suggett and Smith 2020) and numerous studies on cultures of Symbiodiniaceae have suggested that temperature stress "accelerates" the process of photoinhibition (Takahashi and Murata 2008; Takahashi et al. 2009; Hennige et al. 2011; Lesser 2019). Changes in temperature alter the rate of enzyme activity, determining their maximum photosynthesis rates. Whilst colder temperatures appear to do this through "slowing" RuBisCO (Sage 2002; Yamori et al. 2014), the role of higher temperatures are less well understood. A fundamental hypothesis is that temperature

deactivates RuBisCO (Jones et al. 1998); however evidence for this is limited in Symbiodiniaceae (see Lilley et al. 2010), reflecting a lack of focus on DR (section 2.2.4). Recent work suggests a higher potential of DIC acquisition by cultured Symbiodiniaceae under elevated temperatures (30-34ºC), associated with whether a more efficient RuBisCO, whether enhanced CCM activity (Oakley et al. 2014b). More likely, temperature destabilises processes that facilitate high electron flow through PSII (Lesser and Farell 2004) such that excitation pressures build, subjecting cells to enhanced photo-inhibitory pressures (e.g. Tchernov et al. 2004).

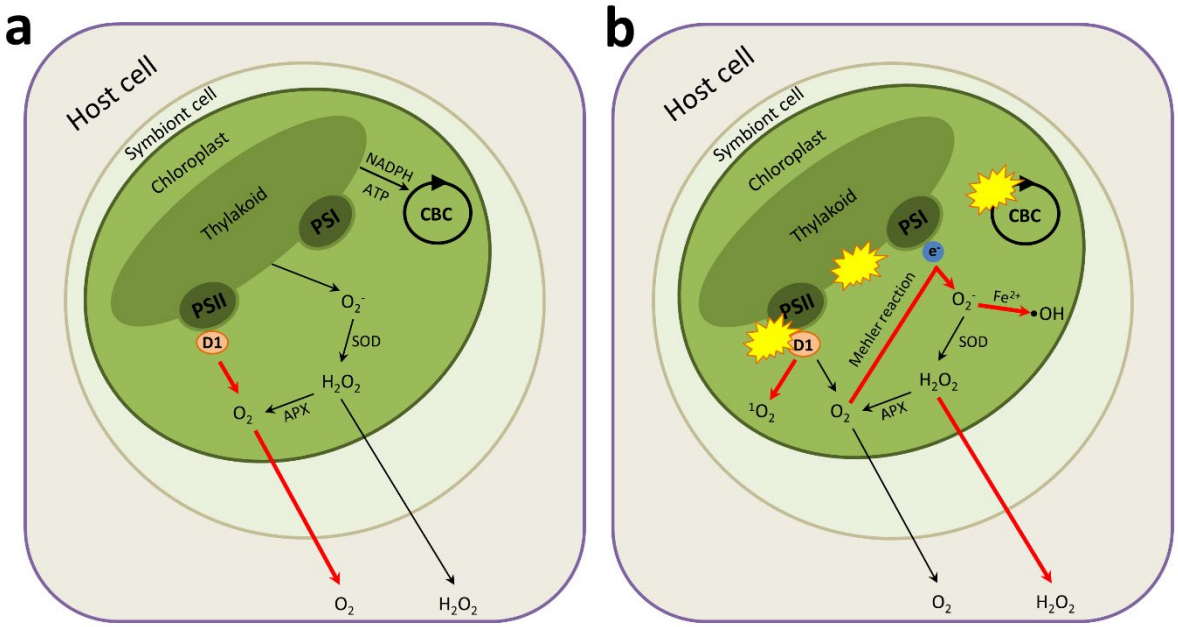

Figure 1.6. Outline of the production and fate of reactive oxygen species (ROS) in a Symbiodiniaceae cell under ambient (**a**), and stressful (**b**) temperature and light conditions. Photosystem I (PSI), photosystem II (PSII), Calvin-Benson cycle (CBC), protein D1 (D1), superoxide dismutase (SOD), ascorbate peroxidase (APX), singlet oxygen ($^1O_2$), superoxide radical (O_2^-), hydroxyl radical (•OH), hydrogen peroxide (H_2O_2), ferrous ion (Fe^{2+}). Yellow flashes represent photoinhibition and damages to cellular pathways. They occur on D1 protein activity (Warner et al. 1999), thylakoid membranes (Tchernov et al. 2004), and RuBisCO (Venn et al. 2008). Modified from Weis (2008).

An increasing quantity of studies is focusing on the acute response of corals to stressful conditions (Tchernov et al. 2004; Bruno et al. 2007; Suggett et al. 2008; Guest et al. 2012) (e.g.

elevated temperature, ocean acidification, and ultraviolet radiation). Such work has reflected the need to better predict the fate of coral reefs towards climate change and to understand the processes underlying coral bleaching (see Smith and Suggett 2020), and potentially drive classification of thermo-tolerant and thermo-sensitive (respectively "winners" and "losers"; *sensu* Baskin 1998; Grottoli et al. 2014) genera of Symbiodiniaceae (Swain et al. 2017). *Durusdinium* is considered as a thermo-tolerant genus based on numerous physiological studies (Rowan, 2004; Silverstein et al. 2017; Wham et al. 2017) while *Cladocopium* is more susceptible but has different levels of tolerance within and between its ITS2 types (Sampayo et al. 2008; Levin et al. 2016) and species, such as *Cladocopium thermophilum* (Hume et al. 2015), prevalent in the southern Persian/Arabian Gulf, the world's hottest sea. Diversity in thermo-tolerance between representatives of different species of same genera is particularly crucial in reconciling Symbiodiniaceae functional diversity with their taxonomic classification. *Symbiodinium* is also considered as thermo-susceptible by Yuyama et al. (2012). However, several studies (Brading et al. 2011; Kramer et al. 2012; Brading et al. 2013) reported some *Symbiodinium* species (or ITS2 types) as being thermo-tolerant, depending on their sampling origin. Consequently, the taxonomic classification of genera based on molecular markers may rarely reflect the actual functional diversity of different Symbiodiniaceae species.

In an attempt to link temperature and seawater acidification effects, Gibbin et al. (2015) suggested that the thermo-tolerance in the coral *Montipora capitata* and thermo-sensitivity in *Pocillopora damicornis* could be explained by their symbionts, without however assessing symbiont taxonomic identity. Such functional diversity in tolerance to thermal stress is building improved knowledge of community-level patterns in stress tolerance for coral species across contrasted habitats (Oliver and Palumbi 2011), and thus disruption in the symbiosis through climate stress inevitably leads to shifts in symbiont community patterns (Jones et al. 2008). Cases of acclimation of corals to elevated temperatures have already been reported (Howells

et al. 2011; Juriaans and Hoogenboom 2019; Wright et al. 2019), depending mostly on the past events of increasing SSTs. However, acclimation processes are relatively costly regarding cell metabolism reorganisation and structure, which may limit the emergence of acclimation mechanisms in coral or symbiont species (or both; Jones and Berkelmans 2011). For this reason, the study of the differential response of Symbiodiniaceae between (and within) genera to stressful events at the cellular level will improve the understanding of their mechanisms of resistance and sensitivity and enrich the insight of functional traits evaluated to explain their functional diversity. We are starting to understand that stress-tolerant corals exploit the fact that there are different available functional Symbiodiniaceae genera (species or genetic variants) in the environment, and bleaching events may provide a means for hosts to select for a type that better withstands – or is more closely functionally optimised – to stressful conditions. This mechanism is also known as symbiont switching (*sensu* Baker et al. 2003), and symbiont communities typically revert back to their native state once the thermal stress abates. However, this is not always the case (Goulet 2006), where the most stress-tolerant coral genera, *Porites*, always associates with *Cladocopium* (ITS2 type C15) in the Indo-Pacific (Fitt et al. 2009) to withstand thermal stress. This ability to be flexible in associating with different symbiont types (Putnam et al. 2012) fundamentally highlights the gap in the knowledge about the niche breadth with which different taxa have evolved to function, and therefore, what is considered optimum *vs.* sub-optimum conditions.

1.5. Methodologies to assess LR and DR diversity

1.5.1. Fast Repetition Rate fluorometry (FRRf)

Characterisation of LR in microalgae starts by examining how efficiently cells can harvest light, this can be resolved using fluorometry techniques based on the inherent capacity of Chl*a* to emit fluorescence after excitation by 450-470 nm wavelengths (Suggett et al. 2009).

These light emissions can then be measured by fluorometers to infer photophysiology parameters, especially the so-called maximum yield of photochemistry (F_v/F_m), a proxy used for determining symbiont photosynthetic capacity (Suggett and Warner 2016). As such, almost all studies studying coral or Symbiodiniaceae physiology are using either pulse-amplified modulated (PAM) or fast repetition rate fluorometers (FRRf). More advanced use of these instruments, such as the establishment of rapid light curves (RLCs), monitors the cells effective quantum yield of photochemistry (Ralph and Gademann 2005) and enables to determine the relative quantum yield of ETR_{PSII} (Hennige et al. 2008; Roberty et al. 2014; Figure 1.2) or absolute ETR_{PSII} (Suggett et al. 2015). Parameterisation from RLCs allows discriminating if the light energy is used for photosynthesis (photochemical quenching; qP) and emitted as fluorescence or converted to heat (non-photochemical quenching; NPQ), a proxy of Symbiodiniaceae metabolic strategies driving their fitness (Suggett et al. 2015; Nitschke et al. 2018; Camp et al. 2019). Both fluorometry techniques measure chlorophyll fluorescence, but while PAM-fluorometers rely on multiple turnovers of RCII, FRRf induce a single turnover rate (by the use of rapid flashlets), making measurements less intrusive in the photosynthetic apparatus and easier to interpret due to a single reduction of the electron transport chain (Hughes et al. 2018). Nonetheless, PAM-fluorometers are widely used due to their ability to be employed directly on corals, where FRRf would mostly be used on cellular cultures or oligotrophic seawater samples given their high sensitivity in assessing low biomass samples (Table 1.1).

1.5.2. Measurements of oxygen evolution

Photosynthesis is characterised by the production of O_2 from the oxidation of water to produce electrons and subsequently ATP and NADPH used by the cell (Figure 1.3). Consequently, one of the earliest (Kawaguti 1937) and most used methods to measure the

efficiency of photosynthesis is measurements of O_2 production by coral symbionts to establish productivity rates. This information is frequently applied to yield the photosynthesis response to irradiance (P-I; *sensu* Muller-Parker 1984; Anthony and Hoegh-Guldberg 2013), allowing characterisation of Symbiodiniaceae photoacclimation strategies (see section 1.2.3.) across their genus diversity (Savage et al. 2002; Suggett et al. 2015). Whilst this technique is useful beyond fluorometry for determining photobiology traits characteristic of Symbiodiniaceae functional diversity, they come with disadvantages inherent to the presence of several organisms within the holobiont making impossible to determine the participation of each organism to the total measured O_2 (Trampe et al. 2015), as well as the fate of O_2 from photosynthesis likely subjected to reallocation to other pathways within the studied organism (Suggett et al. 2008; Brading et al. 2011; Hughes et al. 2018), such as respiration, AEF (see section 1.2.3.) and ROS production (see Figure 1.6). Consequently, the measured rates of O_2 production could be underestimated, and they need to be coupled with direct assessments of carbon assimilation (Table 1.2).

1.5.3. Radioactive and stable isotopes

A more precise and direct measurement of productivity – energy assimilation into organic skeletons – in corals relies on the use of elemental tracers, radioactive or stable, of uptake from the environment or "pulse-chase" through the cells (e.g. Matthews et al. 2018). Tracing labelled elements can be achieved using a wide range of instruments either detecting radioactive emissions (autoradiography or disintegrations per minute counting) or measuring isotope ratios, according to the type of tracer used. Used for the first time by Steemann-Nielsen to measure productivity of phytoplankton in oceanic waters (1952), and by Muscatine and Hand (1958) to demonstrate translocation of photosynthetically fixed carbon compounds by the symbiont to the host; radioisotopes of carbon (^{14}C) have been consistently applied for the

past 60 years to determine productivity of coral symbionts (see Table 1.2). Using this technique enables the separation of the ^{14}C retained by the cells as particulate organic carbon (POC) and excreted (passively or actively) to their surroundings as dissolved organic carbon (DOC) (Thornton et al. 2014). However, the tracking of Ci uptake used for maintenance (as GPC) using carbon isotopes, regardless of their stability, is hindered by a common limitation of loss of the labelled products through respiration readily used by the cell for maintenance (Figure 1.2) (Pei and Laws 2013; Halsey and Jones 2015). As such, it is critical when considering the use of these techniques to keep incubations short, limiting the measurement of NPC over GPC (Halsey et al. 2013; Halsey and Jones 2015), and studies to date (Table 1.2) have generally used long (>1 h) incubations, likely measuring NPC over GPC. Moreover, studies on the holobiont prefer the use of stable over radioactive isotopes due to the inherent hazardous nature of the latter (Table 1.1). Interestingly, the study of natural (without incubations *in situ*) $^{12}C/^{13}C$ ratios in corals make possible the study of long-term adaptations in trophic strategies (Fox et al. 2018; Radice et al. 2019; Wall et al. 2020).

1.5.4. NanoSIMS

Studies on whole corals have turned to nutrient incorporation and transfer approaches, typically with coupling stable-isotopes and imagery techniques using nano-scale secondary ion mass spectrometry (NanoSIMS) to track the fate of carbon and nitrogen, and characterised metabolic interactions between cnidarian host and symbionts at the sub-cellular scale. Clode et al. (2007) were the first to apply this technique to coral tissues to assess the localisation of ^{13}C- and ^{15}N-labelled compounds within the holobiont, followed by Kopp et al. (2013, 2015). Subsequent studies applied the approach to examine the effect of alternate host-Symbiodiniaceae associations on nutrient assimilation (see Table 1.2), and how they were further regulated under future climate change scenarios (Krueger et al. 2017). Using the coral

Stylophora pistillata, Krueger et al. (2018) used NanoSIMS to evaluate how photosynthesis *versus* heterotrophy (feeding) influenced carbon acquisition. Specifically, these authors showed that nutritional intake from heterotrophically supplied carbon, in fact, largely outweighed phototrophic carbon for this coral species, and importantly that symbionts in fed corals exhibited decreased translocation rates of photosynthates to their host. Additional evidence has similarly shown that corals fed when maintained under low light irradiance exhibit reduced carbon translocation rates from symbiont to host by up to 25% (*Cladocora caespitosa*; Tremblay et al. 2012). Such a trade-off in carbon acquisition would suggest that corals that feed can, therefore, associate with Symbiodiniaceae that inherently provide less translocated carbon (are "selfish" or "parasitic", as per Stat et al. 2008 and Mieog et al. 2009) but presumably more stress-tolerant (Stat et al. 2008).

1.5.5. Differences in expression of functional genes

Phenotypes based on the tracing of photosynthetic currencies (electrons, oxygen, carbon, or labelled elements; see Figure 1.2), are ultimately the product of upstream gene expression machinery. Evaluating this genetic machinery has become hugely popular in recent years as crucial means to unlock Symbiodiniaceae evolutive molecular adaptations leading to their immense functional diversity (e.g. Gonzalez-Pech et al. 2019). Recent advances in next-generation sequencing techniques have led coral molecular biologists to decode the genomes of different species from different Symbiodiniaceae genera, such as nuclear genomes of *Breviolum minutum* (Shoguchi et al. 2013), *Fugacium kawagutii* (Lin et al. 2015), *Symbiodinium microadriaticum* (Aranda et al. 2016), and *Cladocopium goreaui* (Liu et al. 2018). Most studies to date investigating the functional diversity and stress response of genetically distinct Symbiodiniaceae focused on genes of LR (such as light-harvesting complexes; Levin et al. 2016; Gierz et al. 2017) and more heavily on genes encoding proteins

involved in response to thermal stress (such as ROS scavenging enzymes and molecular chaperones; Levin et al. 2016; Gierz et al. 2017). Functional diversity of response to stress between Symbiodiniaceae of the same genus such as *Breviolum* (Parkinson et al. 2016) or *Cladocopium* (Levin et al. 2016) has further been demonstrated by the study of their transcripts. As with physiological based approaches, our knowledge of gene expression of proteins involved in the DR (e.g. Ci uptake and assimilation) compared to the LR is scarce. As such, there is to date no evidence at the molecular level of response to thermal stress on DR regulation of photosynthesis and its importance in differential carbon pool allocation inherent to productivity, as well as maintenance and survival.

Table 1.1. Summary of methods (and their associated strengths and limitations) commonly used to assess currencies characteristic of functional diversity in productivity of Symbiodiniaceae, building upon knowledge from Hughes et al. (2018). Gross carbon production (GPC), net carbon production (NPC), particulate organic carbon (POC), dissolved organic carbon (DOC).

Method	Currency	Strengths	Limitations	References
FRRf	Electrons (ETR_{PSII})	High throughput Highly sensitive Non-invasive	No standardised protocols Instrument settings are species-dependent Cannot be used effectively on symbionts *in hospite*	Gorbunov et al. 2001 Hennige et al. 2008 Camp et al. 2019 Leggat et al. 2019
Respirometry	Oxygen (O_2 evolution)	Estimates GPC Estimates NPC	No separation from holobiont constituents Use of photosynthetic quotients to indirectly infer carbon productivity	See Table 1.2 Camp et al. 2019
Radiolabelled isotopes (^{14}C)	Carbon (CO_2 uptake)	Estimate NPC Can separate POC and DOC fractions In use for 60+ years	Time-dependant separation with GPC Cannot measure respiration losses Expensive and hazardous isotopes	See Table 1.2 **Chapter 2-3** of this thesis
Stable-isotopes (^{13}C + NanoSIMS)	Carbon (CO_2 uptake)	Estimate NPC Highly sensitive Imaging of sub-cellular uptake/translocation Can be used in multi-element analyses Safe stable-isotopes	Time-dependant separation with GPC Cannot measure respired losses Lengthy sample preparation Requires knowledge of cellular incorporation High demand for only 22 instruments worldwide	See Table 1.2 **Chapter 4** of this thesis

Table 1.2. Review of the studies from the past 10 years using radioactive and stable isotopes as their major method to track Ci uptake in Symbiodiniaceae *ex* and *in hospite* with subsequent translocation to their host. Outlined are their hypotheses, major results and outcomes, alongside with future directions of research.

Authors (et al.)	Hypothesis	Symbiont	Cnidarian / Host	Methods	Conditions Temp. /Light	Results	Outcomes	Future directions
Brading (2011)	Elevated pCO_2 (OA) affects photosynthesis and growth	*Symbiodinium* spp. (A1-A13-A20) *Breviolum* sp. (B1)	Free living	^{18}O evolution - MIMS (45 min)	26°C 350 µmol photons	A1 - B1 unaffected A13 growth increased A2 increased photosynthetic capacity	OA will impact horizontal transfer of symbionts	Study of different CCM types
Brading (2013)	A13 and A20 have different CCM types – carbonic anhydrase (CA) A20 has inefficient CCMs	*Symbiodinium* spp. (A20-A13)	Free living	^{14}C (1 h) POC content RuBisCO content ETR_{PSII} CA activity	26°C 350 µmol photons	A13-A20 similar rates of Ci uptake RuBisCO in A13 4x greater Preference of CO_2 *vs*. HCO_3 in A13-A20 A20 converts HCO_3 in CO_2 with CA	Different Ci uptake mechanisms Ci could represent a key trait factor influencing productivity	Screen a wider phylogenetic diversity for Ci uptake
Baker (2013)	At non stressful temperature, *Cladocopium* is a better partner than *Durusdinium,* but opposite during thermal stress	*Cladocopium* sp. (C1) *Durusdinium* sp.	*A. tenuis*	^{13}C - ^{15}N (12 h)	28°C 30°C 120 - 320 µmol photons	At 28°C *Cladocopium* uptake 22% more N than *Durusdinium*, but equivalent C At 30°C *Cladocopium* uptake 16% less C than *Durusdinium*, but equivalent N	Competition for limited N affects symbiont abundance and diversity within the host	Target other nutrients uptake rates Effect of high N saturation

Authors (et al.)	Hypothesis	Symbiont	Cnidarian / Host	Methods	Conditions Temp. /Light	Results	Outcomes	Future directions
Oakley (2014b)	CCM damage or inhibition contributes to bleaching	*Symbiodinium* sp. *B. minutum* (B1) *D. trenchii*. (D1a)	Free living	^{13}C (2 h) O_2 evolution DIC evolution Photochem.	22-26-30-34°C 75 µmol photons	No decline in Ci uptake in response to thermal stress	CCM components are not subject to thermal damage Increased temperature enhances Ci acquisition	Study effect of temperature on host carbon delivery system
Pernice (2014)	Different Symbiodiniaceae types that naturally associate with a single coral species possess different metabolic capabilities and affect host metabolism	*Cladocopium* sp. (C3) *Durusdinium* sp. (D1)	*I. palifera*	^{13}C - ^{15}N (48 h) TEM - NanoSIMS	24°C 700 -1000 µmol photons	Type C3 assimilated/ translocated more C and N than type D1	C3 are more efficient at both assimilating C and N from the environment and transferring to the host than D1	Longer incubations to investigate the relationships between metabolism and proliferation rates

Authors (et al.)	Hypothesis	Symbiont	Cnidarian / Host	Methods	Conditions Temp. /Light	Results	Outcomes	Future directions
Kopp (2015)	Incorporation, fate and turnover of Ci assimilation and translocation of photosynthates to the host can be visualised at the sub-cellular level	Unspecified Symbiodiniaceae	*P. damicornis*	^{13}C - ^{15}N (6 h) TEM - NanoSIMS	25°C 100 µmol photons	Uptake of C and N by the symbiont and storage in lipid droplets and starch granules Use of lipid at night for growth and maintenance Photosynthates are accumulated within 15 min in coral lipid droplets Within 6h in glycogen granules Translocation of N compounds happens after 3 h	Lipid droplets and glycogen granules in the coral tissue are sinks for translocated carbon photosynthates by Symbiodiniaceae and confirm their key role in the trophic interactions within the coral-Symbiodiniaceae associations	Need further photosynthesis and respiration measurements
Freeman (2016)	Symbiont metabolism within *C. xamachana* is comparable to other common benthic marine invertebrates	Unspecified Symbiodiniaceae	*C. xamachana*	^{13}C - ^{15}N (6 & 18 h)	Unspecified T°C Light (unspecified levels) and dark	Ci fixation is light dependent N fixation is light-independent	Symbiont metabolism within *C. xamachana* is comparable to other common benthic marine invertebrates	Investigate photosynthates transfers from symbionts to host (NanoSIMS)

Authors (et al.)	Hypothesis	Symbiont	Cnidarian / Host	Methods	Conditions Temp. /Light	Results	Outcomes	Future directions
Tremblay (2016)	Heat stress impacts the nutritional interactions between symbionts and corals maintained under auto- and heterotrophy	Unspecified Symbiodiniaceae	*S. pistillata*	^{13}C (5 h) O_2 evolution Calcification rates	25°C 31°C 250 µmol photons	% of autotrophic carbon retained in the symbionts was higher during heat stress compared to control and % of translocation was lower regardless of feeding supply Restoration of nutrient exchange in fed corals after stress Same calcification between fed and unfed corals	Promotion of parasitism under heat stress Heterotrophy do not mitigate the effects of temperature stress on coral calcification.	Assess quality of photosynthates translocated
LeKieffre (2018)	Dinoflagellates transfer carbon to the host foraminifer	Dinoflagellates	Foraminifera	^{13}C (6 h) TEM - NanoSIMS	22°C 350 µmol photons	Symbionts go outside the cell during day to photosynthesise and come back in the host at night where they translocate lipids to the host	Ci fixation during the day and Ci metabolised at night via respiration, transfer to the host within 45 min	Determine lipid synthesis and transfer pathways between host Foraminifera and symbiont
Radecker (2018)	*Aiptasia* model can be used to study metabolic interactions between Symbiodiniaceae-Cnidarians symbiosis	*Symbiodinium* sp. (A4) *Breviolum* sp. (B1)	*Aiptasia* spp.	^{13}C - ^{15}N (24 h) TEM - NanoSIMS	25°C 80 µmol photons	Rates of C and N assimilation depends on host and symbiont identities Only nutrients in excess are exchanged	Instable symbiosis where there is competition for available resources between partners	Study the role of C translocation in symbiosis maintenance

Authors (et al.)	Hypothesis	Symbiont	Cnidarian / Host	Methods	Conditions Temp. /Light	Results	Outcomes	Future directions
Baker (2018)	Sub-bleaching temperature and excess N promote symbiont parasitism	*Symbiodinium fitti* (A3) *Cladocopium* sp. (C7)	*O. faveolata*	^{13}C - ^{15}N (9.8 h) O_2 evolution Chl*a* Mitotic Index (MI)	26°C 31°C 310-510 µmol photons	Warming reduces holobiont NPC by 60% and C translocated to host by 15% Symbiodiniaceae Ci uptake increased by 14%, N by 32% and MI by 15%	Warming induces greater energetic demands on the holobiont and favours the assimilation of N	Screen more host-symbiont associations
Achlatis (2018)	Contribution to host and symbiont to holobiont energetics	Unspecified Symbiodiniaceae	*C. orientalis* (sponge)	^{13}C - ^{15}N (6 h) TEM - NanoSIMS	27°C 520 µmol photons	Uptake of Ci by Symbiodiniaceae. Organic nutrients translocated to the sponge.	Photosymbiotic bioeroding sponges have advantage against others sponge species	Study non-autotrophic assimilation of C in sponges
Krueger (2018)	There are different sub-cellular sinks for autotrophic and heterotrophic nutrients in *S. pistillata*	Unspecified Symbiodiniaceae	*S. pistillata*	^{13}C - ^{15}N (6 h) TEM - NanoSIMS	24°C 29°C 350 µmol photons	Phototrophic C is channelled into host lipid bodies Heterotrophic C and N to the host tissue Elevated temperature benefits the symbiont Heterotrophy more energetic than autotrophy	Interplay between hetero- and autotrophy could define the ability of corals to recover from a bleaching event	Look at less thermo-tolerant coral-symbiont assemblages

Authors (et al.)	Hypothesis	Symbiont	Cnidarian / Host	Methods	Conditions Temp. /Light	Results	Outcomes	Future directions
Kenkel and Bay (2018)	Vertically transferred symbionts are more efficient than horizontally transferred	Combined communities of *Cladocopium* spp. (C1-C15-C35) and *Durusdinium* spp. (D1a-D6)	*G. acrhelia* *G. astreata* *A. millepora* *M. aequi-tuberculata* *G. columna* *P. lobata*	^{14}C (5 h) O_2 evolution	27°C 31°C (17d) 130-160 µmol photons	All species exhibited similar decreases in symbiont cell density and net photosynthesis in response to elevated temperature. No difference in C translocated between corals	No difference between types of symbiont transmission.	Need to test uniform communities of symbionts

1.6. Thesis roadmap, aims and objectives

In contrast to our rapidly expanding knowledge of Symbiodiniaceae phylogenetic (genus) diversity, the functional diversity of fitness traits that determine the ecological success of these algal symbionts remain largely unknown (Suggett et al. 2017). The light reactions (LR) of photosynthesis have been extensively studied in Symbiodiniaceae for the past four decades, and indeed exhibit high variability in organisation and function across the Symbiodiniaceae (e.g. Jacques and Pilson 1980; Iglesias-Prieto et al. 2004; Suggett et al. 2015; Ziegler et al. 2019). However, knowledge of the dark reactions (DR) of photosynthesis, and the role of Ci-uptake and utilisation that is essential to photosynthesis and Symbiodiniaceae as a coral symbiont (e.g. Wall et al. 2020), remains comparatively overlooked. The primary goal of this thesis is, therefore, to address this fundamental gap in knowledge; specifically, to resolve the nature and variability of Ci uptake and utilisation capacity amongst Symbiodiniaceae – this will increase our understanding of how Symbiodiniaceae (as a family) has evolved to sustain reef functioning across environmental conditions, including in response to climate change. As such, resolving this fundamental unknown will be the stepping stone to further research on the short, medium and long terms leading to the improvement of worldwide reef health.

The specific aims of the thesis are delivered as a series of chapters as follows:

Chapter 2: Determine functional diversity associated with the extent and fate of Ci assimilation across a phylogenetically broad range of Symbiodiniaceae. In this initial Chapter, I identified whether functional diversity of Ci uptake and utilisation exist and reflect evolutionary position (phylogeny based on the ITS2 gene marker). Building on the evidence of contrasting responses to stress within the same genera of Symbiodiniaceae, I hypothesised that their diversity in Ci uptake and utilisation strategies was independent of genus identity, but not growth environment. As such, an initial core goal was to grow 23 evolutionary diverse

Symbiodiniaceae isolates (spanning six genera) maintained in culture to contrast Ci uptake efficiency under the same steady-state growth conditions. Using radiolabelled sodium bicarbonate, I adopted an approach that discriminated carbon assimilated into the cell (particulate) *vs*. excreted externally (dissolved), the latter of which is termed "photosynthate" and assumed to be the fuel for host corals when Symbiodiniaceae are maintained in symbiosis (Davy et al. 2012). I further investigated the effect of different growth temperatures for three distinct isolates with known different tolerances to heat stress to assess whether environment (growth temperature) was also a potent regulator of Ci uptake strategy.

Chapter 3: Identify the physiological and molecular wiring that underpins Ci assimilation strategies, and whether and how they vary under thermal stress. Chapter 2 revealed that variability in Ci capacity was predominantly driven by variability in growth temperature optima. Therefore, I next examined whether sub-optimum temperatures that drive stress similarly result in changes in Ci capacity, by using a combination of physiological and molecular approaches to also identify the underlying metabolic processes at play. From the results of Chapter 2, I hypothesised that in response to stress, a thermo-sensitive symbiont would present lower rates of Ci uptake, characterised by distinct transcriptomic profiles from a thermo-tolerant isolate. Transcriptomic analysis on selected functional genes (LR and DR, metabolism and stress response) was performed in parallel with physiological assessment of Ci uptake (as per Chapter 2) to identify the underlying metabolic network driving how different Symbiodiniaceae invest into growth (steady state) *vs*. maintenance (subsequent heat stress) conditions.

Chapter 4: Determine plasticity in Ci uptake and allocation for Symbiodiniaceae taxa *in hospite* under different (sub-optimum) growth conditions. This final data chapter extended my findings for Symbiodiniaceae isolates grown *ex hospite* (Chapter 2 and 3) to examine next Ci assimilation performance of natural Symbiodiniaceae-coral associations

originating from highly contrasting environments. I hypothesised that Symbiodiniaceae-coral associations found in environments subjected to multiple stressors (such as mangrove lagoons, with environments analogous to future predicted climate change conditions), would yield lower Ci uptake performances than their stable environment counterparts (reefs), as a trade-off to aid survival under sub-optimum growth conditions. For this, I investigated a model coral-environment system on the GBR (Low Isles) to investigate photochemical performance and Ci uptake using the species *Pocillopora acuta* present in both a mangrove lagoon and an adjacent reef. To compare the efficiency in Ci assimilation of symbionts *ex hospite*, I also freshly isolated *in situ* coral symbionts and compared their proportion of fixed radiolabelled carbon with those living *in hospite*. I further quantified and visualised the cellular translocation rates of photosynthates by the symbionts to their host (using stable isotope-based approaches, including NanoSIMS) to characterise further Symbiodiniaceae-coral interactions.

The knowledge gained through Chapters 2-4 is discussed in Chapter 5 in terms of our current understanding of the core biology underpinning broad thermal susceptibility amongst diverse Symbiodiniaceae when cultured *ex hospite* and living *in hospite* in intact symbiotic associations, and the role of Ci uptake in regulating overall ecological fitness. I finally opened the discussion about how my results can be used by future studies over different timeframes, with a common objective to improve the resilience of coral reefs worldwide.

1.7. References

Achlatis, M., M. Pernice, K. Green, P. Guagliardo, M. R. Kilburn, O. Hoegh-Guldberg and S. Dove. 2018. Single-cell measurement of ammonium and bicarbonate uptake within a photosymbiotic bioeroding sponge. ISME J. **12**: 1308-1318. doi:10.1038/s41396-017-0044-2

Aihara, Y., S. Takahashi and J. Minagawa. 2016. Heat induction of cyclic electron flow around photosystem I in the symbiotic dinoflagellate *Symbiodinium*. Plant Physiol. **171**: 522-529. doi:10.1104/pp.15.01886

Ainsworth, T. D., S. F. Heron, J. C. Ortiz, P. J. Mumby, A. Grech, D. Ogawa, C. M. Eakin and W. Leggat. 2016. Climate change disables coral bleaching protection on the Great Barrier Reef. Science. **352**: 338-342.

Alexander, M. A., J. D. Scott, K. D. Friedland, K. E. Mills, J. A. Nye, A. J. Pershing and A. C. Thomas. 2018. Projected sea surface temperatures over the 21st century: Changes in the mean, variability and extremes for large marine ecosystem regions of Northern Oceans. Elem. Sci. Anth. **6**. doi:10.1525/elementa.191

Anthony, K. and O. Hoegh-Guldberg. 2003. Variation in coral photosynthesis, respiration and growth characteristics in contrasting light microhabitats: an analogue to plants in forest gaps and understoreys? Functional Ecology. **17**: 246-259.

Aranda, M., and others. 2016. Genomes of coral dinoflagellate symbionts highlight evolutionary adaptations conducive to a symbiotic lifestyle. Sci. Rep. **6**: 39734. doi:10.1038/srep39734

Armid, A., R. Shinjo, R. Ruslan and Fahmiati. 2017. Distributions and pollution assessment of heavy metals Pb, Cd and Cr in the water system of Kendari Bay, Indonesia. IOP Conference Series: Materials Science and Engineering. **172**. doi:10.1088/1757-899x/172/1/012002

Azam, F. and A. Z. Worden. 2004. Microbes, molecules, and marine ecosystems. Science. **303**: 1622-1624.

Baillie, B., C. Belda-Baillie, V. Silvestre, M. Sison, A. Gomez, E. Gomez and V. Monje. 2000. Genetic variation in *Symbiodinium* isolates from giant clams based on random-amplified-polymorphic DNA (RAPD) patterns. Marine Biology. **136**: 829-836.

Baker, A. and R. Rowan. 1997. Diversity of symbiotic dinoflagellates (zooxanthellae) in scleractinian corals of the Caribbean and eastern Pacific. Proc. 8th Int. Coral Reef Symp.

Baker, A. C. 2003. Flexibility and specificity in coral-algal symbiosis: Diversity, ecology, and biogeography of *Symbiodinium*. Annual Review of Ecology, Evolution, and Systematics. **34**: 661-689. doi:10.1146/annurev.ecolsys.34.011802.132417

Baker, D. M., J. P. Andras, A. G. Jordan-Garza and M. L. Fogel. 2013. Nitrate competition in a coral symbiosis varies with temperature among *Symbiodinium* clades. ISME J. **7**: 1248-1251. doi:10.1038/ismej.2013.12

Baker, A. C., A. M. Correa and R. Cunning. 2017. Diversity, distribution and stability of *Symbiodinium* in reef corals of the eastern tropical pacific. Coral Reefs of the Eastern Tropical Pacific, Springer: 405-420.

Baker, D. M., C. J. Freeman, J. C. Y. Wong, M. L. Fogel and N. Knowlton. 2018. Climate change promotes parasitism in a coral symbiosis. ISME J. **12**: 921-930. doi:10.1038/s41396-018-0046-8

Barott, K. L., A. A. Venn, S. O. Perez, S. Tambutte and M. Tresguerres. 2015. Coral host cells acidify symbiotic algal microenvironment to promote photosynthesis. Proc. Natl. Acad. Sci. U. S. A. **112**: 607-612. doi:10.1073/pnas.1413483112

Baskin, Y. 1998. Winners and losers in a changing world. BioScience. **48**: 788-792.

Bassham, J. A. and M. Calvin. 1960. The path of carbon in photosynthesis. Die CO_2-Assimilation/The Assimilation of Carbon Dioxide, Springer: 884-922.

Beardall, J. and J. A. Raven. 2016. Carbon acquisition by microalgae. The physiology of microalgae, Springer: 89-99.

Ben-Haim, Y., M. Zicherman-Keren and E. Rosenberg. 2003. Temperature-regulated bleaching and lysis of the coral *Pocillopora damicornis* by the novel pathogen *Vibrio coralliilyticus*. Appl. Environ. Microbiol. **69**: 4236-4242. doi:10.1128/aem.69.7.4236-4242.2003

Benham, C. F. 2017. Understanding local community attitudes toward industrial development in the Great Barrier Reef region World Heritage Area: are environmental impacts perceived to overshadow economic benefits? Natural Resources Forum. **41**: 42-54. doi:10.1111/1477-8947.12112

Bertucci, A., E. Tambutte, S. Tambutte, D. Allemand and D. Zoccola. 2009. Symbiosis-dependent gene expression in coral-dinoflagellate association: cloning and characterization of a P-type H^+-ATPase gene. Proc. Biol. Sci. **277**: 87-95. doi:10.1098/rspb.2009.1266

Bessell-Browne, P., A. P. Negri, R. Fisher, P. L. Clode, A. Duckworth and R. Jones. 2017. Impacts of turbidity on corals: The relative importance of light limitation and suspended sediments. Mar. Pollut. Bull. **117**: 161-170. doi:10.1016/j.marpolbul.2017.01.050

Biquand, E., and others. 2017. Acceptable symbiont cell size differs among cnidarian species and may limit symbiont diversity. ISME J. **11**: 1702-1712. doi:10.1038/ismej.2017.17

Birkeland, C. 1997. Life and death of coral reefs, Springer Science & Business Media.

Blackall, L. L., B. Wilson and M. J. van Oppen. 2015. Coral—the world's most diverse symbiotic ecosystem. Molecular Ecology. **24**: 5330-5347.

Bourne, D. G., M. Garren, T. M. Work, E. Rosenberg, G. W. Smith and C. D. Harvell. 2009. Microbial disease and the coral holobiont. Trends Microbiol. **17**: 554-562. doi:10.1016/j.tim.2009.09.004

Brading, P., M. E. Warner, P. Davey, D. J. Smith, E. P. Achterberg and D. J. Suggett. 2011. Differential effects of ocean acidification on growth and photosynthesis among

phylotypes of *Symbiodinium* (Dinophyceae). Limnology and Oceanography. **56**: 927-938. doi:10.4319/lo.2011.56.3.0927

Brading, P., M. E. Warner, D. J. Smith and D. J. Suggett. 2013. Contrasting modes of inorganic carbon acquisition amongst *Symbiodinium* (Dinophyceae) phylotypes. New Phytol. **200**: 432-442. doi:10.1111/nph.12379

Bruno, J. F., E. R. Selig, K. S. Casey, C. A. Page, B. L. Willis, C. D. Harvell, H. Sweatman and A. M. Melendy. 2007. Thermal stress and coral cover as drivers of coral disease outbreaks. PLoS Biol. **5**: e124. doi:10.1371/journal.pbio.0050124

Camp, E. F., V. Schoepf and D. J. Suggett. 2018. How can "Super Corals" facilitate global coral reef survival under rapid environmental and climatic change? Glob. Chang. Biol. **24**: 2755-2757. doi:10.1111/gcb.14153

Camp, E. F., J. Edmondson, A. Doheny, J. Rumney, A. J. Grima, A. Huete and D. J. Suggett. 2019. Mangrove lagoons of the Great Barrier Reef support coral populations persisting under extreme environmental conditions. Marine Ecology Progress Series. **625**: 1-14. doi:10.3354/meps13073

Cardol, P., G. Forti and G. Finazzi. 2011. Regulation of electron transport in microalgae. Biochim. Biophys. Acta. **1807**: 912-918. doi:10.1016/j.bbabio.2010.12.004

Church, M. J., K. M. Björkman, D. M. Karl, M. A. Saito and J. P. Zehr. 2008. Regional distributions of nitrogen-fixing bacteria in the Pacific Ocean. Limnology and Oceanography. **53**: 63-77.

Clode, P. L., R. A. Stern and A. T. Marshall. 2007. Subcellular imaging of isotopically labelled carbon compounds in a biological sample by ion microprobe (NanoSIMS). Microsc. Res. Tech. **70**: 220-229. doi:10.1002/jemt.20409

Cooper, T. F., M. Lai, K. E. Ulstrup, S. M. Saunders, G. R. Flematti, B. Radford and M. J. van Oppen. 2011. *Symbiodinium* genotypic and environmental controls on lipids in reef building corals. PLoS One. **6**: e20434. doi:10.1371/journal.pone.0020434

Crawley, A., D. I. Kline, S. Dunn, K. E. N. Anthony and S. Dove. 2010. The effect of ocean acidification on symbiont photorespiration and productivity in *Acropora formosa*. Global Change Biology. **16**: 851-863. doi:10.1111/j.1365-2486.2009.01943.x

Crossland, C. J., B. G. Hatcher and S. V. Smith. 1991. Role of coral reefs in global ocean production. Coral Reefs. **10**: 55-64. doi:10.1007/bf00571824

Darling, E. S. and S. D'Agata. 2017. Coral Reefs: Fishing for sustainability. Curr. Biol. **27**: R65-R68. doi:10.1016/j.cub.2016.12.005

Darling, E. S., N. A. J. Graham, F. A. Januchowski-Hartley, K. L. Nash, M. S. Pratchett and S. K. Wilson. 2017. Relationships between structural complexity, coral traits, and reef fish assemblages. Coral Reefs. **36**: 561-575. doi:10.1007/s00338-017-1539-z

Davy, S. K., D. Allemand and V. M. Weis. 2012. Cell biology of cnidarian-dinoflagellate symbiosis. Microbiol. Mol. Biol. Rev. **76**: 229-261. doi:10.1128/MMBR.05014-11

De Klein, C., C. Pinares-Patino and G. Waghorn. 2008. Greenhouse gas emissions. Environmental impacts of pasture-based grazing. (Ed. RW McDowell) pp: 1-32.

De'ath, G., K. E. Fabricius, H. Sweatman and M. Puotinen. 2012. The 27-year decline of coral cover on the Great Barrier Reef and its causes. Proc. Natl. Acad. Sci. U. S. A. **109**: 17995-17999. doi:10.1073/pnas.1208909109

del C. Gómez-Cabrera, M., J. C. Ortiz, W. K. W. Loh, S. Ward and O. Hoegh-Guldberg. 2007. Acquisition of symbiotic dinoflagellates (*Symbiodinium*) by juveniles of the coral *Acropora longicyathus*. Coral Reefs. **27**: 219-226. doi:10.1007/s00338-007-0315-x

Deloitte Access Economics. 2017. At what price? The economic, social and icon value of the Great Barrier Reef, Deloitte Access Economics.

Deschaseaux, E. S. M., V. H. Beltran, G. B. Jones, M. A. Deseo, H. B. Swan, P. L. Harrison and B. D. Eyre. 2014. Comparative response of DMS and DMSP concentrations in *Symbiodinium* clades C1 and D1 under thermal stress. Journal of Experimental Marine Biology and Ecology. **459**: 181-189. doi:10.1016/j.jembe.2014.05.018

Descolas-Gros, C. and M. Fontugne. 1985. Carbon fixation in marine phytoplankton: carboxylase activities and stable carbon-isotope ratios; physiological and paleoclimatological aspects. Marine Biology. **87**: 1-6.

Dhingra, A., A. R. Portis and H. Daniell. 2004. Enhanced translation of a chloroplast-expressed RbcS gene restores small subunit levels and photosynthesis in nuclear RbcS antisense plants. Proceedings of the National Academy of Sciences. **101**: 6315-6320.

Diaz, R. J. and R. Rosenberg. 2008. Spreading dead zones and consequences for marine ecosystems. Science. **321**: 926-929. doi:10.1126/science.1156401

Diaz, J. M., C. M. Hansel, A. Apprill, C. Brighi, T. Zhang, L. Weber, S. McNally and L. Xun. 2016. Species-specific control of external superoxide levels by the coral holobiont during a natural bleaching event. Nat. Commun. **7**: 13801. doi:10.1038/ncomms13801

Diaz-Almeyda, E. M., and others. 2017. Intraspecific and interspecific variation in thermotolerance and photoacclimation in *Symbiodinium* dinoflagellates. Proc. R. Soc. B. **284**: 20171767. doi:10.1098/rspb.2017.1767

D'Olivo, J. P., G. Ellwood, T. M. DeCarlo and M. T. McCulloch. 2019. Deconvolving the long-term impacts of ocean acidification and warming on coral biomineralisation. Earth and Planetary Science Letters. **526**. doi:10.1016/j.epsl.2019.115785

Downs, C., J. E. Fauth, J. C. Halas, P. Dustan, J. Bemiss and C. M. Woodley. 2002. Oxidative stress and seasonal coral bleaching. Free Radical Biology and Medicine. **33**: 533-543.

Eakin, C. M., H. P. A. Sweatman and R. E. Brainard. 2019. The 2014–2017 global-scale coral bleaching event: insights and impacts. Coral Reefs. **38**: 539-545. doi:10.1007/s00338-019-01844-2

Elliff, C. I. and R. K. P. Kikuchi. 2017. Ecosystem services provided by coral reefs in a Southwestern Atlantic Archipelago. Ocean & Coastal Management. **136**: 49-55. doi:10.1016/j.ocecoaman.2016.11.021

Elliff, C. I. and I. R. Silva. 2017. Coral reefs as the first line of defense: Shoreline protection in face of climate change. Mar Environ Res. **127**: 148-154. doi:10.1016/j.marenvres.2017.03.007

Erez, J. 1990. On the importance of food sources in coral-reef ecosystems. Ecosystems of the world. **25**: 411-418.

Fabricius, K. E. 2005. Effects of terrestrial runoff on the ecology of corals and coral reefs: review and synthesis. Mar. Pollut. Bull. **50**: 125-146. doi:10.1016/j.marpolbul.2004.11.028

Falkowski, P. G., Z. Dubinsky, L. Muscatine and J. W. Porter. 1984. Light and the bioenergetics of a symbiotic coral. Bioscience. **34**: 705-709.

Falkowski, P. G. and J. LaRoche. 1991. Acclimation to spectral irradiance in algae. Journal of Phycology. **27**: 8-14.

Field, C. B., M. J. Behrenfeld, J. T. Randerson and P. Falkowski. 1998. Primary production of the biosphere: integrating terrestrial and oceanic components. Science. **281**: 237-240.

Finkel, Z. V., J. Beardall, K. J. Flynn, A. Quigg, T. A. V. Rees and J. A. Raven. 2010. Phytoplankton in a changing world: cell size and elemental stoichiometry. Journal of Plankton Research. **32**: 119-137. doi:10.1093/plankt/fbp098

Fournier, A. 2013. The story of symbiosis with zooxanthellae, or how they enable their host to thrive in a nutrient poor environment. Biosci. Master Rev: 1-8.

Fox, M. D., and others. 2018. Gradients in primary production predict trophic strategies of mixotrophic corals across spatial scales. Curr. Biol. **28**: 3355-3363 e3354. doi:10.1016/j.cub.2018.08.057

Frade, P., P. Bongaerts, A. Winkelhagen, L. Tonk and R. Bak. 2008. In situ photobiology of corals over large depth ranges: a multivariate analysis on the roles of environment, host, and algal symbiont. Limnology and Oceanography. **53**: 2711-2723.

Fransolet, D., S. Roberty and J.-C. Plumier. 2012. Establishment of endosymbiosis: The case of cnidarians and *Symbiodinium*. Journal of Experimental Marine Biology and Ecology. **420-421**: 1-7. doi:10.1016/j.jembe.2012.03.015

Fraser, K. A., V. M. Adams, R. L. Pressey and J. M. Pandolfi. 2017. Purpose, policy, and practice: Intent and reality for on-ground management and outcomes of the Great Barrier Reef Marine Park. Marine Policy. **81**: 301-311. doi:10.1016/j.marpol.2017.03.039

Freeman, C. J., E. W. Stoner, C. G. Easson, K. O. Matterson and D. M. Baker. 2016. Symbiont carbon and nitrogen assimilation in the *Cassiopea–Symbiodinium* mutualism. Marine Ecology Progress Series. **544**: 281-286. doi:10.3354/meps11605

Gattuso, J.-P., D. Allemand and M. Frankignoulle. 1999. Photosynthesis and calcification at cellular, organismal and community levels in coral reefs: a review on interactions and control by carbonate chemistry. American Zoologist. **39**: 160-183. doi:10.1093/icb/39.1.160

Genty, B., J.-M. Briantais and N. R. Baker. 1989. The relationship between the quantum yield of photosynthetic electron transport and quenching of chlorophyll fluorescence. Biochimica et Biophysica Acta (BBA)-General Subjects. **990**: 87-92.

Gibbin, E. M., H. M. Putnam, R. D. Gates, M. R. Nitschke and S. K. Davy. 2015. Species-specific differences in thermal tolerance may define susceptibility to intracellular acidosis in reef corals. Marine Biology. **162**: 717-723. doi:10.1007/s00227-015-2617-9

Gierz, S. L., S. Foret and W. Leggat. 2017. Transcriptomic analysis of thermally stressed *Symbiodinium* reveals differential expression of stress and metabolism genes. Front. Plant. Sci. **8**: 271. doi:10.3389/fpls.2017.00271

Giordano, M., J. Beardall and J. A. Raven. 2005. CO_2 concentrating mechanisms in algae: mechanisms, environmental modulation, and evolution. Annu. Rev. Plant. Biol. **56**: 99-131. doi:10.1146/annurev.arplant.56.032604.144052

Goiran, C., S. Al-Moghrabi, D. Allemand and J. Jaubert. 1996. Inorganic carbon uptake for photosynthesis by the symbiotic coral/dinoflagellate association. I. Photosynthetic performances of symbionts and dependence on sea water bicarbonate. Journal of Experimental Marine Biology and Ecology. **199**: 207-225. doi:10.1016/0022-0981(95)00201-4

González-Pech, R. A., and others. 2019. Genomes of Symbiodiniaceae reveal extensive sequence divergence but conserved functions at family and genus levels. bioRxiv: 800482.

Gorbunov, M. Y., Z. S. Kolber, M. P. Lesser and P. G. Falkowski. 2001. Photosynthesis and photoprotection in symbiotic corals. Limnology and Oceanography. **46**: 75-85.

Goulet, T. and M. Coffroth. 2003. Genetic composition of zooxanthellae between and within colonies of the octocoral *Plexaura kuna*, based on small subunit rDNA and multilocus DNA fingerprinting. Marine Biology. **142**: 233-239. doi:10.1007/s00227-002-0936-0

Goulet, T. L. 2006. Most corals may not change their symbionts. Marine Ecology Progress Series, **321**, 1-7. doi:10.3354/meps321001

Goyen, S., M. Pernice, M. Szabó, M. E. Warner, P. J. Ralph and D. J. Suggett. 2017. A molecular physiology basis for functional diversity of hydrogen peroxide production amongst *Symbiodinium* spp. (Dinophyceae). Marine Biology. **164**. doi:10.1007/s00227-017-3073-5

G. B. R. M. P. A. 1981. Nomination of the Great Barrier Reef by the Commonwealth of Australia for inclusion in the World Heritage List: United Nations Educational Scientific and Cultural Organization, Great Barrier Reef Marine Park Authority.

Grottoli, A. G., L. J. Rodrigues and J. E. Palardy. 2006. Heterotrophic plasticity and resilience in bleached corals. Nature. **440**: 1186-1189. doi:10.1038/nature04565

Grottoli, A. G., M. E. Warner, S. J. Levas, M. D. Aschaffenburg, V. Schoepf, M. McGinley, J. Baumann and Y. Matsui. 2014. The cumulative impact of annual coral bleaching can turn some coral species winners into losers. Glob. Chang. Biol. **20**: 3823-3833. doi:10.1111/gcb.12658

Guest, J. R., and others. 2012. Contrasting patterns of coral bleaching susceptibility in 2010 suggest an adaptive response to thermal stress. PLoS One. **7**: e33353. doi:10.1371/journal.pone.0033353

Haas, A. F., and others. 2016. Global microbialization of coral reefs. Nat. Microbiol. **1**: 16042. doi:10.1038/nmicrobiol.2016.42

Hald, S., M. Pribil, D. Leister, P. Gallois and G. N. Johnson. 2008. Competition between linear and cyclic electron flow in plants deficient in Photosystem I. Biochim. Biophys. Acta. **1777**: 1173-1183. doi:10.1016/j.bbabio.2008.04.041

Halsey, K. H., R. T. O'Malley, J. R. Graff, A. J. Milligan and M. J. Behrenfeld. 2013. A common partitioning strategy for photosynthetic products in evolutionarily distinct phytoplankton species. New Phytol. **198**: 1030-1038. doi:10.1111/nph.12209

Halsey, K. H. and B. M. Jones. 2015. Phytoplankton strategies for photosynthetic energy allocation. Ann. Rev. Mar. Sci. **7**: 265-297. doi:10.1146/annurev-marine-010814-015813

Hamilton, R. J., G. R. Almany, C. J. Brown, J. Pita, N. A. Peterson and J. Howard Choat. 2017. Logging degrades nursery habitat for an iconic coral reef fish. Biological Conservation. **210**: 273-280. doi:10.1016/j.biocon.2017.04.024

Hansson, L., K. Isensee, D. Herr, D. Osborn and S. Dupont. 2019. Impacts of climate change and ocean acidification on marine biodiversity. Background briefs for 2020, Ocean Pathways Week. **13**: 32.

Harborne, A. R., A. Rogers, Y. M. Bozec and P. J. Mumby. 2017. Multiple Stressors and the Functioning of Coral Reefs. Ann. Rev. Mar. Sci. **9**: 445-468. doi:10.1146/annurev-marine-010816-060551

Hennige, S. J., D. J. Smith, R. Perkins, M. Consalvey, D. M. Paterson and D. J. Suggett. 2008. Photoacclimation, growth and distribution of massive coral species in clear and turbid waters. Marine Ecology Progress Series. **369**: 77-88. doi:10.3354/meps07612

Hennige, S. J., D. J. Suggett, M. E. Warner, K. E. McDougall and D. J. Smith. 2009. Photobiology of *Symbiodinium* revisited: bio-physical and bio-optical signatures. Coral Reefs. **28**: 179-195. doi:10.1007/s00338-008-0444-x

Hennige, S. J., M. P. McGinley, A. G. Grottoli and M. E. Warner. 2011. Photoinhibition of *Symbiodinium* spp. within the reef corals *Montastraea faveolata* and *Porites astreoides*: implications for coral bleaching. Marine Biology. **158**: 2515-2526. doi:10.1007/s00227-011-1752-1

Hill, R. and P. J. Ralph. 2008. Dark-induced reduction of the plastoquinone pool in zooxanthellae of scleractinian corals and implications for measurements of chlorophyll a fluorescence. Symbiosis-Rehovot. **46**: 45.

Hill, R., C. M. Brown, K. DeZeeuw, D. A. Campbell and P. J. Ralph. 2011. Increased rate of D1 repair in coral symbionts during bleaching is insufficient to counter accelerated photo-inactivation. Limnology and Oceanography. **56**: 139-146. doi:10.4319/lo.2011.56.1.0139

Hoegh-Guldberg, O. 1999. Climate change, coral bleaching and the future of the world's coral reefs. Marine and freshwater research. **50**: 839-866.

Hoegh-Guldberg, O., and others. 2007. Coral reefs under rapid climate change and ocean acidification. Science. **318**: 1737-1742. doi:10.1126/science.1152509

Hoegh-Guldberg, O., and others. 2018. Impacts of 1.5 ºC global warming on natural and human systems. Global Warming of 1.5° C: An IPCC Special Report on the impacts of global warming of 1.5° C above pre-industrial levels and related global greenhouse gas emission pathways, in the context of strengthening the global response to the threat of climate change, sustainable development, and efforts to eradicate poverty, IPCC.

Houlbreque, F. and C. Ferrier-Pages. 2009. Heterotrophy in tropical scleractinian corals. Biol. Rev. Camb. Philos. Soc. **84**: 1-17. doi:10.1111/j.1469-185X.2008.00058.x

Howells, E. J., V. H. Beltran, N. W. Larsen, L. K. Bay, B. L. Willis and M. J. H. van Oppen. 2011. Coral thermal tolerance shaped by local adaptation of photosymbionts. Nature Climate Change. **2**: 116-120. doi:10.1038/nclimate1330

Hughes, D. J., and others. 2018. Roadmaps and detours: active chlorophyll- a assessments of primary productivity across marine and freshwater Systems. Environ. Sci. Technol. doi:10.1021/acs.est.8b03488

Hughes, T. P., J. C. Day and J. Brodie. 2015. Securing the future of the Great Barrier Reef. Nature Climate Change. **5**: 508-511. doi:10.1038/nclimate2604

Hughes, T. P., and others. 2017. Global warming and recurrent mass bleaching of corals. Nature. **543**: 373-377. doi:10.1038/nature21707

Hughes, T. P., and others. 2018. Spatial and temporal patterns of mass bleaching of corals in the Anthropocene. Science. **359**: 80-83. doi:10.1126/science.aan8048

Hughes, T. P., and others. 2019. Ecological memory modifies the cumulative impact of recurrent climate extremes. Nature Climate Change. **9**: 40-43. doi:10.1038/s41558-018-0351-2

Hume, B. C., D'Angelo, C., Smith, E. G., Stevens, J. R., Burt, J. and J. Wiedenmann. 2015. *Symbiodinium thermophilum* sp. nov., a thermotolerant symbiotic alga prevalent in corals of the world's hottest sea, the Persian/Arabian Gulf. Scientific reports, **5**: 1-8. doi: 10.1038/srep08562

Iglesias-Prieto, R. and R. K. Trench. 1994. Acclimation and adaptation to irradiance in symbiotic dinoflagellates. I. Responses of the photosynthetic unit to changes in photon flux density. Marine Ecology Progress Series. **113**: 163-175.

Iglesias-Prieto, R., V. H. Beltran, T. C. LaJeunesse, H. Reyes-Bonilla and P. E. Thome. 2004. Different algal symbionts explain the vertical distribution of dominant reef corals in the eastern Pacific. Proc. Biol. Sci. **271**: 1757-1763. doi:10.1098/rspb.2004.2757

Jacques, T. and M. Pilson. 1980. Experimental ecology of the temperate scleractinian coral *Astrangia danae*. I. Partition of respiration, photosynthesis and calcification between host and symbionts. Marine Biology. **60**: 167-178.

Januar, H. I., N. P. Zamani, D. Soedharma and E. Chasanah. 2017. New cytotoxic cembranoid from Indonesian soft coral *Sarcophyton* sp. Pharmacognosy Research. **9**: 65.

Jeong, H. J., and others. 2012. Heterotrophic feeding as a newly identified survival strategy of the dinoflagellate *Symbiodinium*. Proc. Natl. Acad. Sci. U. S. A. **109**: 12604-12609. doi:10.1073/pnas.1204302109

Jeong, H. J., and others. 2014. Genetics and morphology characterize the dinoflagellate *Symbiodinium voratum*, n. sp., (Dinophyceae) as the sole representative of *Symbiodinium* Clade E. J. Eukaryot. Microbiol. **61**: 75-94. doi:10.1111/jeu.12088

Jones, R. J., O. Hoegh-Guldberg, A. W. D. Larkum and U. Schreiber. 1998. Temperature-induced bleaching of corals begins with impairment of the CO_2 fixation mechanism in zooxanthellae. Plant, Cell and Environment. **21**: 1219-1230. doi:10.1046/j.1365-3040.1998.00345.x

Jones, A. M., R. Berkelmans, M. J. van Oppen, J. C. Mieog and W. Sinclair. 2008. A community change in the algal endosymbionts of a scleractinian coral following a natural bleaching event: field evidence of acclimatization. Proc. Biol. Sci. **275**: 1359-1365. doi:10.1098/rspb.2008.0069

Jones, A. M. and R. Berkelmans. 2011. Tradeoffs to thermal acclimation: energetics and reproduction of a reef coral with heat tolerant *Symbiodinium* type D. Journal of Marine Biology. **2011**: 1-12. doi:10.1155/2011/185890

Jurriaans, S. and M. O. Hoogenboom. 2019. Thermal performance of scleractinian corals along a latitudinal gradient on the Great Barrier Reef. Philos. Trans. R. Soc. Lond. B. Biol. Sci. **374**: 20180546. doi:10.1098/rstb.2018.0546

Kanazawa, A., G. J. Blanchard, M. Szabo, P. J. Ralph and D. M. Kramer. 2014. The site of regulation of light capture in *Symbiodinium*: does the peridinin-chlorophyll a-protein detach to regulate light capture? Biochim. Biophys. Acta. **1837**: 1227-1234. doi:10.1016/j.bbabio.2014.03.019

Karako-Lampert, S., D. J. Katcoff, Y. Achituv, Z. Dubinsky and N. Stambler. 2004. Do clades of symbiotic dinoflagellates in scleractinian corals of the Gulf of Eilat (Red Sea) differ from those of other coral reefs? Journal of Experimental Marine Biology and Ecology. **311**: 301-314. doi:10.1016/j.jembe.2004.05.015

Kawaguti, S. 1937. On the physiology of reef corals. I. On the oxygen exchanges of reef corals. Palao. Trop. Biol. Stn. Stud. **1**: 187-198.

Kenkel, C. D. and L. K. Bay. 2018. Exploring mechanisms that affect coral cooperation: symbiont transmission mode, cell density and community composition. PeerJ. **6**: e6047. doi:10.7717/peerj.6047

Kopp, C., and others. 2013. Highly dynamic cellular-level response of symbiotic coral to a sudden increase in environmental nitrogen. mBio. **4**: e00052-00013. doi:10.1128/mBio.00052-13

Kopp, C., I. Domart-Coulon, S. Escrig, B. M. Humbel, M. Hignette and A. Meibom. 2015. Subcellular investigation of photosynthesis-driven carbon assimilation in the symbiotic reef coral *Pocillopora damicornis*. mBio. **6**. doi:10.1128/mBio.02299-14

Kramer, W. E., I. Caamano-Ricken, C. Richter and K. Bischof. 2012. Dynamic regulation of photoprotection determines thermal tolerance of two phylotypes of *Symbiodinium* clade A at two photon fluence rates. Photochem. Photobiol. **88**: 398-413. doi:10.1111/j.1751-1097.2011.01048.x

Krueger, T., N. Horwitz, J. Bodin, M. E. Giovani, S. Escrig, A. Meibom and M. Fine. 2017. Common reef-building coral in the Northern Red Sea resistant to elevated temperature and acidification. R. Soc. Open. Sci. **4**: 170038. doi:10.1098/rsos.170038

Krueger, T., J. Bodin, N. Horwitz, C. Loussert-Fonta, A. Sakr, S. Escrig, M. Fine and A. Meibom. 2018. Temperature and feeding induce tissue level changes in autotrophic and heterotrophic nutrient allocation in the coral symbiosis - A NanoSIMS study. Sci. Rep. **8**: 12710. doi:10.1038/s41598-018-31094-1

LaJeunesse, T. C. 2001. Investigating the biodiversity, ecology, and phylogeny of endosymbiotic dinoflagellates in the genus *Symbiodinium* using the ITS region: in search of a "species" level marker. Journal of Phycology. **37**: 866-880.

LaJeunesse, T. C., R. Bhagooli, M. Hidaka, L. DeVantier, T. Done, G. Schmidt, W. Fitt and O. Hoegh-Guldberg. 2004. Closely related *Symbiodinium* spp. differ in relative dominance in coral reef host communities across environmental, latitudinal and biogeographic gradients. Marine Ecology Progress Series. **284**: 147-161.

LaJeunesse, T. C., D. T. Pettay, E. M. Sampayo, N. Phongsuwan, B. Brown, D. O. Obura, O. Hoegh-Guldberg and W. K. Fitt. 2010. Long-standing environmental conditions, geographic isolation and host-symbiont specificity influence the relative ecological dominance and genetic diversification of coral endosymbionts in the genus *Symbiodinium*. Journal of Biogeography. **37**: 785-800. doi:10.1111/j.1365-2699.2010.02273.x

LaJeunesse, T. C., J. E. Parkinson and J. D. Reimer. 2012. A genetics-based description of *Symbiodinium minutum* sp. nov. and *S. psygmophilum* sp. nov. (Dinophyceae), two dinoflagellates symbiotic with Cnidaria. J Phycol. **48**: 1380-1391. doi:10.1111/j.1529-8817.2012.01217.x

LaJeunesse, T. C., J. E. Parkinson, P. W. Gabrielson, H. J. Jeong, J. D. Reimer, C. R. Voolstra and S. R. Santos. 2018. Systematic revision of Symbiodiniaceae highlights the antiquity and diversity of coral endosymbionts. Curr. Biol. **28**: 2570-2580 e2576. doi:10.1016/j.cub.2018.07.008

Larkum, A. W. 2016. Photosynthesis and light harvesting in algae. The Physiology of Microalgae, Springer: 67-87.

Lawson, C. A., J. B. Raina, T. Kahlke, J. R. Seymour and D. J. Suggett. 2018. Defining the core microbiome of the symbiotic dinoflagellate, *Symbiodinium*. Environ. Microbiol. Rep. **10**: 7-11. doi:10.1111/1758-2229.12599

Lawson, C. A., M. Possell, J. R. Seymour, J. B. Raina and D. J. Suggett. 2019. Coral endosymbionts (Symbiodiniaceae) emit species-specific volatilomes that shift when exposed to thermal stress. Sci. Rep. **9**: 17395. doi:10.1038/s41598-019-53552-0

Leal, M. C., K. Hoadley, D. T. Pettay, A. Grajales, R. Calado and M. E. Warner. 2015. Symbiont type influences trophic plasticity of a model cnidarian-dinoflagellate symbiosis. J. Exp. Biol. **218**: 858-863. doi:10.1242/jeb.115519

Leggat, W., M. R. Badger and D. Yellowlees. 1999. Evidence for an inorganic carbon-concentrating mechanism in the symbiotic dinoflagellate *Symbiodinium* sp. Plant Physiol. **121**: 1247-1256. doi:10.1104/pp.121.4.1247

Leggat, W., F. Seneca, K. Wasmund, L. Ukani, D. Yellowlees and T. D. Ainsworth. 2011. Differential responses of the coral host and their algal symbiont to thermal stress. PLoS One. **6**: e26687. doi:10.1371/journal.pone.0026687

Leggat, W. P., and others. 2019. Rapid coral decay is associated with marine heatwave mortality events on reefs. Curr. Biol. **29**: 2723-2730 e2724. doi:10.1016/j.cub.2019.06.077

LeKieffre, C., H. J. Spero, A. D. Russell, J. S. Fehrenbacher, E. Geslin and A. Meibom. 2018. Assimilation, translocation, and utilization of carbon between photosynthetic symbiotic dinoflagellates and their planktonic foraminifera host. Marine Biology. **165**. doi:10.1007/s00227-018-3362-7

Lesser, M. P. and J. H. Farrell. 2004. Exposure to solar radiation increases damage to both host tissues and algal symbionts of corals during thermal stress. Coral Reefs. **23**: 367-377. doi:10.1007/s00338-004-0392-z

Lesser, M. P. 2019. Phylogenetic signature of light and thermal stress for the endosymbiotic dinoflagellates of corals (Family Symbiodiniaceae). Limnology and Oceanography. **64**: 1852-1863. doi:10.1002/lno.11155

Levin, R. A., V. H. Beltran, R. Hill, S. Kjelleberg, D. McDougald, P. D. Steinberg and M. J. van Oppen. 2016. Sex, scavengers, and chaperones: transcriptome secrets of divergent *Symbiodinium* thermal tolerances. Mol. Biol. Evol. **33**: 2201-2215. doi:10.1093/molbev/msw119

Lilley, R. M., P. J. Ralph and A. W. Larkum. 2010. The determination of activity of the enzyme Rubisco in cell extracts of the dinoflagellate alga *Symbiodinium* sp. by manganese chemiluminescence and its response to short-term thermal stress of the alga. Plant Cell Environ. **33**: 995-1004. doi:10.1111/j.1365-3040.2010.02121.x

Lin, S., and others. 2015. The *Symbiodinium kawagutii* genome illuminates dinoflagellate gene expression and coral symbiosis. Science. **350**: 691-694.

Liu, H., and others. 2018. *Symbiodinium* genomes reveal adaptive evolution of functions related to coral-dinoflagellate symbiosis. Commun. Biol. **1**: 95. doi:10.1038/s42003-018-0098-3

Logan, D. D. K., A. C. LaFlamme, V. M. Weis and S. K. Davy. 2010. Flow-cytometric characterization of the cell-surface glycans of symbiotic dinoflagellates (*Symbiodinium* spp.). Journal of Phycology. **46**: 525-533. doi:10.1111/j.1529-8817.2010.00819.x

MacIntyre, H. L., T. M. Kana, T. Anning and R. J. Geider. 2002. Photoacclimation of photosynthesis irradiance response curves and photosynthetic pigments in microalgae and cyanobacteria. Journal of Phycology. **38**: 17-38. doi:10.1046/j.1529-8817.2002.00094.x

Madoz, J., J. Fernández-Recio, C. Gómez-Moreno and V. M. Fernández. 1998. Investigation of the diaphorase reaction of ferredoxin-$NADP^+$ reductase by electrochemical methods. Bioelectrochemistry and bioenergetics. **47**: 179-183.

Martin, T. S. H., R. M. Connolly, A. D. Olds, D. M. Ceccarelli, D. E. Fenner, T. A. Schlacher, M. Beger and M. Kaiser. 2017. Subsistence harvesting by a small community does not

substantially compromise coral reef fish assemblages. ICES Journal of Marine Science. **74**: 2191-2200. doi:10.1093/icesjms/fsx043

Matthews, J. L., and others. 2017. Optimal nutrient exchange and immune responses operate in partner specificity in the cnidarian-dinoflagellate symbiosis. Proceedings of the National Academy of Sciences. **114**: 13194-13199. doi:10.1073/pnas.1710733114

Matthews, J. L., C. A. Oakley, A. Lutz, K. E. Hillyer, U. Roessner, A. R. Grossman, V. M. Weis and S. K. Davy. 2018. Partner switching and metabolic flux in a model cnidarian-dinoflagellate symbiosis. Proc. Biol. Sci. **285**. doi:10.1098/rspb.2018.2336

Matthews, J. L., J. B. Raina, T. Kahlke, J. R. Seymour, M. J. H. van Oppen and D. J. Suggett. 2020. Symbiodiniaceae-bacteria interactions: rethinking metabolite exchange in reef-building corals as multi-partner metabolic networks. Environ. Microbiol. doi:10.1111/1462-2920.14918

McCall, C. 2017. Australia's new coal mine plan: a “public health disaster”. The Lancet 389. doi:10.1016/s0140-6736(17)30329-x

McGinty, E. S., J. Pieczonka and L. D. Mydlarz. 2012. Variations in reactive oxygen release and antioxidant activity in multiple *Symbiodinium* types in response to elevated temperature. Microb. Ecol. **64**: 1000-1007. doi:10.1007/s00248-012-0085-z

Mieog, J. C., J. L. Olsen, R. Berkelmans, S. A. Bleuler-Martinez, B. L. Willis and M. J. van Oppen. 2009. The roles and interactions of symbiont, host and environment in defining coral fitness. PLoS One. **4**: e6364. doi:10.1371/journal.pone.0006364

Moore, R., D. Clark, K. R. Stern and D. Vodopich. 1995. Botany. Dubuque: Wm. C, Brown Publishers.

Morris, L. A., C. R. Voolstra, K. M. Quigley, D. G. Bourne and L. K. Bay. 2019. Nutrient availability and metabolism affect the stability of coral-Symbiodiniaceae symbioses. Trends Microbiol. **27**: 678-689. doi:10.1016/j.tim.2019.03.004

Muir, P. R., C. C. Wallace, T. Done and J. D. Aguirre. 2015. Coral reefs. Limited scope for latitudinal extension of reef corals. Science. **348**: 1135-1138. doi:10.1126/science.1259911

Muller-Parker, G. 1984. Photosynthesis-irradiance responses and photosynthetic periodicity in the sea anemone *Aiptasia pulchella* and its zooxanthellae. Marine Biology. **82**: 225-232.

Muscatine, L. and C. Hand. 1958. Direct evidence for the transfer of materials from symbiotic algae to the tissues of a coelenterate. Proceedings of the National Academy of Sciences of the United States of America. **44**: 1259.

Muscatine, L. 1990. The role of symbiotic algae in carbon and energy flux in reef corals. Coral reefs. **25**: 1-29.

Mwaura, J., Y. Umezawa, T. Nakamura and J. Kamau. 2017. Evidence of chronic anthropogenic nutrient within coastal lagoon reefs adjacent to urban and tourism centers, Kenya: A stable isotope approach. Mar. Pollut. Bull. **119**: 74-86. doi:10.1016/j.marpolbul.2017.04.028

Nitschke, M. R., S. K. Davy and S. Ward. 2015. Horizontal transmission of *Symbiodinium* cells between adult and juvenile corals is aided by benthic sediment. Coral Reefs. **35**: 335-344. doi:10.1007/s00338-015-1349-0

Nitschke, M. R., S. G. Gardner, S. Goyen, L. Fujise, E. F. Camp, P. J. Ralph and D. J. Suggett. 2018. Utility of photochemical traits as diagnostics of thermal tolerance amongst Great Barrier Reef corals. Frontiers in Marine Science. **5**. doi:10.3389/fmars.2018.00045

Nitschke, M. R., Craveiro, S. C., Brandão, C., Fidalgo, C., Serôdio, J., Calado, A. J. and J. C. Frommlet. 2020. Description of *Freudenthalidium* gen. nov. and *Halluxium* gen. nov. to formally recognize clades Fr3 and H as genera in the family Symbiodiniaceae (Dinophyceae). Journal of Phycology. doi: 10.1111/jpy.12999

Oakley, C. A., B. M. Hopkinson and G. W. Schmidt. 2014a. Mitochondrial terminal alternative oxidase and its enhancement by thermal stress in the coral symbiont *Symbiodinium*. Coral Reefs. **33**: 543-552. doi:10.1007/s00338-014-1147-0

Oakley, C. A., G. W. Schmidt and B. M. Hopkinson. 2014b. Thermal responses of *Symbiodinium* photosynthetic carbon assimilation. Coral Reefs. **33**: 501-512. doi:10.1007/s00338-014-1130-9

Oliver, T. A. and S. R. Palumbi. 2011. Many corals host thermally resistant symbionts in high-temperature habitat. Coral Reefs. **30**: 241-250. doi:10.1007/s00338-010-0696-0

Parkinson, J. E., Baumgarten, S., Michell, C. T., Baums, I. B., LaJeunesse, T. C., and C. R. Voolstra. 2016. Gene expression variation resolves species and individual strains among coral-associated dinoflagellates within the genus *Symbiodinium*. Genome Biology and Evolution. **8**: 665-680. doi: 10.1093/gbe/evw019

Pei, S. and E. A. Laws. 2013. Does the ^{14}C method estimate net photosynthesis? Implications from batch and continuous culture studies of marine phytoplankton. Deep Sea Research Part I: Oceanographic Research Papers. **82**: 1-9. doi:10.1016/j.dsr.2013.07.011

Pelejero, C., E. Calvo and O. Hoegh-Guldberg. 2010. Paleo-perspectives on ocean acidification. Trends Ecol. Evol. **25**: 332-344. doi:10.1016/j.tree.2010.02.002

Pernice, M., and others. 2014. A nanoscale secondary ion mass spectrometry study of dinoflagellate functional diversity in reef-building corals. Environ. Microbiol. **17**: 3570-3580. doi:10.1111/1462-2920.12518

Pochon, X., T. C. LaJeunesse and J. Pawlowski. 2004. Biogeographic partitioning and host specialization among foraminiferan dinoflagellate symbionts (*Symbiodinium*; Dinophyta). Marine Biology. **146**: 17-27. doi:10.1007/s00227-004-1427-2

Pochon, X. and R. D. Gates. 2010. A new *Symbiodinium* clade (Dinophyceae) from soritid foraminifera in Hawai'i. Mol. Phylogenet. Evol. **56**: 492-497. doi:10.1016/j.ympev.2010.03.040

Putnam, H. M., Stat, M., Pochon, X., and R. D. Gates. 2012. Endosymbiotic flexibility associates with environmental sensitivity in scleractinian corals. Proceedings of the Royal Society B: Biological Sciences. **279**: 4352-4361. doi: 10.1098/rspb.2012.1454

Quigley, K. M., B. L. Willis and L. K. Bay. 2017. Heritability of the *Symbiodinium* community in vertically- and horizontally-transmitting broadcast spawning corals. Sci. Rep. **7**: 8219. doi:10.1038/s41598-017-08179-4

Radecker, N., J. B. Raina, M. Pernice, G. Perna, P. Guagliardo, M. R. Kilburn, M. Aranda and C. R. Voolstra. 2018. Using *Aiptasia* as a model to study metabolic interactions in cnidarian-*Symbiodinium* symbioses. Front. Physiol. **9**: 214. doi:10.3389/fphys.2018.00214

Radice, V. Z., O. Hoegh-Guldberg, B. Fry, M. D. Fox, S. G. Dove and E. Dorrepaal. 2019. Upwelling as the major source of nitrogen for shallow and deep reef-building corals across an oceanic atoll system. Functional Ecology. **33**: 1120-1134. doi:10.1111/1365-2435.13314

Ragni, M., R. L. Airs, S. J. Hennige, D. J. Suggett, M. E. Warner and R. J. Geider. 2010. PSII photoinhibition and photorepair in *Symbiodinium* (Pyrrhophyta) differs between thermally tolerant and sensitive phylotypes. Marine Ecology Progress Series. **406**: 57-70. doi:10.3354/meps08571

Ralph, P. J. and R. Gademann. 2005. Rapid light curves: A powerful tool to assess photosynthetic activity. Aquatic Botany. **82**: 222-237. doi:10.1016/j.aquabot.2005.02.006

Raven, J. 1984. A cost-benefit analysis of photon absorption by photosynthetic unicells. New Phytologist. **98**: 593-625.

Reside, A. E., J. Beher, A. J. Cosgrove, M. C. Evans, L. Seabrook, J. L. Silcock, A. S. Wenger and M. Maron. 2017. Ecological consequences of land clearing and policy reform in Queensland. Pacific Conservation Biology. **23**: 219-230.

Reynolds, J. M., B. U. Bruns, W. K. Fitt and G. W. Schmidt. 2008. Enhanced photoprotection pathways in symbiotic dinoflagellates of shallow-water corals and other cnidarians. Proceedings of the National Academy of Sciences. **105**: 13674-13678.

Roberty, S., B. Bailleul, N. Berne, F. Franck and P. Cardol. 2014. PSI Mehler reaction is the main alternative photosynthetic electron pathway in *Symbiodinium* sp., symbiotic dinoflagellates of cnidarians. New Phytol. **204**: 81-91. doi:10.1111/nph.12903

Rohwer, F., M. Breitbart, J. Jara, F. Azam and N. Knowlton. 2001. Diversity of bacteria associated with the Caribbean coral *Montastraea franksi*. Coral Reefs. **20**: 85-91. doi:10.1007/s003380100138

Roth, E., K. Jeon and G. Stacey. 1988. Homology in endosymbiotic systems: the term "symbiosome".

Rowan, R., S. M. Whitney, A. Fowler and D. Yellowlees. 1996. Rubisco in marine symbiotic dinoflagellates: form II enzymes in eukaryotic oxygenic phototrophs encoded by a nuclear multigene family. The Plant Cell. **8**: 539-553.

Rowan, R. 2004. Thermal adaptation in reef coral symbionts. Nature. **430**: 742-742.

Sabry, O. M., D. E. Goeger and W. H. Gerwick. 2017. Bioactive new metabolites from the green alga *Udotea orientalis* growing on the Gorgonian coral *Pseudopterogorgia rigida*. Nat. Prod. Res. **31**: 1245-1250. doi:10.1080/14786419.2016.1236096

Sage, R. F. 2002. Variation in the k_{cat} of Rubisco in C_3 and C_4 plants and some implications for photosynthetic performance at high and low temperature. Journal of Experimental Botany. **53**: 609-620.

Sampayo, E. M., L. Franceschinis, O. Hoegh-Guldberg and S. Dove. 2007. Niche partitioning of closely related symbiotic dinoflagellates. Mol. Ecol. **16**: 3721-3733. doi:10.1111/j.1365-294X.2007.03403.x

Santos, S., T. Shearer, A. Hannes and M. Coffroth. 2004. Fine-scale diversity and specificity in the most prevalent lineage of symbiotic dinoflagellates (*Symbiodinium*, Dinophyceae) of the Caribbean. Molecular Ecology. **13**: 459-469.

Savage, A., H. Trapido-Rosenthal and A. Douglas. 2002. On the functional significance of molecular variation in *Symbiodinium*, the symbiotic algae of Cnidaria: photosynthetic response to irradiance. Marine Ecology Progress Series. **244**: 27-37.

Shoguchi, E., and others. 2013. Draft assembly of the *Symbiodinium minutum* nuclear genome reveals dinoflagellate gene structure. Curr. Biol. **23**: 1399-1408. doi:10.1016/j.cub.2013.05.062

Shumway, N., M. Maron and J. E. Watson. 2017. Australia needs a wake-up call. Science. **355**: 918. doi:10.1126/science.aam8945

Silverstein, R. N., R. Cunning and A. C. Baker. 2017. Tenacious D: *Symbiodinium* in clade D remain in reef corals at both high and low temperature extremes despite impairment. J. Exp. Biol. **220**: 1192-1196. doi:10.1242/jeb.148239

Simmons, T. L., E. Andrianasolo, K. McPhail, P. Flatt and W. H. Gerwick. 2005. Marine natural products as anticancer drugs. Molecular Cancer Therapeutics. **4**: 333-342.

Smith, D. J., D. J. Suggett and N. R. Baker. 2005. Is photoinhibition of zooxanthellae photosynthesis the primary cause of thermal bleaching in corals? Global Change Biology. **11**: 1-11.

Spalding, M., L. Burke, S. A. Wood, J. Ashpole, J. Hutchison and P. zu Ermgassen. 2017. Mapping the global value and distribution of coral reef tourism. Marine Policy. **82**: 104-113. doi:10.1016/j.marpol.2017.05.014

Sproles, A. E., C. A. Oakley, J. L. Matthews, L. Peng, J. G. Owen, A. R. Grossman, V. M. Weis and S. K. Davy. 2019. Proteomics quantifies protein expression changes in a model cnidarian colonised by a thermally tolerant but suboptimal symbiont. ISME J. **13**: 2334-2345. doi:10.1038/s41396-019-0437-5

Stat, M., E. Morris and R. D. Gates. 2008. Functional diversity in coral–dinoflagellate symbiosis. Proceedings of the National Academy of Sciences. **105**: 9256-9261.

Steemann-Nielsen, E. 1952. The use of radio-active carbon (C^{14}) for measuring organic production in the sea. ICES Journal of Marine Science. **18**: 117-140. doi:10.1093/icesjms/18.2.117

Suggett, D. J., M. E. Warner, D. J. Smith, P. Davey, S. Hennige and N. R. Baker. 2008. Photosynthesis and production of hydrogen peroxide by *Symbiodinium* (Pyrrhophyta) phylotypes with different thermal tolerances. J. Phycol. **44**: 948-956. doi:10.1111/j.1529-8817.2008.00537.x

Suggett, D. J., H. L. MacIntyre, T. M. Kana and R. J. Geider. 2009. Comparing electron transport with gas exchange: parameterising exchange rates between alternative photosynthetic currencies for eukaryotic phytoplankton. Aquatic Microbial Ecology. **56**: 147-162. doi:10.3354/ame01303

Suggett, D. J., R. K. P. Kikuchi, M. D. M. Oliveira, S. Spanó, R. Carvalho and D. J. Smith. 2012. Photobiology of corals from Brazil's near-shore marginal reefs of Abrolhos. Marine Biology. **159**: 1461-1473. doi:10.1007/s00227-012-1925-6

Suggett, D. J., S. Goyen, C. Evenhuis, M. Szabo, D. T. Pettay, M. E. Warner and P. J. Ralph. 2015. Functional diversity of photobiological traits within the genus *Symbiodinium* appears to be governed by the interaction of cell size with cladal designation. New Phytol. **208**: 370-381. doi:10.1111/nph.13483

Suggett, D. J., M. E. Warner and W. Leggat. 2017. Symbiotic dinoflagellate functional diversity mediates coral survival under ecological crisis. Trends Ecol. Evol. **32**: 735-745. doi:10.1016/j.tree.2017.07.013

Suggett, D. J., E. F. Camp, J. Edmondson, L. Boström-Einarsson, V. Ramler, K. Lohr and J. T. Patterson. 2019. Optimizing return-on-effort for coral nursery and outplanting practices to aid restoration of the Great Barrier Reef. Restoration Ecology. **27**: 683-693. doi:10.1111/rec.12916

Suggett, D. J. and D. J. Smith. 2020. Coral bleaching patterns are the outcome of complex biological and environmental networking. Global Change Biology. **26**: 68-79.

Sunda, W., D. Kieber, R. Kiene and S. Huntsman. 2002. An antioxidant function for DMSP and DMS in marine algae. Nature. **418**: 317-320.

Swain, T. D., J. Chandler, V. Backman, L. Marcelino and W. Blanckenhorn. 2017. Consensus thermotolerance ranking for 110 *Symbiodinium* phylotypes: an exemplar utilization of a novel iterative partial-rank aggregation tool with broad application potential. Functional Ecology. **31**: 172-183. doi:10.1111/1365-2435.12694

Takahashi, S. and N. Murata. 2008. How do environmental stresses accelerate photoinhibition? Trends Plant Sci. **13**: 178-182. doi:10.1016/j.tplants.2008.01.005

Takahashi, S., S. M. Whitney and M. R. Badger. 2009. Different thermal sensitivity of the repair of photodamaged photosynthetic machinery in cultured *Symbiodinium* species. Proc. Natl. Acad. Sci. U. S. A. **106**: 3237-3242. doi:10.1073/pnas.0808363106

Tansik, A. L., W. K. Fitt and B. M. Hopkinson. 2017. Inorganic carbon is scarce for symbionts in scleractinian corals. Limnology and Oceanography. **62**: 2045-2055. doi:10.1002/lno.10550

Tchernov, D., M. Y. Gorbunov, C. de Vargas, S. Narayan Yadav, A. J. Milligan, M. Haggblom and P. G. Falkowski. 2004. Membrane lipids of symbiotic algae are diagnostic of sensitivity to thermal bleaching in corals. Proc. Natl. Acad. Sci. U. S. A. **101**: 13531-13535. doi:10.1073/pnas.0402907101

Teh, L. S., L. C. Teh and U. R. Sumaila. 2013. A global estimate of the number of coral reef fishers. PLoS One. **8**: e65397. doi:10.1371/journal.pone.0065397

Thornhill, D. J., Y. Xiang, D. T. Pettay, M. Zhong and S. R. Santos. 2013. Population genetic data of a model symbiotic cnidarian system reveal remarkable symbiotic specificity and vectored introductions across ocean basins. Molecular Ecology. **22**: 4499-4515. doi:10.1111/mec.12416

Thornhill, D. J., Howells, E. J., Wham, D. C., Steury, T. D., and S. R. Santos. 2017. Population genetics of reef coral endosymbionts (*Symbiodinium*, Dinophyceae). Molecular Ecology. **26**: 2640-2659. doi:10.1111/mec.14055

Thornton, D. C. O. 2014. Dissolved organic matter (DOM) release by phytoplankton in the contemporary and future ocean. European Journal of Phycology. **49**: 20-46. doi:10.1080/09670262.2013.875596

Tivey, T. R., and others. 2019. N-linked surface glycan biosynthesis, composition, inhibition, and function in cnidarian-dinoflagellate symbiosis. bioRxiv: 820894.

Trampe, E., P. J. Hansen and M. Kühl. 2015. A comparison of photosynthesis measurements by O_2 evolution, ^{14}C assimilation and variable chlorophyll fluorescence during light acclimatization of the diatom *Coscinodiscus granii*. Algae. **30**: 103-119.

Tremblay, P., C. Ferrier-Pages, J. F. Maguer, C. Rottier, L. Legendre and R. Grover. 2012. Controlling effects of irradiance and heterotrophy on carbon translocation in the temperate coral *Cladocora caespitosa*. PLoS One. **7**: e44672. doi:10.1371/journal.pone.0044672

Tremblay, P., A. Gori, J. F. Maguer, M. Hoogenboom and C. Ferrier-Pages. 2016. Heterotrophy promotes the re-establishment of photosynthate translocation in a symbiotic coral after heat stress. Sci. Rep. **6**: 38112. doi:10.1038/srep38112

van Hooidonk, R., J. A. Maynard and S. Planes. 2013. Temporary refugia for coral reefs in a warming world. Nature Climate Change. **3**: 508-511. doi:10.1038/nclimate1829

van Hooidonk, R., and others. 2016. Local-scale projections of coral reef futures and implications of the Paris Agreement. Sci. Rep. **6**: 39666. doi:10.1038/srep39666

van Woesik, R. and C. J. Randall. 2017. Coral disease hotspots in the Caribbean. Ecosphere. **8**. doi:10.1002/ecs2.1814

Venn, A. A., M. A. Wilson, H. G. Trapido-Rosenthal, B. J. Keely and A. E. Douglas. 2006. The impact of coral bleaching on the pigment profile of the symbiotic alga, *Symbiodinium*. Plant, Cell & Environment. **29**: 2133-2142.

Venn, A. A., J.E. Loram and A. E. Douglas. 2008. Photosynthetic symbioses in animals. Journal of Experimental Botany. **59**: 1069-1080. doi:/10.1093/jxb/erm328

Venn, A. A., E. Tambutte, S. Lotto, D. Zoccola, D. Allemand and S. Tambutte. 2009. Imaging intracellular pH in a reef coral and symbiotic anemone. Proc. Natl. Acad. Sci. U. S. A. **106**: 16574-16579. doi:10.1073/pnas.0902894106

Veron, J., M. Stafford-Smith, L. DeVantier and E. Turak. 2015. Overview of distribution patterns of zooxanthellate Scleractinia. Frontiers in Marine Science. **1**. doi:10.3389/fmars.2014.00081

Vidal-Dupiol, J., and others. 2009. Coral bleaching under thermal stress: putative involvement of host/symbiont recognition mechanisms. BMC Physiol. **9**: 14. doi:10.1186/1472-6793-9-14

Vila-Concejo, A. and P. Kench. 2017. Storms in coral reefs. Coastal Storms: Processes and Impacts: 127-149.

Wall, C. B., M. Kaluhiokalani, B. N. Popp, M. J. Donahue and R. D. Gates. 2020. Divergent symbiont communities determine the physiology and nutrition of a reef coral across a light-availability gradient. ISME J. doi:10.1038/s41396-019-0570-1

Wang, C., C. Deser, J.-Y. Yu, P. DiNezio and A. Clement. 2017. El Niño and Southern Oscillation (ENSO): A Review. Coral Reefs of the Eastern Tropical Pacific: 85-106.

Warner, M. E., W. K. Fitt and G. W. Schmidt. 1999. Damage to photosystem II in symbiotic dinoflagellates: a determinant of coral bleaching. Proc. Natl. Acad. Sci. U. S. A. **96**: 8007-8012. doi:10.1073/pnas.96.14.8007

Warner, M., G. Chilcoat, F. McFarland and W. Fitt. 2002. Seasonal fluctuations in the photosynthetic capacity of photosystem II in symbiotic dinoflagellates in the Caribbean reef-building coral *Montastraea*. Marine Biology. **141**: 31-38. doi:10.1007/s00227-002-0807-8

Warner, M. E. and S. Berry-Lowe. 2006. Differential xanthophyll cycling and photochemical activity in symbiotic dinoflagellates in multiple locations of three species of Caribbean coral. Journal of Experimental Marine Biology and Ecology. **339**: 86-95. doi:10.1016/j.jembe.2006.07.011

Warner, M. E. and D. J. Suggett. 2016. The photobiology of *Symbiodinium* spp.: Linking physiological diversity to the implications of stress and resilience. The Cnidaria, Past, Present and Future: 489-509.

Weis, V. M. 2008. Cellular mechanisms of Cnidarian bleaching: stress causes the collapse of symbiosis. J. Exp. Biol. **211**: 3059-3066. doi:10.1242/jeb.009597

Wham, D. C. and T. C. LaJeunesse. 2016. *Symbiodinium* population genetics: testing for species boundaries and analysing samples with mixed genotypes. Molecular Ecology. **25**: 2699-2712.

Wolfe, K., A. Graba-Landry, S. A. Dworjanyn and M. Byrne. 2017. Superstars: Assessing nutrient thresholds for enhanced larval success of *Acanthaster planci*, a review of the evidence. Mar. Pollut. Bull. **116**: 307-314. doi:10.1016/j.marpolbul.2016.12.079

Wood-Charlson, E. M., L. L. Hollingsworth, D. A. Krupp and V. M. Weis. 2006. Lectin/glycan interactions play a role in recognition in a coral/dinoflagellate symbiosis. Cell Microbiol. **8**: 1985-1993. doi:10.1111/j.1462-5822.2006.00765.x

Wooldridge, S. A. and J. E. Brodie. 2015. Environmental triggers for primary outbreaks of crown-of-thorns starfish on the Great Barrier Reef, Australia. Mar. Pollut. Bull. **101**: 805-815. doi:10.1016/j.marpolbul.2015.08.049

Wright, R. M., H. Mera, C. D. Kenkel, M. Nayfa, L. K. Bay and M. V. Matz. 2019. Positive genetic associations among fitness traits support evolvability of a reef-building coral under multiple stressors. Global Change Biology. **25**: 3294-3304.

Xiang, T., E. A. Hambleton, J. C. DeNofrio, J. R. Pringle and A. R. Grossman. 2013. Isolation of clonal axenic strains of the symbiotic dinoflagellate *Symbiodinium* and their growth and host specificity. J. Phycol. **49**: 447-458. doi:10.1111/jpy.12055

Yamori, W., K. Hikosaka and D. A. Way. 2014. Temperature response of photosynthesis in C_3, C_4, and CAM plants: Temperature acclimation and temperature adaptation. Photosynth. Res. **119**: 101-117. doi:10.1007/s11120-013-9874-6

Yost, D. M. and C. L. Mitchelmore. 2009. Dimethylsulfoniopropionate (DMSP) lyase activity in different strains of the symbiotic alga *Symbiodinium microadriaticum*. Marine Ecology Progress Series. **386**: 61-70. doi:10.3354/meps08031

Yuyama, I., S. Harii and M. Hidaka. 2012. Algal symbiont type affects gene expression in juveniles of the coral *Acropora tenuis* exposed to thermal stress. Mar. Environ. Res. **76**: 41-47. doi:10.1016/j.marenvres.2011.09.004

Ziegler, M., F. O. Seneca, L. K. Yum, S. R. Palumbi and C. R. Voolstra. 2017. Bacterial community dynamics are linked to patterns of coral heat tolerance. Nat. Commun. **8**: 14213. doi:10.1038/ncomms14213

Ziegler, M., C. Arif and C. R. Voolstra. 2019. Symbiodiniaceae diversity in Red Sea coral reefs & coral bleaching. Coral Reefs of the Red Sea. C. R. Voolstra and M. L. Berumen. Cham, Springer International Publishing: 69-89.

Chapter 2

Unlocking the black-box of inorganic carbon-uptake and utilisation strategies amongst coral endosymbionts (Symbiodiniaceae)

Mickael Ros[1], Emma F. Camp[1], David J. Hughes[1], Joseph R. Crosswell[2], Mark E. Warner[3], William P. Leggat[4], David. J. Suggett[1*]

[1] Climate Change Cluster, University of Technology Sydney, Broadway, NSW 2007, Australia

[2] CSIRO Oceans and Atmosphere, Ecosciences Precinct, Dutton Park, QLD 4102, Australia

[3] College of Earth, Ocean, and Environment, University of Delaware, Lewes, DE 19958, USA

[4] School of Environmental and Life Sciences, University of Newcastle, Callaghan, NSW 2308, Australia

* Corresponding author

This Chapter has been accepted for publication in Limnology and Oceanography as:

Ros M., Camp E.F., Hughes D.J., Crosswell J.R., Warner M.E., Leggat W.P., Suggett D.J. 2020. Unlocking the black-box of inorganic carbon-uptake and utilisation strategies amongst coral endosymbionts (Symbiodiniaceae). Limnol. Oceanogr. doi: 10.1002/lno.11416

2.1. Abstract

Dinoflagellates within the family Symbiodiniaceae are widespread and fuel metabolism of reef-forming corals through photosynthesis. Adaptation in capacity to harvest and utilise light, and "safely" process photosynthetically-generated energy is a key factor regulating their broad ecological success. However, whether such adaptive capacity similarly extends to how Symbiodiniaceae species and genotypes assimilate inorganic carbon (Ci) remains unexplored. We build on recent approaches exploring functional diversity of fitness traits to identify whether Ci uptake and incorporation could be reconciled with evolutionary adaptation amongst Symbiodiniaceae. We examined phylogenetically-diverse Symbiodiniaceae cultures (23 isolates, six genera) to track how carbon was invested into cellular uptake, excretion, and growth (cell size, division, storage). Gross carbon uptake rates (GPC) over 1h varied amongst isolates grown at 26°C (0.63 – 3.08 pg C $[cell.h]^{-1}$) with no evident pattern with algal phylogeny. Intriguingly, net carbon uptake rates (24h) were often higher (1.01 – 5.54 pg C $[cell.h]^{-1}$) than corresponding values of GPC – we discuss how such GPC measurements may reflect highly-conserved biological characteristics for cultured cells linked to high metabolic dependency on photorespiration and heterotrophy. Three isolates from different genera (*Cladocopium goreaui*, *Durusdinium trenchii*, and *Effrenium voratum)* were additionally grown at 20°C and 30°C. Here, Ci uptake consistently decreased with temperature-driven declines in growth rate, suggesting environmental regulation outweighs phylogenetic organisation of carbon assimilation capacity amongst Symbiodiniaceae. Together, these data demonstrate environmental regulation and ecological success amongst Symbiodiniaceae likely rests on plasticity of upstream photosynthetic processes (light harvesting, energy quenching, etc.) to overcome evolutionary-conserved limitations in Ci functioning.

2.2. Introduction

Dinoflagellates within the family Symbiodiniaceae are widespread throughout tropical and temperate marine biomes (LaJeunesse et al. 2018), commonly existing as endosymbionts within invertebrates – including corals, gorgonians and jellyfish (Phylum: Cnidaria) and giant clams (Phylum: Mollusca) – but also as free-living cells and attached to substrates (Takabayashi et al. 2012; Cunning et al. 2015). As coral reef endosymbionts, their photosynthesis drives healthy ecosystem functioning by primarily fuelling growth of reef-building corals (Gattuso et al. 1999; Weis and Allemand 2009; Colombo-Pallotta et al. 2010) but also acting to destabilise host survival during stress events, such as temperature-induced coral bleaching (Suggett and Smith 2011; Warner and Suggett 2016; Fordyce et al. 2019). Similarly, photosynthesis by free-living cells drives metabolic exchange with neighbouring bacteria to drive calcification and the formation of unique "symbiolites" (Frommlet et al. 2015). Consequently, for over 50 years, studies have attempted to unlock how algal symbiont photosynthesis functions (Trench 1969; Warner and Suggett 2016) and is optimised across different species (Suggett et al. 2015) and growth environments (Robison and Warner 2006; Silverstein et al. 2017).

A key challenge in trying to establish models describing optimum photosynthetic function for Symbiodiniaceae reflects that the family is comprised of immense genetic (LaJeunesse et al. 2018) and functional (Warner and Suggett 2016; Suggett et al. 2017) diversity. Ease of measuring photobiological traits using active fluorometry-based photosystem II (PSII) activity (Robison and Warner 2006; Suggett et al. 2015) and photosynthetic O_2 evolution (Gregoire et al. 2017) has led to identification of "ecotypes" that are adapted to high or low light availability (Iglesias-Prieto et al. 2004; Hennige et al. 2009; Suggett et al. 2015; Wangpraseurt et al. 2016) as well as temperature (Oakley et al. 2014; Diaz-Almeyda et al.

2017; Goyen et al. 2017) and CO_2 (Brading et al. 2011) extremes. Such techniques have proven powerful in resolving how primary photosynthetic pathways, such as PSII (Roberty et al. 2014; Karim et al. 2015) and photosystem I (PSI) (Roberty et al. 2014; Aihara et al. 2016) turnover operate differently amongst Symbiodiniaceae to regulate functioning under sub-optimal environmental conditions. In comparison to this relative wealth of information describing the functional diversity of the photosynthetic "light reactions", we know far less about the "dark reactions" (more accurately termed "carbon reactions" – reviewed by Mirkovic et al. 2017); specifically, the capacity to assimilate inorganic carbon (Ci) for cellular maintenance and growth (Warner and Suggett 2016) – such limited knowledge is surprising given that different Ci assimilation strategies could confirm their potential "benefit" as symbionts (Warner and Suggett 2016; Suggett et al. 2017; Baker et al. 2018).

Photosynthetic responses retrieved from fluorometric- and O_2-based measurements provide insight into Ci uptake efficiency (Brading et al. 2011; Roberty et al. 2014; Oakley et al. 2014; Suggett et al. 2015; Gregoire et al. 2017), yet few direct Ci assimilation rates have been performed to date despite early foundational work on coral endosymbionts (Goiran et al. 1996; Al-Moghrabi et al. 1996; Allemand et al. 1998). More recent studies on Ci assimilation have adopted diverse approaches using stable (^{13}C; Pernice et al. 2014; Baker et al. 2018; Krueger et al. 2018; Radecker et al. 2018) and radio-isotope methods (^{14}C; Brading et al. 2013; Hoadley et al. 2015, 2016). As such, methodological differences across studies such as variable incubation lengths (Halsey et al. 2013; Hughes et al. 2018b) limit any reconciliation across species and environmental treatments. Therefore, how activity of Ci uptake processes, notably diffusive CO_2 incorporation or carbon concentrating mechanisms (CCMs), potentially varies across Symbiodiniaceae taxa to reflect evolutionary divergence in uptake capacity (efficiency and extent), as has been observed across other closely-related microalgal taxa (Halsey et al. 2013), remains unknown. Such reconciliation is particularly hindered where Symbiodiniaceae

^{14}C-enrichment methodologies have reported only absolute enrichment levels (as per disintegrations per minute (DPM) per cell) that have not been standardised against Ci uptake rates (Wang and Douglas 1997; Loram et al. 2007; Kenkel and Bay 2018) and/or have assumed the dissolved inorganic carbon (DIC) concentration available to cells in the incubation media (Rost et al. 2008; Brading et al. 2013). The few Ci-based studies with symbiotic dinoflagellates that have overcome these limitations have identified important adaptations of Ci "strategies". For example, these algae appear to have evolved different CCM efficiencies (e.g. within the genus *Symbiodinium*; Brading et al. 2013), with comparative genomics based on bicarbonate transporter domains suggesting this pattern may also hold across other genera within the Symbiodiniaceae (Aranda et al. 2016).

How potential differences in Ci uptake in turn translate to strategies of allocation into organic carbon are even less well understood for Symbiodiniaceae. As in other microalgae, photosynthetic fixation of Ci into organic carbon can result in several key pathways (Figure 2.1); notably building of "organic skeletons" for growth (*sensu* MacIntyre et al. 2002) from macronutrients synthesis (Halsey and Jones 2015) or long-term storage under the form of carbohydrates or fatty acids (Hillyer et al. 2017; Matthews et al. 2017). For Symbiodiniaceae, excretion or *sensu stricto* translocation of photosynthetic products to the host is also a major pathway (Davy et al. 2012). Storage of photosynthetically assimilated organic carbon then results in increased particulate organic carbon (POC) inside the algal cells, and symbiont identity can explain the quantity and quality of lipids stored (Cooper et al. 2011). Ultimately, this variability of stored POC could explain variability in growth, but studies to date have not explored the link between variability of POC and growth rates in Symbiodiniaceae. Such unknowns are further confounded by observations that Symbiodiniaceae may supplement their organic carbon acquisition by photosynthetic Ci fixation via feeding on dissolved (Xiang et al. 2013) and particulate carbon sources (Jeong et al. 2012) within cultures (Figure 2.1).

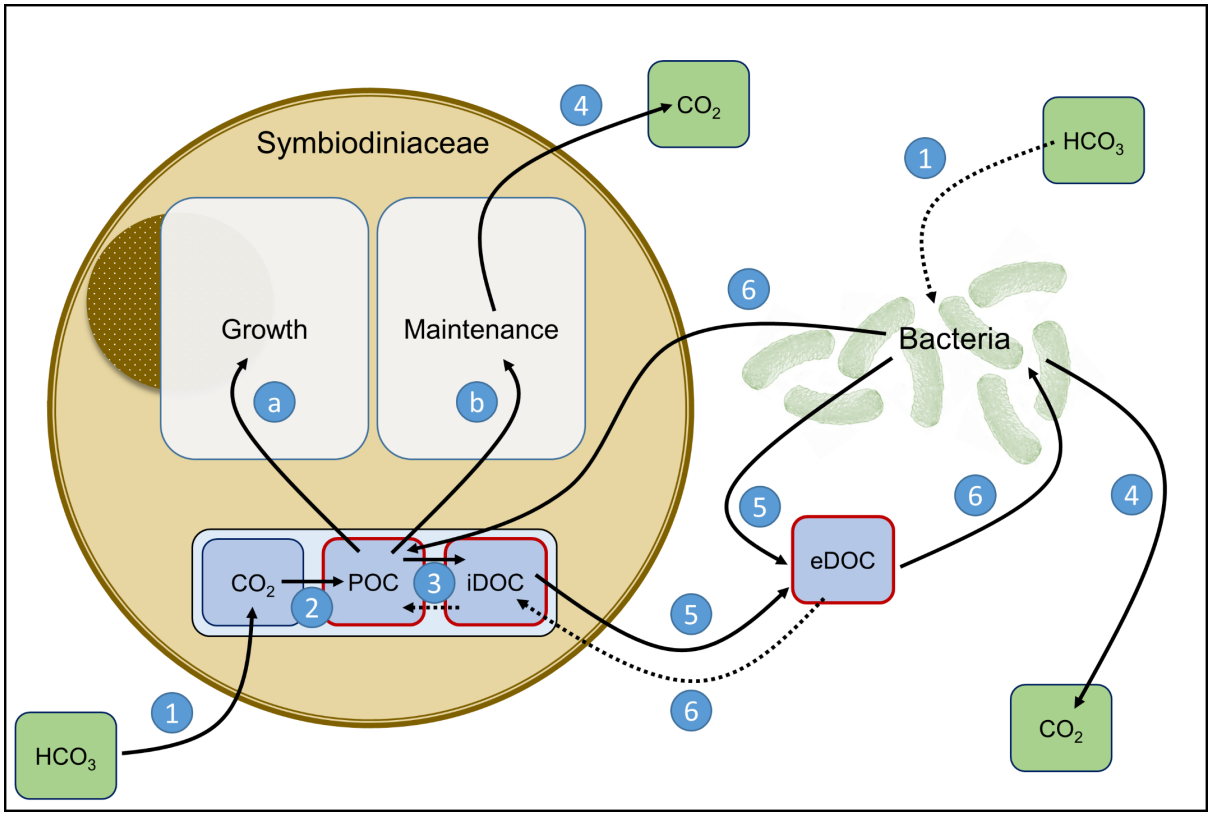

Figure 2.1. Schematic summarising carbon transfers and mechanisms occurring between the Symbiodiniaceae algae and their surrounding environment (here as free-living in culture). **(1)** Uptake. **(2)** Carboxylation. **(3)** Recycling of internal pools. **(4)** Respiration. **(5)** Active excretion or passive leakiness. **(6)** Heterotrophy. **(a)** Long-term storage for growth net carbon production (NPC) as the product of particulate organic carbon (POC) and growth rate (μ × POC). **(b)** Short-term storage for maintenance as gross carbon production (GPC, as ^{14}C fixed). POC: Particulate organic carbon. iDOC: Internal dissolved organic carbon. eDOC: External dissolved organic carbon. Red frames show the parameters measured in the study. Solid lines represent established pathways, and dashed lines represent hypothesised pathways.

Despite several decades of research on these algae, the fundamental physiological properties that define the ecological success and fitness (sensitivity or tolerance) of different species remain poorly resolved (Warner and Suggett 2016; Suggett et al. 2017). Few physiological characteristics have yet been simultaneously investigated across a sufficiently large number of Symbiodiniaceae representatives (light harvesting, (Suggett et al. 2015); reactive oxygen species (ROS) emissions, (Goyen et al. 2017); bacterial associates, (Lawson et al. 2018)), hence the level of complexity required to describe functional diversity is not yet

resolved. We therefore built on recent approaches screening fitness traits across Symbiodiniaceae (Suggett et al. 2015; Goyen et al. 2017; Lawson et al. 2018) to further examine for functional diversity of Ci assimilation across phylogenetically diverse Symbiodiniaceae taxa (23 isolates, spanning former clades A - F). We systematically examined how differences in growth rate reflected differences in Ci assimilation (uptake and incorporation), in the latter case examining how $NaH^{14}CO_3$ is fixed into particulate (cellular skeletons, *sensu* MacIntyre et al. 2002) *versus* dissolved (rapidly excreted) organic fractions (Figure 2.1). For three of the most functionally distinct taxa, we then further demonstrated how optimum *versus* sub-optimum growth temperature moderates the Ci assimilation "strategy" observed. Thus, functional diversity patterns observed amongst Symbiodiniaceae taxa when grown under a single condition reflect adaptive differences in growth optima.

2.3. Material and Methods

2.3.1. Symbiodiniaceae ITS2 type identification

Stock culture identity was verified prior to culturing using a 15 mL aliquot of each isolate concentrated to 100,000 cells mL^{-1}. DNA was extracted using a DNEasy PowerPlant Pro Kit (Qiagen, Hilden, Germany) and the internal transcribed spacer 2 (ITS2) locus (Yao et al. 2010) was amplified by polymerase chain reaction (PCR). Reverse (ITS1intrev2; 5'-GGG ATC CAT ATG CTT AAG TTC AGC GGG T-3') and forward (ITSintfor2; 5'-GAA TTG CAG AAC TCC GTG-3') primers (LaJeunesse and Trench, 2000; Sigma-Aldrich, St. Louis, MO, USA) specific to Symbiodiniaceae were used to flank the amplified sequence. The PCR was performed using the Veriti 96 Well Thermal cycler (Applied Biosystems, Foster City, CA, USA) and the following cycling conditions: 1 cycle at 95°C for 1 min (denaturation), followed by 35 cycles at: (i) 95°C for 15 s (denaturation), (ii) 58°C for 15 s (annealing), (iii) 72°C for 30 s (elongation) and 1 cycle at 72°C for 7 min (additional elongation). The PCR products were

cleaned and concentrated using the DNA Clean & Concentrator™-5 kit (ZYMO Research, Irvine, CA, USA) before being sent to the Australian Genome Research Facility (AGRF) for Sanger sequencing. The resulting sequences were processed through the BLAST algorithm (Basic Local Alignment Search Tool) against the National Center for Biotechnology Information (NCBI) database to confirm ITS2 identity.

2.3.2. Symbiodiniaceae culturing

We initially cultured 23 different isolates spanning six genera (*Symbiodinium*, *Breviolum*, *Cladocopium*, *Durusdinium*, *Effrenium*, and *Fugacium*; formerly clades A to F) to screen for differences in Ci uptake and incorporation strategy. These isolates covered multiple geographic locations (Caribbean Sea and Pacific Ocean), host origin (coral, sea anemone, or other cnidarian hosts), and lifestyle (exclusively free-living and symbiotic) (Table 2.1). All isolates have been maintained at 26°C as free-living cells in culture for at least five years, except for isolates A-2548 and E-3420, which were cryopreserved prior to the experiment but were re-animated and acclimated to growth conditions 3 months prior to experimentation. Isolates were grown in a climate-control chamber (Aralab, Lisbon, Portugal) under an irradiance of 190 ± 42 µmol photons m^{-2} s^{-1} (Hydra 52 HD LED, AquaIllumination, Ames, IA, USA); as measured with a 4π LI-190SA Quantum Sensor (LI-COR, Lincoln, NE, USA) set to a 12:12 light:dark cycle and at a temperature of 26 ± 0.5ºC. Three isolates, one sub-tropical each from the symbiotic genera *Cladocopium* and *Durusdinium* (thermo-sensitive and thermo-tolerant, respectively; see Camp. et al. 2020) as well as one exclusively free-living from temperate waters (genus *Effrenium*) were subsequently selected to evaluate how Ci uptake and incorporation strategies were moderated by growth temperature; specifically, C1-SCF-124, amur-D-MI and E-421 (Table 2.1). For this second experiment, the three isolates were grown exactly as for the initial screening experiment but in parallel incubators set to 20, 26 or 30ºC

Table 2.1. Summary of Symbiodiniaceae type identifiers and source (geographic and host taxa) examined. Isolates are classified according to their genus (formerly clade A – F) and by numerical subtype determined via ITS2 identification. The culture isolate identity denotes the identification number under which a specific isolate is found in the literature or algal collections. The internal isolate label is used internally as the University of Technology of Sydney (UTS) and is used throughout this study to refer to a specific isolate. The geographic region where the isolates were originally isolated from is shown, as well as their original host taxa, or as a non-symbiotic isolate (free-living).

Genus	Species	ITS2 type	Culture isolate identity	Internal isolate label	Geographic origin	Host taxa
Symbiodinium	*S. microadriaticum*	A1	CCMP2464, rt61	A1-61	Florida (Caribbean Sea)	*Cassiopeia xamachana* (jellyfish)
	S. pilosum	A2	rt104	A2-104	Enewetak (Pacific)	*Heliopora* sp.(octocoral)
	S. pilosum		rt154	A2-154	Jamaica (Caribbean Sea)	*Discosoma sanctithomae* (corallimorph)
	S. pilosum		CCMP2461, rt185	A2-185	Jamaica (Caribbean Sea)	*Zoanthus sociatus* (zoanthid)
	S. tridacnidorum	A3	CS73, SCF022-01, UTS-A	A3-UTS-A	Heron Island (Pacific)	*Tridacna maxima* (giant clam)
	S. natans		CCMP2548, HA3-5, MBIC10, rt796	A-2548	Hawaii (Pacific)	Free-living
	S. lincheaea	A4	CCMP2456, rt379	A4-379	Sargasso Sea (Caribbean Sea)	*Plexaura homomalla* (gorgonian)
	S. necroappetens	A13	CCMP2469, JS879, rt80	A13-80	Jamaica (Caribbean Sea)	*Condylactis gigantea* (sea anemone)
Breviolum	*B. minutum*	B1	B (UTS)	B1-UTS-B	S. Taiwan (Indo-Pacific)	*Euphyllia glabrescens* (coral)
	Breviolum sp.		CCMP2460, CCMP3345, rt2	B1-2	Florida (Caribbean Sea)	*Aiptasia pallida* (sea anemone)
	B. pseudominutum		CCMP2463, rt12	B1-12	Puerto Rico (Caribbean Sea)	*Aiptasia tagetes* (sea anemone)
Cladocopium	*C. goreaui*	C1	AIMS-aten-C1-MI-cfu-B2, SCF055	C1-Hetero-M	Magnetic Island (Pacific)	*Acropora tenuis* (coral)
	C. goreaui		AIMS-aten-C1-WSY	C1-Hetero-W	South Molle Isl. (Pacific)	*Acropora tenuis* (coral)
	C. goreaui		SCF058-04	SCF123	Magnetic Island (Pacific)	*Acropora millepora* (coral)
	C. goreaui		SCF055-06	SCF124	Magnetic Island (Pacific)	*Acropora tenuis* (coral)
	Cladocopium sp.	C2	rt203	C2-203	Palau (Pacific)	*Hippopus hippopus* (giant clam)
Durusdinium	*D. trenchii*	D1a	amur-D-MI, SCF082, D (UTS)	amur-D-MI	Magnetic Island (Pacific)	*Acropora muricata* (coral)
	D. trenchii		CCMP3408, A001, JS1313	D1a-3408	Okinawa (Japan)	*Acropora* sp. (coral)
Effrenium	*E. voratum*	E	CCMP3420	E-3420	Santa Barbara (California)	Free-living
	E. voratum		CCMP421, CHANG4	E-421	Cooks Strait (New Zealand)	Free-living
Fugacium	*F. kawagutii*	F1	CCMP2468, CS156	F1-156	Hawaii (Pacific)	*Montipora verrucosa* (coral)
	F. kawagutii		SCF089-01, UTS-C	F1-UTS-C	Heron Island (Pacific)	*Pocillopora damicornis* (coral)
	Fugacium sp.	F2	CCMP2455, rt133	F2-133	Jamaica (Caribbean Sea)	*Meandrina meandrites* (coral)

Cultures were grown semi-continuously (i.e. supplied with new medium when required to maintain cultures in exponential growth) in 250 mL conical flasks of sterile 0.2 µm filtered artificial seawater (modified from Berges et al. 2002) enriched with Daigo's IMK medium (Nihon Pharmaceutical, Tokyo, Japan) and harvested during the middle of the photoperiod whilst maintained in steady-state growth in triplicate from consecutive generations to ensure biological replication (as per Hennige et al. 2009; Brading et al. 2011). Each new biological replicate was initiated after transfer into freshly-prepared IMK medium with a starting density of 50,000 cells mL^{-1}. Cultures were then monitored daily using cell counts to define the exponential division rate (μ, d^{-1}) and sampled for all subsequent analyses whilst still within exponential growth phase. During this period, culture health was regularly assessed using FastOcean (Chelsea Technologies, West Molesey, UK) and LIFT (Soliense, Shoreham, NY, USA) Fast Repetition Rate fluorometers (FRRf) to probe photophysiological status (as per Suggett et al. 2015). Cell counts were performed using four aliquots of 10 µL of cultures fixed with glutaraldehyde (25%, Grade II, Sigma-Aldrich, 1% final concentration), loaded onto a Neubauer haemocytometer chamber for quantification using microscopy. Imaging of all aliquots was also performed to retrieve cell volume (Fujise et al. 2018). For each sample, 16 images were captured of the counting chamber using NIS-Elements AR software (v.4.30.000) and an Eclipse Ni-U optical microscope coupled with a DS-Fi2 colour camera (Nikon, Tokyo, Japan). Photographs were processed with ImageJ2 software (Rueden et al. 2017) loaded with Fiji package (Schindelin et al. 2012) and using a high-throughput image processing script (Suggett et al. 2015; Fujise et al. 2018). This set-up determined the number of cells present on each photograph and estimated the cell volume of each counted element. Values of cell density and volume were then averaged. Manual cell counts were performed periodically throughout the experiment to verify the accuracy of the automated counting method.

2.3.3. Inorganic carbon uptake and excretion

Inorganic carbon uptake was determined using radiolabelled sodium bicarbonate ($NaH^{14}CO_3$) with a specific activity of 40-60 mCi $mmol^{-1}$ (PerkinElmer, Waltham, MA, USA) (Steemann-Nielsen 1952). Triplicate aliquots (10 mL) from each culture were incubated under a light intensity of 185±20 µmol photons m^{-2} s^{-1} (Hydra 52 HD LED, Aqua Illuminations, USA) to match that used for growth. A preliminary experiment was performed to determine the shortest incubation length at which we could reliably measure excretion rate, whilst simultaneously minimising uncertainty arising from ^{14}C uptake methods that employ longer incubation times and so introduce uncertainty in discriminating between gross and net carbon production (Pei and Laws 2013; Milligan et al. 2015; Hughes et al. 2018a) (Supplementary Figure S2.1a). Specifically, this experiment, which assessed both the fastest and slowing growing isolates, yielded an optimum incubation length of 60 min (Supplementary Figure S2.1b). After incubation, samples were held on ice in the dark to slow metabolism (and hence ^{14}C uptake and cellular incorporation) as per Hughes et al. (2018b), before gentle filtering using a hand pump through glass-fibre filters (GF/F, Whatman, Maidstone, UK) to separate the cells trapped on the filter (containing cellular particulate organic carbon (POC) and internal DOC (iDOC) *versus* excreted DOC (eDOC) (Table 2.2) into the medium (Moran et al. 2001). Residual, unfixed $NaH^{14}CO_3$ was removed by addition of 200 µL HCl (6 M) and the samples fixed with 150 µL glutaraldehyde 25% then left to degas in a fume hood for 24 h. 10 mL of scintillation liquid (Ultima Gold LLT, PerkinElmer) was added to each sample, and shaken firmly until the filter was dissolved. Disintegrations per minute (DPM) were then counted with a Liquid Scintillation Analyzer Tri-Carb 2810 TR (PerkinElmer) averaged from a 5 min count. To measure DIC, an additional aliquot from each culture was transferred to 12 mL gas-tight Exetainer vials (Labco Ltd., Lampeter, UK), and biological activity was immediately terminated with 180 µL of saturated solution of $HgCl_2$ (to a final concentration of 1.5%), and

subsequently stored in the dark at 4°C for analysis. Concentration of DIC for samples was determined at the Commonwealth Scientific and Industrial Research Organisation (CSIRO, Brisbane, Australia), using an AS-C3 DIC analyser (Apollo SciTech, Newark, DE, USA) against a reference material for oceanic CO_2 measurements (Batch 174, A.G. Dickson, UC San Diego). Inorganic carbon fixation and organic carbon excretion rates (C_{fix} and C_{exc}, respectively; pg C [cell h]$^{-1}$) were calculated according to Brading et al. (2013) as follows:

$$C_{fix\,(exc)} = \frac{DPM_{sample} - DPM_{T0}}{DPM_{100\%}} \times \frac{Volume_{100\%}}{Volume_{sample}} \times \frac{DIC}{t} \quad \text{[Eq. 1]}$$

Where the subscripts "sample", "T0" and "100%" refer to the sample, the initial measurement at the start of the incubation and the total activity count respectively; *t* is the incubation time, in hours (see Supplementary Methods for details and Tables S2.15 and S2.16 for results). From these values, gross primary production (GPC – as per Halsey and Jones 2015) was calculated as the sum of C_{fix} and C_{exc} (Table 2.2).

Table 2.2. Abbreviations and their definitions and units used throughout the main text.

Abbreviation	Definition	Unit
Ci	Inorganic Carbon	N/A
eDOC	External dissolved organic Carbon	N/A
iDOC	Internal Dissolved Organic Carbon	N/A
Chl*a*	Chlorophyll-*a*	N/A
μ	Growth rate	d^{-1}
POC	Particulate Organic Carbon (POC + iDOC)	pg C cell^{-1}
C_{fix}	Rate of inorganic carbon fixation	pg C (cell h)$^{-1}$
C_{exc}	Rate of organic carbon excretion as eDOC production	pg C (cell h)$^{-1}$
GPC	Gross Carbon Production (C_{fix} + C_{exc})	pg C (cell h)$^{-1}$
$\%C_{fix}$	Fraction of GPC retained in the cell (C_{fix}/GPC × 100)	%
$\%C_{exc}$	Fraction of GPC excreted in the media (C_{exc}/GPC × 100)	%
NPC	Net Carbon Production ([μ × POC] / 12)	pg C (cell h)$^{-1}$
DIC	Dissolved Inorganic Carbon	μM

2.3.4. Organic carbon content analysis

Particulate organic carbon (POC) per cell was determined following a slightly modified protocol of Brading et al. (2013). Specifically, aliquots of 3 mL were passed through pre-combusted GF/F filters then immediately snap-frozen in liquid nitrogen. Filters were then placed in 20 mL borosilicate vials, acidified with 200 µL HCl (6 M) to remove residual Ci, and then vacuum oven-dried at 60°C for 24 h. POC was determined using a TruMac CN Analyser (Leco, Castle Hill, Australia) against an EDTA calibration standard, and subsequently normalised to cell density, yielding pg C cell^{-1} and pg N cell^{-1}, respectively. The POC accumulation rate, or net carbon production (NPC – as per Halsey and Jones 2015) often considered as a rate of primary productivity (Sackett et al. 2016), was then calculated as follows:

$$\mathrm{NPC} = \frac{\mu \times POC}{12} \qquad \text{[Eq. 2]}$$

Where NPC represents the photosynthetically fixed carbon that is used for the duration of a cell cycle (pg C [cell h]$^{-1}$), µ is the specific growth rate (d^{-1}), and 12 accounts for the hours of daylight during the incubator photoperiod for CO_2 uptake. Nitrogen and chlorophyll content were additionally measured (see Supplementary Methods) to determine their ratios to carbon (see Supplementary Figure S2.3).

2.3.5. Statistical analysis

Statistical analyses on biological replicates ($n = 3$) were performed using SPSS Statistics (version 24, IBM, Armonk, NY, USA) to assess for variance in growth rates, cell volumes, C_{fix}, C_{exc}, $\%C_{exc}$, and NPC between isolates of the same genus. When data met assumptions of normality (Shapiro-Wilk test), but not homoscedasticity (Levene's homogeneity test), a Welch's ANOVA combined with Games-Howell post-hoc tests of unequal variances were performed (used on sub-optimal temperature growth dataset). When

neither normality nor homoscedasticity assumptions were met, the non-parametric Kruskal-Wallis test combined with Dunn-Bonferroni post-hoc pairwise comparisons were used (used for the screening dataset and the study of PCA outputs). Spearman's rank-order correlation was used to examine for co-variance between $\%C_{exc}$ (or $\%C_{fix}$) and cell volume. Linear regression analysis and Pearson's product-moment correlation were used to examine covariance between cell volume and growth rates, and between GPC and NPC. For all statistical tests, alpha (α) was set to 0.05. A principal component analysis (PCA) across the 23 different isolates was performed using RStudio (version 0.99.903, Boston, MA, USA) and the FactoMineR package (Lê et al. 2008), based on the parameters of NPC, cell volume, C_{fix}, and C_{exc}. This integrative approach aimed to identify potential functional groups and visually represented using the PRIMER-e PCA module (version 6, Auckland, New Zealand). The first two components of the PCA were selected for the representation with the generalised cross-validation approximation (Josse and Husson 2012).

2.4. Results

2.4.1. Variability of Ci assimilation across isolates

Under steady state growth at 26°C, growth (division) rates generally varied only two-fold across the 23 Symbiodiniaceae isolates, 0.24-0.49 d^{-1}, with only C1-Hetero-W (0.216 ± 0.008 (mean ± standard error) d^{-1}) and C1-SCF124 (0.222 ± 0.009 d^{-1}) growing slower than F1-UTS-C (0.720 ± 0.073 d^{-1}) (Supplementary Tables S2.1 and S2.2). In contrast, mean cell-normalised GPC (C_{fix} + C_{exc}) rates varied four-fold (Figure 2.2a; Supplementary Table S2.3), from 0.63 ± 0.13 pg C (cell h)$^{-1}$ (D1a-3408) to 3.16 ± 0.37 pg C (cell h)$^{-1}$ (A2-185), but were not statistically different across isolates. All isolates within the genera *Cladocopium* and *Fugacium* maintained remarkably conserved GPC rates, with 1.61 ± 0.04 –

1.85 ± 0.12 pg C (cell h)$^{-1}$. Thus, overall no phylogenetic trends were observed in GPC rates amongst Symbiodiniaceae.

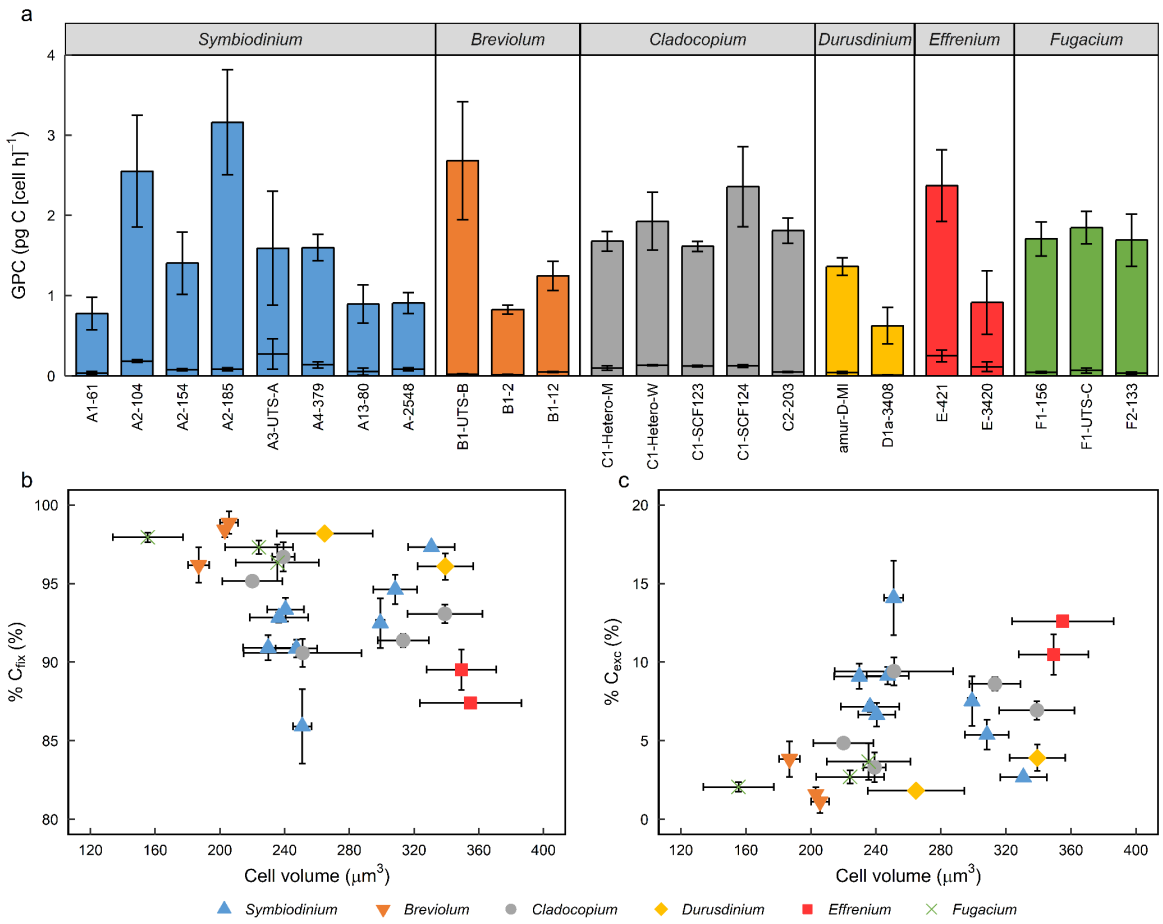

Figure 2.2. Carbon fluxes (as ^{14}C) occurring within the 23 Symbiodiniaceae isolates after 1h of photosynthesis at 26°C. Data shown is the mean (n = 3) ± standard deviation for each Symbiodiniaceae isolate. Isolates are grouped by genus; *Symbiodinium* (blue), *Breviolum* (orange), *Cladocopium* (grey), *Durusdinium* (yellow), *Effrenium* (red), and *Fugacium* (green). **(a)** The gross carbon production (GPC) rates (pg C [cell h]$^{-1}$), where the upper bar is the rate of inorganic carbon fixation (C_{fix}) and the lower bar is the rate of organic carbon excretion in the media (as eDOC, C_{exc}). Relationships between the cell volume (µm^3) and **(b)** the percentage (%C_{fix}) of GPC retained in the cell (i.e. C_{fix}/GPC × 100); and **(c)** the percentage (%C_{exc}) of GPC excreted in the media (i.e. C_{exc}/GPC × 100).

Most GPC was measured as the POC fraction (%C_{fix} = C_{fix} / [C_{fix} + C_{exc}] × 100), and not DOC fraction, and hence retained by the cells (85.91 ± 2.37 – 98.87 ± 0.72%). Values of C_{exc} were generally higher for isolates of *Symbiodinium*, *Cladocopium* and *Effrenium* (combined range for the three genera 0.04 ± 0.02 – 0.27 ± 0.19 pg C [cell h]$^{-1}$) than *Breviolum*,

Durusdinium and *Fugacium* (combined range for the three genera 0.01 ± 0.01 – 0.07 ± 0.03 pg C [cell h]$^{-1}$), but only C_{exc} for *E. voratum* (E-421; 0.25 ± 0.07 pg C [cell h]$^{-1}$) was higher (Supplementary Table S2.2) than *D. trenchii* (D1a-3408, 0.01 ± 0.01 pg C [cell h]$^{-1}$). Cell volumes exhibited a wide range across all isolates (from a minimum of 155.47 ± 21.71 µm^3 for F2-133 (*Fugacium* sp.) to a maximum of 354.90 ± 31.29 µm^3 for E-3420 (*E. voratum*) (Supplementary Tables S2.1 and S2.2). While cell volume is known to influence cell-normalised Ci uptake rates in microalgae (Popp et al. 1998), variability of cell-normalised Ci uptake rates amongst the Symbiodiniaceae isolates here did not correlate with cell volume (Supplementary Figure S2.2). In contrast, $\%C_{fix}$ or $\%C_{exc}$ ($\%C_{exc} = C_{exc} / [C_{fix} + C_{exc}] \times 100$) were negatively and positively correlated with cell volume, respectively ($r_S(67) = -0.446$ and 0.446, $P < 0.001$) (Figure 2.2b). Thus, isolates generally retained less carbon within cells (and excreted more) as cell volume increased and hence the surface area-to-volume ratio decreased.

In comparison to GPC, NPC characterises longer-term carbon uptake and retention by the cell and was similar across isolates in this study (Figure 2.3a). Surprisingly, in comparing GPC with NPC (Figure 2.3b), carbon uptake rates were always higher (by 17-106%) for NPC than GPC. The GPC:NPC ratio was lowest for D1a-3408 (0.15) and highest for C1-SCF124 (1.16), but there was no significant correlation between GPC and NPC across the entire dataset ($r_S(67) = 0.143$, $P = 0.240$), suggesting highly variable conversion of GPC to NPC amongst isolates. In fact, only 4.4% of the variation in GPC could be explained by that in NPC ($R^2 = 0.044$, $F_{(2.67)}$, $P = 0.083$) (Supplementary Table S2.4).

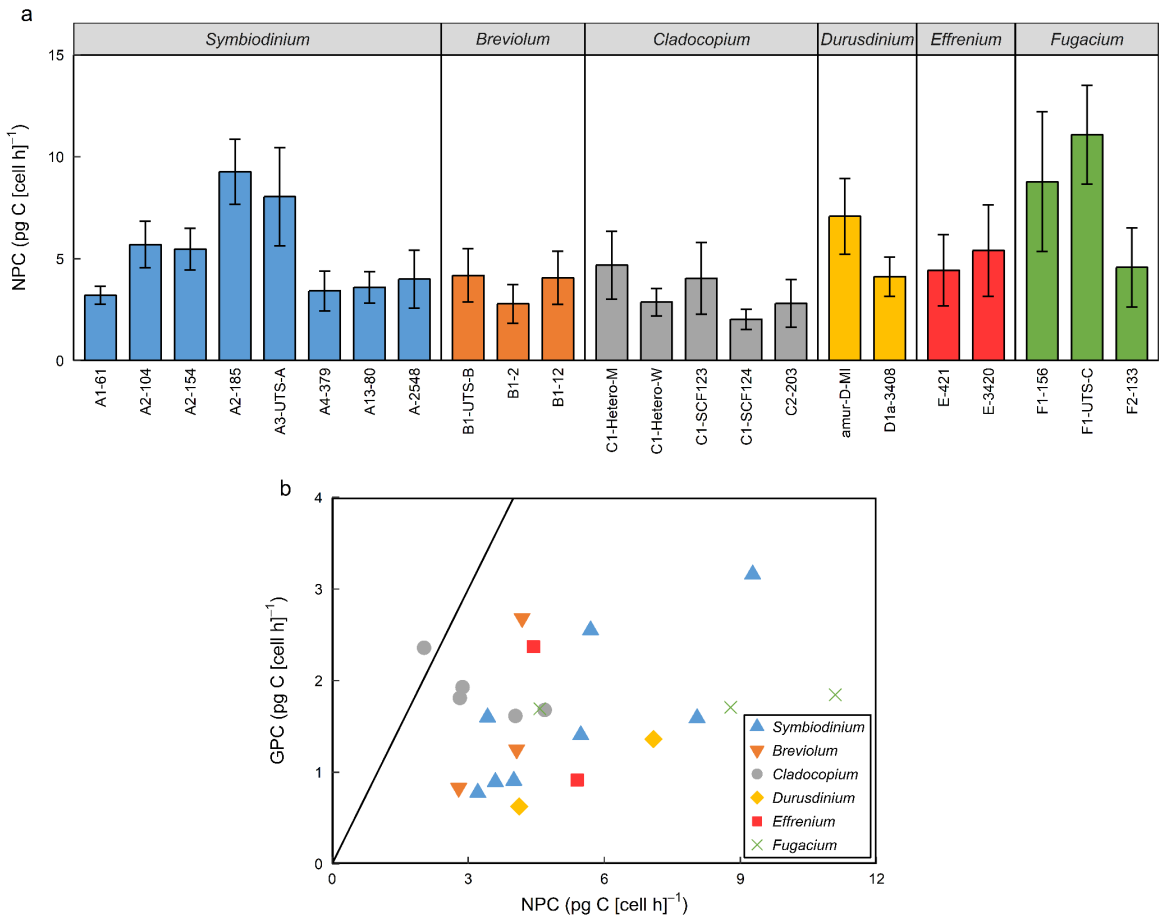

Figure 2.3. Carbon productivity of the 23 Symbiodiniaceae isolates grown at 26°C. Data shown is the mean (n = 3) ± standard deviation for each Symbiodiniaceae isolate. Isolates are grouped by genus; *Symbiodinium* (blue), *Breviolum* (orange), *Cladocopium* (grey), *Durusdinium* (yellow), *Effrenium* (red), and *Fugacium* (green). **(a)** The net carbon production (NPC), as the product of particulate organic carbon (POC) and growth rate, normalised per illumination time (12h). **(b)** Relationship between gross carbon production (GPC) and NPC, where the black line represents the 1:1 ratio between the two variables. Each dot represents the mean (n = 3) data of one isolate. Error bars were not shown for clarity of the representation but can be found in the Supplementary Table S2.3.

We next conducted a PCA of key measured carbon parameters (NPC, cell volume, C_{fix}, and C_{exc}) to identify whether functional groups could be identified based on potential trade-offs in Ci incorporation amongst growth, C_{fix}, and C_{exc} (Figure 2.4). From this, the first principle component, comprising C_{fix} and C_{exc} (Supplementary Table S2.5) contributed to 43.6% of the observed differences between genera. Samples for *Breviolum* were separated from those for *Effrenium* for this first component, with the greatest separation between isolates B1-2 and E-

421 (Supplementary Table S2.6). The second principle component explained 27.3% of the differences between genera, largely from NPC and C_{exc} (Supplementary Table S2.5), where *Fugacium* was separate from *Symbiodinium, Cladocopium* and *Effrenium*, and with isolates E-421 and F1-156 driving these differences (Supplementary Table S2.6). Isolates from the genus *Breviolum*, *Cladocopium* and *Effrenium* were not grouped following hierarchical clustering based on their Euclidean distance.

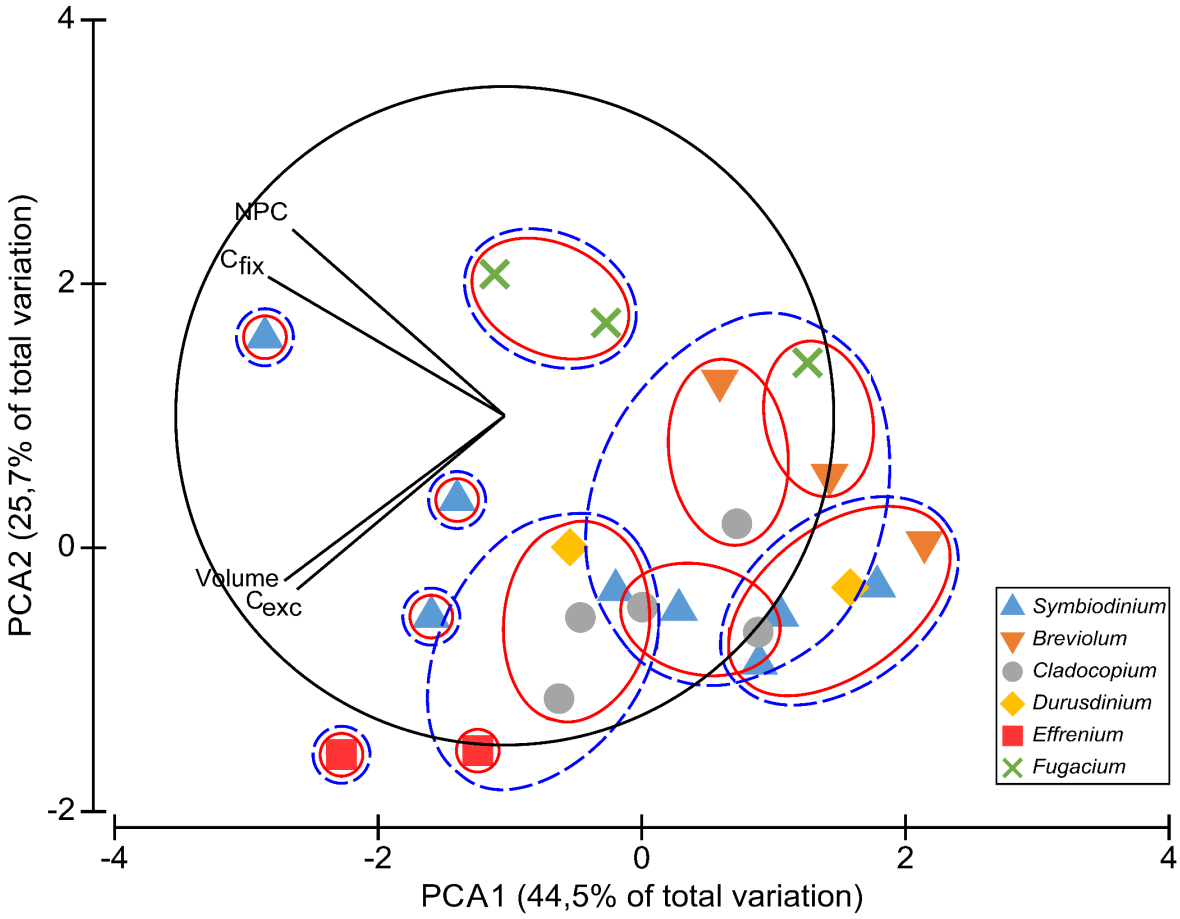

Figure 2.4. Functional groupings based on measured factors associated with inorganic carbon uptake and utilisation (cell volume, C_{fix}, C_{exc} and NPC) across all 23 Symbiodiniaceae isolates grown at 26°C. Cluster analysis and principal component analysis (PCA) were performed on the average of each variable (n = 3) per isolate. Axes X and Y represent the first and second component of the PCA, respectively. Similarity at 95% level is shown at the 1.5 (red line) and 2 (dashed blue line) Euclidean distance levels, and vectors driving the clustering are shown in black. Isolates are grouped by genus for clarity; *Symbiodinium* (blue), *Breviolum* (orange), *Cladocopium* (grey), *Durusdinium* (yellow), *Effrenium* (red), and *Fugacium* (green).

2.4.2. Effect of sub-optimal growth temperature on Ci assimilation

Subsequent Ci analysis of the three isolates (C1-SCF124, amur-D-MI, E-421) grown at 20°C and 30°C in addition to 26°C demonstrated taxon-specific differences in growth temperature performance. Growth rates were equivalent at 20ºC-26°C (0.205 ± 0.009 to 0.289 ± 0.039) but substantially reduced at 30ºC (0.002 ± 0.003 to 0.069 ± 0.007) for both C1-SCF124 and E-421 (Figure. 2.5a; Supplementary Table S2.7). In contrast, whilst growth was arrested entirely at 20°C for amur-D-MI, growth at 26°C (0.353 ± 0.025) was higher than at 30°C (0.096 ± 0.010) (Supplementary Table S2.8). Thus, growth was optimum (based on the three temperatures tested) at 26°C but generally sustained under warmer (amur-D-MI, E-421) and cooler (C1-SCF124, E-421) temperatures. Cell volumes were almost always larger for isolates exhibiting reduced growth rates. Notably, cell volume (Figure 2.5b) of C1-SCF124 was larger (Supplementary Tables S2.7 and S2.8) at 30°C (477 ± 3 μm^3) than at 26°C (220 ± 18 μm^3), of amur-D-MI was increased by 330% at 20°C (1121 ± 95 μm^3) compared to 26°C (339 ± 14 μm^3), and of E-421 was larger at 30°C (883 ± 63 μm^3) compared to 26°C (349 ± 21 μm^3). Higher cell volumes corresponded to a lower growth rate (Figure. 2.5a), with the two variables negatively correlated ($r = -0.643$, $n = 27$, $P < 0.001$) (Supplementary Table S2.9).

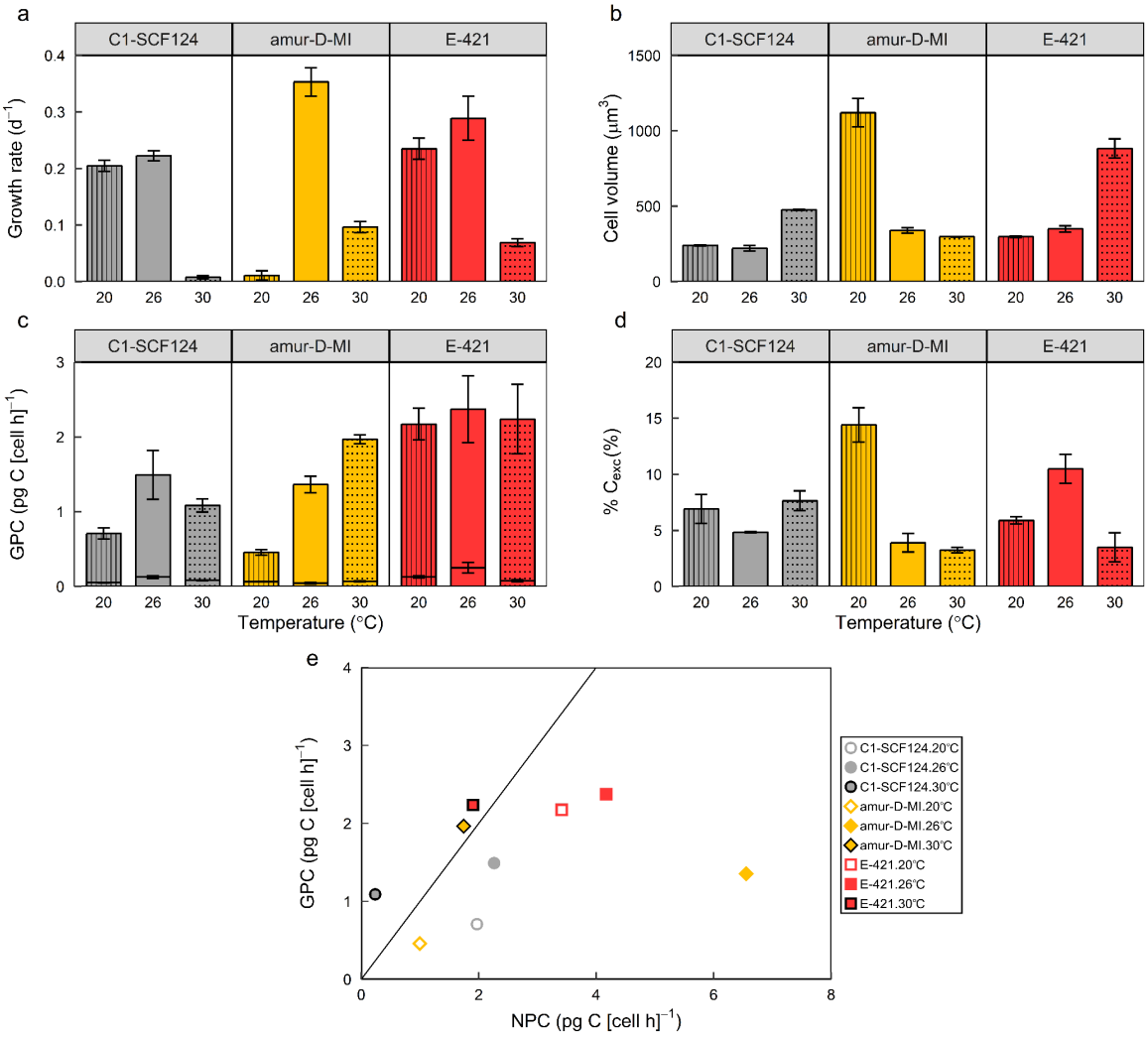

Figure 2.5. Physiological parameters of the Symbiodiniaceae *Cladocopium* (C1-SCF124), *Durusdinium* (amur-D-MI) and *Effrenium* (E-421) isolates grown at 20°C, 26°C and 30°C. Data shown is the mean (n = 3) ± standard deviation for each Symbiodiniaceae isolate. Isolates and temperatures of growth are represented as: C1-SCF124 (grey), amur-D-MI (yellow), E-421 (red), 20°C (vertical hatches), 26°C (plain bars), and 30°C (dotted bars). **(a)** Growth rates (d^{-1}) of the three isolates. **(b)** Cell volumes (μm^3) of the three isolates. **(c)** Gross carbon production (GPC) rates (pg C [cell h]$^{-1}$), where the upper bar is the rate of inorganic carbon fixation (C_{fix}) and the lower bar is the rate of organic carbon excretion in the media (as eDOC, C_{exc}). **(d)** Percentage (%C_{exc}) of GPC excreted in the media (i.e. C_{exc}/GPC × 100). **(e)** Relationship between gross and net carbon production (respectively GPC and NPC; pg C [cell h]$^{-1}$), where the black line represents the 1:1 ratio between GPC and NPC. Each dot represents the mean (n = 3) data of one isolate grown at one temperature: 20°C (white-centre shapes), 26°C (regular shapes), and 30°C (black-bordered shapes). Error bars are not shown for clarity but are provided in Supplementary Table S2.10.

Taxon-specific differences in GPC across temperatures were also observed, but with patterns that were not the same as those for growth rate (Figure 2.5a and 2.5c; Supplementary Table S2.8 and S2.10); here, GPC increased with temperature for amur-D-MI, from 0.391 ± 0.037 pg C (cell h)$^{-1}$ at 20°C to 1.899 ± 0.061 pg C (cell h)$^{-1}$ at 30°C. The $\%C_{exc}$ for amur-D-MI cells grown at 20°C (14.41 ± 1.52%; Figure. 2.5d) was higher than the cells grown at both 26°C (3.91 ± 0.84%) and 30°C (3.25 ± 0.24%; Supplementary Table S2.8). For this isolate, $\%C_{exc}$ was positively correlated with cell volume ($r_S(7) = 0.783$, $P = 0.013$). Indeed, the cells grown at 20°C were the largest and had the highest $\%C_{exc}$, and the cells grown at 30°C were the smallest (297 ± 1 μm^3) and presented the lowest $\%C_{exc}$. Conversely, this trend was reversed for E-421, where the cells grown at 30°C were the largest and had the lowest $\%C_{exc}$ (3.50 ± 1.30%), and the cells grown at 20°C and 26°C were smaller (297 ± 4 μm^3 and 349 ± 21 μm^3, respectively) and presented a higher $\%C_{exc}$ (5.90 ± 0.32% and 10.48 ± 1.28%, respectively). However, cell volume and $\%C_{exc}$ were not correlated for the isolate E-421 ($r_S(7) = -0.450$, $P = 0.224$).

Further comparison of GPC with NPC (Figure 2.5e) for the three isolates grown at 20°C, 26°C and 30°C, revealed a very different outcome to that observed for all isolates under only 26°C (Figure 2.3b). For all isolates grown at 30°C, values of GPC were higher than their corresponding values of NPC, and subsequently had GPC:NPC > 1 , ranging from 1.13 to 5.52. All the other isolates grown at 20°C and 26°C had ratios ranging from 0.21 to 0.66. Thus, GPC remained closely coupled to NPC for all isolates at high temperature.

Finally, PCA analysis demonstrated that amongst the studied variables (NPC, cell volume, C_{fix}, and C_{exc}), C_{fix} and NPC better explained the first and second component, respectively (Supplementary Table S2.11). Overall, samples at their growth optima clustered together (Figure 2.6; 26°C for C1-SCF124, 30°C for amur-D-MI and 20°C for E-421). Samples under sub-optimum growth temperatures did not adhere to any specific clustering pattern, with

C1-SCF124 exhibiting a relatively conserved response for 20 and 30°C (Supplementary Table S2.12).

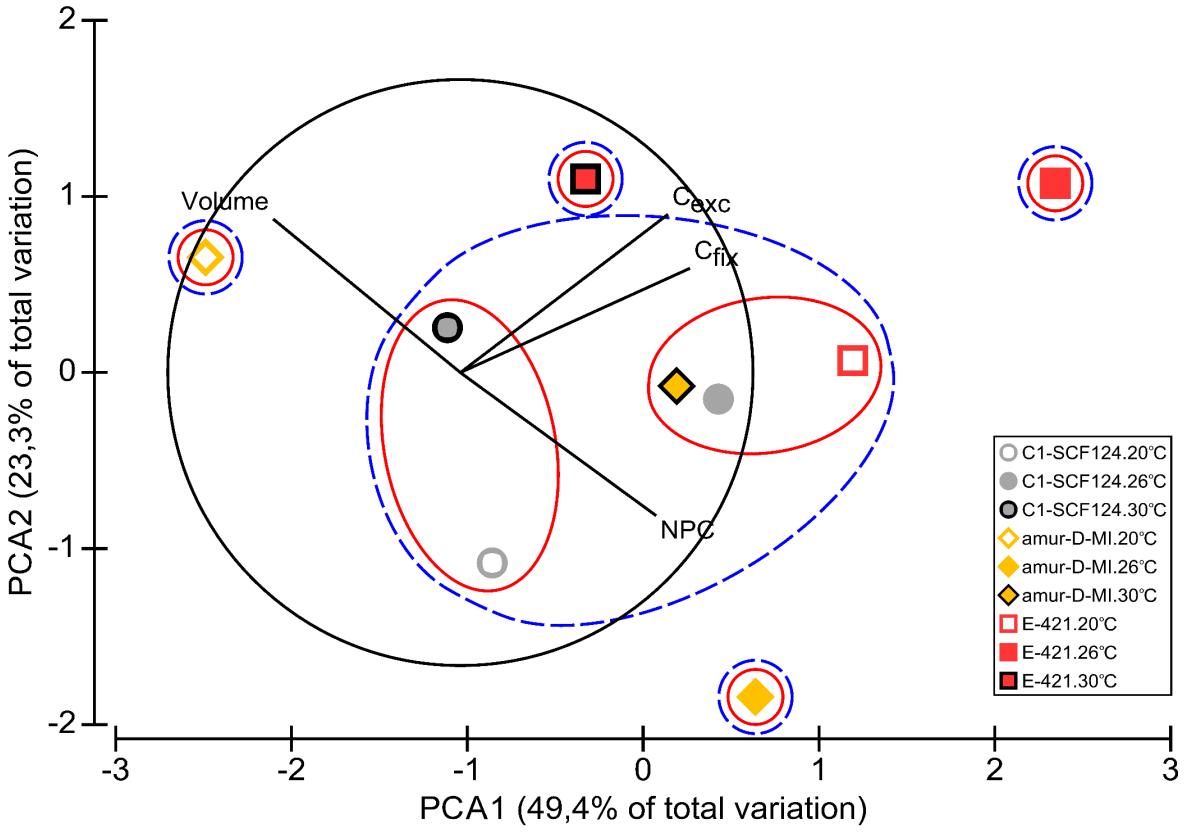

Figure 2.6. Functional groupings based on measured factors associated with inorganic carbon uptake and utilisation (cell volume, C_{fix}, C_{exc} and NPC) of the Symbiodiniaceae *Cladocopium* (C1-SCF124), *Durusdinium* (amur-D-MI) and *Effrenium* (E-421) isolates grown at 20°C, 26°C and 30°C. Cluster analysis and principal component analysis (PCA) were performed on the average of each variable (n = 3) per isolate. Axes X and Y represent the first and second components of the PCA, respectively. Similarity at 95% level is shown at the 1.5 (red line) and 2 (dashed blue line) Euclidean distance levels, and vectors driving the clustering are shown in black. Isolates and temperatures of growth are represented as: C1-SCF124 (grey), amur-D-MI (yellow), E-421 (red), 20°C (white-centre shapes), 26°C (regular shapes), and 30°C (black-bordered shapes).

2.5. Discussion

2.5.1. Patterns of Ci assimilation are not explained by Symbiodiniaceae phylogeny

In contrast to rapidly growing knowledge of Symbiodiniaceae phylogenetic (taxonomic) diversity (LaJeunesse et al. 2018), functional diversity of fundamental physiological properties that ultimately determine the ecological success of these algae remains largely unresolved (Suggett et al. 2017). This is particularly true for factors governing the acquisition and utilisation of Ci, which fuels symbiont photosynthesis (Warner and Suggett 2016; Suggett et al. 2017). A recent analysis of functional diversity of light harvesting strategies of photosynthesis revealed that algal isolates maintained in long-term cultures persisted as low-light and high-light adapted ecotypes, broadly (but not exclusively) separated by genus (Suggett et al. 2015). Our examination of 23 phylogenetically-distinct algal isolates spanning six genera using standardised Ci uptake and incorporation methods did not observe any such groupings by phylogeny. Such lack of functional grouping for traits associated with "dark reactions" (i.e. carbon reactions) of photosynthesis suggests that these isolates may actively employ diverse physiological processes to overcome evolutionary constraints imposed on Ci uptake and incorporation (Brading et al. 2011, 2013; Suggett et al. 2017) compared to light-harvesting.

Of all physiological variables examined, only differences in cell volume explained some the isolate-wide Ci responses. Whilst previous studies on phytoplankton have noted that increasing surface area-to-volume results in more cell content leakage (Irwin et al. 2006), dinoflagellate cells in our study retained less ($\%C_{fix}$) and excreted more ($\%C_{exc}$) fixed carbon as cell volume increased (i.e. a decrease in surface area-to-volume ratio). In this case, observed eDOC is therefore more likely representative of active excretion rather than passive leakage

that is thought to arise from higher surface area-to-volume ratios (Kriest and Oschlies 2007; Thornton 2014). Cell volume did not show any effect on C_{fix}, supporting previous observations of different strategies of Ci uptake that are independent of cell volume amongst Symbiodiniaceae (see also Brading et al. 2011). Given that Ci fixation does not appear subject to allometric scaling constraints that govern light-harvesting for Symbiodiniaceae (Suggett et al. 2015), the efficiency of mechanisms involved in acquisition and utilisation of Ci, e.g. CCM capacity and carbonic anhydrase (CA) activity (Brading et al. 2013), and presumably RuBisCO activity turnover rates (Lilley et al. 2010), are likely highly variable between isolates.

An unexpected outcome of this study was the observation that NPC was approximately three-fold higher than GPC when averaged across all isolates (i.e. GPC:NPC <1), a finding that contradicts reported GPC:NPC values for other key phytoplankton groups (ranging from 1.2 – 7.0, Halsey and Jones 2015) – although notably no dinoflagellate representatives were included within the Halsey and Jones (2015) data set. Our values are, however, consistent with the sole study of ^{14}C metabolism in cultured Symbiodiniaceae to date reporting parameters necessary to establish GPC:NPC ratios (Brading et al. 2013) that, based on their reported values of growth rate, POC or ^{14}C-uptake, observed a GPC:NPC ratio of 0.36 for the isolate A13-80 (Table 2.3). This outcome is intriguing since NPC is usually defined as GPC minus dark respiration, light-enhanced respiration and photorespiration (Halsey an Jones, 2015); thus GPC:NPC values <1 suggest presence of either: i) non-photosynthetic supplementation of carbon used for growth, or ii) bias in methodological determination of either μ, POC or ^{14}C-uptake, or iii) a combination of both. We discuss potential contributions of heterotrophy and methodology in driving such low observed GPC:NPC ratios to ask the important question, is this a genuine biological response common to Symbiodiniaceae or rather due to an artefact(s) in methodology?

Table 2.3. Comparison of carbon fluxes and productivity characteristics between Symbiodiniaceae from the genus *Symbiodinium* previously studied in Brading et al. (2013) and those from the present study (shown in bold). Data is the mean (n = 4 and n = 3, respectively; and the row "All" are the average values of all the 23 Symbiodiniaceae isolates from the present study.) of growth rate (μ, d^{-1}), particulate organic carbon content (POC, pg C $cell^{-1}$), gross carbon production (GPC, as ^{14}C fixed (pg C [cell h]$^{-1}$), net carbon production (NPC, as μ × POC (pg C [cell h]$^{-1}$) and GPC:NPC (dimensionless).

Reference	Organism	Isolate	μ	POC	GPC	NPC	GPC:NPC
Brading et al. (2013)	*Symbiodinium* sp.	A20	0.425	358	3.288	10.868	0.303
	S. necroappetens	A13-80	0.287	111	0.814	2.276	0.358
Present study	*S. necroappetens*	**A13-80**	**0.298**	**145**	**0.894**	**3.597**	**0.249**
	Symbiodiniaceae	**All**	**0.356**	**167**	**1.633**	**5.030**	**0.378**

Some algae within the Symbiodiniaceae routinely source organic carbon through osmotrophy (Xiang et al. 2013) and through direct feeding upon bacteria (Jeong et al. 2012) – the latter of which are both abundant and diverse in non-axenic cultures as per those used in this study (Lawson et al. 2018). It is thus highly plausible that the isolates studied here supplemented photosynthetic carbon by bacterial consumption over the duration of our study. Respiratory contributions to energy and reductant driving cellular maintenance and growth fuelled by heterotrophic carbon acquisition could lead to increased NPC (estimated as μ × POC) yet would not affect GPC from short-term ^{14}C-incubations, thus potentially driving GPC:NPC values < 1. Ultimately, as we did not directly quantify heterotrophy, its relative contribution to the total carbon budget, and thus the magnitude of this potential effect on our GPC:NPC ratios are unknown. Importantly, algal (and thus presumably bacterial) densities were similar across isolates at the time of sampling (see Lawson et al. 2018), although possible species-specific differences in heterotrophy should be considered when interpreting GPC:NPC ratios – however to our knowledge no study has examined this to date. Given the low GPC:NPC ratios observed by Brading et al. (2013), and now ours from a wider diversity of Symbiodiniaceae isolates, it is clear that a better understanding of heterotrophic capacity should

be a critical research priority for future studies aiming to definitively close the carbon budget of Symbiodiniaceae.

Our POC, growth rate and hence NPC measurements appear to compare well with previous independently conducted work (Niggl et al. 2009; Brading et al. 2011, 2013; Suggett et al. 2015), and so it is reasonable to assume that none of these measurements is driving significant overestimation of NPC. Therefore, if our GPC:NPC ratios are indeed related to methodology, this would suggest GPC was underestimated during the ^{14}C incubations. Potential pitfalls of the ^{14}C method have been well-documented and mostly relate to the choice of protocol employed (Milligan et al. 2015; Halsey and Jones 2015). Arguably, growth rate dependency of newly-fixed ^{14}C retention when incubations lengths exceed 20 min (Halsey et al. 2011; Pei and Laws 2013; Hughes et al. 2018b), only appears problematic for studies of nutrient-limited cells, which is not the case for our study where isolates were grown under nutrient-replete conditions (IMK media). We therefore propose an alternative explanation:

As with other dinoflagellates, Symbiodiniaceae possess the form II of RuBisCO (Brading et al. 2011, 2013; Roberty et al. 2014), which exhibits poor discrimination between O_2 and CO_2 (Oakley et al. 2014), leading to high photorespiration rates by oxygenase activity (Geider and Osborne 1992) unless mitigated through employment of CCMs (Leggat et al. 1999; Brading et al. 2013). It is plausible that photosynthetic build-up of O_2 within the small incubation chambers used for ^{14}C incubations may have induced transient hyperoxia (thus increasing photorespiration) compared to under usual growth conditions where the volume of media was both larger and had a greater surface area to facilitate gas exchange. As photorespiration leads to fixation of O_2 rather than $^{14}CO_2$ activation of this pathway would be expected to contribute towards underestimation of GPC (Smith and Platt 1984; Lancelot and Mathot 1985). While Symbiodiniaceae do exhibit CCM activity (Leggat et al. 1999; Brading et al. 2013; Oakley et al. 2014), it is not clear how much photorespiration CCMs could

overcome at potentially hyperoxic levels. Whilst we did not measure (photo)respiration in this study, we further compared the GPC:NPC to retrieved data of light-dependent O_2 consumption (Figure 2.7, Supplementary Tables S2.13 and S2.14) for the isolates A1-61 (*Symbiodinium microadriaticum*), A13-80 (*Symbiodinium necroappetens*) and B1-2 (*Breviolum* sp.) from Brading et al. (2011) grown at the same temperature, but at higher light intensity (350 µmol photons m^{-2} s^{-1}), as for our study. Indeed, algal cells with lower values of GPC:NPC exhibit consistently higher O_2 consumption rates (Figure 2.7). Carpenter and Roenneberg (1995) previously reported low values of GPC:NPC in marine phytoplankton communities, and similarly concluded that RuBisCO carboxylase activity was reduced to the profit of oxygenase activity (Li et al. 1980). Importantly, whilst this O_2 consumption can come from light-dependent processes in the chloroplasts and mitochondria (Roberty et al. 2014; Warner and Suggett 2016), heterotrophically derived carbon-fuelled catabolic pathways will particularly enhance NPC (Jeong et al. 2012) and reduce C_{fix} (Jeong et al. 2016). Overall, given that our measurements match well with those of previous work (Brading et al. 2013) and the fact that we have adopted standard ^{14}C protocols (e.g. Hughes et al. 2018b), it therefore seems plausible that such unusually low GPC:NPC may represent a previously unrecognised but conserved biological characteristic of Symbiodiniaceae cultures, however, the key mechanism to explain this (e.g. heterotrophy, photorespiration, etc.) warrants targeted examination in future studies.

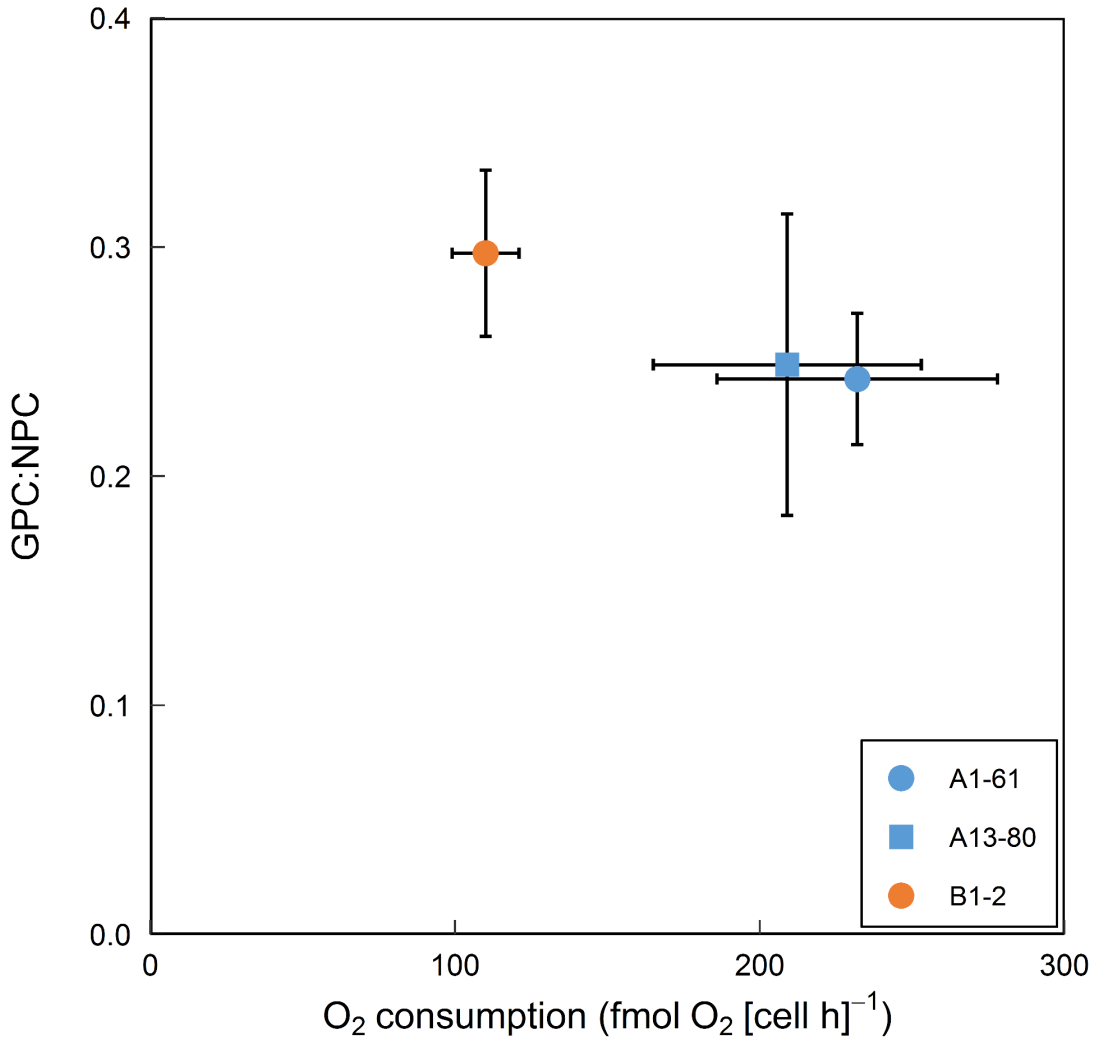

Figure 2.7. Relationship between gross carbon production and net carbon production ratios (GPC:NPC) and O_2 consumption rates (fmol O_2 [cell h]$^{-1}$) for the Symbiodiniaceae *Symbiodinium* (A1-61 and A13-80) and *Breviolum* (B1-2) isolates grown at 26°C. Data shown is the mean (n = 3) ± standard deviation for each Symbiodiniaceae isolate. GPC:NPC ratios are calculated from the present study, whilst O_2 consumption rates are retrieved from Brading et al. (2011). The linear relationship between the two sets of variables is described by the equation GPC:NPC = (- 0.000461 × O_2 consumption rate) + 0.347. $R^2 = 0.996$, $P = 0.039$ (see Supplementary Table S2.14).

2.5.2. Symbiodiniaceae functional diversity is driven by their growth environments

No distinct functional groupings were observed based on the Ci parameters of C_{fix}, C_{exc}, NPC, and cell volume amongst isolates all grown under 26°C. However, whether long term maintenance as cultures impacts culture-based evolution of Symbiodiniaceae functioning (e.g. Chakravarti et al. 2017) differently for light harvesting *versus* Ci-uptake pathways, and hence explains why functional groups are seen for light but not dark reactions, remains to be explored. In contrast, we observed different functional patterns for Ci acquisition and growth amongst three key Symbiodiniaceae isolates (C1-SCF124, amur-D-MI, and E-421) when grown at different temperatures (20°C, 26°C, and 30°C), suggesting that the concept of functional diversity for Ci acquisition amongst Symbiodiniaceae may be primarily driven by the short-term local environment rather than evolutionary separation of function. This suggests that evolutionary pathways and Ci uptake capacity may be reasonably well-conserved. Indeed, it is known that temperature regulates Symbiodiniaceae photosynthetic "strategies" (Robison and Warner 2006; Diaz-Almeyda et al. 2017; Goyen et al. 2017) and plays a major role in determining how effective cells are at acquiring and utilising Ci (Lesser 1996; Oakley et al. 2014). The differences in physiology we noted under sub-optimal growth conditions appear to reflect alternate inherent temperature optima (e.g. Klueter et al. 2017), 26°C for C1-SCF124, 30°C for amur-D-MI, and 20°C for E-421.

Variability in Ci uptake and/or C-excretion rates between taxa were only apparent when isolates were subjected to temperatures sub-optimum for growth. Such variability may indicate that cellular adjustment to environmental perturbation predominately relies on regulation of upstream photosynthetic pathways such as light-harvesting and non-photochemical quenching, rather than those associated with downstream carbon reactions. Even so, C_{fix} was not impaired

for Symbiodiniaceae under elevated temperatures, which is consistent with previous studies suggesting primarily that algal CCM activity is sustained during sub-optimum growth (or "stress") (Oakley et al. 2014). However, Graham et al. (2015) demonstrated reduced CA activity of Symbiodiniaceae *in hospite* in response to thermal stress, which could reflect that C_{fix} under some instances is affected by impairment (or slowing) of the carboxylation potential within the Calvin Cycle (Jones et al. 1998), and specifically RuBisCO (Lilley et al. 2010). In order to increase the clustering resolution of functional groups, knowledge of other parameters involved in Ci uptake (activity of CA or RuBisCO) or photosynthate excretion (response to the presence of host release factor) pathways may therefore be required to capture alternate "strategies" of carbon acquisition, as has been demonstrated for light absorption and utilisation pathways (Suggett et al. 2015) and ROS-antioxidant production (Goyen et al. 2017). Whereas the isolates here did not cluster according to phylogeny based on Ci uptake and incorporation, functional groupings were notably distinct from those recently generated for light reactions (Suggett et al. 2015; Goyen et al. 2017). Consequently, our results would suggest that any functional divergence is driven by assessing their response to environmental stressors, such as light and temperature.

2.6. Conclusion

Direct Ci fixation measurements are a useful tool to benchmark carbon fate in Symbiodiniaceae, and most importantly to study the rates of excretion of organic photosynthates that could ultimately be translocated to the coral host. However, results obtained from *ex hospite* studies should be interpreted with care when extrapolating to *in hospite* situations, where growth, Ci fixation and loss can be substantially different. We have shown for the first time that Ci uptake and excretion rates were highly conserved across 23 Symbiodiniaceae isolates under the same growth condition but were not for the same isolate

when grown under sub-optimum growth temperature. As such, functional groupings of Ci "strategy" – based on the few key descriptors we employed here – are mostly driven by growth environment and not genus diversity. Thus, how Symbiodiniaceae respond to changing environments is likely heavily governed by upstream processes related to photosynthesis, such as effectiveness of light harvesting and non-photochemical quenching, instead of downstream Ci uptake, assimilation and excretion. Major advances are still required in understanding plasticity in the metabolic network with which carbon is acquired and incorporated into these dinoflagellates, not only through the metabolic wiring available (e.g. the potentially over-arching regulatory role of photorespiration) but also how heterotrophy may be a key surrogate in meeting energetic demands.

2.7. Acknowledgements

The authors would like to thank Paul Brooks for technical assistance in setting up incubation and growth experiments, Matthew Nitschke and Jörg Frommlet for providing Symbiodiniaceae isolates, Lochlan de Beyer and Joel Burke for maintaining the Symbiodiniaceae culture collection, and Susan Fenech for her assistance with the imaging microscope and the TCN analyser. Contribution of DJS was supported by an Australian Research Council Future Fellowship (FT130100202), and MR, EFC, and DJH through ARC Discovery Grants (DP160100271 to WL and DJS; DP180100074 to DJS).

2.8. References

Aihara, Y., S. Takahashi and J. Minagawa. 2016. Heat induction of cyclic electron flow around photosystem I in the symbiotic dinoflagellate *Symbiodinium*. Plant Physiol. **171**: 522-529. doi:10.1104/pp.15.01886

Allemand, D., P. Furla and S. Bénazet-Tambutté. 1998. Mechanisms of carbon acquisition for endosymbiont photosynthesis in Anthozoa. Can. J. Bot. **76**: 925-941. doi:10.1139/b98-086

Al-Moghrabi, S., C. Goiran, D. Allemand, N. Speziale and J. Jaubert. 1996. Inorganic carbon uptake for photosynthesis by the symbiotic coral-dinoflagellate association II. Mechanisms for bicarbonate uptake. J. Exp. Mar. Biol. Ecol. **199**: 227-248. doi:10.1016/0022-0981(95)00202-2

Aranda, M., and others. 2016. Genomes of coral dinoflagellate symbionts highlight evolutionary adaptations conducive to a symbiotic lifestyle. Sci. Rep. **6**: 39734. doi:10.1038/srep39734

Baker, D. M., C. J. Freeman, J. C. Y. Wong, M. L. Fogel and N. Knowlton. 2018. Climate change promotes parasitism in a coral symbiosis. ISME J. **12**: 921-930. doi:10.1038/s41396-018-0046-8

Berges, J. A., D. J. Franklin and P. J. Harrison. 2002. Evolution of an artificial seawater medium: Improvements in enriched seawater, artificial water over the last two decades. J. Phycol. **37**: 1138-1145. doi:10.1046/j.1529-8817.2001.01052.x

Brading, P., M. E. Warner, P. Davey, D. J. Smith, E. P. Achterberg and D. J. Suggett. 2011. Differential effects of ocean acidification on growth and photosynthesis among phylotypes of *Symbiodinium* (Dinophyceae). Limnol. Oceanogr. **56**: 927-938. doi:10.4319/lo.2011.56.3.0927

Brading, P., M. E. Warner, D. J. Smith and D. J. Suggett. 2013. Contrasting modes of inorganic carbon acquisition amongst *Symbiodinium* (Dinophyceae) phylotypes. New Phytol. **200**: 432-442. doi:10.1111/nph.12379

Camp, E. F., and others. 2020a. Revealing changes in the microbiome of Symbiodiniaceae under thermal stress. Environmental Microbiology.

Carpenter, E. J. and T. Roenneberg. 1995. The marine planktonic cyanobacteria *Trichodesmium* spp.: photosynthetic rate measurements in the SW Atlantic Ocean. Mar. Ecol. Prog. Ser. **118**: 267-273. doi:10.3354/meps118267

Chakravarti, L. J., V. H. Beltran and M. J. H. van Oppen. 2017. Rapid thermal adaptation in photosymbionts of reef-building corals. Glob. Change Biol. **23**: 4675-4688. doi:10.1111/gcb.13702

Colombo-Pallotta, M. F., A. Rodríguez-Román and R. Iglesias-Prieto. 2010. Calcification in bleached and unbleached *Montastraea faveolata*: evaluating the role of oxygen and glycerol. Coral Reefs. **29**: 899-907. doi:10.1007/s00338-010-0638-x

Cooper, T. F., M. Lai, K. E. Ulstrup, S. M. Saunders, G. R. Flematti, B. Radford and M. J. van Oppen. 2011. *Symbiodinium* genotypic and environmental controls on lipids in reef building corals. PLoS One. **6**: e20434. doi:10.1371/journal.pone.0020434

Cunning, R., D. M. Yost, M. L. Guarinello, H. M. Putnam and R. D. Gates. 2015. Variability of *Symbiodinium* communities in waters, sediments, and corals of thermally distinct reef pools in American Samoa. PLoS One. **10**: e0145099. doi:10.1371/journal.pone.0145099

Davy, S. K., D. Allemand and V. M. Weis. 2012. Cell biology of cnidarian-dinoflagellate symbiosis. Microbiol. Mol. Biol. Rev. **76**: 229-261. doi:10.1128/MMBR.05014-11

Diaz-Almeyda, E. M., and others. 2017. Intraspecific and interspecific variation in thermotolerance and photoacclimation in *Symbiodinium* dinoflagellates. Proc. R. Soc. B. **284**: 20171767. doi:10.1098/rspb.2017.1767

Fordyce, A. J., T. D. Ainsworth, S. F. Heron and W. Leggat. 2019. Marine heatwave hotspots in coral reef environments: physical drivers, ecophysiological outcomes, and impact upon structural complexity. Front. Mar. Sci. **6**: 498. doi:10.3389/fmars.2019.00498

Frommlet, J. C., M. L. Sousa, A. Alves, S. I. Vieira, D. J. Suggett and J. Serodio. 2015. Coral symbiotic algae calcify *ex hospite* in partnership with bacteria. Proc. Natl. Acad. Sci. U. S. A. **112**: 6158-6163. doi:10.1073/pnas.1420991112

Fujise, L., M. R. Nitschke, J. C. Frommlet, J. Serodio, S. Woodcock, P. J. Ralph and D. J. Suggett. 2018. Cell cycle dynamics of cultured coral endosymbiotic microalgae (*Symbiodinium*) across different types (species) under alternate light and temperature conditions. J. Eukaryotic Microbiol. **65**: 505-517. doi:10.1111/jeu.12497

Gattuso, J.-P., D. Allemand and M. Frankignoulle. 1999. Photosynthesis and calcification at cellular, organismal and community levels in coral reefs: a review on interactions and control by carbonate chemistry. Am. Zool. **39**: 160-183. doi:10.1093/icb/39.1.160

Goiran, C., S. Al-Moghrabi, D. Allemand and J. Jaubert. 1996. Inorganic carbon uptake for photosynthesis by the symbiotic coral/dinoflagellate association I. Photosynthetic performances of symbionts and dependence on sea water bicarbonate. J. Exp. Mar. Biol. Ecol. **199**: 207-225. doi:10.1016/0022-0981(95)00201-4

Goyen, S., M. Pernice, M. Szabó, M. E. Warner, P. J. Ralph and D. J. Suggett. 2017. A molecular physiology basis for functional diversity of hydrogen peroxide production amongst *Symbiodinium* spp. (Dinophyceae). Mar. Biol. **164**: 46. doi:10.1007/s00227-017-3073-5

Graham, E. R., A. Parekh, R. K. Devassy and R. W. Sanders. 2015. Carbonic anhydrase activity changes in response to increased temperature and pCO_2 in *Symbiodinium*–zoanthid associations. J. Exp. Mar. Biol. Ecol. **473**: 218-226. doi:10.1016/j.jembe.2015.08.017

Grégoire, V., F. Schmacka, M. A. Coffroth and U. Karsten. 2017. Photophysiological and thermal tolerance of various genotypes of the coral endosymbiont *Symbiodinium* sp. (Dinophyceae). J. Appl. Phycol. **29**: 1893-1905. doi:10.1007/s10811-017-1127-1

Halsey, K. H., A. J. Milligan and M. J. Behrenfeld. 2011. Linking time-dependent carbon-fixation efficiencies in *Dunaliella tertiolecta* (Chlorophyceae) to underlying metabolic Pathways. J. Phycol. **47**: 66-76. doi:10.1111/j.1529-8817.2010.00945.x

Halsey, K. H., R. T. O'Malley, J. R. Graff, A. J. Milligan and M. J. Behrenfeld. 2013. A common partitioning strategy for photosynthetic products in evolutionarily distinct phytoplankton species. New Phytol. **198**: 1030-1038. doi:10.1111/nph.12209

Halsey, K. H. and B. M. Jones. 2015. Phytoplankton strategies for photosynthetic energy allocation. Ann. Rev. Mar. Sci. **7**: 265-297. doi:10.1146/annurev-marine-010814-015813

Hennige, S. J., D. J. Suggett, M. E. Warner, K. E. McDougall and D. J. Smith. 2009. Photobiology of *Symbiodinium* revisited: bio-physical and bio-optical signatures. Coral Reefs. **28**: 179-195. doi:10.1007/s00338-008-0444-x

Hillyer, K. E., D. A. Dias, A. Lutz, U. Roessner and S. K. Davy. 2017. Mapping carbon fate during bleaching in a model cnidarian symbiosis: the application of ^{13}C metabolomics. New Phytol. **214**: 1551-1562. doi:10.1111/nph.14515

Hoadley, K. D., D. Rollison, D. T. Pettay and M. E. Warner. 2015. Differential carbon utilization and asexual reproduction under elevated pCO_2 conditions in the model anemone, *Exaiptasia pallida*, hosting different symbionts. Limnol. Oceanogr. **60**: 2108-2120. doi:10.1002/lno.10160

Hoadley, K. D., D. T. Pettay, D. Dodge and M. E. Warner. 2016. Contrasting physiological plasticity in response to environmental stress within different cnidarians and their respective symbionts. Coral Reefs. **35**: 529-542. doi:10.1007/s00338-016-1404-5

Hughes, D. J., and others. 2018a. Roadmaps and detours: active chlorophyll-a assessments of primary productivity across marine and freshwater systems. Environ. Sci. Technol. **52**: 12039-12054. doi:10.1021/acs.est.8b03488

Hughes, D. J., D. Varkey, M. A. Doblin, T. Ingleton, A. McInnes, P. J. Ralph, V. van Dongen-Vogels and D. J. Suggett. 2018b. Impact of nitrogen availability upon the electron requirement for carbon fixation in Australian coastal phytoplankton communities. Limnol. Oceanogr. **63**: 1891-1910. doi:10.1002/lno.10814

Iglesias-Prieto, R., V. H. Beltran, T. C. LaJeunesse, H. Reyes-Bonilla and P. E. Thome. 2004. Different algal symbionts explain the vertical distribution of dominant reef corals in the eastern Pacific. Proc. R. Soc. B. **271**: 1757-1763. doi:10.1098/rspb.2004.2757

Irwin, A. J., Z. V. Finkel, O. M. E. Schofield and P. G. Falkowski. 2006. Scaling-up from nutrient physiology to the size-structure of phytoplankton communities. J. Plankton Res. **28**: 459-471. doi:10.1093/plankt/fbi148

Jeong, H. J., and others. 2012. Heterotrophic feeding as a newly identified survival strategy of the dinoflagellate *Symbiodinium*. Proc. Natl. Acad. Sci. U. S. A. **109**: 12604-12609. doi:10.1073/pnas.1204302109

Jeong, H. J., K. Lee, Y. D. Yoo, J.-M. Kim, T. H. Kim, M. Kim, J.-H. Kim and K. Y. Kim. 2016. Reduction in CO_2 uptake rates of red tide dinoflagellates due to mixotrophy. Algae. **31**: 351-362. doi:10.4490/algae.2016.31.11.17

Jones, R. J., O. Hoegh-Guldberg, A. W. D. Larkum and U. Schreiber. 1998. Temperature-induced bleaching of corals begins with impairment of the CO_2 fixation mechanism in zooxanthellae. Plant, Cell Environ. **21**: 1219-1230. doi:10.1046/j.1365-3040.1998.00345.x

Josse, J. and F. Husson. 2012. Selecting the number of components in principal component analysis using cross-validation approximations. Comput. Stat. Data Anal. **56**: 1869-1879. doi:10.1016/j.csda.2011.11.012

Karim, W., S. Nakaema and M. Hidaka. 2015. Temperature effects on the growth rates and photosynthetic activities of *Symbiodinium* cells. J. Mar. Sci. Eng. **3**: 368-381. doi:10.3390/jmse3020368

Kenkel, C. D. and L. K. Bay. 2018. Exploring mechanisms that affect coral cooperation: symbiont transmission mode, cell density and community composition. PeerJ. **6**: e6047. doi:10.7717/peerj.6047

Klueter, A., J. Trapani, F. I. Archer, S. E. McIlroy and M. A. Coffroth. 2017. Comparative growth rates of cultured marine dinoflagellates in the genus *Symbiodinium* and the effects of temperature and light. PLoS One. **12**: e0187707. doi:10.1371/journal.pone.0187707

Kriest, I. and A. Oschlies. 2007. Modelling the effect of cell-size-dependent nutrient uptake and exudation on phytoplankton size spectra. Deep Sea Res., Part I. **54**: 1593-1618. doi:10.1016/j.dsr.2007.04.017

Krueger, T., J. Bodin, N. Horwitz, C. Loussert-Fonta, A. Sakr, S. Escrig, M. Fine and A. Meibom. 2018. Temperature and feeding induce tissue level changes in autotrophic and heterotrophic nutrient allocation in the coral symbiosis - A NanoSIMS study. Sci. Rep. **8**: 12710. doi:10.1038/s41598-018-31094-1

LaJeunesse, T. C. and R. K. Trench. 2000. Biogeography of two species of *Symbiodinium* (Freudenthal) inhabiting the intertidal sea anemone *Anthopleura elegantissima* (Brandt). Biol. Bull. **199**: 126-134. doi:10.2307/1542872

LaJeunesse, T. C., J. E. Parkinson, P. W. Gabrielson, H. J. Jeong, J. D. Reimer, C. R. Voolstra and S. R. Santos. 2018. Systematic revision of Symbiodiniaceae highlights the antiquity and diversity of coral endosymbionts. Curr. Biol. **28**: 2570-2580 e2576. doi:10.1016/j.cub.2018.07.008

Lancelot, C., Mathot, S. 1985. Biochemical fractionation of primary production by phytoplankton in Belgian coastal waters during short- and long-term incubations with ^{14}C-bicarbonate. Mar. Biol. **86**, 219–226. doi:10.1007/BF00397507

Lawson, C. A., J. B. Raina, T. Kahlke, J. R. Seymour and D. J. Suggett. 2018. Defining the core microbiome of the symbiotic dinoflagellate, *Symbiodinium*. Environ. Microbiol. Rep. **10**: 7-11. doi:10.1111/1758-2229.12599

Lê, S., J. Josse and F. Husson. 2008. FactoMineR: an R package for multivariate analysis. J. Stat. Softw. **25**: 1-18. doi:10.18637/jss.v025.i01

Leggat, W., M. R. Badger and D. Yellowlees. 1999. Evidence for an inorganic carbon-concentrating mechanism in the symbiotic dinoflagellate *Symbiodinium* sp. Plant Physiol. **121**: 1247-1256. doi:10.1104/pp.121.4.1247

Lesser, M. P. 1996. Elevated temperatures and ultraviolet radiation cause oxidative stress and inhibit photosynthesis in symbiotic dinoflagellates. Limnol. Oceanogr. **41**: 271-283. doi:10.4319/lo.1996.41.2.0271

Li, W. K. W., H. E. Glover and I. Morris. 1980. Physiology of carbon photoassimilation by *Oscillatoria thiebautii* in the Caribbean Sea. Limnol. Oceanogr. **25**: 447-456. doi:10.4319/lo.1980.25.3.0447

Lilley, R. M., P. J. Ralph and A. W. Larkum. 2010. The determination of activity of the enzyme Rubisco in cell extracts of the dinoflagellate alga *Symbiodinium* sp. by manganese chemiluminescence and its response to short-term thermal stress of the alga. Plant, Cell Environ. **33**: 995-1004. doi:10.1111/j.1365-3040.2010.02121.x

Loram, J. E., H. G. Trapido-Rosenthal and A. E. Douglas. 2007. Functional significance of genetically different symbiotic algae *Symbiodinium* in a coral reef symbiosis. Mol. Ecol. **16**: 4849-4857. doi:10.1111/j.1365-294X.2007.03491.x

MacIntyre, H. L., T. M. Kana, T. Anning and R. J. Geider. 2002. Photoacclimation of photosynthesis irradiance response curves and photosynthetic pigments in microalgae and cyanobacteria. J. Phycol. **38**: 17-38. doi:10.1046/j.1529-8817.2002.00094.x

Matthews, J. L., and others. 2017. Optimal nutrient exchange and immune responses operate in partner specificity in the cnidarian-dinoflagellate symbiosis. Proc. Natl. Acad. Sci. U. S. A. **114**: 13194-13199. doi:10.1073/pnas.1710733114

Milligan, A. J., K. H. Halsey and M. J. Behrenfeld. 2015. Advancing interpretations of ^{14}C-uptake measurements in the context of phytoplankton physiology and ecology. J. Plankton Res. **37**: 692-698. doi:10.1093/plankt/fbv051

Mirkovic, T., E. E. Ostroumov, J. M. Anna, R. van Grondelle, Govindjee and G. D. Scholes. 2017. Light absorption and energy transfer in the antenna complexes of photosynthetic organisms. Chem. Rev. **117**: 249-293. doi:10.1021/acs.chemrev.6b00002

Morán, X. A. G., J. M. Gasol, C. Pedrós-Alió and M. Estrada. 2001. Dissolved and particulate primary production and bacterial production in offshore Antarctic waters during austral summer: coupled or uncoupled? Mar. Ecol.: Prog. Ser. **222**: 25-39. doi:10.3354/meps222025

Niggl, W., M. Glas, C. Laforsch, C. Mayr and C. Wild. 2009. First evidence of coral bleaching stimulating organic matter release by reef corals. In 'Proceedings of the 11th International Coral Reef Symposium'. (Ed. B. Riegl.) pp. 905–910. (International Society for Reef Studies: Ft. Lauderdale, FL, USA.)

Oakley, C. A., G. W. Schmidt and B. M. Hopkinson. 2014. Thermal responses of *Symbiodinium* photosynthetic carbon assimilation. Coral Reefs. **33**: 501-512. doi:10.1007/s00338-014-1130-9

Osborne, B., and R. Geider. 1992. Algal photosynthesis: the measurement of algal gas exchange, Chapman and Hall.

Pei, S. and E. A. Laws. 2013. Does the ^{14}C method estimate net photosynthesis? Implications from batch and continuous culture studies of marine phytoplankton. Deep Sea Res., Part I. **82**: 1-9. doi:10.1016/j.dsr.2013.07.011

Pernice, M., and others. 2014. A nanoscale secondary ion mass spectrometry study of dinoflagellate functional diversity in reef-building corals. Environ. Microbiol. **17**: 3570-3580. doi:10.1111/1462-2920.12518

Popp, B. N., E. A. Laws, R. R. Bidigare, J. E. Dore, K. L. Hanson and S. G. Wakeham. 1998. Effect of phytoplankton cell geometry on carbon isotopic fractionation. Geochim. Cosmochim. Acta. **62**: 69-77. doi:10.1016/s0016-7037(97)00333-5

Radecker, N., J. B. Raina, M. Pernice, G. Perna, P. Guagliardo, M. R. Kilburn, M. Aranda and C. R. Voolstra. 2018. Using *Aiptasia* as a model to study metabolic interactions in cnidarian-*Symbiodinium* symbioses. Front. Physiol. **9**: 214. doi:10.3389/fphys.2018.00214

Roberty, S., B. Bailleul, N. Berne, F. Franck and P. Cardol. 2014. PSI Mehler reaction is the main alternative photosynthetic electron pathway in *Symbiodinium* sp., symbiotic dinoflagellates of cnidarians. New Phytol. **204**: 81-91. doi:10.1111/nph.12903

Robison, J. D. and M. E. Warner. 2006. Differential impacts of photoacclimation and thermal stress on the photobiology of four different phylotypes of *Symbiodinium* (Pyrrhophyta). J. Phycol. **42**: 568-579. doi:10.1111/j.1529-8817.2006.00232.x

Rost, B., I. Zondervan and D. Wolf-Gladrow. 2008. Sensitivity of phytoplankton to future changes in ocean carbonate chemistry: current knowledge, contradictions and research directions. Mar. Ecol.: Prog. Ser. **373**: 227-237. doi:10.3354/meps07776

Rueden, C. T., J. Schindelin, M. C. Hiner, B. E. DeZonia, A. E. Walter, E. T. Arena and K. W. Eliceiri. 2017. ImageJ2: ImageJ for the next generation of scientific image data. BMC Bioinf. **18**: 529. doi:10.1186/s12859-017-1934-z

Sackett, O., K. Petrou, B. Reedy, R. Hill, M. Doblin, J. Beardall, P. Ralph and P. Heraud. 2016. Snapshot prediction of carbon productivity, carbon and protein content in a Southern Ocean diatom using FTIR spectroscopy. ISME J. **10**: 416-426. doi:10.1038/ismej.2015.123

Schindelin, J., and others. 2012. Fiji: an open-source platform for biological-image analysis. Nat. Methods. **9**: 676-682. doi:10.1038/nmeth.2019

Silverstein, R. N., R. Cunning and A. C. Baker. 2017. Tenacious D: *Symbiodinium* in clade D remain in reef corals at both high and low temperature extremes despite impairment. J. Exp. Biol. **220**: 1192-1196. doi:10.1242/jeb.148239

Smith, R., and Platt, T. 1984. Carbon exchange and ^{14}C tracer methods in a nitrogen-limited diatom, *Thalassiosira pseudonana*. Marine Ecology Progress Series, 16(1/2), 75-87.

Steemann-Nielsen, E. 1952. The use of radio-active carbon (C^{14}) for measuring organic production in the sea. J. Cons., Cons. Int. Explor. Mer. **18**: 117-140. doi:10.1093/icesjms/18.2.117

Suggett, D. J. and D. J. Smith. 2011. Interpreting the sign of coral bleaching as friend vs. foe. Glob. Change Biol. **17**: 45-55. doi:10.1111/j.1365-2486.2009.02155.x

Suggett, D. J., S. Goyen, C. Evenhuis, M. Szabo, D. T. Pettay, M. E. Warner and P. J. Ralph. 2015. Functional diversity of photobiological traits within the genus *Symbiodinium* appears to be governed by the interaction of cell size with cladal designation. New Phytol. **208**: 370-381. doi:10.1111/nph.13483

Suggett, D. J., M. E. Warner and W. Leggat. 2017. Symbiotic dinoflagellate functional diversity mediates coral survival under ecological crisis. Trends Ecol. Evol. **32**: 735-745. doi:10.1016/j.tree.2017.07.013

Takabayashi, M., L. M. Adams, X. Pochon and R. D. Gates. 2012. Genetic diversity of free-living *Symbiodinium* in surface water and sediment of Hawai'i and Florida. Coral Reefs. **31**: 157-167. doi:10.1007/s00338-011-0832-5

Thornton, D. C. O. 2014. Dissolved organic matter (DOM) release by phytoplankton in the contemporary and future ocean. Eur. J. Phycol. **49**: 20-46. doi:10.1080/09670262.2013.875596

Trench, R. K. 1969. Chloroplasts as functional organelles in animal tissues. J. Cell Biol. **42**: 404-417. doi:10.1083/jcb.42.2.404

Wang, J. T. and A. E. Douglas. 1997. Nutrients, signals, and photosynthate release by symbiotic algae (the impact of taurine on the dinoflagellate alga *Symbiodinium* from the sea anemone *Aiptasia pulchella*). Plant Physiol. **114**: 631-636. doi:10.1104/pp.114.2.631

Wangpraseurt, D., M. Pernice, P. Guagliardo, M. R. Kilburn, P. L. Clode, L. Polerecky and M. Kuhl. 2016. Light microenvironment and single-cell gradients of carbon fixation in tissues of symbiont-bearing corals. ISME J. **10**: 788-792. doi:10.1038/ismej.2015.133

Warner, M. E., and D. J. Suggett. 2016. The photobiology of *Symbiodinium* spp.: linking physiological diversity to the implications of stress and resilience, p. 489-509. In S. Goffredo and Z. Dubinsky [eds.], The Cnidaria, Past, Present and Future. Springer, Cham.

Weis, V. M. and D. Allemand. 2009. Physiology. What determines coral health? Science. **324**: 1153-1155. doi:10.1126/science.1172540

Xiang, T., E. A. Hambleton, J. C. DeNofrio, J. R. Pringle and A. R. Grossman. 2013. Isolation of clonal axenic strains of the symbiotic dinoflagellate *Symbiodinium* and their growth and host specificity. J. Phycol. **49**: 447-458. doi:10.1111/jpy.12055

Yao, H., and others. 2010. Use of ITS2 region as the universal DNA barcode for plants and animals. PLoS One. **5**: e13102. doi:10.1371/journal.pone.0013102

2.9. Supplementary information

2.9.1. Supplementary Methods

2.9.1.1. Photophysiology

All samples were acclimated to low light (ca. ~20 µmol photons m^{-2} s^{-1}) for at least 20 min prior to photophysiology measurements. All samples were then analysed using a FastOcean and Light Induced Fluorescence Transient (LIFT) Fast Repetition Rate fluorometers (FRRf) (respectively Chelsea Technologies Group, UK and Soliense Inc., CA). Excitation was delivered using a blue LED excitation source (peak excitation 450 nm) delivering a ST induction protocol of 100 flashlets of 1.1 µs at 2.8 µs (see Suggett et al. 2015). The FRRf was programmed to record the average of 40 sequential single turnover acquisitions at 150 ms intervals. Photosystem II (PSII) photophysiological characteristics were then determined by fitting acquisitions to the KPF model (Kolber et al. 1998) using FastPRO software (Chelsea Technologies Group, UK) to yield the minimum (F_o) and maximum (F_m) PSII fluorescence yields (instrument units), and PSII absorption cross section (σ_{PSII}; nm^2). All fluorescence yields were adjusted for baseline fluorescence using sample filtrate (see Suggett et al. 2015).

2.9.1.2. Chlorophyll-*a* (Chl*a*) measurements

Aliquots of 6 mL culture were filtered through GF/F filters under a gentle vacuum. Pigments were then extracted by placing filters in glass vials containing 3 mL of 90% acetone at 4ºC for 24 h in darkness. Absolute values of extracted Chl*a* were measured at 630 and 664 nm with a UV-1280 UV-Visible Spectrophotometer (Shimadzu, Kyoto, Japan) and determined from the coefficients and equations of Ritchie et al. (2006) for dinoflagellates. Chl*a* concentrations were normalised to the cell density to provide units of pg Chl*a* $cell^{-1}$ (Supplementary Figure S2.3).

2.9.2. Supplementary Figures

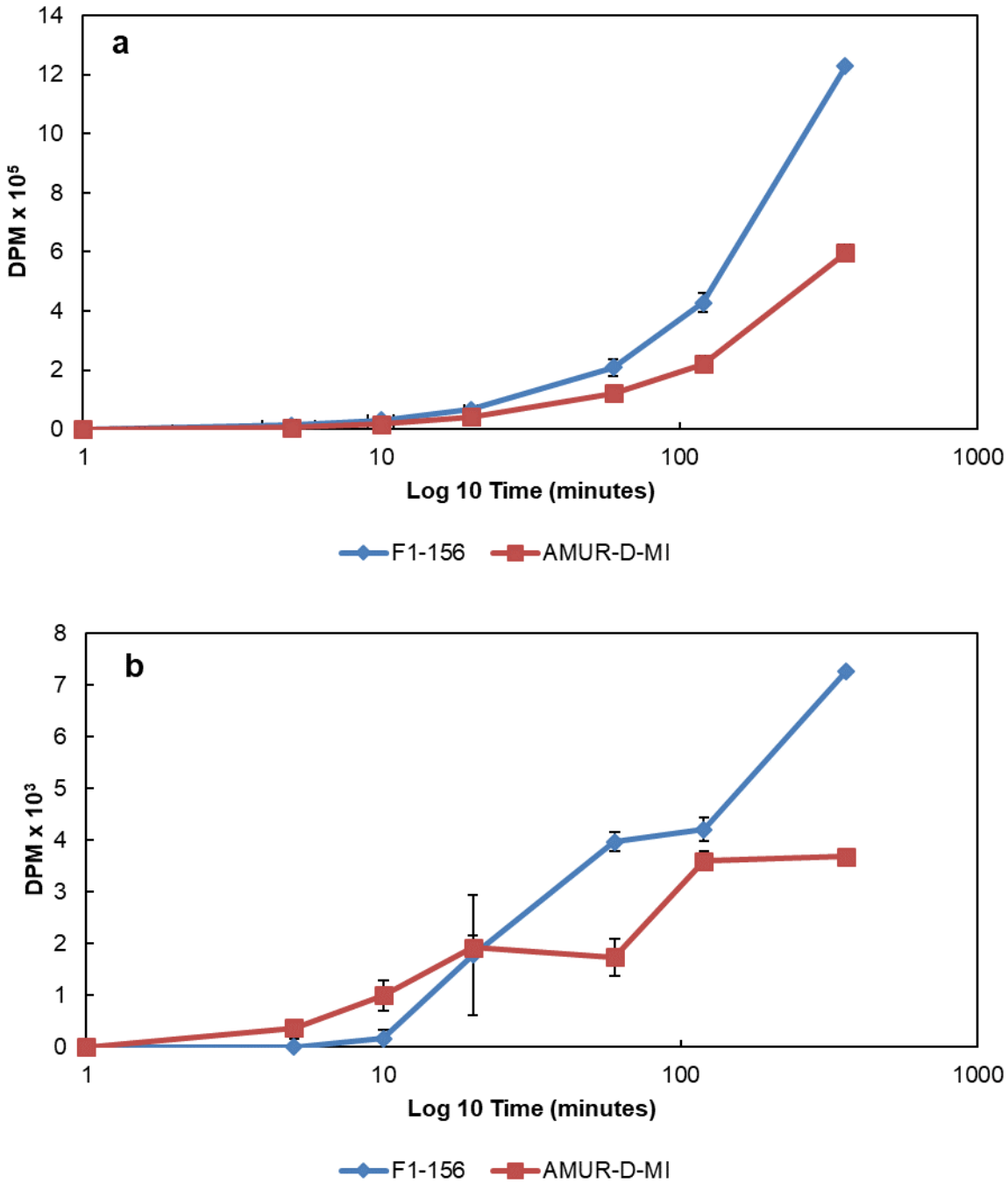

Supplementary Figure S2.1. Relative ^{14}C fixation (DPM) as (**a**) C_{fix} and (**b**) C_{exc} over time (5, 10, 20, 60, 120 and 360 minutes) of F1-156 and amur-D-MI, characterised as fastest and slowest growing isolates at the time of the assay, respectively.

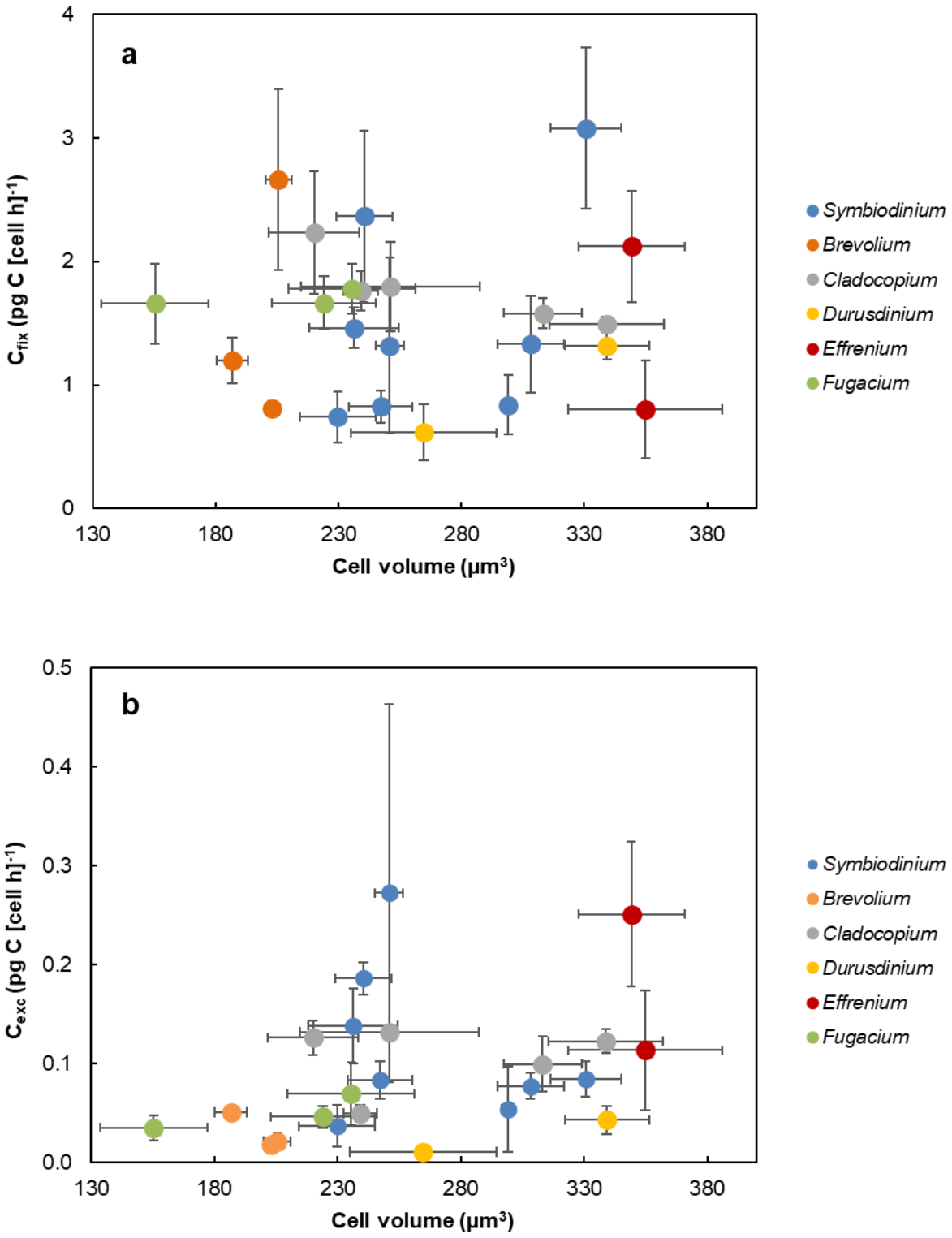

Supplementary Figure S2.2. Carbon fluxes as (**a**) C_{fix} and (**b**) C_{exc} occurring within the 23 Symbiodiniaceae isolates grouped per genus after 1h of photosynthesis, as a function of their respective cell volumes.

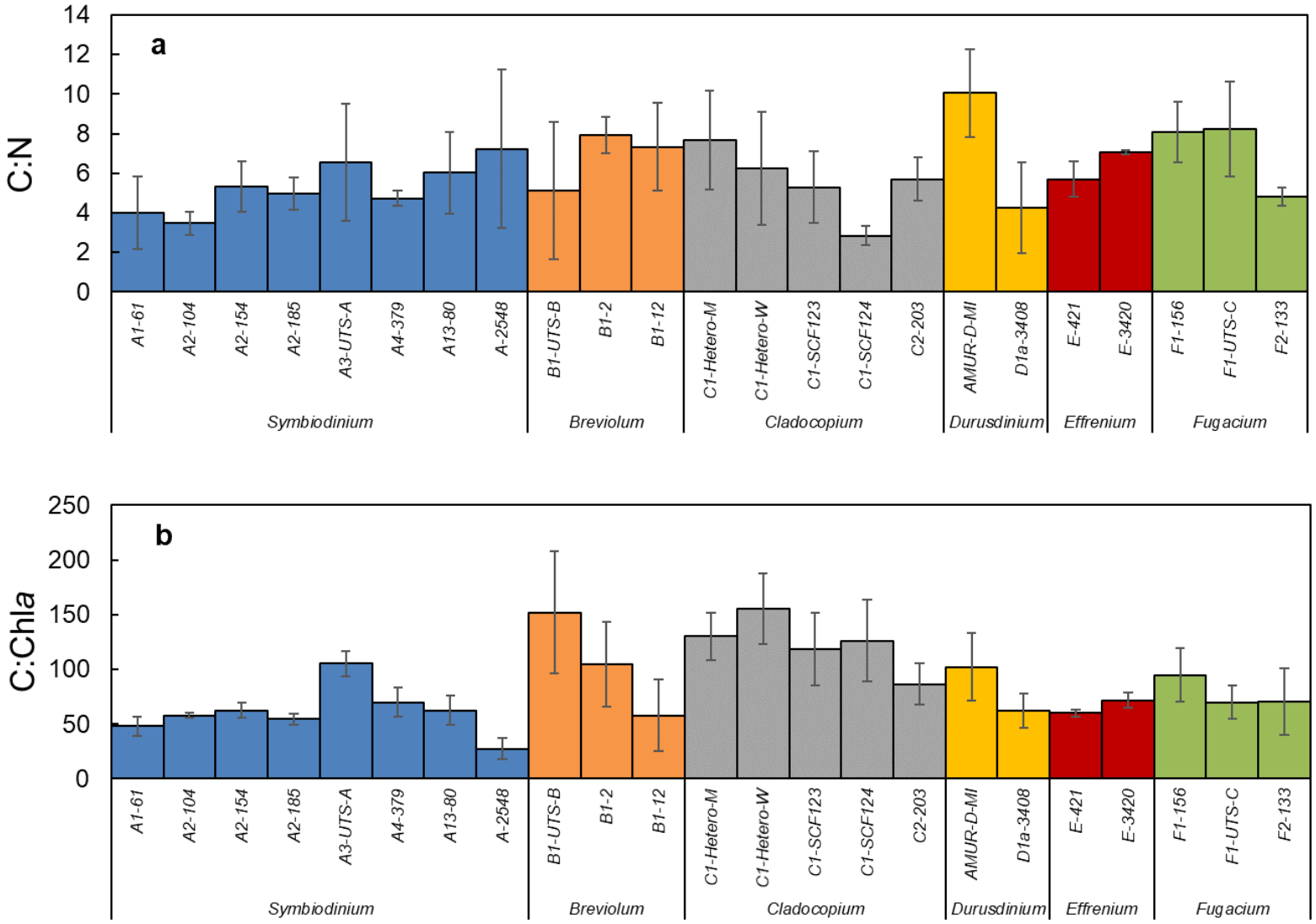

Supplementary Figure S2.3. Summary of (**a**) C:N and (**b**) C:Chl*a* ratios for each of the 23 studied Symbiodiniaceae isolates.

2.9.3. Supplementary Tables

Supplementary Table S2.1. Steady-state growth characteristics and cell contents of studied Symbiodiniaceae isolates: mean (±SD) (n = 3) of growth rate (μ, day^{-1}), cell volumes (μm^3), POC (pg C $cell^{-1}$), TN (pg N $cell^{-1}$), and Chl*a* (pg Chl*a* $cell^{-1}$).

Isolate	μ	Volume	POC	TN	Chl*a*
A1-61	0.350 (0.007)	229.805 (15.372)	110.071 (16.874)	24.063 (4.864)	2.292 (0.063)
A2-104	0.382 (0.017)	240.504 (11.444)	179.100 (70.396)	43.344 (11.388)	3.530 (1.041)
A2-154	0.329 (0.011)	308.318 (13.443)	199.680 (7.410)	47.887 (7.730)	3.214 (0.225)
A2-185	0.391 (0.013)	330.705 (14.308)	284.256 (71.439)	52.737 (7.178)	7.016 (1.000)
A3-UTS-A	0.444 (0.053)	250.905 (5.761)	217.373 (24.562)	22.753 (8.589)	2.100 (0.482)
A4-379	0.404 (0.040)	236.412 (18.064)	101.839 (32.871)	21.976 (8.912)	1.406 (0.261)
A13-80	0.298 (0.012)	299.109 (2.459)	144.706 (7.875)	35.039 (10.062)	2.400 (0.564)
A-2548	0.454 (0.077)	247.256 (12.912)	105.919 (22.348)	21.103 (3.471)	2.916 (0.516)
B1-UTS-B	0.286 (0.024)	205.623 (5.414)	175.569 (35.996)	27.471 (6.535)	1.028 (0.097)
B1-2	0.272 (0.025)	203.037 (1.946)	122.785 (65.313)	18.904 (3.050)	1.049 (0.241)
B1-12	0.295 (0.027)	186.839 (6.508)	165.119 (111.441)	18.564 (4.783)	1.516 (0.259)
C1-Hetero-M	0.315 (0.037)	313.246 (15.771)	178.185 (54.732)	29.043 (2.494)	1.506 (0.081)
C1-Hetero-W	0.216 (0.008)	251.126 (36.405)	159.426 (58.237)	35.217 (1.166)	1.135 (0.135)
C1-SCF123	0.369 (0.077)	339.038 (23.197)	131.282 (34.838)	20.315 (4.802)	1.082 (0.070)
C1-SCF124	0.223 (0.009)	220.094 (18.471)	109.154 (17.748)	32.857 (1.570)	0.773 (0.094)
C2-203	0.244 (0.031)	239.196 (6.864)	138.424 (88.404)	39.083 (7.089)	2.158 (0.425)
amur-D-MI	0.353 (0.025)	339.306 (17.108)	240.624 (118.045)	44.869 (7.455)	2.095 (0.103)
D1a-3408	0.388 (0.024)	264.688 (29.673)	127.471 (60.303)	45.795 (11.950)	1.807 (0.137)
E-421	0.289 (0.039)	349.278 (21.492)	184.251 (36.028)	37.652 (11.372)	3.166 (0.308)
E-3420	0.363 (0.068)	354.899 (31.291)	178.754 (7.706)	35.08 (15.857)	2.707 (0.193)
F1-156	0.493 (0.110)	224.099 (20.953)	213.697 (43.679)	28.894 (2.018)	2.277 (0.118)
F1-UTS-C	0.720 (0.074)	235.547 (25.686)	184.944 (37.759)	20.946 (4.153)	2.656 (0.115)
F2-133	0.310 (0.051)	155.466 (21.719)	177.420 (95.379)	36.034 (16.326)	2.444 (0.243)

Supplementary Table S2.2. Summary of significant non-parametric ANOVA (Kruskal-Wallis) with discrimination of significantly different isolates using Dunn-Bonferroni post-hoc tests, carried out on the variables measured in the study (growth rate μ, cell volume, C_{fix}, C_{exc}, $\%C_{exc}$, NPC, C:N and C:Chl*a*).

Variable	Comparisons	Statistic H	*P*
μ	C1-Hetero-W × F1-UTS-C	-64.000	0.024
	C1-SCF124 × F1-UTS-C	-63.330	0.028
Volume	F2-133 × E-3420	61.333	0.046
	F2-133 × E-421	61.667	0.042
C_{fix}	D1a-3408 × A2-185	61.000	0.050
C_{exc}	E-421 × D1a-3408	-62.667	0.033
$\%C_{exc}$	B1-UTS-B × E-3420	-62.000	0.039
	B1-UTS-B × A3-UTS-A	63.000	0.030
	B1-2 × A3-UTS-A	61.000	0.050
NPC	N/A	N/A	N.S.
C:N	N/A	36.99	0.024
C:Chl*a*	C1-Hetero-W × A-2548	51.128	0.046

"N/A" and "N.S." denote for "not applicable" and "not significant", respectively.

Supplementary Table S2.3. Carbon fluxes and productivity characteristics across studied Symbiodiniaceae isolates: mean (±SD) (n = 3) of GPC (pg C [cell h]$^{-1}$), the detail of C_{fix} (pg C [cell h]$^{-1}$) and C_{exc} (pg C [cell h]$^{-1}$), and NPC (pg C [cell h]$^{-1}$).

Isolate	GPC	C_{fix}	C_{exc}	NPC
A1-61	0.778 (0.118)	0.741 (0.203)	0.037 (0.021)	3.209 (0.441)
A2-104	2.551 (0.402)	2.364 (0.697)	0.186 (0.017)	5.695 (1.139)
A2-154	1.406 (0.224)	1.328 (0.387)	0.077 (0.013)	5.479 (1.020)
A2-185	3.161 (0.378)	3.077 (0.654)	0.084 (0.018)	9.267 (1.590)
A3-UTS-A	1.591 (0.425)	1.318 (0.710)	0.272 (0.191)	8.043 (2.414)
A4-379	1.600 (0.096)	1.462 (0.162)	0.138 (0.038)	3.425 (0.981)
A13-80	0.894 (0.139)	0.840 (0.238)	0.054 (0.043)	3.597 (0.770)
A-2548	0.908 (0.077)	0.825 (0.132)	0.083 (0.019)	4.004 (1.421)
B1-UTS-B	2.682 (0.424)	2.660 (0.734)	0.022 (0.008)	4.186 (1.314)
B1-2	0.829 (0.032)	0.811 (0.055)	0.018 (0.002)	2.788 (0.946)
B1-12	1.248 (0.105)	1.197 (0.182)	0.051 (0.006)	4.065 (1.305)
C1-Hetero-M	1.679 (0.073)	1.579 (0.123)	0.100 (0.027)	4.684 (1.655)
C1-Hetero-W	1.928 (0.208)	1.796 (0.360)	0.132 (0.007)	2.875 (0.673)
C1-SCF123	1.614 (0.037)	1.491 (0.063)	0.123 (0.013)	4.040 (1.751)
C1-SCF124	2.358 (0.288)	2.232 (0.498)	0.126 (0.018)	2.027 (0.498)
C2-203	1.811 (0.091)	1.761 (0.158)	0.050 (0.009)	2.814 (1.172)
amur-D-MI	1.363 (0.065)	1.319 (0.111)	0.043 (0.014)	7.082 (1.854)
D1a-3408	0.627 (0.132)	0.616 (0.229)	0.011 (0.007)	4.122 (0.962)
E-421	2.371 (0.262)	2.119 (0.447)	0.251 (0.073)	4.437 (1.746)
E-3420	0.915 (0.231)	0.802 (0.396)	0.114 (0.060)	5.401 (2.241)
F1-156	1.709 (0.123)	1.663 (0.213)	0.046 (0.011)	8.782 (3.420)
F1-UTS-C	1.847 (0.118)	1.777 (0.202)	0.070 (0.032)	11.089 (2.429)
F2-133	1.693 (0.189)	1.657 (0.326)	0.035 (0.012)	4.577 (1.938)

Supplementary Table S2.4. Summary of the regression analyses carried out between the mean (±SD) of GPC and NPC of the different Symbiodiniaceae genera.

Genus	N	GPC	NPC	R^2	Std. Error	Stat. F	*P*	Slope (lower bound, upper bound - 95% CI)	Intercept (lower bound, upper bound - 95% CI)
Symbiodinium	24	1.613 (0.912)	5.396 (2.178)	0.338	0.759	11.221	0.003	0.239 (0.091, 0.386)	0.321 (-0.542, 1.183)
Breviolum	9	1.596 (0.948)	3.540 (2.042)	0.451	0.751	5.751	0.048	0.352 (0.005, 0.699)	0.225 (-1.251, 1.701)
Cladocopium	15	1.885 (0.373)	3.318 (1.272)	0.127	0.362	1.892	0.192	-0.105 (-0.269, 0.060)	2.232 (1.651, 2.814)
Durusdinium	6	0.994 (0.434)	5.305 (2.721)	0.308	0.404	1.776	0.253	0.089 (-0.096, 0.273)	0.525 (-0.556, 1.605)
Effrenium	6	1.643 (0.908)	5.064 (1.706)	0.271	0.867	1.484	0.290	-0.277 (-0.908, 0.354)	3.046 (-0.299, 6.391)
Fugacium	9	1.749 (0.245)	8.296 (3.515)	0.046	0.256	0.335	0.581	-0.015 (-0.076, 0.046)	1.873 (1.330, 2.416)
All data	69	1.637 (0.741)	5.027 (2.647)	0.044	0.730	3.094	0.083	0.059 (-0.008, 0.127)	1.334 (0.948, 1.720)

Supplementary Table S2.5. Contribution of variables (in %) to each component of the PCA carried out on the screening dataset.

Variable	1st PCA component	2nd PCA component
NPC	13.755	59.157
Volume	19.582	8.146
C_{fix}	31.479	6.596
C_{exc}	35.185	26.101

Supplementary Table S2.6. Summary of significant nonparametric ANOVA (Kruskal-Wallis) with discrimination of the genera (and isolates, when applicable) significantly apart from each other using Dunn-Bonferroni post-hoc tests, carried out on each dimension of the PCA carried out on the screening dataset.

Variable	Comparisons	Statistic H	*P*
1st PCA component	*Breviolum* × *Effrenium*	-37.944	0.005
	B1-2 × E-421	-62.667	0.033
2nd PCA component	*Breviolum* × *Effrenium*	31.444	0.044
	Symbiodinium × *Fugacium*	-26.694	0.010
	Cladocopium × *Fugacium*	-39.778	0.000
	Effrenium × *Fugacium*	-47.111	0.000
	E-421 × F1-156	-61.667	0.042

Supplementary Table S2.7. Steady-state growth characteristics and cell contents of the three studied Symbiodiniaceae isolates grown at 20°C, 26°C and 30°C: mean (±SD) (n = 3) of growth rate (μ, day^{-1}), cell volumes (μm^3), POC (pg C $cell^{-1}$), TN (pg N $cell^{-1}$), and Chl*a* (pg Chl*a* $cell^{-1}$).

Isolates	Temperature	Growth rate	Volume	POC	TN	Chl*a*
C1-SCF124	20	0.205 (0.010)	240.524 (3.580)	124.944 (18.6)	30.043 (3.706)	0.411 (0.043)
	26	0.223 (0.009)	220.094 (18.471)	109.154 (17.748)	32.857 (1.570)	0.773 (0.094)
	30	0.023 (0.031)	477.101 (3.101)	283.878 (107.298)	57.475 (8.563)	0.451 (0.265)
amur-D-MI	20	0.016 (0.013)	1120.940 (95.272)	764.190 (28.196)	147.979 (25.977)	2.453 (0.239)
	26	0.353 (0.025)	339.306 (17.108)	240.624 (118.045)	44.869 (7.455)	2.095 (0.103)
	30	0.096 (0.010)	297.170 (0.842)	216.504 (61.630)	36.664 (4.686)	1.352 (0.087)
E-421	20	0.235 (0.019)	297.338 (4.436)	157.031 (31.777)	29.242 (5.439)	2.741 (0.567)
	26	0.289 (0.039)	349.278 (21.492)	184.251 (36.028)	37.652 (11.372)	3.166 (0.308)
	30	0.069 (0.007)	883.391 (63.65)	327.301 (67.91)	34.469 (7.470)	5.142 (0.956)

Supplementary Table S2.8. Summary of significant non-parametric ANOVA (Kruskal-Wallis) with discrimination of significantly different temperatures of growth using Dunn-Bonferroni post-hoc tests, carried out on the variables measured on the three studied Symbiodiniaceae isolates (growth rate μ, cell volume, C_{fix}, C_{exc}, $\%C_{exc}$, and NPC).

Variable	Isolates	Temperature	Statistic F	*P*
μ	C1-SCF124	26 x 30	153.182	0.001
		20 x 30		0.002
	amur-D-MI	20 x 26		0.008
		26 x 30		0.007
		20 x 30		0.017
	E-421	26 x 30		0.042
		20 x 30		0.010
Volume	C1-SCF124	26 x 30	189.515	0.007
		20 x 30		0.000
	amur-D-MI	20 x 26		0.020
		20 x 30		0.021
	E-421	20 x 30		0.018
C_{fix}	amur-D-MI	20 x 26	19.712	0.013
		26 x 30		0.026
		20 x 30		0.000
C_{exc}	C1-SCF124	20 x 30	17.571	0.008
$\%C_{exc}$	amur-D-MI	20 x 26	40.717	0.011
		20 x 30		0.026
	E-421	26 x 30		0.024
NPC	N/A	N/A	N/A	N.S.

"N/A" and "N.S." denote for "not applicable" and "not significant", respectively.

Supplementary Table S2.9. Summary of the regression analyses carried out between the mean (±SD) of cell volume (μm^3) and growth rate (μ, d^{-1}) of the three Symbiodiniaceae isolates grown at 20°C, 26°C and 30°C.

Isolate	N	Volume	μ	R^2	Std. Error	Stat. F	*P*	Slope (lower bound, upper bound - 95% CI)	Intercept (lower bound, upper bound - 95% CI)
C1-SCF124	9	313 (124)	0.137 (0.101)	0.995	9.676	1308.609	0.000	-1194.6 (-1272.7, -1116.5)	485.9 (472.3, 499.6)
amur-D-MI	9	586 (405)	0.141 (0.151)	0.427	327.346	5.226	0.056	-1707.3 (-3473.4, 58.7)	847.9 (473.6, 1222.1)
E-421	9	510 (283)	0.198 (0.102)	0.847	118.413	38.679	0.000	-2562.6 (-3536.9, -1588.3)	1016.5 (802.5, 1230.6)
All data	27	469 (306)	0.157 (0.120)	0.414	238.784	17.651	0.000	-1638.5 (-2441.7, -835.3)	740.5 (577.4, 903.6)

Supplementary Table S2.10. Carbon fluxes and productivity characteristics of the three studied Symbiodiniaceae isolates grown at 20°C, 26°C and 30°C: mean (±SD) (n = 3) of GPC (pg C [cell h]$^{-1}$), the detail of C_{fix} (pg C [cell h]$^{-1}$) and C_{exc} (pg C [cell h]$^{-1}$), and NPC (pg C [cell h]$^{-1}$).

Isolates	Temperature	GPC	C_{fix}	C_{exc}	NPC
C1-SCF124	20	0.708 (0.043)	0.656 (0.075)	0.052 (0.003)	0.986 (0.277)
	26	1.493 (0.188)	1.366 (0.325)	0.126 (0.018)	1.131 (0.278)
	30	1.085 (0.051)	1.002 (0.088)	0.082 (0.004)	0.098 (0.415)
amur-D-MI	20	0.456 (0.022)	0.391 (0.037)	0.065 (0.002)	0.349 (1.704)
	26	1.363 (0.065)	1.319 (0.111)	0.043 (0.014)	3.277 (0.858)
	30	1.969 (0.036)	1.899 (0.061)	0.070 (0.006)	0.870 (0.522)
E-421	20	2.171 (0.123)	2.043 (0.212)	0.128 (0.016)	1.707 (0.575)
	26	2.371 (0.262)	2.119 (0.447)	0.251 (0.073)	2.086 (0.821)
	30	2.239 (0.268)	2.162 (0.464)	0.077 (0.012)	0.954 (0.653)

Supplementary Table S2.11. Contribution of variables (in %) to each component of the PCA carried out on the dataset of isolates grown at sub-optimal temperatures.

Variable	1st PCA component	2nd PCA component
NPC	20.6301	32.0036
Volume	21.2733	23.9233
C_{fix}	32.6125	11.6947
C_{exc}	25.4841	32.3785

Supplementary Table S2.12. Summary of significant non-parametric ANOVA (Kruskal-Wallis) with discrimination of the isolates specifically grown at the mentioned temperature, significantly apart from each other using Dunn-Bonferroni post-hoc tests, carried out on each dimension of the PCA carried out on the dataset of isolates grown at sub-optimal temperatures.

Variable	Comparisons			Stat. F	*P*
	Isolate 1.Temp.		Isolate 2.Temp.		
1st PCA component	C1-SCF124.20	×	amur-D-MI.20	37.795	0.011
	C1-SCF124.20	×	amur-D-MI.30		0.028
	C1-SCF124.20	×	E-421.20		0.024
	C1-SCF124.26	×	amur-D-MI.20		0.018
	C1-SCF124.30	×	amur-D-MI.20		0.024
	C1-SCF124.30	×	amur-D-MI.30		0.025
	C1-SCF124.30	×	E-421.20		0.024
	amur-D-MI.20	×	amur-D-MI.26		0.039
	amur-D-MI.20	×	amur-D-MI.30		0.001
	amur-D-MI.20	×	E-421.20		0.001
	amur-D-MI.20	×	E-421.26		0.024
	amur-D-MI.20	×	E-421.30		0.029
2nd PCA component	C1-SCF124.20	×	C1-SCF124.26	119.699	0.049
	C1-SCF124.20	×	C1-SCF124.30		0.006
	C1-SCF124.20	×	amur-D-MI.20		0.019
	C1-SCF124.20	×	amur-D-MI.30		0.009
	C1-SCF124.20	×	E-421.20		0.038
	C1-SCF124.20	×	E-421.30		0.006
	C1-SCF124.30	×	E-421.30		0.005
	amur-D-MI.30	×	E-421.30		0.024

Supplementary Table S2.13. Mean (±SD) GPC:NPC ratios (present study) of specific isolates used in Brading et al. (2011) and their retrieved O2 production rates (fmol O_2 [cell h]$^{-1}$). GPC:NPC ratios averaged per genus are from the present study.

Isolate/Genus	GPC:NPC	O_2 light	O_2 dark
A1-61	0.240 (0.080)	232 (46)	83 (15)
A13-80	0.610 (0.091)	209 (44)	60 (19)
B1-2	0.770 (0.097)	110 (11)	29 (4)
Symbiodinium	0.304 (0.104)		
Breviolum	0.415 (0.195)		
Cladocopium	0.647 (0.321)		
Durusdinium	0.172 (0.029)		
Effrenium	0.352 (0.258)		
Fugacium	0.244 (0.110)		
All	0.378 (0.241)		

Supplementary Table S2.14. Summary of the regression analyses carried out between the mean (±SD) GPC:NPC and O_2 production rates (fmol O_2 [cell h]$^{-1}$) of the three Symbiodiniaceae isolates retrieved from Brading et al. (2011), in light and dark conditions.

Treatment	N	GPC:NPC	O_2 prod.	R^2	Std. Error	Stat. F	*P*	Slope (lower bound, upper bound - 95% CI)	Intercept (lower bound, upper bound - 95% CI)
Light	9	0.263 (0.042)	184 (65)	0.996	0.003	266.582	0.039	-0.000461 (-0.000820, -0.000102)	0.347 (0.279, 0.416)
Dark	9	0.263 (0.042)	57 (27)	0.900	0.013	9.0391	0.204	-0.001048 (-0.005479, 0.003382)	0.323 (0.050, 0.595)

Supplementary Table S2.15. Photobiology characteristics of studied Symbiodiniaceae isolates: mean ± SD (n = 3) of photosystem II (PSII) maximum photochemical efficiency (F_v/F_m, dimensionless) and PSII absorption cross-section (σ_{PSII}, nm^2).

Isolate	F_v/F_m	σ_{PSII}
A1-61	0.530 (0.004)	3.374 (0.173)
A2-104	0.485 (0.018)	2.890 (0.212)
A2-154	0.507 (0.017)	2.694 (0.123)
A2-185	0.537 (0.014)	2.717 (0.099)
A3-UTS-A	0.530 (0.039)	1.713 (0.871)
A4-379	0.566 (0.004)	2.980 (0.148)
A13-80	0.553 (0.011)	2.944 (0.136)
A-2548	0.536 (0.011)	2.751 (0.133)
B1-UTS-B	0.510 (0.022)	3.844 (0.318)
B1-2	0.480 (0.015)	3.073 (0.129)
B1-12	0.557 (0.011)	2.575 (0.022)
C1-Hetero-M	0.485 (0.019)	2.444 (0.414)
C1-Hetero-W	0.530 (0.008)	2.175 (0.358)
C1-SCF123	0.527 (0.019)	1.548 (0.500)
C1-SCF124	0.534 (0.018)	2.137 (0.359)
C2-203	0.480 (0.023)	2.625 (0.088)
amur-D-MI	0.497 (0.031)	2.467 (0.338)
D1a-3408	0.521 (0.008)	2.644 (0.130)
E-421	0.494 (0.011)	2.776 (0.071)
E-3420	0.543 (0.015)	2.291 (0.066)
F1-156	0.571 (0.008)	1.902 (0.170)
F1-UTS-C	0.525 (0.023)	2.071 (0.195)
F2-133	0.519 (0.015)	2.619 (0.116)

Supplementary Table S2.16. Photobiology characteristics of the three studied Symbiodiniaceae isolates grown at 20°C, 26°C and 30°C: mean ± SD (n = 3) of photosystem II (PSII) maximum photochemical efficiency (F_v/F_m, dimensionless) and PSII absorption cross-section (σ_{PSII}, nm^2).

Isolates	Temperature	F_v/F_m	σ_{PSII}
C1-SCF124	20	0.405 (0.009)	4.439 (0.110)
	26	0.534 (0.018)	2.137 (0.359)
	30	0.363 (0.005)	4.352 (0.106)
amur-D-MI	20	0.154 (0.015)	6.065 (0.143)
	26	0.497 (0.031)	2.467 (0.338)
	30	0.469 (0.010)	4.293 (0.330)
E-421	20	0.425 (0.006)	4.486 (0.159)
	26	0.494 (0.011)	2.776 (0.071)
	30	0.336 (0.022)	3.954 (0.221)

2.9.4. Supplementary References

Brading, P., M. E. Warner, P. Davey, D. J. Smith, E. P. Achterberg and D. J. Suggett. 2011. Differential effects of ocean acidification on growth and photosynthesis among phylotypes of *Symbiodinium* (Dinophyceae). Limnol. Oceanogr. **56**: 927-938.

Kolber, Z. S., O. Prášil and P. G. Falkowski. 1998. Measurements of variable chlorophyll fluorescence using fast repetition rate techniques: defining methodology and experimental protocols. Biochim. Biophys. Acta, Bioenerg. **1367**: 88-106.

Ritchie, R. J. 2006. Consistent sets of spectrophotometric chlorophyll equations for acetone, methanol and ethanol solvents. Photosynth. Res. **89**: 27-41.

Suggett, D. J., S. Goyen, C. Evenhuis, M. Szabo, D. T. Pettay, M. E. Warner and P. J. Ralph. 2015. Functional diversity of photobiological traits within the genus *Symbiodinium* appears to be governed by the interaction of cell size with cladal designation. New Phytol. **208**: 370-381.

Chapter 3

Molecular and physiological signatures of light-harvesting and carbon assimilation in thermo-tolerant and sensitive Symbiodiniaceae

Mickael Ros[1], Emma F. Camp[1], Tim Kahlke[1], David J. Hughes[1], Deepa Varkey[1,2], Nerissa Fisher[1], Lisa Fujise[1], Samantha Goyen[1], Caitlin A. Lawson[1], William Leggat[3], David J. Suggett[1]

[1]University of Technology Sydney, Climate Change Cluster, Ultimo NSW 2007, Australia

[2]Department of Molecular Sciences, Macquarie University, NSW 2109, Australia

[3] School of Environmental and Life Sciences, University of Newcastle, NSW 2308, Australia

Whilst this chapter is written as a stand-alone draft for publication, data and experimental contributions from MR also supported an additional publication examining bacteria community shifts:

Camp EF, Nitschke M, Kahlke T, Varkey D, Fisher N, Fujise R, Goyen S, Hughes DJ, Lawson C, Ros M, Woodcock S, Xiao K, Leggat W, Suggett DJ. 2020. Revealing changes in the microbiome of Symbiodiniaceae under thermal stress. Environmental Microbiology. doi:10.1111/1462-2920.14935

3.1. Abstract

Dysfunction of the photosynthetic light reactions is commonly observed when Symbiodiniaceae cells are exposed to short term heating. How functions of the inorganic carbon (Ci) dark reactions – specifically uptake and assimilation – potentially accompany stress responses under heat exposure remain largely unknown, and no study has specifically examined expression of genes encoding proteins involved in dark reactions of photosynthesis dictating Ci assimilation. Here, we investigated the response to thermal stress by three Symbiodiniaceae isolates (*Breviolum minutum*, *Cladocopium goreaui*, *Durusdinium trenchii*) with known differences in thermal tolerance. We adopted a novel approach combining physiological assessment and transcriptomics to characterise functional groups of genes involved in light harvesting and photochemistry and corresponding dark reactions (Ci uptake rates and functional groups of genes involved in carbon concentrating mechanisms and the Calvin-Benson cycle [CBC] of photosynthesis). Our results revealed distinct metabolic responses between isolates, where *Breviolum minutum* exhibited the largest decline in F_v/F_m to thermal stress, with a significant interruption of Ci uptake. This was accompanied by a strong down-regulation of genes involved in both light (light-harvesting and encoding the D1 and D2 proteins of photosystem II) and dark reactions (carbonic anhydrase and genes involved in the CBC). Acute thermal stress had a less pronounced effect on the physiology of *C. goreaui* with minimal decreases in Ci uptake, and no specific changes in gene expression. Conversely, *D. trenchii* exhibited increased rate of Ci uptake, yet surprisingly, this was accompanied by down-regulation of genes involved in both light and dark reactions, with a similar extent of fold-change as *B. minutum* for genes involved in the CBC functioning. Together, our results highlight that Ci uptake responses are consistent with F_v/F_m that are conventionally used as indicators of relative thermal susceptibility, thus can potentially be used as a proxy to detect declines in Ci uptake. Transcriptomics confirmed that the light reactions of photosynthesis

appear primarily impacted for more thermo-sensitive symbionts. As such, the relatively conserved and low transcriptional response between species for dark reaction gene expression, regardless of their thermal tolerance, suggests that "upstream reactions", notably light-harvesting (and excitation energy dissipation) presumably regulate differences in Ci uptake performance observed under heat stress.

3.2. Introduction

The ecological success of coral reefs is highly dependent on the viability of the symbiosis between the reef-forming corals and microalgal cells from the family Symbiodiniaceae. Photosynthetic activity by these microalgal cells fuels host metabolic activity, with up to 60% of their photosynthates translocated to their coral host (Davy et al. 2012; Tanaka et al. 2018), and in turn, the extent with which corals grow and calcify (Ezzat et al. 2015; Jokiel et al. 2016). Coral reefs worldwide have deteriorated over the past two decades, notably by mass-bleaching events induced by heatwaves that have increased in frequency and intensity through climate change (Hughes et al. 2018; Eakin et al. 2019). Under abnormal temperature stress, Symbiodiniaceae cells can rapidly transition to metabolic states that are no longer beneficial to the host (Cziesielski et al. 2019; Suggett and Smith 2020), which results in bleaching and ultimately coral mortality. Whilst widespread evidence has repeatedly shown that alternate Symbiodiniaceae taxa exhibit different extents of sensitivity to heat stress based on their ability to cope with stressful conditions of light and temperature (e.g. Goyen et al. 2017; Swain et al. 2017; Quigley et al. 2018), whether and how mechanisms of thermal sensitivity are conserved – or rather have adapted as various "functionally diverse" states (e.g. Suggett et al. 2017) – amongst taxa remains entirely unresolved.

Symbiodiniaceae functional diversity for various environmental scenarios has mostly been characterised to date via different organisation and operation of their photosynthetic

apparatus, notably the "light reactions" (light harvesting, electron transport, photosystem I [PSI] and II [PSII] functioning; see Warner and Suggett 2016), which have been extensively studied via measurement of PSII turnover rates and activity (Roberty et al. 2014; Karim et al. 2015; Suggett et al. 2015; Goyen et al. 2017). Exposure of Symbiodiniaceae to heat stress can impair many functional aspects of the photosynthetic apparatus, such as PSII repair capacity (Takahashi et al. 2004, 2009), increasing the rate of PSII photodamage through the loss of D1 protein, an essential component of PSII (Hill et al. 2011). Consequently, heat stress can damage the PSII repair machinery directly, leading to PSII repair functions unable to keep pace with rates of damage elsewhere (Warner and Suggett 2016). Cellular metabolic homeostasis, which is characterised by a balance of reactive oxygen species (ROS) production from photosynthesis and their scavenging by antioxidants, can rapidly become deregulated through overproduction of ROS, leading to oxidative stress (Cziesielski et al. 2019). The ability of Symbiodiniaceae to sustain homeostasis under stressful conditions of light and temperature involves regulation of the protection of their photosynthetic apparatus (Kramer et al. 2012) leading do photoinhibition of the PSII (Warner et al. 1999) and subsequently to elevated levels of ROS, triggering endosymbiont expulsion – coral bleaching (Lesser 2006).

In contrast with our knowledge of the light reactions, activity of the dark photosynthetic reactions (or "carbon reactions"; *sensu* Mirkovic et al. 2017) that encompasses uptake of inorganic carbon (Ci) and transformation into organic carbon remains overlooked for Symbiodiniaceae when under heat stress (see Chapter 2). Early work demonstrated that carbon-concentrating mechanisms (CCMs) such as carbonic anhydrase (CA) used to acquire Ci were not the primary site of damage in response to thermal stress (Leggat et al. 2004). A subsequent study demonstrated that the core enzyme for assimilating Ci, the RuBisCO enzyme, appears prone to heat-induced damage (Lilley et al. 2010), which in turn would impair the Calvin-Benson cycle (CBC) activity and ultimately PSII repair function (Jones et al. 1998; Takahashi

and Murata 2008; Bhagooli 2013) leading to the production of singlet oxygen, damaging PSII machinery (Vass 2012). Such processes are likely exacerbated where suboptimal temperatures slow down the "dark reactions" occurring downstream of light reactions (Jones et al. 1998; Ros et al. 2020 – Chapter 2), initiating "bottlenecking" of energy (electrons) in the photosynthetic apparatus leading to photodamage and photosynthetic impairment (Warner et al. 1999; Oakley et al. 2014). Consequently, it has been suggested that the carbon reactions would be the primary site of damage due to thermal stress but can also be variable according to endosymbiont taxonomic identity (Buxton et al. 2012). However, there is still no consensus about the role of CBC in balancing stressors during thermal stress (Warner and Suggett 2016). Symbiodiniaceae can rely on different strategies to uptake Ci (Brading et al. 2013), and recent work has shown that variation of CBC functioning appears to be driven mainly by environment rather than taxa (Ros et al. 2020 – Chapter 2), suggesting relatively evolutionary conserved dark reactions. As such, the ecological success of different genera of Symbiodiniaceae likely rests on the plasticity of upstream light reactions to overcome evolutionary-conserved limitations in Ci uptake performance. Nevertheless, the nature and extent with which the dark reactions are impacted by heat stress alongside better-characterised dysfunction of the light reactions remain unexplored.

Recent advances in decoding the Symbiodiniaceae genome highlight the interest in understanding the underlying molecular causes of their functional diversity (e.g. González-Pech et al. 2019). Examining Symbiodiniaceae transcriptomes have led to new functional insight through differential gene expression under altered light intensities (*Breviolum* sp., Xiang et al. 2015), heat stress (*Cladocopium* sp., Levin et al. 2016; *Fugacium* sp., Gierz et al. 2017) or lifestyles (*Durusdinium trenchii*, Bellantuono et al. 2019); highlighting critical genes involved in regulating stress, such as ROS scavenging enzymes and molecular chaperones (Levin et al. 2016; Gierz et al. 2017), and encoding light-harvesting complexes (Gierz et al.

2017). Levin et al. (2016) specifically contrasted differential expression of stress response genes within thermal tolerant and sensitive genetic variants of *Cladocopium* species but did not detect changes in genes constituting dark reactions. However, in response to thermal stress, Bellantuono et al. (2019) noted a difference in processes that are downstream of the dark reactions, i.e. the utilisation of products of photosynthesis (via genes involved in the glyoxylate cycle), in both *in hospite* and free-living *D. trenchii* cells. As such, little evidence exists to date at the molecular level of the effect of thermal stress on dark reactions of photosynthesis and their importance in homeostasis maintenance. Whether the expression of genes encoding carbon reactions remain unchanged in response to thermal stress or have been overlooked in existing transcriptomic studies. Moreover, a direct link between the functional physiology of carbon reactions and the expression of genes involved in these pathways under thermal stress is yet to be examined.

Here we build on recent advances in using transcriptomics to unlock Symbiodiniaceae photosynthetic metabolism under heat stress when *ex hospite* (Levin et al. 2016; Gierz et al. 2017; Bellantuono et al. 2019) and identify whether/how this metabolism is functionally conserved across different Symbiodiniaceae isolates previously shown to have different thermal optima e.g. *Breviolum minutum*, *Cladocopium goreaui* and *Durusdinium trenchii* (Ros et al. 2020 – Chapter 2). We conducted a heat stress experiment periodically using Fast Repetition Rate fluorometry (FRRf) and radiolabelled $NaH^{14}CO_3$ to track simultaneously photosynthetic capacity and Ci uptake rates for control (26°C) and treatment (32°C) conditions. These data were accompanied by transcriptome profiling to examine differentially expressed genes encoding proteins associated with photosynthetic light reaction and carbon reaction metabolism. We demonstrated that each species of Symbiodiniaceae exhibits a different physiological response to stress, despite exhibiting similar trends in global gene expression

with the exception of *B. minutum*. which had down-regulated expression of PSI and PSII genes in response to thermal stress.

3.3. Materials and Methods

3.3.1. Symbiodiniaceae cultures genotyping

Three Symbiodiniaceae isolates were used for this study, *Breviolum minutum* (internal transcribed spacer 2 [ITS2] type B1, "UTS-B"), *Cladocopium goreaui* (ITS2 Type C1; "C1-124"), and *Durusdinium trenchii* (ITS2 type D1a, "amur-D-MI") (Suggett et al. 2015; Camp et al. 2020). Isolate ITS2 type identity was verified before culturing using steady-state growth aliquots of 15 mL at ~ 250,000 cells mL^{-1}, whereby a DNEasy PowerPlant Pro Kit (Qiagen, Hilden, Germany) was used to extract the DNA of cells according to the manufacturer's guidelines. Amplification of the ITS2 was performed via PCR using forward (SYM2f; 5'-GAA TTG CAG AAC TCC GTG-3') and reverse (SYM2r; 5'-GGG ATC CAT ATG GTT AAG TTC AGC GG GT-3') primers (Sigma-Aldrich, St. Louis, MO, USA). The PCR was performed according to the following conditions: one cycle at 95°C for 1 min (denaturation), followed by 35 cycles at (i) 95°C for 15 s (denaturation), (ii) 58°C for 15 s (annealing), (iii) 72°C for 30 s (elongation) and one cycle at 72°C for 7 min (additional elongation). Amplicons were then purified using the DNA Clean and Concentrator™-5 kit (ZYMO Research, Irvine, CA, USA) before being Sanger-sequenced at the Australian Genome Research Facility. Output sequences were then compared with the NCBI database using the BLAST algorithm to corroborate ITS2 identity.

3.3.2. Symbiodiniaceae growth and experimental conditions

Symbiodiniaceae isolates were grown in 750 mL vented culture flasks and acclimated for two weeks at 26.0 ± 0.5°C (mean ± SD) in one of two water baths (n = 4 per isolate per water bath) controlled by water heaters (JULABO GmbH, Germany) under an irradiance of 207.0 ± 0.05 µmol photons m^{-2} s^{-1} (Hydra 52 HD LED, AquaIllumination, Ames, IA, USA) on a 12:12 hours light:dark cycle; as measured with a 4π LI-190SA Quantum Sensor (LI-COR, Lincoln, NE, USA). All cultures were grown in autoclaved 0.2 µm-filtered seawater sourced from Rose Bay (New South Wales, Australia) and nutrient-enriched with 0.2 µm filter-sterilised Daigo's IMK medium (Nihon Pharmaceutical, Tokyo, Japan). One water bath was used as a control and maintained at 26°C throughout the entire experiment. The second water bath served as the treatment, whereby temperature on the first day of the experiment (T0) was increased by 2°C every day for three days to reach 32.4 ± 0.1°C (TI). The temperature was then maintained at ca. 32°C until the end of the experiment seven days later (TE) (see Camp et al. 2020 for further details). Both temperature and light were recorded at 5 min increments for the duration of the experiment by HOBO Pendant data loggers (Onset, MA, USA).

An aliquot of 5 mL was withdrawn every two days from each replicate flask to assess photophysiology and cell density monitoring. Samples were dark-acclimated for 15 min prior to being analysed with a Light-Induced Fluorescence Transient (LIFT) Fast Repetition Rate fluorometer (FRRf) (Soliense Inc., CA, USA) as per Camp et al. (2020). Excitation was delivered using a 450 nm blue LED according to a single turnover induction protocol of 100 flashlets of 1.1 µs at 2.8 µs (Suggett et al. 2015). The FRRf was programmed to record the average of 40 sequential single turnover acquisitions at 150 ms intervals. Photosystem II (PSII) photophysiological characteristics were then determined by fitting acquisitions to the KPF model (Kolber et al. 1998) to yield the minimum (F_o) and maximum (F_m) PSII fluorescence

yields (instrument units). All fluorescence yields were adjusted for baseline fluorescence using sample filtrate (Suggett et al. 2015). Maximum PSII photochemical efficiency (F_v/F_m, where $F_v = F_m - F_0$; dimensionless) was then recorded and used as a proxy of cellular health through the experiment.

Cell density was monitored from a 100 µL aliquot of culture fixed with glutaraldehyde (25%, Grade II, Sigma-Aldrich, 1% final concentration), where four technical replicates of 10 µL were loaded onto a Neubauer-improved haemocytometer chamber for quantification using microscopy. For each replicate, 16 images of the counting chamber were captured using NIS-Elements AR software (v.4.30.000) and an Eclipse Ni-U optical microscope coupled with a DS-Fi2 colour camera (Nikon, Tokyo, Japan). Subsequent photographs were then processed with ImageJ2 software (Rueden et al. 2017) loaded with Fiji package (Schindelin et al. 2012) and using a high-throughput image processing script circumventing cell debris and lysed cells by applying dimension and sphericity filters (Suggett et al. 2015; Fujise et al. 2018). The output counts were then ordered by the number of cells counted per frame, with the minimal and maximal values trimmed to remove any potential counting artefacts before averaging the count values. Cell volume was recorded in the same way as cell counts and determined for each counted cell. The median of the resulting series of cell volume was then recorded. Cell densities in both treatments were maintained at ~150,000 cells mL^{-1} throughout the experiment, with dilutions with new media as required to prevent nutrient limitation and self-shading (Camp et al. 2020).

3.3.3. Inorganic carbon uptake

At each sampling time (T0, TI, and TE), aliquots of 5 mL of each incubation flask were transferred into six 20 mL borosilicate scintillation vials. All vials were then incubated in the presence of radiolabelled sodium bicarbonate ($NaH^{14}CO_3$) with a specific activity of 40-60 mCi $mmol^{-1}$ (PerkinElmer, Waltham, MA, USA) (Nielsen 1952). Five vials were incubated 15 min in their original conditions (control or treatment), three of which were exposed to ambient light and two in darkness wrapped in aluminium foil. The sixth vial was kept as an initial measurement (i.e. used to determine background noise) immediately kept on ice in the dark. From the initial measurement vial, 150 µL of radiolabelled culture was preserved in 5 mL of NaOH 0.1M and kept on ice in the dark to determine the actual quantity of radioisotope (noted as "100%"). After the incubation, samples were immediately transferred on ice and kept in the dark (Hughes et al. 2018a). All vials except the "100%" vial were then acidified with 200 µL HCl (6M) to remove any residual $NaH^{14}CO_3$ and fixed with 150 µL glutaraldehyde 25% and left to degas in a fume hood for 24 hours. For each vial, 10 mL of scintillation liquid (Ultima Gold LLT, PerkinElmer) was added and shaken vigorously to ensure even distribution of the scintillation cocktail. Disintegrations per min (DPM) of the $NaH^{14}CO_3$ remaining in the samples were counted with a Liquid Scintillation Analyzer Tri-Carb 2810 TR (PerkinElmer), then averaged from 5 min counts. Dissolved inorganic carbon (DIC) concentration was required to determine Ci uptake rates and hence determined from an additional 12 mL aliquot of each culture transferred in gas-tight Exetainer vials (Labco Ltd., Lampeter, UK) with no overhead space to limit gas exchange, where any biological activity was immediately terminated with 180 µL of saturated solution of $HgCl_2$ (to a final concentration of 1.5%) and sealed prior to being stored in the dark at 4°C for analysis. The concentration of DIC in samples was determined using an AS-C3 DIC analyser (Apollo SciTech, Newark, DE, USA) standardised with referenced seawater (A.G. Dickson Batch #154, Scripps Institution of

Oceanography, UC San Diego, CA, USA). Inorganic carbon uptake rates (pg C [cell h]$^{-1}$) were then calculated according to Ros et al. (2020 – Chapter 2) as follows:

$$\text{Carbon uptake} = \frac{\text{DPM}_{\text{sample}} - \text{DPM}_{\text{T0}}}{\text{DPM}_{100\%}} \times \frac{\text{Volume}_{100\%}}{\text{Volume}_{\text{sample}}} \times \frac{\text{DIC}}{t} \quad \text{[Eqn. 1]}$$

Where the subscripts "sample", "T0" and "100%" refer to the sample, the initial measurement at the start of the incubation and the total activity count, respectively; *t* is the incubation time, in hours.

3.3.4. RNA extraction and sequencing

Parallel samples on T0, TI, and TE (aliquots of 20 mL) for all flasks were immediately snap-frozen and held at -80°C until further processing of all samples to minimise batch effect according to Levin et al. (2016). Aliquots were thawed and centrifuged at 4°C at 3000g for 5 min. Cell pellets were lysed in RLT buffer from the RNeasy Plant Mini Kit (Qiagen, Hilden, Germany) and β-mercaptoethanol by bead-beating with 200 µL of 0.5 mm sterile glass beads (BioSpec, OK, USA) using a TissueLyser II (Qiagen) at 30 Hz for 90 s. RNA was extracted using the RNeasy Plant Mini Kit (Qiagen) and then purified with an added on-column DNase I treatment (Qiagen). Quality of RNA (150-500 ng) was checked using the Agilent 2100 Bioanalyzer (Agilent Technologies, CA, USA) and polyA-purified at the Australian Genome Research Facility, Melbourne, Australia. Sequencing libraries were created using Illumina TruSeq stranded library preparation kit and sequenced with two flow cells of Illumina HiSeq2500 resulting in a total of 3,667,316,020 100 bp paired-end Illumina read pairs per sample.

3.3.5. Transcript assembly, differential gene expression quantification and functional annotation

Fastq files were trimmed using Trim Galore! (v0.6.0; Babraham Bioinformatics) with default settings. Trimmed fastq files were combined into a single fastq for each isolate, and then transcripts assembled using Trinity (v2.8.4) with default parameters (Haas et al. 2013). Transcript read counts for each sample were quantified using the Trinity script align_and_estimate_abundance.pl using kallisto (v0.43.1) as the abundance estimation method (est_method), and the appropriate Trinity fasta assembly for each species (Haas et al. 2013; Bray et al. 2016). Counts for each gene were calculated by combining the read counts for each gene isoform. Differential expression was performed in R using voom and limma on gene read counts (Law et al. 2014; Ritchie et al. 2015). Before normalisation, genes with a read count of at least 10 were filtered in at least four samples. Reads were normalised using voom(), with normalisation factors calculated using calcNormFactors(). For each comparison (Treatment TE *vs.* Control TE, and Treatment TI *vs.* Control TI), linear models were fitted using lmFit(), contrasts for each gene estimated using contrasts.fit(), and empirical Bayes smoothing of standard errors performed using eBayes(). Functional annotation of transcripts was performed using InterproScan v5.30-69 with local lookup server (Mitchell et al. 2019). Annotations were manually searched for Interpro domains, gene names and functional annotations of 156 proteins for the 12 functions listed in Table 3.1 (full list of proteins is in Supplementary Table S3.1. Differentially expressed genes (DEGs) were characterised at each sampling point (TI and TE) for each isolate according to a log2 fold change (FC) ≥ 1 and false discovery rate (FDR) ≤ 0.05 as per Levin et al. (2016) to establish major trends in gene expression levels. To examine low fold change gene expression, selection of further DEGs when not meeting the previously stated cut-off were set to log2 FC ≥ 0.5. The full annotation list for each isolate at each TI and TE can be found in Supplementary Tables S3.2-S3.7.

Table 3.1. Summary of the number of unique functional proteins queried to carry the transcriptome analysis, the total number of functions matched in the transcripts and the number of functions encoded by differentially expressed genes (DEGs) effectively matched amongst the analysed transcripts and used for the rest of the analysis. Full list of genes and their associated proteins can be found in Supplementary Table S3.1 (Abbreviations: CBC: Calvin-Benson cycle; PPP: pentose phosphate pathway; TCA: tricarboxylic acid – Krebs cycle).

		Number of functions		
Functional group	**Function**	**Queried**	**Matched (total genes)**	**Matched (DEGs)**
Light reactions	Light harvesting	12	3	3
	Electron transport	18	12	8
	Photosystem I	7	6	6
	Photosystem II	26	14	6
Carbon reactions	CBC	11	11	8
	PPP	4	4	1
	Carbon fixation	6	1	1
Carbon utilisation	Metabolism	25	10	8
	Photorespiration	18	3	2
	Transport	8	0	0
	TCA cycle	2	2	2
Stress response	Stress response	19	10	9
	Total	156	76	54

3.3.6. Statistical analysis

Statistical analyses on physiological data (n = 4) were carried out using SPSS Statistics 25 (IBM, Armonk, NY, USA). F_v/F_m and Ci uptake rates were both tested for normality (Shapiro-Wilk test), homoscedasticity (Levene's homogeneity test), and sphericity (Mauchly's test). Where these assumptions were confirmed (Ci uptake data), the continuity of physiological parameters across each of the experimental conditions for each isolate was

assessed with one-way repeated measures ANOVAs with post-hoc Bonferroni-adjusted pairwise comparisons to determine at which time point the difference occurred. Differences in physiology between each experimental condition for each isolate were assessed with a two-way ANOVA repeated measures with post-hoc Tukey HSD to determine at which time point the difference occurred. Where normality was not met (F_v/F_m), Friedman tests with post-hoc Bonferroni-adjusted pairwise comparisons were performed to assess the continuity of physiological parameters across each of the experimental conditions; and Mann-Whitney U tests with post-hoc to assess the differences between the control and heat treatments. For all statistical tests, alpha (α) was set to 0.05.

3.4. Results

3.4.1. Physiological response of Symbiodiniaceae to heat stress

Changes in F_v/F_m over time were primarily used to track the response of the three isolates to the heat stress treatment (as per Camp et al. 2020). Under heat stress, *B. minutum*, *C. goreaui* and *D. trenchii* exhibited a decline in F_v/F_m by 79, 35 and 25% respectively from TE relative to TI (Figure 3.1), representing seven days maintained at 32°C. Values of F_v/F_m in the controls remained unchanged for *B. minutum* through the experiment but declined by 16 and 22% for *C. goreaui* and *D. trenchii* respectively. Although these declines were significant, they were substantially less (*C. goreaui*), or the same as (*D. trenchii*), compared to the declines observed in the corresponding heat stress treatment.

Inorganic carbon uptake rates of the three isolates exhibited no change throughout the experiment for the control (Figure 3.1), except for an increase of carbon uptake (ca. 68%) for *D. trenchii* at TI compared to both the beginning (T0) and the end (TE) of the experiment (One-way repeated measures ANOVA, $P = 0.016$ and $P = 0.006$, respectively). However, each species exhibited a different pattern of Ci uptake under heat stress: *B. minutum* exhibited a

continued decrease in Ci assimilation during the heat stress treatment, with a notable interruption after seven days of stress at 32°C (96% decrease; $P = 0.037$). Ci uptake rates for *C. goreaui* were unchanged between T0 and TI but decreased at TE compared to TI (49% decrease, $P = 0.017$). In contrast to both *B. minutum* and *C. goreaui*, *D. trenchii* exhibited a gradually increased Ci assimilation throughout the experiment (125% increase from the beginning of the experiment, $P = 0.032$). For all isolates subjected to heat stress, Ci uptake rates were only different relative to their control at TE (see Supplementary Table S3.8). At this time point, *B. minutum* had the lowest values of Ci uptake rates (mean ± SD; 0.065 ± 0.003 pg [cell h]$^{-1}$), followed by *C. goreaui* (1.137 ± 0.032 pg [cell h]$^{-1}$), and *D. trenchii* had the highest (2.046 ± 0.178 pg [cell h]$^{-1}$).

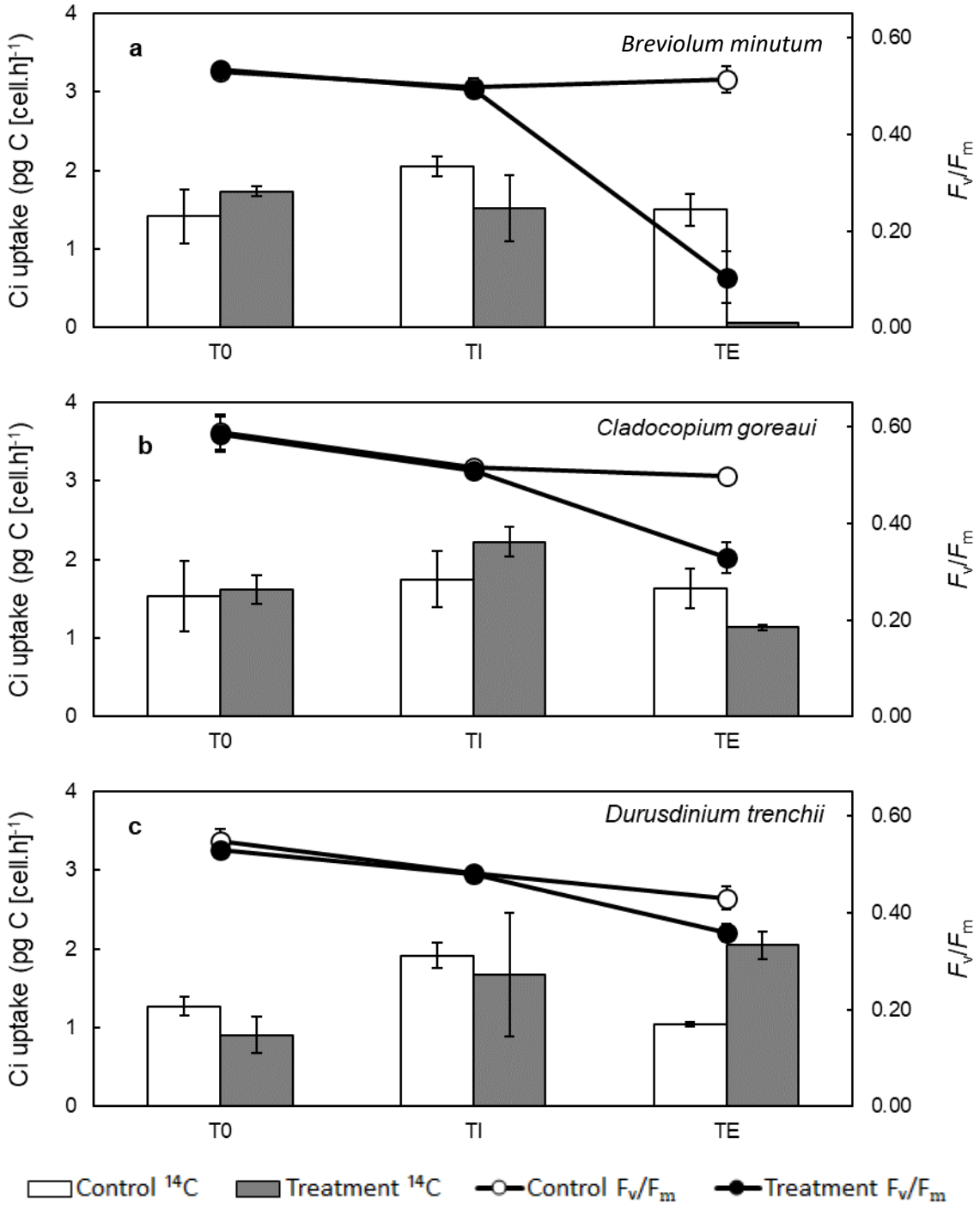

Figure 3.1. Inorganic carbon (Ci) uptake (bars; pg C [cell.h]$^{-1}$) of the three studied Symbiodiniaceae isolates (**a**) B1-UTS-B: *Breviolum minutum*, (**b**) C1-SCF124: *Cladocopium goreaui*, and (**c**) amur-D-MI: *Durusdinium trenchii* as labelled ^{14}C after 20 min of photosynthesis, matched with the photochemical efficiency of their PSII (lines; F_v/F_m) the day of the incubation. Control (white bars and dots ○) stayed at 26°C for the duration of the experiment. Treatment (grey bars and black dots ●) consisted of acclimation phase at 26°C (T0), ramping phase from 26°C to 32°C in two days (TI), and stress phase at 32°C for seven days (TE).

3.4.2. Symbiodiniaceae transcriptome patterns under thermal stress

The total transcriptome extracted at TE from *B. minutum*, *C. goreaui* and *D. trenchii* was composed of 33,712; 28,103 and 36,679 contigs, respectively. Based on the cut-off criteria (log2 FC ≥ 1, FDR ≤ 0.05), 49%, 15%, and 45% (from *B. minutum*, *C. goreaui* and *D. trenchii*, respectively) of contigs characterised DEGs. Out of the 156 proteins of interest, 76 matched the extracted transcripts sequences (Figure 3.2a). However, of these, only 54 functions encoded by differentially genes across the three Symbiodiniaceae isolates were found to have transcripts with 2-fold changes in expression (log2 FC ≥1; FDR ≤ 0.05; see Table 3.1 and Figure 3.2b).

At the onset of exposure to 32°C (TI), following ramping of temperature from 26°C to 32°C by 2°C per day over three days, only two differentially expressed genes (DEGs) were found in the list of proteins of interest for *B. minutum* (*cyb5r2*, encoding the NADH-cytochrome b5 reductase involved in lipid metabolism; and *GPX*, encoding the glutathione peroxidase-1 involved in stress response), and one for *C. goreaui* isolate (*HSP90*, encoding a 90 kDa heat-shock protein involved in stress response), both of which were down-regulated. No DEGs were observed at TI for *D. trenchii*. Given this general lack of response at TI, we focussed the analysis on the end of the experiment, TE (after seven days of exposure at 32°C).

A higher number of DEGs were observed after seven days exposure to 32°C (TE) than TI; specifically, 120, 13 and 135 DEGs for *B. minutum*, *C. goreaui* and *D. trenchii*, respectively (Figure 3.2). Two DEGs were similarly expressed in both *B. minutum* and *C. goreaui*, *rpe* (encoding chloroplastic ribulose-phosphate 3-epimerase, involved in the CBC) and an unspecified chloroplastic peridinin-Chl*a* binding protein (involved in light-harvesting). Two DEGs were also similarly regulated between *C. goreaui* and *D. trenchii*, *leuA*, (encoding 3-isopropylmalate dehydratase, involved in L-leucine metabolism) and *MDH2* (encoding malate dehydrogenase, involved in the TCA cycle). The most extensive suite of common transcripts

differentially expressed (both up and down) was 80 for *B. minutum* and *D. trenchii*, with 38 differentially expressed transcripts identified to be involved in the light reactions, 21 in the dark reactions, 7 in carbon utilisation and 14 in stress response (Supplementary Table S3.9). All three species shared only nine DEGs encoding six proteins: *prkB* (encoding phosphoribulokinase of the CBC), *petF* (encoding ferredoxin-1 in electron transport), an unspecified gene encoding unspecified Chl*a*-b binding proteins for light-harvesting, a gene encoding an unspecified class I/II aminotransferase potentially involved in photorespiration, *CYP-1* (encoding cytochrome P_{450}) and *HSP70* (encoding a 70 kDa heat shock protein).

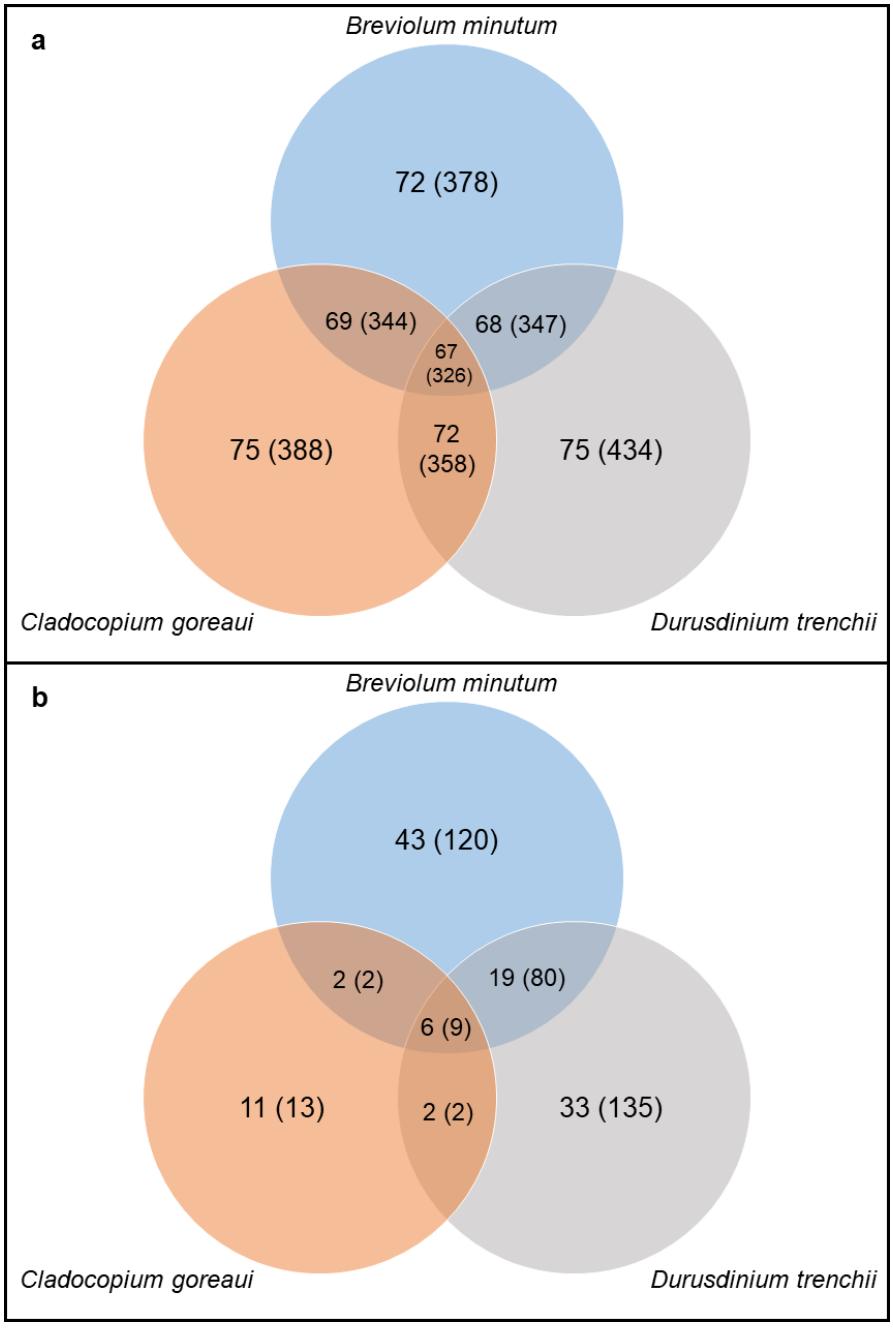

Figure 3.2. Venn diagrams illustrating the outcome of the analysis targeting 156 functional proteins of interest, returning **(a)** 76 total functions found in the extracted transcripts and **(b)** 54 functions encoded by differentially expressed genes (DEGs; log2 FC ≥1; FDR ≤ 0.05) of the three studied Symbiodiniaceae species (*Breviolum minutum*, *Cladocopium goreaui*, and *Durusdinium trenchii*) between the control (26°C) and treatment at the end of the experiment (TE, after seven days at 32°C). For both **(a)** and **(b)**, the number of gene isoforms is indicated between brackets (number of functions can be found in Table 3.1, list in Supplementary Table S3.1). Numbers over superposed circles correspond to the number of the conserved functions (and similar isoforms) expressed between the species that were allocated to the said circles. The list of commonly expressed transcripts associated to their functional groups can be found in Supplementary Table S3.9.

Of all matched transcripts across isolates/selected protein functions, 88% (237 out of 268) DEGs were down-regulated for the heat stress relative to control compared to only 12% (31 out of 268) (Figure 3.3) up-regulated. *B. minutum* and *D. trenchii* predominantly drove this trend with 84% (101 out of 120) and 96% (130 transcripts out of 135) of all DEGs down-regulated, respectively. In contrast, the extent of down- *versus* up-regulated DEGs for *C. goreaui* were similar (46% *versus* 54% of the 13 DEGs), respectively. These various changes captured very different heat stress responses for the three species.

Most down-regulated genes for *B. minutum* at TE (Supplementary Table S3.10) encoded proteins involved with photosynthesis via PSI (4.97 - 5.68 log2 fold change for the *psaA* gene encoding the P700 apoprotein A1) and PSII (4.82 and 4.91 log2 fold change for *psbA* and *psbD*, encoding the D1 and D2 proteins, respectively). The gene encoding the subunit 4 of the cytochrome b6-f complex (*petD*), involved in electron transport was also down-regulated (4.69 log2 fold change); interestingly, these same genes were the most up-regulated during TI (0.88 – 1.12 for *psaA*; 1.00 for *psbA*; 1.11 for *psbD*; and 1.25 for *petD*). At TE, additional genes encoding PSI (*psaC*, *psaD*, *psaE*, and *psaF*) and PSII (*psbJ*, *psbP*, and *psbU*) subunits were up-regulated, but which were not up-regulated (at least according to log2 fold expressions < 1) at TI suggesting a lack of expression change at the early onset of heat stress. Genes encoding proteins of the CBC and stress response pathways were increasingly down-regulated between TI and TE, except for *rpe* (encoding the chloroplastic ribulose-phosphate 3-epimerase) and a gene encoding an unspecified redoxin (from 0.77 at TI to 2.05 log2 fold change at TE, and from 0.60 at TI to 2.10 log2 fold change at TE, respectively).

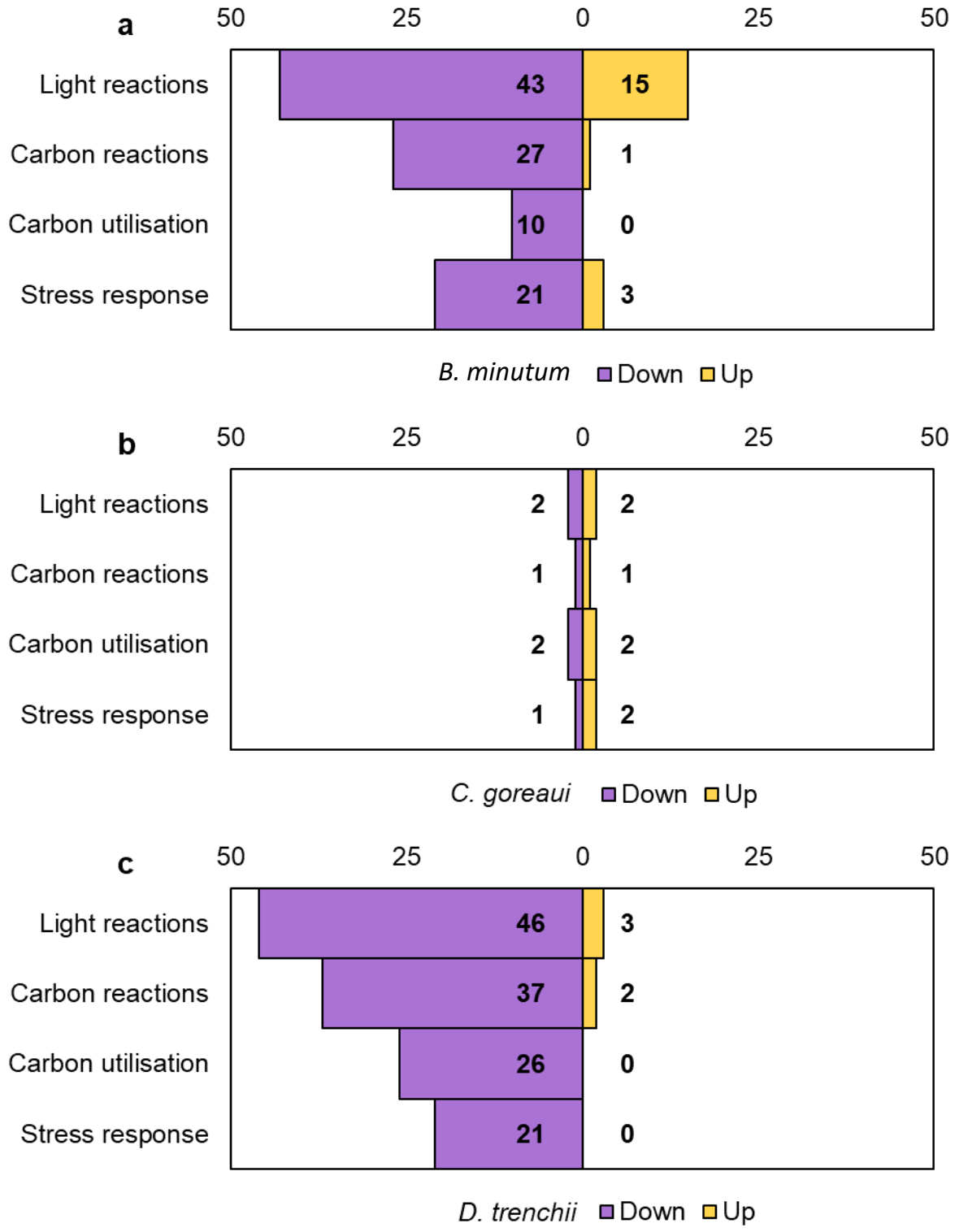

Figure 3.3. Number of functional gene isoforms of interest found to be differentially down- (purple) or up-regulated (yellow) in the three studied Symbiodiniaceae isolates (**a**) B1-UTS-B: *Breviolum minutum*, (**b**) C1-SCF124: *Cladocopium goreaui*, and (**c**) amur-D-MI: *Durusdinium trenchii* at the end of the experiment (TE, after seven days at 32°C), relative to their control (26°C). Transcripts are grouped by function, and the full list of genes can be found in Supplementary Table S3.10).

Down-regulated DEGs for *D. trenchii* at TE (Supplementary Table S3.10) were mostly those encoding proteins associated with light-harvesting (1.03 – 3.45 log2 fold change for 39 gene isoforms encoding unspecified Chl*a*-b binding proteins, with two gene isoforms up-regulated). The gene encoding the iron-sulphur subunit of the cytochrome b6-f complex (*petD*) involved in electron transport was up-regulated from 0.31 log2 fold change at TI (albeit not being significant) to 1.58 log2 fold change at TE. Similarly, two other gene isoforms encoding the RuBisCO (*rbcL*) and carbonic anhydrase (*AN1805*) were up-regulated; however, it should be noted that these genes were not the majority compared to transcripts matched with down-regulated genes encoding the same proteins, but rather only accounted for one out of four gene isoforms for *rbcL*, and one out of 15 for *AN1805*.

Fewer DEGs were observed for *C. goreaui*, and generally exhibited lower fold changes in expression (up and down-regulated between 1.41 log2 fold change), than for the other two species at TE (Supplementary Table S3.10). Genes encoding an unspecified Chl*a*-b binding protein involved in light-harvesting were both down-regulated (1.41 log2 fold change) and up-regulated (1.11 log2 fold change). The same trend was observed for *CYP-1* (encoding for the cytochrome P450, previously reported to be involved in stress response), which had two transcripts either down- or up-regulated (1.15 log2 fold change and 1.27 log2 fold change, respectively). Whilst one other gene involved in the stress response, *HSP70*, was up-regulated under heat stress only at TE (1.30 log2 fold change), a second heat shock protein gene, *HSP90* gene had an increased expression between TI and TE albeit still being down-regulated compared to the control (from 1.11 log2 fold change to 0.84 log2 fold change). Several genes were regulated in the opposite way compared to *B. minutum*. and *D. trenchii*: genes *petF* and *prkB* encoding the ferredoxin-1 (involved in electron transport) and a phosphoribulokinase (involved in the CBC), respectively were both substantially up-regulated for *C. goreaui*, while they were down-regulated within the two other species. This was also the case for one isoform

of a gene encoding an unspecified Chl*a*-b binding protein, one isoform of a gene encoding a 70 kDa heat-shock protein, and two isoforms of a gene encoding unspecified class I/II aminotransferases.

3.5. Discussion

Global sea surface temperatures (Bopp et al. 2013; reviewed in Suggett and Smith 2020) as well as the frequency and intensity of marine heatwave events (Ainsworth et al. 2016) are expected to rise over the next decades, and coral reefs of the world will thus be increasingly subjected to thermal stress (Hughes et al. 2018). Resolving the role of endosymbiont photosynthetic performance in determining coral success or failure during thermal stress is therefore essential to better understand and predict trajectories of future reef assemblages (McIlroy et al. 2019). Here, we subjected three species of Symbiodiniaceae (representing three genera) with different extents of thermal tolerance (Camp et al. 2020; Ros et al. 2020 – Chapter 2), assessing both physiological and molecular responses to understand whether and how mechanisms of photosynthetic light-harvesting and carbon metabolism potentially vary under heat stress. The thermo-sensitive *B. minutum* and -resistant *D. trenchii* isolates showed drastically different responses of their photophysiology and Ci uptake capacity to thermal stress. However, the corresponding regulation patterns of the studied functional groups of genes (light and dark reactions, carbon utilisation and stress response), whilst different at the onset of stress, were surprisingly similar after seven days of exposure to 32°C, with an overall majority of down-regulated genes (Table 3.2). *C. goreaui* was not impacted by thermal stress as much as *B. minutum*, (but more than *D. trenchii*), yet interestingly, the *C. goreaui* transcripts did not reveal notable trends in gene expression, where most genes were not differentially expressed. The findings suggest that for these specific isolates of *B. minutum*, *C. goreaui* and *D. trenchii* under nutrient replete culture conditions, our transcriptional profiling provided little

elucidation of the mechanisms of thermal stress – at least at the temperature and duration of stress we examined – since gene expression patterns showed no apparent patterns with the emergent physiological properties of photochemical efficiency and Ci-uptake. Consequently, these processes are likely both regulated at the onset of thermal stress to trigger the ability of Symbiodiniaceae to adjust to thermal stress through post-transcriptional modifications, which are known to be a key characteristic for dinoflagellates (Jones et al. 2015).

Table 3.2. Summary of trends found across the studied Symbiodiniaceae isolates. Numbers between brackets represent the number of differentially expressed genes (DEGs) in a sequential order of isolate appearance in the table (*Breviolum minutum*, *Cladocopium goreaui*, *Durusdinium trenchii*). The percent of change of all DEGs indicate how are allocated the DEGs between down- and up-regulated genes. Arrows thickness represent the number of DEGs found in each functional group.

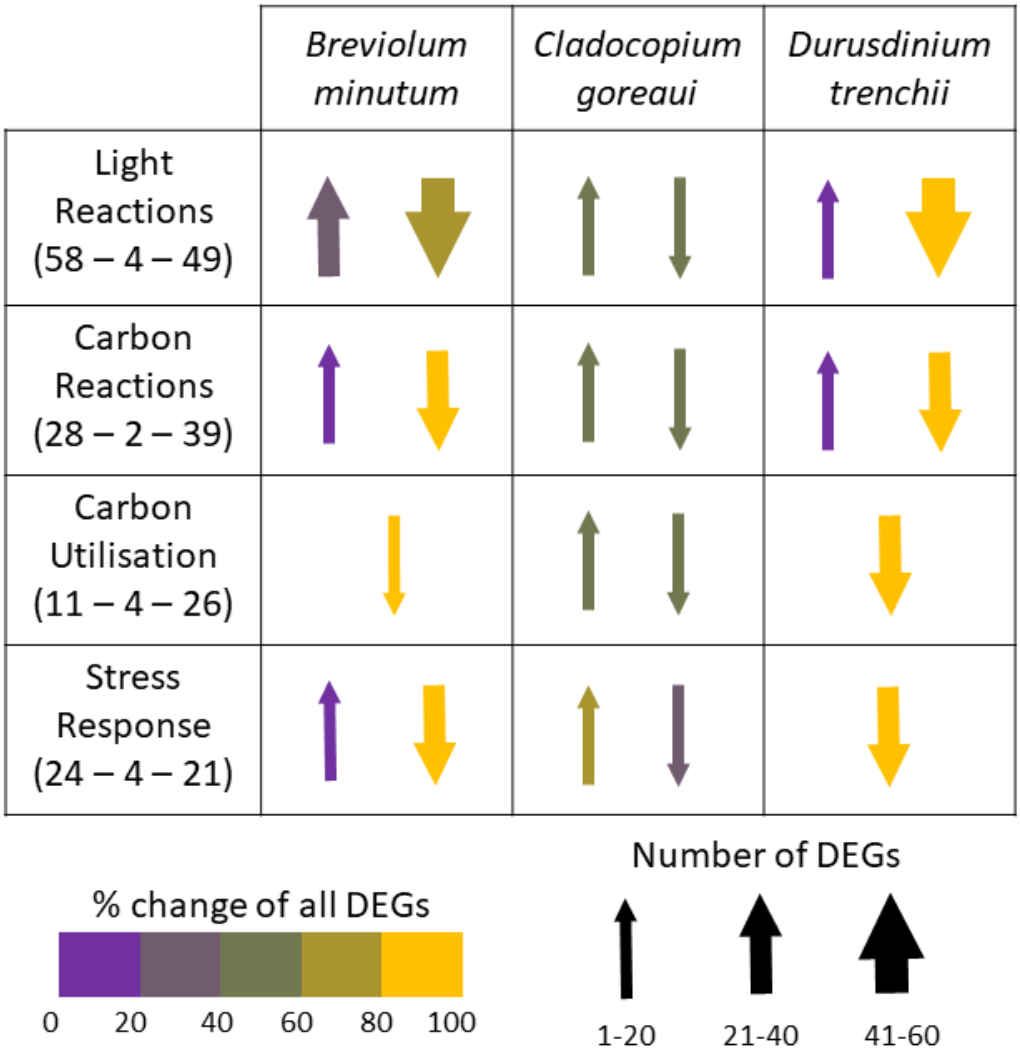

3.5.1. Light reactions

Inhibition of light reactions constituents is well reported in describing thermo-sensitivity amongst different members of Symbiodiniaceae, such as declines in F_v/F_m (e.g. *Breviolum* sp. in Karim et al. 2015; *Cladocopium* sp. in Levin et al. 2016), expression of light-harvesting genes (*Symbiodinium* sp. and *Cladocopium* sp. in McGinley et al. 2012) and repair of photosynthetic machinery (*Symbiodinium* spp. in Takahashi et al. 2009). As expected, under thermal stress we observed an overall decline of F_v/F_m for all isolates throughout the study. More specifically, at the onset of stress, light reaction genes in *B. minutum* started to be down-regulated (at a low log2 fold-change approximating 0.22), an observation accentuated after seven days under heat stress at 32°C, where both light and carbon reactions of *B. minutum* were interrupted. Genes encoding for light reaction proteins were both largely down- (*psaA*/*psaB* genes encoding the P_{700} protein of PSI, and *psbA*/*psbD* encoding the D1 and D2 protein of PSII, respectively) and up-regulated (other PSI subunits such as *psaC*, *psaD*, *psaE* and *psaF*), a pattern previously observed for a thermo-sensitive *Symbiodinium* sp. (ITS type A13) and *Cladocopium* sp. (ITS type C1b-c) subjected to similar duration and intensities of thermal stress (McGinley et al. 2012). Up-regulation of genes encoding these subunits of PSI (*psaC*, *psaD*, *psaE* and *psaF*) under thermal stress were also found in recent works (Salas et al. 2017), where they likely act as photoreductant proteins within the PSI complex (Bengis and Nelson 1977). Photoreduction in PSI is known to be associated with the Mehler reaction, an alternative electron flow acting as a photoprotective mechanism in Symbiodiniaceae (Roberty et al. 2014). Interestingly, the *psaE* gene is also involved in mechanisms of prevention of ROS formation as response to stress in cyanobacteria (Jeanjean et al. 2008), and this family of genes may act to counteract the degradation of photosynthetic protein repair machinery (McGinley et al.

2012). The up-regulation of genes encoding the subunits of PSI in *B. minutum* thus appears crucial where cells attempt to reroute excess energy with alternative electron flows – albeit seemingly unsuccessfully – to minimise oxidative damage occurred in response to thermal stress.

We noted an interesting difference in the response of light-harvesting genes between the thermo-sensitive *B. minutum* and the thermo-tolerant *D. trenchii*, where at the onset of stress *B. minutum* exhibited down-regulation of light-harvesting genes, *D. trenchii* moderately up-regulated their genes at low fold change (log2 FC approximately 0.46). *D. trenchii* further exhibited a slight decrease of F_v/F_m and subsequent down-regulation of light reaction genes (mostly *LHCB*) under prolonged heat stress compared to the control. A recent study demonstrated that in response to thermal stress, cultured *D. trenchii* do not show differential expression of genes associated with photosynthetic light harvesting, electron transport or PSII repair (Bellantuono et al. 2019). The study of Bellantuono et al. (2019) also compared *D. trenchii* living *in hospite* and in culture and found that under ambient conditions, *in hospite* cells are characterised by up-regulated light reaction genes compared to cultures. Furthermore, in response to six hours of thermal stress at 34°C, *D. trenchii* cells living *in hospite* and in culture had an unaffected expression of light-harvesting and electron transport genes, but PSII repair genes *in hospite* were up-regulated compared to cultured *D. trenchii*. Their experimental design was similar to ours in the ramping period (T0 to TI). However, in Bellantuono et al. (2019), transcripts were extracted after six hours of exposure to 34°C, which therefore represents a considerably shorter exposure to heat stress than our time point TE. Thus, it compares in effect better to our post-ramping sampling time point (TI), where transcripts were sampled as soon as temperature reached 32°C. The combination of our results and those from Bellantuono et al. (2019) suggest that thermal ramping of 2°C per day may provide the *D. trenchii* cells' machinery the time to acclimate to higher temperatures, hence not triggering the

"stressed" condition of the cells. The effect of the host could also play a role in symbionts regulation of their light reaction genes where the host can significantly modify the symbiont light environment (Wangpraseurt et al. 2016), but Bellantuono et al. (2019) did not provide physiological data to support this statement. The difference at the onset of stress in light reaction genes between *B. minutum* and *D. trenchii* perhaps indicate different strategies of stress response and acclimation, which we revisit later.

A somewhat intriguing outcome of our experiment with *C. goreaui* is that despite exhibiting significant F_v/F_m decreases at TE, no trends in light reaction gene regulation were apparent relative to the control. Levin et al. (2016) found that in response to thermal stress, a thermo-tolerant *Cladocopium* sp. isolate (ITS type C1) had a sustained photosynthetic ability compared to a thermo-sensitive isolate (also *Cladocopium* sp. ITS type C1) which exhibited a decline in photochemical efficiency. They however did not report any difference in transcriptional response between the genes involved in the light reactions of these two isolates. Study of light-harvesting genes expression in *Cladocopium* sp. (ITS type C3) *in hospite* (Gierz et al. 2016) revealed that isoforms of this category of genes have a variable response and can be both up-regulated and not differentially expressed. In our study, there was a higher proportion of differential expression at low FC (log2 FC $\leq$ 0.5) compared to the other isolates, suggesting a predisposition for *Cladocopium* to post-transcriptional modifications, an outcome consistent with previous studies (Leggat et al. 2011; McGinley et al. 2012; Gierz et al. 2016).

3.5.2. Dark reactions

In comparison to light reaction processes, dark reactions of photosynthesis – and more specifically the ability of Symbiodiniaceae to uptake and utilise Ci in response to stress – are often overlooked, and not well characterised in transcriptome studies to date. Overall, within our study, there were fewer trends observed for dark reactions than light reactions. Instead,

there were several contradictions observed in fact between gene expression and physiological performance. For example, carbonic anhydrase (CA) gene expression was down-regulated in both *B. minutum* and *D. trenchii*, yet Ci fixation was low in *B. minutum* and high in *D. trenchii*. The primary entry point of Ci is dictated by carbon concentrating mechanisms (CCMs) such as carbonic anhydrase (CA), which breaks down dissolved HCO_3 in the media into CO_2 usable by the cell. Thus, it is plausible to expect that down-regulation of CA gene expression would mean less Ci uptake and less carbon fixed. In Chapter 2 (Ros et al. 2020) using the same isolate, we also noted for *B. minutum* an impairment of Ci uptake at 30°C – i.e. 2°C lower than in the present study, suggesting this phenomenon is likely to happen with this species under thermal stress. Our results appear to therefore contradict findings of Oakley et al. (2014) who suggested that CCM activity (through measurement of a reduction in dissolved Ci in the media) was not impacted under 34°C, even for Symbiodiniaceae species considered to be thermo-sensitive (e.g. *B. minutum* ITS type B1).

More importantly, Ci uptake in the thermo-tolerant *D. trenchii* increased with elevated temperature. Oakley et al. (2014) also showed for *D. trenchii* that CCMs were not damaged – but in fact increased activity – under heat stress at temperatures up to 34°C, suggesting a fully functional CCM capable of sustaining Ci uptake for our study at 32°C. We therefore hypothesise that our thermo-tolerant species may be benefitting from increased CCM enzyme activity and thus capable of maintaining Ci uptake with less energetic expenditure – thus freeing-up available energy for other cellular maintenance processes. A study of *C. goreaui in hospite* (Ogawa et al. 2013) corroborates this hypothesis, where increased temperatures did not affect the gene expression of CA in *Cladocopium* sp. (ITS type C3). Interestingly, the animal isoform of the enzyme supplying the symbiont with Ci (Weis et al. 1989; Allemand et al. 1998) was down-regulated, limiting endosymbiont access to Ci during thermal stress, highlighting the importance of the host in regulating Ci assimilation capacity across studies.

Given that the primary site of Ci intake in relation to expressed transcripts did not show a response matching physiology, we investigated the gene expression levels of an enzyme further downstream of the carbon assimilation process in the Calvin-Benson cycle (CBC). RuBisCO, which plays a critical role in breaking down newly formed CO_2 by the into usable organic carbon skeletons by the cell, and thus could be one of the main sites of damage explaining decreased Ci fixation performance. As with the CA genes, we noted a down-regulation for the genes encoding for the large subunit of RuBisCO (*rbcL*; Brown et al. 2008) in both *B. minutum* and *D. trenchii* in response to thermal stress. This response of our thermo-tolerant *D. trenchii* was in contrast with Gierz et al. (2017) whereby for the thermo-tolerant *Fugacium kawagutii*, the expression of the *rbcL* gene was up-regulated in response to thermal stress, only after 28 days of exposure (but not after 19 days). This could suggest that the seven-day timeframe of heat stress in our experiment is too long to see light-harvesting gene expression patterns, and not long enough to see dark reactions expression responses. Lilley et al. (2010) demonstrated that the RuBisCO activity of *Symbiodinium microadriaticum* rapidly declines by up to 80% after acute thermal stress and could perhaps be a primary site of damage inhibiting upstream light reaction processes (Jones et al. 1998; Bhagooli et al. 2013). However, this study was conducted on crude symbiont cell extracts, and the possible mechanisms of repair or stabilisation of RuBisCO (RuBisCO activases, see Bhat et al. 2017; Mueller-Cajar 2017) may apply to thermal stress *in vivo*. Different symbiont taxa isolated from *Pocillopora damicornis* and *Stylophora pistillata* have varying CBC sensitivity in response to thermal stress (Buxton et al. 2012). However, Levin et al. (2016) demonstrated that within the same genus, different *Cladocopium* isolates could have different responses to thermal stress, but without showing any emergent physiological data on any differential CBC sensitivity. Whether the identity of host indeed plays a role in CBC sensitivity of Symbiodiniaceae is yet to be determined.

In summary, gene expression patterns were the same for our thermo-sensitive *B. minutum* isolate and the thermo-tolerant *D. trenchii* for dark reactions encompassing Ci intake and the CBC under heat stress. We observed universal down-regulation of genes associated with both CA and CBC across all isolates, but this did not confirm to differences in physiological performance. Dinoflagellates (and Symbiodiniaceae) possess the form II of RuBisCO (Morse et al. 1995), which is rare among eukaryotes, and there has been no targeted examination of differential CBC performance across different Symbiodiniaceae taxa via either direct enzyme assessment or transcriptional response under temperature stress against which to contextualise findings of the present study. As such, there is limited evidence from the broader literature to contextualise our findings. Therefore, we next explore two possible explanations for why we saw a lack of consistency between gene expression and Ci fixation for our two isolates with very different thermal tolerance.

First and foremost, genuine differential performance in the CBC may exist for *B. minutum* and *D. trenchii*, but cannot be resolved by transcriptomics only, either due to post-transcriptional modifications, the timeframe of the experiment, or both. Mechanisms of post-transcriptional and translational control in dinoflagellates have been extensively reviewed by Roy et al. (2018), to provide insight of those likely inherent to Symbiodiniaceae. Recent studies on Symbiodiniaceae post-transcriptional mechanisms have begun to show a vast array of cellular processes at play, such as production of micro RNA (Baumgarten et al. 2013), RNA editing (Liew et al. 2017) and silencing (in *Prorocentrum*, Zhang and Lin 2019). The combination of proteomic and transcriptomic studies has shown that inconsistencies between the transcriptome and the phenotype of thermally stressed Symbiodiniaceae are common (e.g. Putnam et al. 2013; Mayfield et al. 2016). The study of epigenetic mechanisms now start to emerge for coral-symbiont associations (Liew et al. 2018; Li et al. 2018), and they could further help in lifting the veil still laying on the mechanisms of transcriptional differences underlying

thermal acclimation of Symbiodiniaceae to sustain coral symbiosis (Eirin-Lopez and Putnam 2019). As recommended by Morse et al. (2018), future high-throughput functional studies should focus on proteomics, which directly assess the nature of the proteins functionally active. With the combination of proteomics at a time-resolved sampling, we could be able to resolve the upstream processes of functional response to thermal stress in Symbiodiniaceae.

Secondly, activity of CBC was indeed impacted in both isolates (as evidenced from the transcriptional response), reflecting different upstream delivery of substrates (energy and reductant) to the site of carbon fixation. As light reactions were not impaired in *D. trenchii*, we can hypothesise that energy (ATP) and reductant (NADPH) generated from the linear electron flow (Warner and Suggett 2016) can be redirected to maintenance pathways rather than invested into Ci uptake and CBC pathway. A recent study led by Dang et al. (2019) confirmed Suggett et al. (2008) findings, showing that *Breviolum* spp. do not rely as much as the *Symbiodinium* spp. (categorised as more thermo-tolerant than the *B. minutum* of the present study) on circular electron flow in response to stress, possibly highlighting the differences found in metabolic plasticity to cope with photodamage compared to thermo-tolerant species such as *D. trenchii*. Such a process could be verified by tracking the distribution of photosynthetically-generated electrons by PSII to Ci-fixing and non-Ci-fixing pathways (i.e. linear *vs.* cyclic *vs.* alternative electron flows; Dang et al. 2019) using mass inlet mass spectrometry (MIMS) techniques (Cardol et al. 2011; Hughes et al. 2018b).

3.5.3. Metabolism and stress response

Given the down-regulation of light and dark reactions associated genes for *B. minutum*, it is perhaps unsurprising that metabolism genes also were down-regulated from TI to TE. The physiological shutdown of Ci uptake and the down-regulation of the final gene of the CBC, (*FBP*, encoding the fructose-1,6-biphosphate) would interrupt the metabolism of

photosynthates by arresting glyceraldehyde-3-phosphate (GAP) to the carbohydrate production chain, (glyceraldehyde-3-phosphate dehydrogenase, GAPDH; Takishita et al. 2003). Interestingly, we found the same fate for these genes in *D. trenchii*, which was on par with the downregulation of CBC genes. Recent studies have shown that *D. trenchii* cells can up-regulate their cell cycle processes in response to stress (Bellantuono et al. 2019) and that the cells arrest their division cycle but remain photosynthetically viable after four days of thermal stress (Fujise et al. 2018) in contrast with other isolates that degrade, supporting the hypothesis of *D. trenchii* investing into "metabolic maintenance" under heat stress. Leggat et al. (2011) did not detect any changes in the expression of GAPDH in *Cladocopium* spp. *in hospite* in response to stress (which is consistent with the behaviour of our *Cladocopium* isolate), but this could be genus-specific. Expression of genes involved in the TCA cycle was down-regulated in *D. trenchii* only, suggesting that this species is unlikely to use fatty acids for their maintenance compared to the others. Overall, no particular trend towards lipolytic or glycolytic pathways to obtain energy in response to stress in our studied Symbiodiniaceae species could be determined. Others (Leggat et al. 2011; Gierz et al. 2017) found that the metabolism of fatty acids is likely to occur in response to stress *in hospite* and as a free-living state through an up-regulation of fatty acids desaturases.

Expression of stress response genes (encoding ROS-scavenging enzymes and HSP proteins) followed the same trend as these of metabolism genes. *B. minutum* exhibited a continuous down-regulation of stress response genes from TI to TE, suggesting an inability for these genes to respond to the heat dosing applied through this experiment, and importantly of genes encoding ROS-scavenging enzymes. A similar response was described for a thermo-sensitive *Cladocopium* sp. isolate (ITS type C1, Levin et al. 2016). Such a response is species-specific, where McGinty et al. (2012) further demonstrated a differential production of ROS in

two sensitive species of *Breviolum* sp. (ITS type B1) and *Cladocopium* sp. (ITS type C1) that could also express different levels of ROS-scavenging enzymes.

Stress response genes in *D. trenchii* were up-regulated at TI (CYP-1 encoding the protective cytochrome P_{450} and both *HSP70* and *HSP90*) at low FC (log2 FC $\leq$ 0.5) and then down-regulated at TE (at a log2 FC of approximately 1.60). Response to oxidative stress was also found to be down-regulated by Bellantuono et al. (2019) in *D. trenchii* both *in hospite* and as a free-living state, as soon as six hours after similar thermal stress exposure. They also found a highly up-regulated response of protein folding pathways in their free-living *D. trenchii*, to possibly maintain this species' proteins functional in response to stress, which is characteristic of increased production of chaperone proteins (e.g. HSP70 and HSP90; Levin et al. 2016). This response found after six hours of stress in their experiment may not be detected in ours, as it is likely that expression of proteins occurs at the very early stages of heat stress but not after longer durations (e.g. after 72 hours; Rosic et al. 2014). This early response was not found in our *B. minutum*, perhaps indicating a more rapid synthesis at the onset of stress as a means of acclimation by the thermo-tolerant isolate, and the lack of late response would suggest a persistence of these protective proteins throughout the stress experiment compared to *D. trenchii* after 21 days of stress at 32°C (Lesser 2019).

As for all other pathways described before, *C. goreaui* did not exhibit substantial differences in their expression of genes involved in stress response. We could argue that our length and severity of stress could not be enough, as most differences found in Levin et al. (2016) between thermo-sensitive and tolerant *Cladocopium* spp. occurred after a 13-day exposure to stress. However, both their sensitive and tolerant isolates did not show evidence of physiological stress after nine days, while ours already has a significant decrease in photochemical efficiency by day seven. Consequently, this suggests that our *C. goreaui* was indeed experiencing stress, but that their molecular stress response is happening at low fold

change, as reviewed by Leggat et al. (2011) and further confirmed by studies on Symbiodiniaceae transcriptomes (e.g. Gierz et al. 2016).

3.6. Conclusion

Our study is the first to simultaneously assess the photophysiology, Ci uptake and the subsequent variation of gene expression in response to thermal stress of three distinct Symbiodiniaceae genera. The strong down-regulation of PSI genes in a thermo-sensitive isolate (*Breviolum minutum*) indicates a stronger effect of heat stress on light reaction pathways, which affects both photosynthetic efficiency and Ci uptake. Conversely, an apparent down-regulation of photosynthetic genes and efficiency in a thermo-tolerant isolate (*Durusdinium trenchii*) does not seem to impair their ability to uptake carbon. An early response to thermal (chaperone proteins) and oxidative (ROS-scavenging enzymes) stress in *D. trenchii* suggests employment of protective cellular responses to maintain photosynthetic processes and Ci uptake. Thermo-tolerant species of Symbiodiniaceae such as *D. trenchii* could be able to reroute their energy initially to protective systems (after a possible acclimation to stress), to maintain these essential protective processes. Interestingly, our results suggest that this early response to stress is not found in heat sensitive species such as *B. minutum* further highlighting the pivotal role of genus-specific ability to cope rapidly with thermal stress. Finally, despite starting to detect a physiological response at the end of the experiment (TE), *Cladocopium goreaui* did not show any specific trends in their gene expression, potentially highlighting a high level of post-transcriptional or post-translational modifications.

Our work shows that in comparing three different Symbiodiniaceae species with different thermal stress tolerance, there is a diversity of responses observed that are particularly clear in terms of emergent physiologies rather than molecular wiring. This reinforces the core paradigm of functional diversity but the challenges in drawing divergent physiologies from

transcriptional data. Whether this holds for these isolates once they are *in hospite*, and across different time scales of heat stress (see Suggett and Smith 2020) requires further detailed assessment to further elucidate how light *versus* carbon reactions are impacted by thermal stress. The inclusion of proteomic studies would resolve the uncertainty of transcript fate in stressed cells, whether degraded or subjected to post-transcriptional modifications, and are an obvious area for future studies. Altogether, these results would be useful to help to predict the fate of coral reefs and understand why specific genera of corals are winning – or losing – against the increasing effects of climate change. This knowledge could help in targeting priority areas of management to preserve biodiversity of threatened coral reefs.

3.7. References

Ainsworth, T. D., S. F. Heron, J. C. Ortiz, P. J. Mumby, A. Grech, D. Ogawa, C. M. Eakin and W. Leggat. 2016. Climate change disables coral bleaching protection on the Great Barrier Reef. Science. **352**: 338-342. doi:10.1126/science.aac7125

Allemand, D., P. Furla and S. Bénazet-Tambutté. 1998. Mechanisms of carbon acquisition for endosymbiont photosynthesis in Anthozoa. Canadian Journal of Botany. **76**: 925-941.

Baumgarten, S., T. Bayer, M. Aranda, Y. J. Liew, A. Carr, G. Micklem and C. R. Voolstra. 2013. Integrating microRNA and mRNA expression profiling in *Symbiodinium microadriaticum*, a dinoflagellate symbiont of reef-building corals. BMC Genomics. **14**: 704. doi:10.1186/1471-2164-14-704

Bellantuono, A. J., K. E. Dougan, C. Granados-Cifuentes and M. Rodriguez-Lanetty. 2019. Free-living and symbiotic lifestyles of a thermo-tolerant coral endosymbiont display profoundly distinct transcriptomes under both stable and heat stress conditions. Mol. Ecol. **28**: 5265-5281. doi:10.1111/mec.15300

Bengis, C. and N. Nelson. 1977. Subunit structure of chloroplast photosystem I reaction center. Journal of Biological Chemistry. **252**: 4564-4569.

Bhagooli, R. 2013. Inhibition of Calvin–Benson cycle suppresses the repair of photosystem II in *Symbiodinium*: implications for coral bleaching. Hydrobiologia. **714**: 183-190. doi:10.1007/s10750-013-1535-4

Bhat, J. Y., G. Thieulin-Pardo, F. U. Hartl and M. Hayer-Hartl. 2017. Rubisco activases: AAA+ chaperones adapted to enzyme repair. Front. Mol. Biosci. **4**: 20. doi:10.3389/fmolb.2017.00020

Bopp, L., and others. 2013. Multiple stressors of ocean ecosystems in the 21st century: projections with CMIP5 models. Biogeosciences. **10**: 6225-6245. doi:10.5194/bg-10-6225-2013

Brading, P., M. E. Warner, D. J. Smith and D. J. Suggett. 2013. Contrasting modes of inorganic carbon acquisition amongst *Symbiodinium* (Dinophyceae) phylotypes. New Phytol. **200**: 432-442. doi:10.1111/nph.12379

Bray, N. L., H. Pimentel, P. Melsted and L. Pachter. 2016. Near-optimal probabilistic RNA-seq quantification. Nat. Biotechnol. **34**: 525-527. doi:10.1038/nbt.3519

Brown, C. M., J. D. MacKinnon, A. M. Cockshutt, T. A. Villareal and D. A. Campbell. 2008. Flux capacities and acclimation costs in *Trichodesmium* from the Gulf of Mexico. Marine Biology. **154**: 413-422. doi:10.1007/s00227-008-0933-z

Buxton, L., S. Takahashi, R. Hill and P. J. Ralph. 2012. Variability in the primary site of photosynthetic damage in *Symbiodinium* sp. (Dinophyceae) exposed to thermal stress. J. Phycol. **48**: 117-126. doi:10.1111/j.1529-8817.2011.01099.x

Camp, E. F., and others. 2020a. Revealing changes in the microbiome of Symbiodiniaceae under thermal stress. Environmental Microbiology.

Cardol, P., G. Forti and G. Finazzi. 2011. Regulation of electron transport in microalgae. Biochim. Biophys. Acta. **1807**: 912-918. doi:10.1016/j.bbabio.2010.12.004

Cziesielski, M. J., S. Schmidt-Roach and M. Aranda. 2019. The past, present, and future of coral heat stress studies. Ecol. Evol. **9**: 10055-10066. doi:10.1002/ece3.5576

Dang, K. V., M. Pierangelini, S. Roberty and P. Cardol. 2019. Alternative photosynthetic electron transfers and bleaching phenotypes upon acute heat stress in *Symbiodinium* and *Breviolum* spp. (Symbiodiniaceae) in culture. Frontiers in Marine Science. **6**. doi:10.3389/fmars.2019.00656

Davy, S. K., D. Allemand and V. M. Weis. 2012. Cell biology of cnidarian-dinoflagellate symbiosis. Microbiol. Mol. Biol. Rev. **76**: 229-261. doi:10.1128/MMBR.05014-11

Eakin, C. M., H. P. A. Sweatman and R. E. Brainard. 2019. The 2014–2017 global-scale coral bleaching event: insights and impacts. Coral Reefs. **38**: 539-545. doi:10.1007/s00338-019-01844-2

Eirin-Lopez, J. M. and H. M. Putnam. 2019. Marine environmental epigenetics. Ann. Rev. Mar. Sci. **11**: 335-368. doi:10.1146/annurev-marine-010318-095114

Ezzat, L., J. F. Maguer, R. Grover and C. Ferrier-Pages. 2015. New insights into carbon acquisition and exchanges within the coral-dinoflagellate symbiosis under NH^{4+} and NO^{3-} supply. Proc. Biol. Sci. **282**: 20150610. doi:10.1098/rspb.2015.0610

Fujise, L., M. R. Nitschke, J. C. Frommlet, J. Serodio, S. Woodcock, P. J. Ralph and D. J. Suggett. 2018. Cell cycle dynamics of cultured coral endosymbiotic microalgae (*Symbiodinium*) across different types (species) under alternate light and temperature conditions. J. Eukaryot. Microbiol. **65**: 505-517. doi:10.1111/jeu.12497

Gierz, S. L., B. R. Gordon and W. Leggat. 2016. Integral light-harvesting complex expression in *Symbiodinium* within the coral *Acropora aspera* under thermal stress. Sci. Rep. **6**: 25081. doi:10.1038/srep25081

Gierz, S. L., S. Foret and W. Leggat. 2017. Transcriptomic analysis of thermally stressed *Symbiodinium* reveals differential expression of stress and metabolism genes. Front. Plant. Sci. **8**: 271. doi:10.3389/fpls.2017.00271

González-Pech, R. A., and others. 2019. Genomes of Symbiodiniaceae reveal extensive sequence divergence but conserved functions at family and genus levels. bioRxiv: 800482.

Goyen, S., M. Pernice, M. Szabó, M. E. Warner, P. J. Ralph and D. J. Suggett. 2017. A molecular physiology basis for functional diversity of hydrogen peroxide production amongst *Symbiodinium* spp. (Dinophyceae). Marine Biology. **164**. doi:10.1007/s00227-017-3073-5

Haas, B. J., and others. 2013. De novo transcript sequence reconstruction from RNA-seq using the Trinity platform for reference generation and analysis. Nat. Protoc. **8**: 1494-1512. doi:10.1038/nprot.2013.084

Hill, R., C. M. Brown, K. DeZeeuw, D. A. Campbell and P. J. Ralph. 2011. Increased rate of D1 repair in coral symbionts during bleaching is insufficient to counter accelerated

photo-inactivation. Limnology and Oceanography. **56**: 139-146. doi:10.4319/lo.2011.56.1.0139

Hughes, D. J., D. Varkey, M. A. Doblin, T. Ingleton, A. McInnes, P. J. Ralph, V. van Dongen-Vogels and D. J. Suggett. 2018a. Impact of nitrogen availability upon the electron requirement for carbon fixation in Australian coastal phytoplankton communities. Limnology and Oceanography. **63**: 1891-1910. doi:10.1002/lno.10814

Hughes, D. J., and others. 2018b. Roadmaps and detours: Active chlorophyll-a assessments of primary productivity across marine and freshwater systems. Environ. Sci. Technol. **52**: 12039-12054. doi:10.1021/acs.est.8b03488

Hughes, T. P., and others. 2018. Spatial and temporal patterns of mass bleaching of corals in the Anthropocene. Science. **359**: 80-83. doi:10.1126/science.aan8048

Jeanjean, R., A. Latifi, H. C. Matthijs and M. Havaux. 2008. The PsaE subunit of photosystem I prevents light-induced formation of reduced oxygen species in the cyanobacterium *Synechocystis* sp. PCC 6803. Biochim. Biophys. Acta. **1777**: 308-316. doi:10.1016/j.bbabio.2007.11.009.

Jokiel, P. L., C. P. Jury and I. B. Kuffner. 2016. Coral calcification and ocean acidification. Coral Reefs at the Crossroads: 7-45.

Jones, R. J., O. Hoegh-Guldberg, A. W. D. Larkum and U. Schreiber. 1998. Temperature-induced bleaching of corals begins with impairment of the CO_2 fixation mechanism in zooxanthellae. Plant, Cell and Environment. **21**: 1219-1230. doi:10.1046/j.1365-3040.1998.00345.x

Jones, G. D., E. P. Williams, A. R. Place, R. Jagus and T. R. Bachvaroff. 2015. The alveolate translation initiation factor 4E family reveals a custom toolkit for translational control in core dinoflagellates. BMC Evol. Biol. **15**: 14. doi:10.1186/s12862-015-0301-9

Karim, W., S. Nakaema and M. Hidaka. 2015. Temperature effects on the growth rates and photosynthetic activities of *Symbiodinium* cells. Journal of Marine Science and Engineering. **3**: 368-381. doi:10.3390/jmse3020368

Kolber, Z. S., O. Prášil and P. G. Falkowski. 1998. Measurements of variable chlorophyll fluorescence using fast repetition rate techniques: defining methodology and experimental protocols. Biochimica et Biophysica Acta (BBA) – Bioenergetics. **1367**: 88-106. doi:10.1016/s0005-2728(98)00135-2

Kramer, W. E., I. Caamano-Ricken, C. Richter and K. Bischof. 2012. Dynamic regulation of photoprotection determines thermal tolerance of two phylotypes of *Symbiodinium* clade A at two photon fluence rates. Photochem. Photobiol. **88**: 398-413. doi:10.1111/j.1751-1097.2011.01048.x

Law, C. W., Y. Chen, W. Shi and G. K. Smyth. 2014. voom: Precision weights unlock linear model analysis tools for RNA-seq read counts. Genome Biol. **15**: R29. doi:10.1186/gb-2014-15-2-r29

Leggat, W., S. Whitney and D. Yellowlees. 2004. Is coral bleaching due to the instability of the zooxanthellae dark reactions? Symbiosis. **37**: 137-153.

Leggat, W., D. Yellowlees and M. Medina. 2011. Recent progress in *Symbiodinium* transcriptomics. Journal of Experimental Marine Biology and Ecology. **408**: 120-125. doi:10.1016/j.jembe.2011.07.032

Lesser, M. P. 2006. Oxidative stress in marine environments: biochemistry and physiological ecology. Annu. Rev. Physiol. **68**: 253-278. doi:10.1146/annurev.physiol.68.040104.110001

Lesser, M. P. 2019. Phylogenetic signature of light and thermal stress for the endosymbiotic dinoflagellates of corals (Family Symbiodiniaceae). Limnology and Oceanography. **64**: 1852-1863. doi:10.1002/lno.11155

Levin, R. A., V. H. Beltran, R. Hill, S. Kjelleberg, D. McDougald, P. D. Steinberg and M. J. van Oppen. 2016. Sex, scavengers, and chaperones: Transcriptome secrets of divergent *Symbiodinium* thermal tolerances. Mol. Biol. Evol. **33**: 2201-2215. doi:10.1093/molbev/msw119

Li, Y., Y. J. Liew, G. Cui, M. J. Cziesielski, N. Zahran, C. T. Michell, C. R. Voolstra and M. Aranda. 2018. DNA methylation regulates transcriptional homeostasis of algal endosymbiosis in the coral model *Aiptasia*. Sci. Adv. **4**: eaat2142. doi:10.1126/sciadv.aat2142

Liew, Y. J., Y. Li, S. Baumgarten, C. R. Voolstra and M. Aranda. 2017. Condition-specific RNA editing in the coral symbiont *Symbiodinium microadriaticum*. PLoS Genet. **13**: e1006619. doi:10.1371/journal.pgen.1006619

Liew, Y. J., and others. 2018. Epigenome-associated phenotypic acclimatization to ocean acidification in a reef-building coral. Sci. Adv. **4**: eaar8028. doi:10.1126/sciadv.aar8028

Lilley, R. M., P. J. Ralph and A. W. Larkum. 2010. The determination of activity of the enzyme Rubisco in cell extracts of the dinoflagellate alga *Symbiodinium* sp. by manganese chemiluminescence and its response to short-term thermal stress of the alga. Plant Cell Environ. **33**: 995-1004. doi:10.1111/j.1365-3040.2010.02121.x

Mayfield, A. B., Y. B. Wang, C. S. Chen, S. H. Chen and C. Y. Lin. 2016. Dual-compartmental transcriptomic + proteomic analysis of a marine endosymbiosis exposed to environmental change. Mol. Ecol. **25**: 5944-5958. doi:10.1111/mec.13896

McGinley, M. P., M. D. Aschaffenburg, D. T. Pettay, R. T. Smith, T. C. LaJeunesse and M. E. Warner. 2012. Transcriptional response of two core photosystem genes in *Symbiodinium* spp. exposed to thermal stress. PLoS One. **7**: e50439. doi:10.1371/journal.pone.0050439

McIlroy, S. E., R. Cunning, A. C. Baker and M. A. Coffroth. 2019. Competition and succession among coral endosymbionts. Ecol. Evol. **9**: 12767-12778. doi:10.1002/ece3.5749

Mirkovic, T., E. E. Ostroumov, J. M. Anna, R. van Grondelle, Govindjee and G. D. Scholes. 2017. Light absorption and energy transfer in the antenna complexes of photosynthetic organisms. Chem. Rev. **117**: 249-293. doi:10.1021/acs.chemrev.6b00002

Mitchell, A. L., and others. 2019. InterPro in 2019: improving coverage, classification and access to protein sequence annotations. Nucleic Acids Res. **47**: D351-D360. doi:10.1093/nar/gky1100

Morse, D., P. Salois, P. Markovic and J. W. Hastings. 1995. A nuclear-encoded form II RuBisCO in dinoflagellates. Science. **268**: 1622-1624. doi:10.1126/science.7777861

Morse, D., S. P. K. Tse and S. C. L. Lo. 2018. Exploring dinoflagellate biology with high-throughput proteomics. Harmful Algae. **75**: 16-26. doi:10.1016/j.hal.2018.03.010

Mueller-Cajar, O. 2017. The diverse AAA+ machines that repair inhibited Rubisco active sites. Front. Mol. Biosci. **4**: 31. doi:10.3389/fmolb.2017.00031

Oakley, C. A., G. W. Schmidt and B. M. Hopkinson. 2014. Thermal responses of *Symbiodinium* photosynthetic carbon assimilation. Coral Reefs. **33**: 501-512. doi:10.1007/s00338-014-1130-9

Ogawa, D., T. Bobeszko, T. Ainsworth and W. Leggat. 2013. The combined effects of temperature and CO_2 lead to altered gene expression in *Acropora aspera*. Coral Reefs. **32**: 895-907. doi:10.1007/s00338-013-1046-9

Putnam, H. M., A. B. Mayfield, T. Y. Fan, C. S. Chen and R. D. Gates. 2012. The physiological and molecular responses of larvae from the reef-building coral *Pocillopora damicornis* exposed to near-future increases in temperature and pCO_2. Marine Biology. **160**: 2157-2173. doi:10.1007/s00227-012-2129-9

Quigley, K. M., A. C. Baker, M. A. Coffroth, B. L. Willis and M. J. H. van Oppen. 2018. Bleaching resistance and the role of algal endosymbionts. Coral Bleaching: Patterns, Processes, Causes and Consequences. M. J. H. van Oppen and J. M. Lough. Cham, Springer International Publishing: 111-151.

Ritchie, M. E., B. Phipson, D. Wu, Y. Hu, C. W. Law, W. Shi and G. K. Smyth. 2015. limma powers differential expression analyses for RNA-sequencing and microarray studies. Nucleic Acids Res. **43**: e47. doi:10.1093/nar/gkv007

Roberty, S., B. Bailleul, N. Berne, F. Franck and P. Cardol. 2014. PSI Mehler reaction is the main alternative photosynthetic electron pathway in *Symbiodinium* sp., symbiotic dinoflagellates of cnidarians. New Phytol. **204**: 81-91. doi:10.1111/nph.12903

Ros, M., E. F. Camp, D. J. Hughes, J. R. Crosswell, M. E. Warner, W. P. Leggat and D. J. Suggett. 2020. Unlocking the black-box of inorganic carbon-uptake and utilization strategies among coral endosymbionts (Symbiodiniaceae). Limnology and Oceanography. doi:10.1002/lno.11416

Rosic, N., P. Kaniewska, C. K. Chan, E. Y. Ling, D. Edwards, S. Dove and O. Hoegh-Guldberg. 2014. Early transcriptional changes in the reef-building coral *Acropora aspera* in response to thermal and nutrient stress. BMC Genomics. **15**: 1052. doi:10.1186/1471-2164-15-1052

Roy, S., R. Jagus and D. Morse. 2018. Translation and translational control in dinoflagellates. Microorganisms. **6**. doi:10.3390/microorganisms6020030

Rueden, C. T., J. Schindelin, M. C. Hiner, B. E. DeZonia, A. E. Walter, E. T. Arena and K. W. Eliceiri. 2017. ImageJ2: ImageJ for the next generation of scientific image data. BMC Bioinformatics. **18**: 529. doi:10.1186/s12859-017-1934-z

Salas, B. H., J. A. Haslun, K. B. Strychar, P. H. Ostrom and J. M. Cervino. 2017. Site-specific variation in gene expression from *Symbiodinium* spp. associated with offshore and inshore *Porites astreoides* in the lower Florida Keys is lost with bleaching and disease stress. PLoS One. **12**: e0173350. doi:10.1371/journal.pone.0173350

Schindelin, J., and others. 2012. Fiji: an open-source platform for biological-image analysis. Nat. Methods. **9**: 676-682. doi:10.1038/nmeth.2019

Steemann-Nielsen, E. 1952. The use of radio-active carbon (C^{14}) for measuring organic production in the sea. Journal de Conseil. **18**: 117-140.

Suggett, D. J., M. E. Warner, D. J. Smith, P. Davey, S. Hennige and N. R. Baker. 2008. Photosynthesis and production of hydrogen peroxide by *Symbiodinium* (Pyrrhophyta) phylotypes with different thermal tolerances. J. Phycol. **44**: 948-956. doi:10.1111/j.1529-8817.2008.00537.x

Suggett, D. J., S. Goyen, C. Evenhuis, M. Szabo, D. T. Pettay, M. E. Warner and P. J. Ralph. 2015. Functional diversity of photobiological traits within the genus *Symbiodinium* appears to be governed by the interaction of cell size with cladal designation. New Phytol. **208**: 370-381. doi:10.1111/nph.13483

Suggett, D. J., M. E. Warner and W. Leggat. 2017. Symbiotic dinoflagellate functional diversity mediates coral survival under ecological crisis. Trends Ecol. Evol. **32**: 735-745. doi:10.1016/j.tree.2017.07.013

Suggett, D. J. and D. J. Smith. 2020. Coral bleaching patterns are the outcome of complex biological and environmental networking. Glob. Chang. Biol. doi:10.1111/gcb.14871

Swain, T. D., and others. 2016. Coral bleaching response index: a new tool to standardize and compare susceptibility to thermal bleaching. Glob. Chang. Biol. **22**: 2475-2488. doi:10.1111/gcb.13276

Takahashi, S., T. Nakamura, M. Sakamizu, R. van Woesik and H. Yamasaki. 2004. Repair machinery of symbiotic photosynthesis as the primary target of heat stress for reef-building corals. Plant Cell Physiol. **45**: 251-255. doi:10.1093/pcp/pch028

Takahashi, S. and N. Murata. 2008. How do environmental stresses accelerate photoinhibition? Trends Plant Sci. **13**: 178-182. doi:10.1016/j.tplants.2008.01.005

Takahashi, S., S. M. Whitney and M. R. Badger. 2009. Different thermal sensitivity of the repair of photodamaged photosynthetic machinery in cultured *Symbiodinium* species. Proc. Natl. Acad. Sci. U. S. A. **106**: 3237-3242. doi:10.1073/pnas.0808363106

Takishita, K., K. Ishida and T. Maruyama. 2003. An enigmatic GAPDH gene in the symbiotic dinoflagellate genus *Symbiodinium* and its related species (the order Suessiales): possible lateral gene transfer between two eukaryotic algae, dinoflagellate and euglenophyte. Protist. **154**: 443-454. doi:10.1078/143446103322454176

Tanaka, Y., A. Suzuki and K. Sakai. 2018. The stoichiometry of coral-dinoflagellate symbiosis: carbon and nitrogen cycles are balanced in the recycling and double translocation system. ISME J. **12**: 860-868. doi:10.1038/s41396-017-0019-3

Vass, I. 2012. Molecular mechanisms of photodamage in the Photosystem II complex. Biochim. Biophys. Acta. **1817**: 209-217. doi:10.1016/j.bbabio.2011.04.014

Wangpraseurt, D., M. Pernice, P. Guagliardo, M. R. Kilburn, P. L. Clode, L. Polerecky and M. Kuhl. 2016. Light microenvironment and single-cell gradients of carbon fixation in tissues of symbiont-bearing corals. ISME J. **10**: 788-792. doi:10.1038/ismej.2015.133

Warner, M. E., W. K. Fitt and G. W. Schmidt. 1999. Damage to photosystem II in symbiotic dinoflagellates: a determinant of coral bleaching. Proc. Natl. Acad. Sci. U. S. A. **96**: 8007-8012. doi:10.1073/pnas.96.14.8007

Warner, M. E. and D. J. Suggett. 2016. The photobiology of *Symbiodinium* spp.: Linking physiological diversity to the implications of stress and resilience. The Cnidaria, Past, Present and Future: 489-509.

Weis, V. M., G. J. Smith and L. Muscatine. 1989. A "CO_2 supply" mechanism in zooxanthellate cnidarians: role of carbonic anhydrase. Marine Biology. **100**: 195-202. doi:10.1007/bf00391958

Xiang, T., W. Nelson, J. Rodriguez, D. Tolleter and A. R. Grossman. 2015. *Symbiodinium* transcriptome and global responses of cells to immediate changes in light intensity when grown under autotrophic or mixotrophic conditions. Plant J. **82**: 67-80. doi:10.1111/tpj.12789

Zhang, C. and S. Lin. 2019. Initial evidence of functional siRNA machinery in dinoflagellates. Harmful Algae. **81**: 53-58. doi:10.1016/j.hal.2018.11.014

3.8. Supplementary Information

Supplementary Table S3.1 Full list of proteins and their associated genes and functions used to target and refine the transcripts analysis in all the studied Symbiodiniaceae (*Breviolum minutum*, *Cladocopium goreaui,* and *Durusdinium trenchii*). Shade of cells represent the functional grouping proteins were associated with green: light reactions; blue: dark reactions; yellow: metabolism; orange: stress response; grey: transport. Information of protein function was retrieved from the UniProt database.

See Appendix p.224

Supplementary Table S3.2. Summary of DEGs for *Breviolum minutum* at the TI of the experiment (post-temperature ramping).

See attached electronic Supplementary Material

Supplementary Table S3.3. Summary of DEGs for *Cladocopium goreaui* at the TI of the experiment (post-temperature ramping).

See attached electronic Supplementary Material

Supplementary Table S3.4. Summary of DEGs for *Durusdinium trenchii* at the TI of the experiment (post-temperature ramping).

See attached electronic Supplementary Material

Supplementary Table S3.5. Summary of DEGs for *Breviolum minutum* at the TE of the experiment (after seven days at 32°C).

See attached electronic Supplementary Material

Supplementary Table S3.6. Summary of DEGs for *Cladocopium goreaui* at the TE of the experiment (after seven days at 32°C).

See attached electronic Supplementary Material

Supplementary Table S3.7. Summary of DEGs for *Durusdinium trenchii* at the TE of the experiment (after seven days at 32°C).

See attached electronic Supplementary Material

Supplementary Table S3.8. Summary of one-way ANOVAs carried out on the ^{14}C uptake data. Differences are between control and treatment for each time point. The star symbol denotes a significant difference at alpha = 0.05

Isolate	Time point	ANOVA
Breviolum minutum	T0	$F_{(1,6)} = 1.322$ $P = 0.294$
	TI	$F_{(1,6)} = 0.215$ $P = 0.659$
	TE	$F_{(1,6)} = 43.338$ **$P < 0.001$***
Cladocopium goreaui	T0	$F_{(1,6)} = 0.031$ $P = 0.866$
	TI	$F_{(1,6)} = 1.143$ $P = 0.326$
	TE	$F_{(1,6)} = 2.458$ **$P = 0.024$***
Durusdinium trenchii	T0	$F_{(1,6)} = 9.545$ $P = 0.422$
	TI	$F_{(1,6)} = 11.326$ $P = 0.447$
	TE	$F_{(1,6)} = 5.269$ **$P = 0.002$***

Supplementary Table S3.9. Summary of genes (functional proteins between brackets) sharing a difference in expression between the studied Symbiodiniaceae isolates (B1: *B. minutum*; C1: *C. goreaui*; D1a: *D. trenchii*) after seven days of thermal stress (32°C)

Functional group	DEGs (Proteins)			
	B1-C1	C1-D1a	B1-D1a	All
Light reactions	1 (1)	0	38 (4)	3 (2)
Carbon reactions	1 (1)	0	21 (7)	1 (1)
Carbon utilisation	0	2 (2)	7 (4)	2 (1)
Stress response	0	0	14 (4)	3 (2)
Total	2 (2)	2 (2)	80 (19)	9 (6)

Supplementary Table S3.10. Heat-map summarising the differential gene expression at the end of the temperature ramping (TI) and after seven days of thermal stress at 32°C (TE) in our three Symbiodiniaceae isolates (B1: *B. minutum*; C1: *C. goreaui*; D1a: *D. trenchii*). Heat-map was populated first for the DEGs conforming to our threshold cut-off (log2 fold change [FC] ≥1 and false discovery rate [FDR] ≤ 0.05) for either TI and TE, and then the corresponding DEG for the same gene at the other time point was reported regardless of significance and log2 fold change. Blank cells denote the lack of DEGs according to our set cut-off for both TI and TE. The presence of a star in the column "Sig" denotes a FDR < 0.05. Shade of "Protein" column represent the functional grouping proteins were associated with green: light reactions; blue: dark reactions; yellow: metabolism; orange: stress response. Colour scale of heat-map varies from a gradient of purple (most down-regulated) to gold (most up-regulated).

Protein name (gene)	*B. minutum* (B1-UTS-B)				*C. goreaui* (C1-SCF124)				*D. trenchii* (D1a-UTS-D)			
	TI		TE		TI		TE		TI		TE	
	Log2 FC	Sig	Log2 FC	Sig	Log2 FC	Sig	Log2 FC	Sig	Log2 FC	Sig	Log2 FC	Sig
Light harvesting												
Chlorophyll-*a*-b binding proteins	-0.46		-1.29	*	0.23		1.11	*	0.26		-1.15	*
	-0.26		-1.16	*	-0.29		-1.41	*	0.49		-1.46	*
	-0.41		-1.44	*					0.70		-2.67	*
	-0.24		-1.66	*					0.56		-3.39	*
	-0.37		-1.44	*					0.28		-1.17	*
	0.59		2.36	*					0.38		-1.71	*
	-0.24		-1.18	*					0.47		-1.03	*
	-0.40		-1.05	*					0.35		-1.16	*
	-0.20		-2.06	*					1.17		-3.19	*
	-0.35		-1.69	*					0.32		-1.11	*
	-0.51		-1.75	*					0.47		-2.75	*
	-0.41		-2.06	*					0.54		-2.10	*
	-0.35		-1.36	*					0.41		-2.42	*
	0.08		-1.27	*					0.19		-1.08	*
	-0.35		-1.91	*					1.20		-3.16	*

Chlorophyll-*a*-b binding proteins	-0.33		-1.08	*					-0.05		-1.07	*
	0.49		1.15	*					0.29		-1.16	*
	-0.63		-2.17	*					0.06		-1.25	*
	0.03		-1.30	*					0.88		-2.98	*
	-0.46		-2.54	*					0.08		-1.30	*
	-0.36		-1.55	*					0.50		-2.46	*
	-0.34		-2.06	*					0.71		-2.92	*
	-0.13		-1.31	*					-0.19		1.68	*
	-0.09		-1.38	*					0.62		-2.31	*
	0.26		1.04	*					0.95		-3.21	*
	0.43	*	1.07	*					0.48		-2.02	*
	-0.52		-1.66	*					0.23		-1.54	*
	-0.33		-1.80	*					0.63		-3.00	*
	-0.28		-2.40	*					0.81		-2.84	*
	-0.13		-2.25	*					-0.11		-1.10	*
	-0.08		-1.05	*					0.95		-2.42	*
	-0.35		-1.52	*					0.20		-1.72	*
	-0.31		-1.45	*					0.26		-1.26	*
	-0.51		-2.35	*					0.66		-2.58	*
									1.14		-3.33	*
									0.48		-2.01	*
									0.15		-1.28	*
									-0.35		1.13	*
									0.84		-3.45	*
									0.54		-1.65	*
									0.29		-1.17	*
Peridinin-chlorophyll-*a* binding protein, chloroplastic	0.00		-1.18	*	-0.05		-1.18	*				
Photosystem antenna protein-like	0.59		-4.90	*								

Electron transport												
Cytochrome c oxidase subunit 1 (*ctaD*)	1.10		1.69	*								
Cytochrome c oxidase subunit 2 (*COX2*)	0.17		1.13	*					0.16		-1.24	*
Succinate dehydrogenase [ubiquinone] flavoprotein subunit, mitochondrial (*SDH1*)									0.21		-1.66	*
Cytochrome b6-f complex iron-sulphur subunit, chloroplastic (*petC*)							*		0.31		1.58	*
Cytochrome b6-f complex subunit 4 (*petD*)	1.25		-4.69	*								*
Cytochrome f (*petA*)	0.25		2.00	*								
Ferredoxin-1 (*petF*)	-0.34		-1.24	*	0.42		1.40	*	0.32		-1.64	*
	-0.31		-1.67	*					0.38		-1.84	*
	-0.37		-1.37	*					-0.02		-1.69	*
	-0.77		-1.02	*								
PSI - Photosynthesis												
Photosystem I P700 chlorophyll-*a* apoprotein A1 (*psaA*)	0.88		-5.68	*								
Photosystem I PsaA/PsaB (*psaA*/*psaB*)	1.12		-5.36	*								
	1.05		-4.97	*								
Photosystem I iron-sulphur center (*psaC*)	0.49		1.33	*								
	0.39		1.34	*								
Photosystem I reaction center subunit II, chloroplastic (*psaD*)	0.29		1.16	*								
Photosystem I reaction center subunit III, chloroplastic (*psaF*)	0.23		1.25	*								
Photosystem I reaction center subunit IV, chloroplastic (*psaE*)	0.49		1.17	*								

PSII - Photosynthesis												
Oxygen-evolving enhancer protein 2-1, chloroplastic (*psbP*)	0.27		1.53	*					-0.04		-1.31	*
	-0.34		-1.54	*								
Oxygen-evolving enhancer protein 3-1, chloroplastic (*psbQ*)									0.23		-1.47	*
Photosystem II 12 kDa extrinsic protein, chloroplastic (*psbU*)	0.20		1.25	*								
Photosystem II D1 protein (*psbA*)	1.00		-4.82	*								
Photosystem II D2 protein (*psbD*)	1.11		-4.91	*								
Photosystem II reaction center protein J (*psbJ*)	0.52		1.13	*								
Calvin-Benson cycle												
Fructose-1,6-bisphosphatase, chloroplastic (*FBP*)	-0.48		-1.72	*					0.27		-1.82	*
Fructose-bisphosphate aldolase (*fba*)	-0.43		-1.53	*					0.20		-1.81	*
	-0.36		-1.02	*					0.32		-1.32	*
	-0.30		-2.14	*								
Phosphoglycerate kinase (*pgk*)	0.01		-1.45	*					-0.09		-1.20	*
	-0.56		-2.10	*					0.34		-2.16	*
									0.18		-1.28	*
Phosphoribulokinase (*prkB*)	-0.27		-1.01	*	0.44	*	1.08	*	-0.52	*	-1.06	*
	-0.23		-2.31	*					0.21		-1.57	*
									0.14		-1.04	*
Ribulose bisphosphate carboxylase (*rbcL*)	-0.51		-2.15	*					0.26		-1.31	*
	-0.34		-1.47	*					0.38		-1.32	*
	-0.50		-1.47	*					0.16		1.41	*
									0.59		-2.88	*
Ribulose-phosphate 3-epimerase, chloroplastic (*rpe*)	0.77	*	2.05	*	0.02		-1.00	*				

Transketolase (*tkt*)	-0.37		-1.02	*		0.06		-1.46	*
	-0.32		-1.05	*		0.04		-1.34	*
	-0.50		-1.29	*		0.34		-2.08	*
	-0.44		-1.06	*		-0.01		-1.58	*
	-0.24		-1.69	*		0.15		-1.55	*
	-0.41		-1.54	*		0.13		-1.29	*
	-0.31		-1.42	*		0.10		-1.33	*
	-0.28		-1.23	*		0.46		-1.12	*
						0.45		-1.74	*
						0.22		-1.42	*
Triose phosphate isomerase (*tpiA*)	-0.75	*	-1.05	*		0.18		-1.72	*
	-0.18		-1.12	*					
	-0.43		-1.43	*					
Pentose-phosphate pathway									
Glucose-6-phosphate isomerase (*pgi*)	-0.35		-1.03	*					
	-0.29		-1.12	*					
Carbon fixation									
Carbonic anhydrase (AN1805)	0.00		-1.12	*		-0.04		1.23	*
	-0.53		-3.14	*		0.40		-2.04	*
	-0.61		-1.69	*		0.19		-1.97	*
						0.43		-2.07	*
						0.49		-2.01	*
						0.47		-2.29	*
						0.54		-1.71	*
						0.11		-1.67	*
						0.45		-2.67	*
						0.30		-1.77	*
						0.39		-1.70	*
						0.53		-1.75	*

Metabolism																
Glutamate synthase (*GLT1*)	-0.48		-2.47	*								0.51		-1.05	*	
	-0.79		-1.72	*								0.53		-2.55	*	
3-isopropylmalate dehydratase (*leuA*)						-0.24	*	-1.06	*			0.14		-1.24	*	
Light-dependent protochlorophyllide reductase; iron-sulphur ATP-binding protein (*DPOR*)												0.03		-1.02	*	
												0.48		-1.15	*	
												0.21		-1.09	*	
												0.43		-2.12	*	
												0.54		-1.68	*	
												0.30		-1.23	*	
												0.39		-1.43	*	
Glycerol-3-phosphate dehydrogenase [NAD(P)+] (*gpsA*)												0.19		-1.14	*	
ATP-citrate synthase (*Acly*)	-0.32		-1.57	*								0.18		-1.06	*	
												0.15		-1.65	*	
NADH-cytochrome b5 reductase 2 (*cyb5r2*)	-1.05	*	-0.86	*								0.33		-2.75	*	
	-0.22		-2.53	*								0.09		-1.64	*	
												0.16		-1.41	*	
4-hydroxyphenylpyruvate dioxygenase (*lly*)	-0.38		-1.47	*												
Photorespiration																
Aminotransferase, class I/class II	-0.23		-1.73	*		-0.03		1.07	*			0.12		-1.02	*	
	-0.40		-1.35	*		-0.06		1.02	*			0.23		-1.28	*	
	-0.45		-1.53	*								0.21		-1.05	*	
	-0.19		-1.41	*								0.17		-1.32	*	
Serine hydroxymethyltransferase 1, mitochondrial (*SHM1*)												0.10		-1.20	*	

TCA cycle															
Citrate synthase (*gltA*)	-0.32		-1.57	*						-0.09		-1.03	*		
										0.18		-1.06	*		
										0.15		-1.65	*		
										0.29		-1.03	*		
Malate dehydrogenase, mitochondrial (*MDH2*)					-0.04		-1.11	*		0.13		-1.77	*		
Stress response															
Photosystem II repair protein PSB27-H1, chloroplastic (*psb27-1*)										-0.04		-1.12	*		
Catalase-peroxidase (*katG*)	-0.60		-2.05	*						0.00		-1.12	*		
Cytochrome P450 (*CYP-1*)	-0.43		-1.29	*	-0.13		-1.15	*		-0.01		-1.43	*		
	-0.57	*	-3.20	*	-0.21		1.27	*		0.49		-1.93	*		
	-0.47		-1.01	*						0.19		-1.21	*		
	0.65		2.58	*						0.07		-1.84	*		
	0.00		1.17	*						0.58		-1.70	*		
	-0.25		-1.03	*						0.42	*	-1.15	*		
	0.17		-1.89	*						0.19		-1.27	*		
	-0.61		-1.14	*											
	-0.62		-1.56	*											
Glutathione peroxidase 1, mitochondrial (*GPX*)	-1.10	*	-1.99	*						0.06		-2.66	*		
	-0.53		-2.32	*											
	-0.64		-2.63	*											
	-0.65		-1.11	*											
Heat shock 70 kDa protein (*HSP70*)	-0.39	*	-1.45	*	0.20		1.30	*		0.43		-2.16	*		
	-0.28		-1.16	*						0.40		-1.45	*		
	-0.26		-1.45	*						0.14		-1.33	*		
	-0.21		-1.01	*						0.34		-1.85	*		
										0.22		-1.36	*		

Heat shock protein 90 (*HSP90*)	0.10		-1.58	*	-1.11	*	-0.84	*	0.25		-1.16	*
	-0.47		-1.81	*					0.04		-1.39	*
	-0.51		-1.92	*					0.35		-1.80	*
									0.18		-1.93	*
									0.05		-2.11	*
Redoxin	0.60		2.10	*								
Superoxide dismutase [Cu-Zn] (*sodC*)	-0.51		-2.21	*					0.41		-2.10	*
Superoxide dismutase [Ni] (*sodB*)	0.17		-1.28	*								

Chapter 4

Extreme mangrove corals exhibit lower ^{13}C uptake and translocated compounds than their reef counterparts as a trade-off for survival

Mickael Ros[1], David J. Suggett[1], John Edmondson[2], Trent Haydon[1], David J. Hughes[1], Mikael Kim[1], Paul Guagliardo[3], Jeremy Bougoure[3], Mathieu Pernice[1], Jean-Baptiste Raina[1], Emma F. Camp[1]

[1]University of Technology Sydney, Climate Change Cluster, Ultimo NSW 2007, Australia

[2]Wavelength Reef Cruises, Port Douglas, QLD 4877, Australia

[3]Centre for Microscopy, Characterisation and Analysis, University of Western Australia, Perth, WA, Australia

This chapter is written as a stand-alone draft paper for publication.

4.1. Abstract

Fixation of inorganic carbon (Ci) by Symbiodiniaceae and translocation to the coral host are essential to symbiosis; however, we have little information on how these processes change for corals adapted to survive across environmental gradients. Here, we investigate the reef-building coral *Pocillopora acuta* that persists from a reef habitat into an extreme mangrove lagoon on the Great Barrier Reef. The mangrove lagoon is a model system to evaluate the effects future predicted climate conditions (specifically warmer waters, low pH and low oxygen) will have on coral physiology and carbon translocation potential. We combined respirometry measurements to characterise light reactions, and on both freshly isolated symbionts and whole coral used stable isotope ^{13}C labelling coupled with NanoSIMS imaging to track the incorporation of Ci and subsequent translocation to the host. Our results suggest that *P. acuta* has metabolic strategies that differ between habitats, associated with a shift in dominant associated Symbiodiniaceae from *Cladocopium* in the reef corals to *Durusdinium* in the mangrove corals. This shift in major ITS2 symbiont type was associated with a change in "photosynthetic strategy", with *P. acuta* in the mangroves preferentially utilising absorbed light for photochemistry over non-photochemical quenching (photoprotection). Mangrove colonies were less able to fix Ci (but had the same proportion of translocated photosynthates) than *P. acuta* found on the reef (~ 30% decrease), possibly due to the need to sustain cellular maintenance processes – a trade-off to tolerating the multiple stressors of the mangrove location. In both habitats, Ci uptake was greatly enhanced by the presence of the host compared to isolated symbionts. Collectively our results build on the body of literature demonstrating that corals utilise diverse physiological strategies to survive under extreme environmental conditions, and specifically that the extent of carbon translocation in mangroves is the same as in the reefs, despite a lower Ci uptake compared to the reef.

4.2. Introduction

The ecological success of reef-building corals resides on their ability to establish and maintain metabolic exchanges through an effective symbiotic association in resource exchange with dinoflagellates from the family Symbiodiniaceae. Associations of the cnidarian host with different genera, species or even genetic types of the same species of Symbiodiniaceae have been found to influence profoundly the stress resilience of the coral holobiont (e.g. Berkelmans and van Oppen. 2006; Abrego et al. 2008; Howells et al. 2011; Oliver and Palumbi 2011). Corals commonly appear to host different Symbiodiniaceae associations across environmental gradients, presumably since the landscape of resources available to any given coral host changes (e.g. Matthews et al. 2017; Suggett et al. 2017). For example, Hennige et al. (2010) observed a flexibility (*sensu* Baker 2003) of symbiont types between *Cladocopium* and *Durusdinium* from optimal reef environments to mangrove waters for the coral *Goniastrea aspera*. Conversely, Howells et al. (2016) found that *Platygyra deadala* corals in the Persian-Arabian Gulf are flexible between *Durusdinium* and *Cladocopium*. Thus, host-Symbiodiniaceae plasticity is a central means for corals to acclimatise to a broad range of conditions and expand their effective niche.

Whilst associating with different Symbiodiniaceae taxa clearly provides benefits towards thriving into extreme environments (Berkelmans and van Oppen 2006; Howells et al. 2016), these relationships inevitably come with a "trade-off". For example, *Durusdinium* (type D1) symbionts translocate less photosynthetic compounds to their hosts than *Cladocopium* (types C1 and C3; Cooper et al. 2011), and thus have been considered somewhat "parasitic" (Lesser et al. 2013; Baker et al. 2018) or "selfish" (Stat and Gates 2011). Under thermal stress, such "parasitism" can promote higher resource uptake but unchanged resource translocation to the host for both *Symbiodinium* (type A3) and *Cladocopium* (type C7; Baker et al. 2018).

Consequently, such host-Symbiodiniaceae associations that may promote stress resilience may come with other metabolic costs that ultimately influence fitness; for example, reduced reproduction and calcification rates when associating with *Durusdinium* spp. (Jones and Berkelmans 2011; Cunning et al. 2015). What host-Symbiodiniaceae associations have occurred for corals to persist under particularly suboptimal environments where multiple abiotic parameters vary remain largely unresolved, despite such knowledge being fundamental in driving changes in the corals metabolic performance and productivity (e.g. Camp et al. 2018, 2019).

Extreme environments support reefs and reef-building corals by providing environmental refugia or selecting more stress-tolerant populations (see Camp et al. 2018), and include low light waters (mesophotic, Baird et al. 2018; turbid, Suggett et al. 2012, Sully and van Woesik 2019), inherently hot waters (e.g. Persian-Arabian Gulf; Ziegler et al. 2019), estuaries (Syahrir et al. 2018) and inshore habitats such as mangroves (Camp et al. 2019). Mangrove lagoons are of particular interest since they can exhibit extremes in the range and variability of several abiotic factors simultaneously (e.g. temperature, light, pH and O_2) that are reflective of multiple stressors conditions predicted under future climate shifts (Camp et al. 2017, 2018). Reef-building corals have been recently shown to thrive under these extreme conditions (Camp et al. 2017, 2019) providing unique ecological systems with which to study physiological trade-offs associated with coral adaptation to stressful scenarios (Palumbi et al. 2014; Camp et al. 2018). Notably, studies of corals within and adjacent to mangroves have shown that corals colonies can be flexible in their associations with different symbiont types (Hennige et al. 2010) and often exhibit a down-regulation of the photosynthesis-to-respiration ratio (P:R), mainly through enhanced respiration rather than photosynthesis (Hennige et al. 2010; Camp et al. 2016, 2017, 2019). Whilst the nature with which enhanced respiration occurs remains unresolved, it is likely from one or more factors including increased host heterotrophy

(feeding), increased biological O_2 demand of associated bacteria (Gregg et al. 2013; Zhang et al. 2015), and/or increased basal metabolism of the associated endosymbionts (Hill 2014).

Symbiodiniaceae fuel their hosts with organic carbon by fixing inorganic carbon (Ci) through photosynthesis (e.g. Davy et al. 2012). While Ci uptake rates by the algal symbionts have been rarely measured, they appear strongly regulated by environmental factors, such as availability of CO_2 (pCO_2, Suggett et al. 2012; Brading et al. 2013) and temperature (Oakley et al. 2014). In a recent study, Ros et al. (2020 – Chapter 2), demonstrated that different environmental optima across Symbiodiniaceae taxa primarily drive variation in Ci uptake rates in cultured isolates. While being useful to pinpoint different Ci uptake mechanisms at play, studies on free-living symbionts are ultimately limited in scope when trying to reconcile host-Symbiodiniaceae interactions, largely since cells are subjected to completely different environments when living *in hospite*. Within reef systems where Symbiodiniaceae are sustained *in hospite* cnidarian hosts, symbiont cells are typically carbon-limited (Smith and Muscatine 1999; Doherty 2009; Towanda and Thuesen 2012); as such, cnidarians such as symbiotic anemones can exhibit a stimulated carbon metabolism under naturally higher pCO_2 (more acidic) environments (Suggett et al. 2012). Under typical Ci-limited conditions *in hospite*, endosymbionts rely heavily on inherent biological processes such as carbon concentrating mechanisms (Cunning et al. 2017) like carbonic anhydrase to convert HCO_3^- from the seawater into CO_2 and increase their productivity, photosynthetic rates, and ultimately the photosynthates potentially translocated to their host (Sproles et al. 2019). Consequently, measurements of gross photosynthesis (P_G) and respiration (R) are directly linked to Ci metabolism for the symbiont and the host, respectively (Suggett et al. 2012). As these measurements typically encapsulate Ci exchange for the whole holobiont (or colony), they are inevitably limited in resolving finer scale Ci uptake by symbionts. Recent studies have therefore employed a combination of stable isotopes and imagery techniques (e.g. nano-scale

secondary ion mass spectrometry; NanoSIMS, see section 1.5.3.) to track the fate of carbon to assess and visualise more directly metabolic transfers in coral-Symbiodiniaceae associations (Pernice et al. 2014; Krueger et al. 2018).

Given the generally reduced net photosynthetic capacity and enhanced respiration observed recently for corals adapted to mangrove lagoon environments (Camp et al. 2018, 2019), we tested the hypothesis that this altered metabolism reflects reduced carbon uptake and translocation capacity by autotrophy of the algal symbionts. To address this, we sampled *Pocillopora acuta* coral colonies from both the reef and neighbouring mangrove lagoon at Low Isles (Great Barrier Reef). We first assessed coral metabolism using pulse-amplitude modulated (PAM) fluorometry (energy quenching and photosynthetic potential), oxygen respirometry (photosynthesis and respiration), as well the symbiont ITS2 diversity. We then quantified and visualised with NanoSIMS cellular ^{13}C-labelled Ci ($NaH^{13}CO_3$) uptake by freshly isolated Symbiodiniaceae cells *versus* within the coral (in intact symbiosis), and the extent of translocation of photosynthetically produced organic compounds to their coral host. In doing so, we evaluate whether and how the adaptive metabolic response for *P. acuta* carbon acquisition was consistent with that previously observed for two other coral species also commonly found in this mangrove lagoon habitat (*Acropora millepora* and *Porites lutea*; Camp et al. 2019). We show that *P. acuta* sampled from the mangrove lagoon compared to reef have different Symbiodiniaceae taxa with alternate photobiological strategies. Whilst *P. acuta* from the mangroves fix less carbon those from the reef, extent of carbon translocated to the host was similar (~22%), suggesting a potential supplementation of energetic requirements via heterotrophic feeding in mangrove corals.

4.3. Materials and Methods

4.3.1. Collection of corals

Fifty coral fragments (< 5 cm) were sampled in May 2018 from 38 colonies of *Pocillopora acuta* (see detail on Supplementary Table S4.1) at Woody Isles (16°23'10.3"S 145°33'53.9"E) mangrove lagoon (23 branches, 18 colonies) and the adjacent Low Isles reef (27 branches, 20 colonies) (see Supplementary Figure S4.1). Both sites have been previously sampled and detailed as per Camp et al. (2019). Briefly, pH, temperature, dissolved O_2, and salinity of the mangrove lagoon waters had more substantial diel variations than those of the reef, and with overall lower pH and dissolved O_2 and warmer temperatures (see Table 4.1), but similar irradiance (see Camp et al. 2019). Coral fragments were returned to the operations vessel (*Wavelength 5*) and processed immediately. Respirometry and ^{13}C-uptake incubations, as well as PAM fluorometry, were conducted on board the vessel, and additional samples preserved for genomic analyses by flash freezing in liquid N_2 whilst on site. Preserved samples were subsequently processed for stable isotope and NanoSIMS analyses back at the University of Technology Sydney, Australia.

4.3.2. Symbiodiniaceae photophysiology

Photophysiology measurements (n = 4) were made following low light acclimation (as per Camp et al. 2019) using a Pulse Amplitude-Modulated fluorometer (Diving PAM, Walz GmbH, Germany) configured (MI: 12, Gain: 12, SI: 6 12, SW: 0.8s, LC-INT: 3) to collect rapid light curves (RLCs) using eight actinic light sequences (0, 186, 214, 360, 456, 670, 1070, 1547, and 1975 μmol photons m^{-2} s^{-1}; E) of 20 seconds duration. For each light sequence, minimum (F_0, F_0', F') and maximum (F_m, F_m') fluorescence yields (where the prime annotation represents measurements performed during a light-acclimated state; instrument units) were recorded. These parameters were then used to calculate the maximum yield of photosystem II (PSII)

photochemistry (F_v/F_m, where $F_v = F_m - F_0$; dimensionless), the relative electron transport rate (*rETR*; µmol e^- m^{-2} s^{-1}, see Eqn. 1 and Supplementary Figure S4.2), the photochemical and dynamic non-photochemical quenching ([1-C] and [1-Q], respectively; dimensionless; see Eqn. 3 and 4) as per Suggett et al. (2015):

$$rETR = (F_v/F_m) \times E \quad \text{Eqn. 1}$$

$$E_k = ETR_{max}/\alpha \quad \text{Eqn. 2}$$

$$[1 - C] = ((F_m' - F')/(F_m' - F_0')) \quad \text{Eqn. 3}$$

$$[1 - Q] = ([F_m' - F_0']/F_m')/([F_m - F_0]/F_m) \quad \text{Eqn. 4}$$

Further photophysiology characteristics were resolved by fitting the model of Platt et al. (1980) on the RLCs, such as the maximal ETR (ETR_{max}), and the light saturation coefficient (E_k; µmol photons m^{-2} s^{-1}; see Eqn. 2, where α is the slope of the fitted line of the model), a parameter estimating light levels to which corals are predominantly acclimated (Suggett et al. 2012) and subsequently used to determine the irradiance levels of the incubations. Here, all values of E_k were determined to be 350 – 400 µmol photons m^{-2} s^{-1} for both reef and mangrove colonies (and consistent with observations of generally equivalent irradiances for the two habitats sampled Camp et al. 2019).

4.3.3. Coral holobiont photosynthesis and respiration rates

Coral nubbins collected from both the mangrove lagoon and reef sites (n = 5 per habitat) were incubated for 2 hours (in the light and dark, respectively) in gas tight sealed 250 mL glass incubation chambers as per Camp et al. (2019). Prior to incubation, any non-live coral tissue was covered with Parafilm to prevent other biological alterations influencing the seawater. A seawater blank from each habitat was also incubated to correct readings for any biological activity in the seawater. Chambers were continuously agitated using a magnetic stirrer. Each

chamber was filled with seawater from the source habitat and placed in a water bath maintained at 28.0 ± 0.2°C (and periodically resupplied with fresh seawater where temperature was observed to increase beyond 28.2°C) matching discrete measurements of seawater temperature for the same day and time of collection (reef: 28.2°C and mangrove: 28.1°C) as measured using a 3430 multi-meter (WTW GmBH, Germany). The water bath was maintained under artificial white-LED irradiance of 350-400 µmol photons m^{-2} s^{-1} (Hydra Fifty-Two HD LED, AquaIllumination, Ames, IA, USA), approximating E_k values determined from the PAM-based RLC acquisitions (above, Eqn. 2). Irradiance was verified using a 4π LI-190SA Quantum Sensor (LI-COR, Lincoln, NE, USA). Rates of light and dark respiration (R), net photosynthesis (P_N) and subsequently gross photosynthesis (P_G, where $P_G = P_N + R$) were determined by measuring O_2 values at the beginning and the end of the incubation with an O_2 probe connected to a FireStingO_2 oxygen meter (PyroScience GmbH, Germany) (as per Camp et al. 2017, 2019), blanked using native seawater controls and normalised by incubation volume, time, and either Symbiodiniaceae cell density or coral skeleton surface area (as described below).

Table 4.1. Summary of abiotic conditions characterising Woody Isles mangrove lagoon and the adjacent Low Isles reef in June 2017 and February-April 2018. Data were retrieved from Camp et al. (2019) and collected with a SeapHOx sensor set at 1-minute sampling frequency over 48 hours (2017 dataset) and at 5 minutes sampling frequency over 50 days (2018 dataset). Mean is provided with standard error (SE) and diel range of measurements with coefficient of variance (CV). Data for the reef in February-April 2018 is not available.

	Reef (2017) (n = 2,880)		Mangrove (2017) (n = 2,880)		Mangrove (2018) (n = 14,400)	
	Mean (SE)	Range (CV)	Mean (SE)	Range (CV)	Mean (SE)	Range (CV)
pH (total scale)	8.075 (0.003)	0.035 (0.001)	7.871 (0.004)	0.488 (0.019)	7.828 (0.001)	1.316 (0.031)
Temperature (°C)	22.300 (0.036)	0.400 (0.005)	22.600 (0.008)	1.600 (0.015)	28.300 (0.006)	7.700 (0.034)
O_2 (mg L^{-1})	6.510 (0.018)	0.190 (0.010)	3.91 (0.015)	3.190 (0.153)	3.020 (0.007)	7.330 (0.366)
Salinity (ppm)	35.300 (0.020)	0.200 (0.002)	33.900 (0.013)	2.000 (0.016)	32.500 (0.015)	16.500 (0.072)

4.3.4. Stable ^{13}C isotope incubations

Inorganic carbon uptake incubations were performed on two different fractions of the corals: freshly isolated symbionts (FIS) and intact coral fragment (holobiont). Both fractions were from different branches of the same colony for both mangrove lagoon and reef environments, and for 5-7 colony replicates. Both fractions were then incubated for 3 hours within gas-tight Parafilm-sealed 400 mL glass incubation chambers (see Supplementary Figure S4.3) with autoclaved artificial seawater (ASW, Berges et al. 2001) at pH 8.02, freshly labelled with 2 mM $NaH^{13}CO_3$ (^{13}C isotopic abundance of 98%, Sigma-Aldrich), and attached with carabineers to a metallic grid fitted at the bottom of the same water bath setup as for respirometry incubations, but with a white-LED irradiance of 700-800 µmol photons m^{-2} s^{-1}, a value two times E_k to ensure a maximal rate of carbon fixation (see Ros et al. 2020 – Chapter 2). Agitation of the incubation chambers was from wave movement of the operations vessel. Both light and temperature were monitored as per respiratory incubations and were recorded every 5 minutes for the duration of the experiment by HOBO Pendant data loggers (Onset, MA, USA).

4.3.4.1. Freshly isolated symbionts fractions

For generating samples of Symbiodiniaceae free from the host, coral fragments were airbrushed in 10 mL of ASW, and the resulting slurry centrifuged at 3,000 relative centrifuge force (RCF) for 5 minutes. Pellets of Symbiodiniaceae were then resuspended in 1 mL of ASW and subjected to three more cycles centrifugation and washing in ASW times to remove any animal fraction. Resulting cell extracts were separated into three aliquots: 50 µL, 250 µL (for cell counting described below, section 4.3.6.), and flash frozen in liquid N_2 for later assessment of natural isotope abundance, respectively), and 700 µL of extracted symbionts for incubation. Samples were incubated in 7 mL scintillation vials and filled with freshly labelled ASW, taking

care to remove any headspace. Scintillation vials containing the FIS were then placed in the same incubation chamber as the holobiont fraction, to ensure same conditions of incubation. After the incubation, samples were spun down at 3,000 RCF for 5 minutes and rinsed three times with 1 mL of non-labelled ASW. The rinsed cell pellets were resuspended in 1 mL of ASW and separated into two aliquots: 750 µL were pelleted and flash frozen in liquid N_2 for later enrichment analysis, and 250 µL for chemical fixation for later NanoSIMS analysis. Upon return to the laboratory, all frozen cell pellets were thawed for further preparation for enrichment analysis.

4.3.4.2. Intact host-Symbiodiniaceae fractions

Before incubation, small subsample fragments (1 cm) of each replicate coral fragment were flash frozen in liquid N_2 to assess the natural carbon isotope ratio. Corresponding fragments (4 cm) were incubated as per the FIS (above), and upon termination of incubation, were immediately rinsed with non-labelled ASW. For each replicate, one additional fragment (1 cm) was subsampled post-incubation and kept for chemical fixation before NanoSIMS analysis. The remaining fragment was flash frozen in liquid N_2 for later enrichment analysis. Upon return to the laboratory, all frozen coral fragments were thawed, airbrushed in filtered ultrapure water, and symbionts were separated from the host fraction at 3,000 RCF for 5 minutes (as per Treignier et al. 2008). Both host and symbiont fractions were treated separately for stable isotope analysis.

4.3.5. Enrichment analysis preparation

Samples for all three fractions generated from the incubation experiment (FIS incubated *ex hospite*, symbionts *in hospite* and host coral) as well as their corresponding controls sampled before incubation were resuspended and rinsed after three extra steps of centrifugation-resuspension in ultrapure water to remove residual salts interfering with the elemental analysis.

Suspensions were placed in acid-washed, pre-combusted (in a muffle furnace at 480°C for 8 hours) borosilicate vials, flash frozen in liquid N_2 and freeze-dried (Alpha 2–4 LDplus, Martin Christ GmbH, Germany) for 48 hours prior to encapsulation according to UC Davis Stable Isotope Facility (Davis, CA, USA) guidelines. Enrichment analysis was performed with a PDZ Europa ANCA-GSL elemental analyser interfaced to a PDZ Europa 20-20 isotope ratio mass spectrometer (EA-IMRS, Sercon Ltd., Cheshire, UK), where samples were interspersed with five different enriched and non-enriched internal laboratory reference materials. Enrichment levels were normalised relative to the natural isotope abundance in unlabelled samples and expressed using $\delta^{13}C$ notation. Enrichment of $\delta^{13}C$ (expressed in ‰) was quantified as follows:

$$\delta^{13}C = \left(\left(\frac{C_{sample}}{C_{unlabelled}}\right) - 1\right) \times 10^3 \qquad \text{Eqn. 4}$$

Where C is the $^{13}C/^{12}C$ atom ratio of the incubated sample or unlabelled control, respectively.

4.3.6. NanoSIMS preparation and analysis

Subsequent NanoSIMS analysis was performed on both freshly extracted symbionts and holobionts to visualise and confirm cellular Ci uptake and, in the case of the holobiont fraction, translocation of labelled compounds from the symbionts to their host. Labelled holobiont fragments (1 cm) and aliquots (250 µL) of the symbiont extracts were chemically fixed following the methods of Pernice et al. (2014) for 24 hours at 4°C in a solution containing 1% formaldehyde and 2.5% in PBS-sucrose buffer (0.1 M phosphate, 0.65 M sucrose, and 2.5 mM $CaCl_2$), pH 7.5. After fixation, samples were rinsed and stored in PBS-sucrose buffer at 4°C. Holobiont fragments underwent an extra step of decalcification process at 4°C and pH 7.5 using PBS-EDTA (0.1 M phosphate, 0.5 M EDTA) changed every 24 hours, until complete dissolution of the skeleton, and then stored in PBS buffer (0.1 M phosphate, pH 7.5) at 4°C until further processing (Pernice et al. 2014). Two coral polyps were dissected from the coral

tissue of the fragment and fixed in 1% OsO_4 - PBS (0.1 M phosphate, pH 7.5). Dissected polyps and FIS were then dehydrated in increasing gradients of ethanol (50%, 70%, 90% and 100%) followed by acetone (100%) and infiltrated with incremental gradients of SPURR resin (25%, 50%, 75%, and 100%) before embedding in moulds and polymerisation of the resin at 65°C. Sections of 80-100 nm were then cut using an ultramicrotome equipped with a diamond saw, where sequential sections were stained with 5% toluidine blue (1% NaCl, pH 2.0 ~ 2.5) and observed on a light compound microscope, and selected upon gastrodermal orientation and cell integrity (for polyps and cell pellets samples, respectively). Unstained sections from the selected observed sequence were then mounted on silicon wafers and gold-coated for NanoSIMS analysis.

Sections were analysed on a NanoSIMS-50 (Cameca, Gennevilliers, France) at the Centre for Microscopy, Characterisation and Analysis at the University of Western Australia. Simultaneous collection of five isotopic species were simultaneously collected ($^{12}C_2^-$, $^{12}C^{13}C^-$, $^{12}C^{14}N^-$, $^{12}C^{15}N^-$, and ^{32}S). Enrichment of ^{13}C was confirmed by an increase in the carbon ($^{13}C/^{12}C$) ratio above natural abundance values recorded in controls (0.011). Samples of interest were rastered with a ~ 2.5 pA Cs^+ beam (~100 nm diameter) across 50 μm^2 areas (512 × 512 pixels), with a dwell time of 15 ms per pixel. Data were simultaneously collected for $^{12}C^{12}C^-$, $^{13}C^{12}C^-$, and $^{12}C^{14}N^-$secondary molecular ions with mass resolving power (MRP, Cameca definition) > 8000 (sufficient to separate $^{13}C^{12}C^-$ from $^{12}C_2{}^1H^-$). NanoSIMS data were processed and analysed using Fiji (Schindelin et al. 2012; http://fiji.sc/Fiji) with the Open-MIMS plug-in (https://github.com/BWHCNI/OpenMIMS). Images were corrected for detector dead time (44 ns) on individual pixels before $^{13}C^{12}C^-/^{12}C^{2-}$ ratio images were generated using a colour-coded transform (hue saturation intensity, HSI) showing natural abundance levels in blue, and increasing enrichment of ^{13}C represented by the shift in colour towards magenta (set to represent maximum enrichment). Regions of interest (ROIs) were manually selected to

represent key features (symbiont cells, FIS and *in hospite*; and gastrodermal host tissue surrounding endosymbionts) and total ion counts calculated for each and used to generate ^{13}C enrichment of each ($^{13}C^{12}C^{-}/^{12}C^{2-}$). Ratios were calibrated by taking daily measurements of a *Saccharomyces cerevisiae* standard independently analysed by IRMS (corrected against Vienna-Pee-Dee Belemnite).

4.3.7. Symbiodiniaceae cell density and skeletal surface area

Aliquots of 50 µL of FIS stored in ASW (see section 4.3.4.1.) were counted on the same day of extraction using a Neubauer chamber and a compound light microscope. Triplicate counting of each sample was made to reach a minimum of 200 cells per chamber and then averaged to obtain the cell concentration. The skeletal surface areas of airbrushed branches were estimated using the wax weight method following Ros et al. (2016). Coral skeletons were cleaned thoroughly from any residual tissue and oven-dried overnight at 60°C. Surface areas of any broken parts resulting from the sampling of the different fractions (natural isotope abundance, enrichment analysis and NanoSIMS) was measured with digital callipers (and calculated as being ellipses, rectangles or squares depending on the shape). Skeletons were weighed prior to wax coating; dipped for five seconds in a bath of paraffin wax held at 75°C, the post-coating weight was recorded, and the weight of wax coating the skeleton was calculated by the difference of the pre- and post-coating skeleton weights. Eight metallic objects of known surface area (10.3 – 60.9 cm^2) were wax-coated in the same way as corals skeletons to produce a standard curve of wax weight per surface area ($y = 0.0405x – 0.1051$; $R^2 = 0.9957$). Measured surface areas of the broken parts of the coral skeletons were then subtracted from the value obtained with the standard curve to consider areas where Symbiodiniaceae were not present.

4.3.8. Symbiodiniaceae ITS2 identity

Fragments of 1 cm were taken from independent colonies of *P. acuta* at each site (n = 4), preserved in RNAlater (Ambion, Life Technologies, Australia) and stored at -20°C until further processing. Excess RNAlater solution was removed prior to DNA extraction with sterile Kimwipes™. Fragments were then airbrushed into sterile PBS-EDTA (0.1 M phosphate, 0.5 M EDTA). Extraction of the DNA from the slurry was performed using the Qiagen DNeasy Plant Mini Kit (Qiagen, Hilden, Germany). Disruption of the cells was insured by bead beating at 30 Hz for 90 seconds with a Tissue Lyser II (Qiagen, Hilden, Germany) and using 200 µL of 0.5 mm sterile glass beads (BioSpec, OK, USA). The quantity and quality of the extracted DNA were checked using a NanoDrop 2000C spectrophotometer (Thermo Fisher Scientific, MA, USA). Amplification of the DNA (aliquoted to 12-50 ng L^{-1}) via PCR was performed using the Qiagen Multiplex PCR Kit (Qiagen, Hilden, Germany) in triplicates reactions. Symbiodiniaceae ITS2 region was amplified using the primers (Illumina sequencing adapters underlined) reverse (ITS2-reverse; 5'-GTC TCG TGG GCT CGG AGA TGT GTA TAA GAG ACA GGG GAT CCA TAT GCT TAA GTT CAG CGG GT-3') and forward (ITSintfor2; 5'-TCG TCG GCA GCG TCA GAT GTG TAT AAG AGA CAG GAA TTG CAG AAC TCC GTG-3'), and following the same PCR conditions as in Arif et al. (2014) with an initial denaturing cycle at 94°C for 15 minutes, followed by 35 cycles of 94°C for 30 seconds, 51°C for 30 seconds, and 72°C for 30 seconds, and a final extension step at 72°C for 10 minutes. Products of the PCR amplification were loaded on a 1% agarose gel to control the quality of the product, prior to purification, indexation, and addition of sequencing adapters with the Nextera XT DNA Library Preparation Kit (Illumina, CA, USA). Amplicons were purified again and quantified on the Invitrogen QuBit 4 fluorometer (Quant-IT dsDNA Broad Range Assay Kit; Thermo Fisher Scientific, MA, USA), prior to being pooled in equimolar ratios using the Agilent 2100 Bioanalyzer (Agilent Technologies, CA, USA). Excess primer dimer

was then removed by purification of the final pooled library on a 2% agarose gel and sequenced at the Ramaciotti Centre for Genomics (University of New South Wales, Australia). Output files of the Illumina sequencing were then submitted to the SymPortal analytical framework (Hume et al. 2019) and quality controlled using Mothur 1.39.5 (Schloss et al. 2009), minimum entropy decomposition (Eren et al. 2015), and BLAST+ executable suites (Camacho et al. 2009) to predict Symbiodiniaceae taxa (LaJeunesse et al. 2018) from the ITS2 marker.

4.3.9. Host coral identity

Extraction of the coral DNA was performed on the coral holobiont slurry using a phenol-chloroform-isoamyl alcohol protocol (see Supplementary Methods) modified from Guthrie et al. (2000). Extracted DNA was amplified by PCR towards the mitochondrial open reading frame (ORF) region (Flot and Tillier 2007) using host-specific forward (Pdam-F: 5'-AAG AAG ATT CGG GCT CGT TT-'3) and reverse (Pdam-R: 5'-CGC CTC CTC TAC CAA GAC AG-'3) primers (Torda et al. 2013). PCR cycles conditions consisted of a denaturing cycle at 95°C for 10 minutes, followed by 35 cycles of 95°C for 30 seconds, 58.5°C for 30 seconds, and 72°C for 30 seconds, and a final extension step at 72°C for 10 minutes. Amplified host sequences were then Sanger-sequenced at the Australian Genomic Research Facility, NSW. Sequences were aligned in Geneious v.6.0.6 against reference sequences for *Pocillopora* from NCBI and matched with reference sequences for *Pocillopora acuta* (Schmidt-Roach et al. 2014) and confirmed initial identification based on morphology.

4.3.10. Statistical analysis

Statistical analyses on physiological data were carried out on SPSS Statistics 25 (IBM, Armonk, NY, USA). Data series were tested for normality (Shapiro-Wilk test) and homoscedasticity (Levene's homogeneity test). Upon confirmation of normality and homoscedasticity, independent sample t-tests were used to compare differences between

mangrove and reef (respirometry and cell density). Differences in Ci uptake between each site across all sample fractions, and between all sample fractions across each site were assessed with One-way ANOVAs with post-hoc Tukey HSD to determine between which samples fractions the differences occurred (elemental analysis) and with Mann-Whitney U tests (NanoSIMS). Significant outliers were removed using the Grubb's test for outliers. For all statistical tests, alpha (α) was set to 0.05.

4.4. Results

4.4.1. Reef and mangrove corals physiology

Respiration (R) and gross photosynthesis (P_G) rates were similar for *P. acuta* from the reef and the mangrove (Figure 4.1a). Mean (± SE) respiration rates were ca. 75% higher, but statistically indistinguishable ($t_{(8)}$ = -1.24, P = 0.251), for samples from the mangrove (0.27 ± 0.09 µmol O_2 cm^{-2} h^{-1}) than from the reef (0.16 ± 0.02 µmol O_2 cm^{-2} h^{-1}). Similarly, P_G were ca. 20% higher, but again statistically indistinguishable ($t_{(8)}$ = -0.68, P = 0.519), for the mangrove (0.67 ± 0.14 µmol O_2 cm^{-2} h^{-1}) than reef corals (0.56 ± 0.07 µmol O_2 cm^{-2} h^{-1}). Symbiodiniaceae cell density per surface area (see supplementary Figure S4.4) were higher ($t_{(10)}$ = -5.05, P < 0.001) for the mangrove ($1.31 \times 10^6 \pm 4.87 \times 10^4$ cells) than the reef ($6.88 \times 10^5 \pm 9.79 \times 10^4$ cells) corals. Consequently, values of P_G normalised per symbiont cell (P_G $cell^{-1}$; Figure 4.1b) was ultimately 37.80% lower ($t_{(8)}$ = 2.06, P = 0.074) for the mangrove (0.51 ± 0.11 pmol O_2 $cell^{-1}$ h^{-1}) compared to the reef (0.82 ± 0.10 pmol O_2 $cell^{-1}$ h^{-1}) corals. Interestingly, subsequent analysis of PSII photochemical quenching patterns (Figure 4.1c) demonstrated that *P. acuta* preferentially utilises absorbed excitation energy through photochemical quenching ([1-C], PSII photosynthesis) rather than dissipating it as heat via non-photochemical quenching ([1-Q] photoprotection) for samples from the mangrove

compared to the reef, and thus somewhat contrary to the lower values of P_G cell^{-1} observed for the mangrove *P. acuta*. We return to this point in the discussion (Section 4.5).

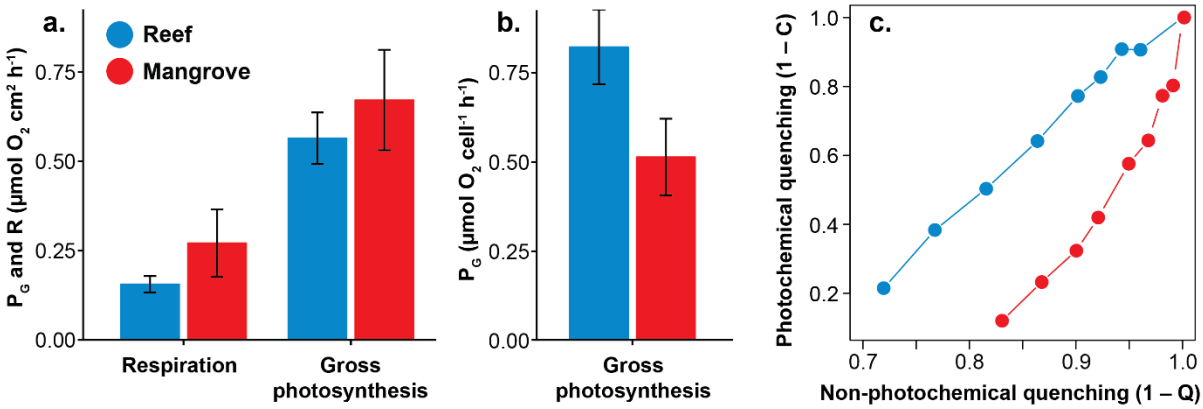

Figure 4.1. Physiology of *Pocillopora acuta* (n = 5; mean ± SE) in the Low Isles reef site (blue) and Woody Isles mangrove lagoon (red). (**a**) respiration and gross photosynthesis (P_G) (as the sum of net photosynthesis and respiration) normalised per surface area, and (**b**) per endosymbiont cell , (**c**) photochemical quenching (1 – C) *versus* non-photochemical quenching (1 – Q).

Patterns of ^{13}C uptake by Symbiodiniaceae and translocation to their host at the bulk scale (Figure 4.2a), followed the trends observed for P_G cell^{-1} for *P. acuta* from the two habitats. Symbionts living *in hospite* in the mangrove corals fixed ($F_{1.8}$ = 8.52, P = 0.019) and translocated ($F_{1.8}$ = 12.65, P = 0.007) 29.88% less carbon than those *in hospite* in the reef corals. However, the proportion of translocated carbon relative to total ^{13}C uptake was the same for corals from both habitats (ca. 22% of total fixed carbon was in the host fraction). ^{13}C uptake by FIS was the same for samples from both habitats ($F_{1.8}$ = 1.082, P = 0.329), but approximately 91% less than for the Symbiodiniaceae when *in hospite*.

^{13}C uptake at the single cell level revealed that Ci uptake was generally 2.65 times greater (U = 7, P < 0.01) *in hospite* (Figure 4.2b) for samples from the reef compared to the mangrove. Additionally, FIS followed the same trend. Both holobiont fractions exhibited

enriched areas around the symbiont cells, corresponding to host storage bodies (Figure 4.2c-f), with no significantly different $\delta^{13}C$ in enriched areas (~ 344 ‰) between reef and mangrove corals (Figure 4.2b).

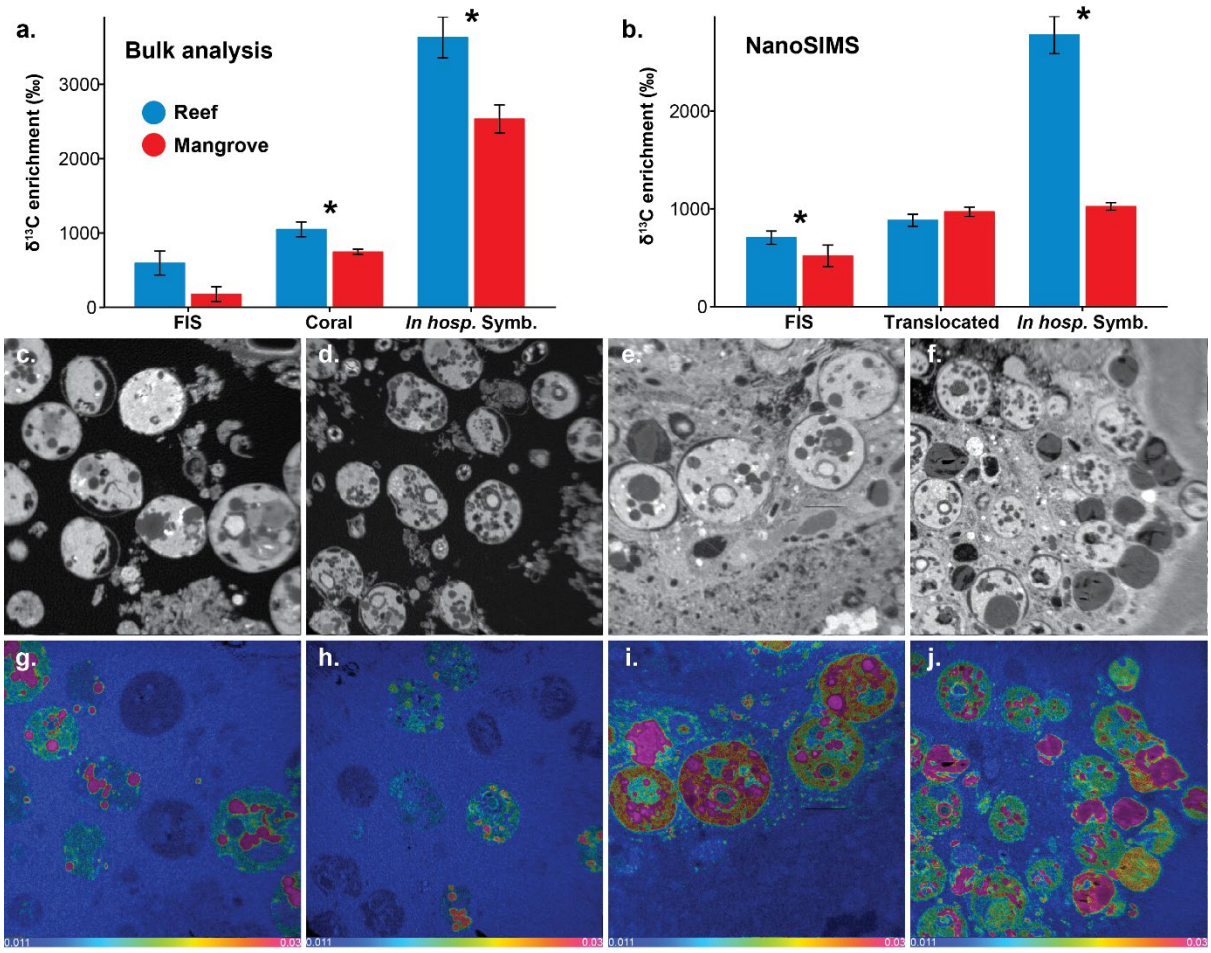

Figure 4.2. Carbon enrichments at the bulk and single-cell levels. (**a**) Bulk (n = 4) $\delta^{13}C$ enrichment levels (normalised to natural abundances) for the different incubated fractions of the coral: ("Coral" and "In hosp. Sym." refer to the incubated holobiont, later separated between animal and algae fractions, respectively; "FIS" refer to freshly isolated Symbiodiniaceae). (**b**) Single cell $\delta^{13}C$ enrichment levels with NanoSIMS. The errors bars represent the standard error, the asterisk symbols denote statistical differences ($p < 0.05$) between (**c-d**; **g-h**) and mangrove (**e-f**; **i-j**) sites. Representative NanoSIMS images showing (**c-f**) the distribution of $^{12}C^{14}N^-$, indicative of the biological structure of the sample, and (**g-j**) the isotope ratio of $^{13}C/^{12}C^-$, with natural abundance in blue, changing to pink with increasing ^{13}C levels. Number of cells analysed: FIS (n = 18); in hospite Symbiodiniaceae (n = 19); and enriched areas in host tissue (n = 5).

4.4.2. Symbiont identities from mangrove and reef corals

Differences in photobiology, P_G and Ci uptake (and translocation) for reef *versus* mangrove were consistent with a shift in dominant Symbiodiniaceae taxa within *P. acuta* across habitats. No major ITS2 type profiles were shared between corals from the mangrove or reef habitats (Figure 4.3) – colonies of *P. acuta* associated with Symbiodiniaceae species of the genus *Cladocopium* on the reef. Three different major ITS2 type profiles (proxies for Symbiodiniaceae genotypes) were observed, where three replicates had a symbiont community composed of both C1/C1b and C1d-C42.2, with the major ITS2 type profile C1k-C3cg also present in one replicate. In the mangrove corals, most of the associations were with the genus *Durusdinium*, where the majority were of the D6/D1-D4-D2.2 major ITS2 type profile, with a replicate also presenting the D1h type exclusively. Notably, no ITS2 sequence for *Durusdinium* was found for symbionts associated with reef corals. Four ITS2 sequences affiliated with *Cladocopium* from the reef corals (C15, C1, C1d and C3) were found within the mangroves, but at less than 0.02% cumulatively in three of the four replicates.

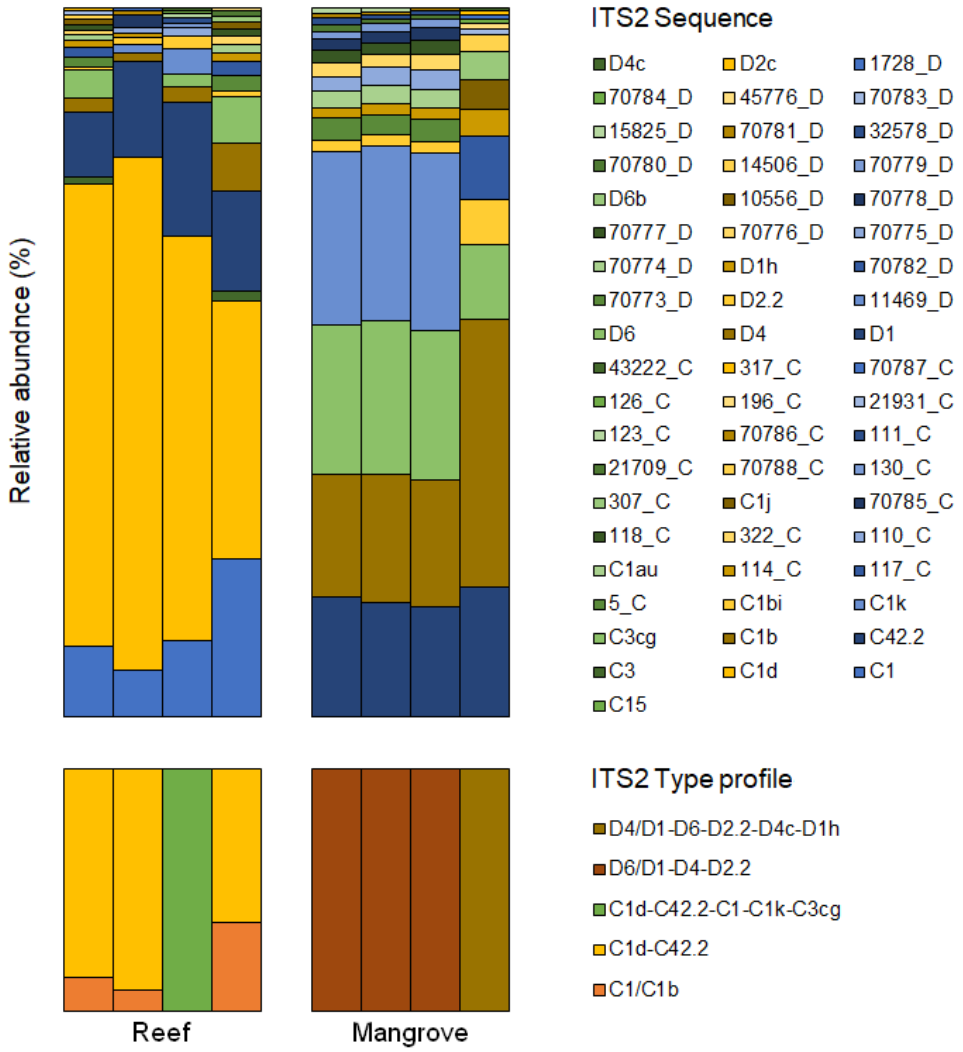

Figure 4.3. Relative abundances (%) of recovered ITS2 sequences (upper section) and predicted major ITS type profiles (lower section) for *Pocillopora acuta* across the Low Isles reef and Woody Isles mangrove habitats on the Great Barrier Reef. Each stacked bar corresponds to a biological replicate of a different colony, and each replicate is plotted relative to each other between the upper and lower sections of the figure. Sequences with designated names (e.g. C1b, D4c, or D6) refer to sequences frequently found in the literature or already characterising ITS2 profiles previously ran through the SymPortal analytical framework (Hume et al. 2019). Other sequences designated by a unique database ID and their associated genus (e.g. 70776_D) refer to sequences that are less common and not previously used to characterise ITS type profiles.

4.5. Discussion

Accelerating degradation and loss of coral reefs worldwide due to anthropogenic impacts have created an urgent need to identify coral populations with greater natural resilience to stress (Hoegh-Guldberg et al. 2018). Corals that already persist in present-day environmental extremes present important model organisms to identify mechanisms that support resilience (e.g. Camp et al. 2018). Here, we contrasted *Pocillopora acuta* corals inhabiting extreme mangrove habitats and adjacent reefs to identify the mechanisms enabling them to survive the warmer temperatures, low pH and low O2 conditions, analogous to future climate predictions. By assessing photosynthetic and respiratory rates, light-dependent dynamic quenching patterns and direct inorganic carbon (Ci) uptake by the symbiont and translocation to the host, we demonstrate that the coral *P. acuta* employs metabolic strategies that differ between habitats. In the mangrove lagoon, *P. acuta* endosymbionts appear more efficient at utilising absorbed light for photochemistry but are less able to fix Ci (or translocate fewer photosynthates to their host), confirmed by both stable isotope analysis and NanoSIMS imaging.

4.5.1. Symbiont flexibility across environmental gradients

P. acuta associated with Symbiodiniaceae from the genus *Durusdinium* in the mangrove lagoons but *Cladocopium* on the reef. Previous work from Low Isles (Camp et al. 2019) also demonstrated a flexibility between *Cladocopium* and *Durusdinium* for *Acropora millepora* between mangrove and reef. In accordance with our findings, flexibility between *Cladocopium* and *Durusdinium* symbionts has been commonly observed when environmental conditions become suboptimal (e.g. Hennige et al. 2010; Boulotte et al. 2016; Cunning et al. 2018). However, corals can persist in suboptimal environments in association with other Symbiodiniaceae genera, e.g. the back-reef pools of American Samoa (*Cladocopium,* Barshis et al. 2010), the extreme hot waters of the Persian/Arabian Gulf (*C. thermophilum*, Hume et al.

2015, D'Angelo et al. 2015) and the mangroves of New Caledonia (*Symbiodinium* and *Cladocopium*, Camp et al. 2020b) and Australia (*Cladocopium*, Camp et al. 2019). Our findings support the body of evidence that plasticity in associations with different symbiont types within a given environment is host-specific.

4.5.2. Reliance of mangrove *P. acuta* on photochemical quenching

Light-dependant dynamic quenching assessment is a diagnostic tool to assess photosynthetic "strategy" (Suggett et al. 2015; Nitschke et al. 2018) and the preference of cells to direct absorbed excitation energy towards photochemical ([1-C]) or non-photochemical ([1-Q]) pathways (Kanazawa and Kramer 2002). A previous study (Camp et al. 2019) also investigated physiological trade-offs associated with the survival in the same mangrove lagoon of two other coral species (*Acropora millepora* and *Porites lutea*). *A. millepora* and *P. acuta* exhibit the same metabolic strategies, with an increase of both P_G and respiration (normalised to coral surface area) – but overall decrease in P_G:R – from the reef to the mangrove. However, when normalised to cell density present *in hospite*, we see a convergence of strategies for all three species as a reduction in P_G and R from reef to mangrove (Figure 4.4) that appears to be mainly driven by the large increase in cell density of the mangrove corals. Moreover, the extent of variation was different between coral species, with a higher shift for *A. millepora* compared to *P. acuta*. Absorbed excitation energy was preferentially dissipated via [1-Q] for *A. millepora* but by [1-C] for *P. acuta* for mangrove compared to reef populations (Figure 4.5), despite the fact that irradiance is generally similar across the two habitats (Camp et al. 2019). The reduced reliance on photochemical quenching is consistent with reduced P_G cell^{-1} for *A. millepora*. However, the preferential reliance on [1-C], but reduced P_G cell^{-1} we observed here for *P. acuta* in the mangroves is hard to reconcile based on the data available, but suggests a high capacity to process absorbed excitation energy that does not result in net O_2 release from the cells

through "light-dependent O_2 consumption". Such a strategy has been observed for Symbiodiniaceae taxa that are inherently more tolerant of heat and/or light stress (Suggett et al. 2008; Roberty et al. 2014). This strategy is conducive to a lower overall PSII electron flow (Gorbunov et al. 2011) yet may allow a higher proportion of electrons to flow linearly to Ci fixation and thus may explain the high P_G yet lower PSII electron flow observed for the reef corals. However, whether these patterns indeed conform to enhanced internal light-dependent O_2 consumption remains to be tested.

P. lutea exhibited further differences in its metabolic strategy compared to *A. millepora* and *P. acuta* when normalised to coral surface area, with a decrease of P_G and an increase of respiration from the reef to the mangrove, but with the same energy-quenching pattern as *A. millepora*. However, in this case, symbionts of *P. lutea* from reef and mangrove were conserved from the genus *Cladocopium* but with different ITS2 major types (C15) between habitats. Recent observations reported a similar outcome for major ITS2 type for corals in New Caledonian mangroves and adjacent reefs, whereby *Acropora muricata* always associated with Symbiodiniaceae of the genus *Cladocopium*, but *Acropora pulchra* associated with *Symbiodinium* spp. in the mangrove *versus Cladocopium* spp. on the reef (Camp et al. 2020). Thus, together, these sets of observations suggest numerous "solutions" which corals may use to thrive in mangrove lagoons, via shifts in metabolic strategy that may or may not accompany associations with different Symbiodiniaceae taxa.

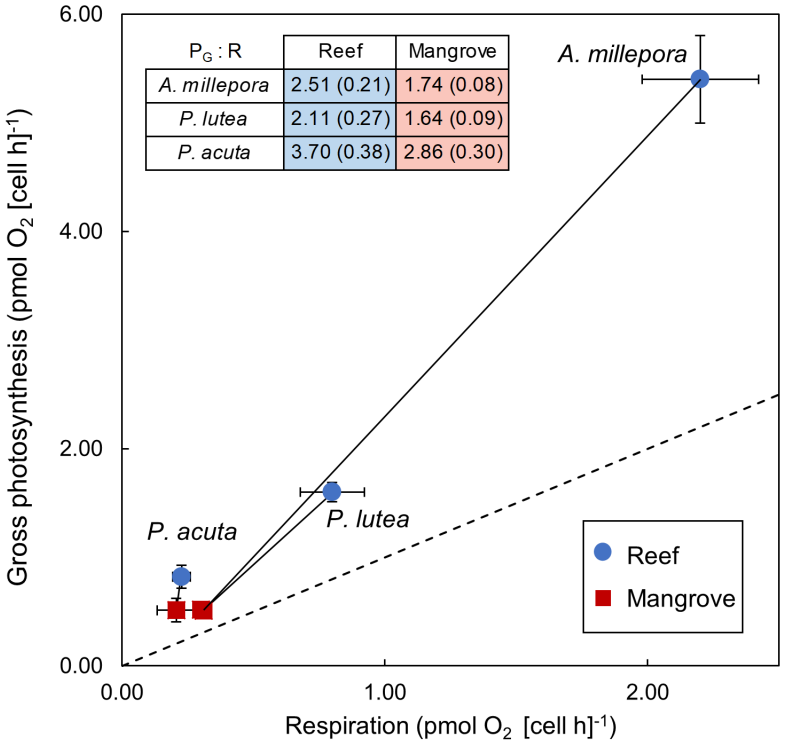

P_G : R	Reef	Mangrove
A. millepora	2.51 (0.21)	1.74 (0.08)
P. lutea	2.11 (0.27)	1.64 (0.09)
P. acuta	3.70 (0.38)	2.86 (0.30)

	Reef → Mangrove		
	P. acuta	*P. lutea*	*A. millepora*
P_G:R	↓	↓	↓
P_G (O_2 [cell h]$^{-1}$)	↓	↓	↓
R (O_2 [cell h]$^{-1}$)	=	↓	↓
[1-C]/[1-Q]	↓	↑	↑
Density (cells cm^{-2})	↑	↑	↑
Ci (^{13}δ‰)	↓	-	-
C translocation (%)	=	-	-
ITS2	C1-C1b-C1d-C1k-C3cg-C42.2 → D1-D1h-D2.2-D4-D4c	C15-C15bp-C15l-C15n-C15.8 → C15-C15bn-C15by	C3-C3b-C50a-C50c → D2-D1ak-D1-D2.2

Figure 4.4. Comparisons of (a) mean (± SE) gross photosynthesis (P_G, as the sum of net photosynthesis and respiration R) and respiration rates between reef (blue dots) and mangrove (red squares) sites. Species-specific metabolic shifts are represented by lines (black), and the dashed line indicates the 1:1 ratio. The table summarises the mean (± SE) P_G:R ratios for reef and mangrove sites. (b) Summary of key metrics shifts from reef and mangrove sites. Data for *Acropora millepora* and *Porites lutea* are retrieved from Camp et al. (2019) and for *Pocillopora acuta* come from the present study.

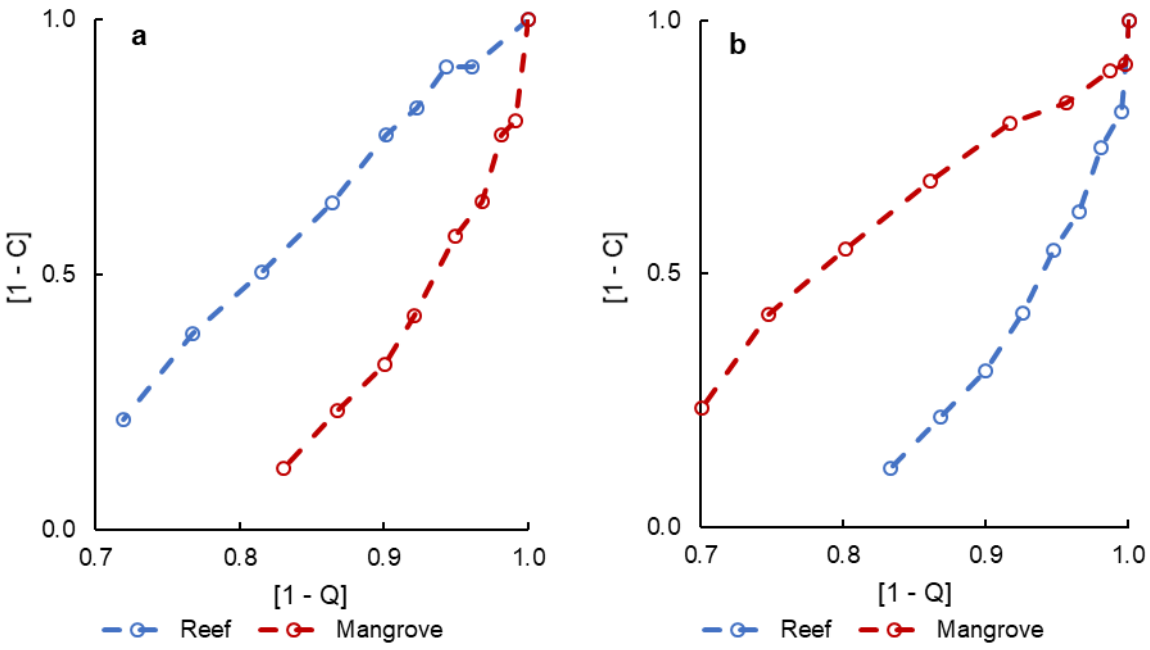

Figure 4.5. Comparisons of light-dependant dynamic quenching patterns between (**a**) *Pocillopora acuta* (present study) and (**b**) *Acropora millepora* (Camp et al. 2019) in the Low Isles reef (blue dashed lines) and Woody Isles mangrove lagoon (red dashed lines). Values of [1 – C] stand for photochemical quenching (qP) and [1 – Q] for non-photochemical quenching (NPQ) (see Methods).

4.5.3. Carbon fixation and translocation in mangrove corals

Symbiodiniaceae *in hospite* were less efficient at fixing Ci and translocating photosynthates in the mangrove compared to reef populations. In both habitats, Ci uptake was greatly enhanced by the presence of the host compared to isolated symbionts. Overall, mangrove corals fixed less Ci (29.88% decrease), as demonstrated by stable isotope tracking both at the bulk scale and at the single-cell levels. Mangrove corals also had similar reductions in P_G per cell compared to the reef (37.80% decrease), suggesting that the loss of Ci in mangrove corals could come from a loss of P_G. However, as the mangrove lagoon is more acidic (and has higher pCO_2 availability), we expected to observe an increase in productivity (Brading et al. 2011; Suggett et al. 2012; Hoadley et al. 2015) but in fact measured the opposite. This decrease in Ci uptake therefore might be driven by an upstream pathway independent of pCO_2 availability. As physiological processes did not allow for an increased uptake of Ci

despite the additional carbon available in the mangrove waters, it is likely that the observed reduction is characteristic of a trade-off linked to stress tolerance. Interestingly, despite a different absolute Ci uptake between corals of the two sites, the proportion of translocated carbon to the host remains the same (~ 22%). These findings shared some consistencies with those of Hoadley et al. (2015), who found that in *Exaiptasia pallida*, increased pCO_2 did not have an effect on carbon translocation, but enhanced Ci fixation by *Breviolum minutum* symbionts. Interestingly, translocation rates of *Cladocopium* sp. in the zoanthid *Palythoa* sp., found by Graham and Sanders (2016) were similar (~26%) to ours (~22%) when the holobionts were incubated at 27°C at a controlled pH of 8.1, which are similar conditions of our incubations (28.0°C at pH 8.02). Moreover, Graham and Sanders (2016) also found that the combination of high temperature (31°C) and high pCO_2 (pH 7.65; which are characteristic of mangrove environments) increased productivity and translocation rates (up to 40%) of *Cladocopium* sp. symbionts. In our study, the incubation conditions of temperature and pH were similar between reef and mangrove corals, thus it is possible that the trends observed will be shifted towards a better performance of mangrove holobionts in response to elevated temperature and/or pCO_2 (Mora et al. 2013). Whilst responses to increased pCO_2 levels point towards an enhanced productivity and translocation of Symbiodiniaceae in symbiosis with anemones (Suggett et al. 2012; Hoadley et al. 2015) and zoanthids (Graham and Sanders 2016), our results suggest that carbon assimilation and transfers are likely to be species-specific, particularly when considering calcifying hosts. The combination of increased respiratory rates and the relative decrease of organic photosynthates translocated to corals by endosymbionts in mangroves compared to the reef, corroborated by a decrease in enriched storage lipid bodies suggest that heterotrophy is likely an additional way of supplementing the energetic requirements of corals in inhospitable conditions (which require an increased energetic demand to sustain homeostasis and survival; Palardy et al. 2008). Such diversity in response presumably

reflects diverse resource requirements of different host-coral species (Suggett et al. 2017), how they are able to meet their requirements via heterotrophic supplementation (Fox et al. 2018), and potential co-evolution of host-Symbiodiniaceae associations (Qin et al. 2019; Wright et al. 2019).

4.5.4. Are mangrove habitats the cause of a reduced Ci uptake, or symbiont identity?

In our study, incubation of FIS revealed a decrease in Ci uptake by 88.98 and 93.05 % (reef and mangrove, respectively) compared to symbionts incubated in the intact holobiont, and FIS from both environments did not show significantly different Ci uptake rates when incubated under the same conditions, an observation also found by Ros et al. (2020 – Chapter 2) in cultured symbionts. It is interesting that even when there are considerable long-term environmental differences, as we see between the mangrove and reef habitats, Ci uptake rates remain similar, possibly due to the host promoting microenvironment stability surrounding the symbionts, which would not happen *ex hospite*. Effect of the host on Ci uptake by the symbiont has already been characterised in previous laboratory-based studies, notably by changing the physicochemical microenvironment surrounding the symbiotic cells inside of the symbiosome (Barott et al. 2015), a specialised vacuole of the coral accommodating the endosymbionts (Roth et al. 1988), however, this has not been directly measured for mangrove corals in particular. Since in the present study both symbiont identity and environments are different, we cannot conclude if *in hospite*, the difference in Ci uptake is solely due to the environment of growth or the taxonomic identity. Previous work by Camp et al. (2019) at Low Isles did not measure Ci uptake (or translocation), but their parallel measurements of respirometry and photochemical quenching patterns highlight that each of the three taxa commonly found across the Low Isles reef and mangrove lagoon (*A. millepora*, *P. lutea*, *P. acuta*) all exhibit three very

different metabolic strategies, suggesting that growth environments and both host and symbiont identity could have a role to play in diversity of Ci uptake and translocation. The study of the Ci uptake of *in hospite* symbionts of identical major ITS2 types but from different environments (see *P. lutea* from Camp et al. 2019; and *A. muricata* in New Caledonia from Camp et al. 2020b) could help in determining the effect of different growth environments on Ci assimilation strategies inherently characteristic of extreme environments. It is noted that FIS extractions from the host could induce physical stress or cell damage that cannot be discounted as contributing to the results. However, the trend between habitats remained constant (higher in reef than mangroves) irrespective of FIS or *in hospite*, suggesting a consistent environmental influence.

4.5.5. The importance of the holobiont

Most coral physiology studies to date have focused on the coral host and the algal endosymbiont, but the role of the microbiome in stress resistance is also essential (Ziegler et al. 2017; Matthews et al. 2020) and often overlooked, especially in relation to carbon transfer (Silveira et al. 2017). Under heat stress, the microbiome of cultured thermo-tolerant *Durusdinium trenchii* is more stable than other thermo-sensitive isolates (*Breviolum minutum* and *Cladocopium goreaui*) and potentially contributes to thermal resistance (Camp et al. 2020a). A recent study carried out on the *P. acuta* microbial communities from a fringing reef (Epstein et al. 2019) highlighted their importance for resistance to thermal stress. More recently, Camp et al. (2020b) characterised the microbial communities between coral colonies from the reef and the mangrove in New Caledonia and demonstrated that different host-bacteria associations from the reef are required to sustain adaptation of corals to mangrove environments. Further work understanding how the microbiome functions to contribute to thermal stress resistance and coral survival across different resource landscapes will be

important to improve on our current understanding of coral survival across environmental gradients.

4.6. Conclusion

Rapid degradation of coral reefs worldwide has created an urgent need to locate local refuge environments as well as stress-tolerant coral populations that could aid the long-term survival of corals. Our work builds on the growing body of evidence (e.g. Camp et al. 2016; 2018, 2019; Morikawa and Palumbi 2019) that corals from extreme environments, including mangrove lagoons, have the potential to act as important stocks of stress-hardened corals (Parker et al. 2020). However, our findings highlight costs associated with survival into extreme environments, specifically lower quantities of Ci uptake by Symbiodiniaceae and organic carbon translocated to their coral host, *P. acuta*. Our results confirm that corals exhibit species-specific differences in their adaptation to extremes, highlighting the complexities of resolving stress tolerance to multiple abiotic parameters, characteristic of future global climate change conditions.

4.7. References

Abrego, D., K. E. Ulstrup, B. L. Willis and M. J. van Oppen. 2008. Species-specific interactions between algal endosymbionts and coral hosts define their bleaching response to heat and light stress. Proc. Biol. Sci. **275**: 2273-2282. doi:10.1098/rspb.2008.0180

Arif, C., C. Daniels, T. Bayer, E. Banguera-Hinestroza, A. Barbrook, C. J. Howe, T. C. LaJeunesse and C. R. Voolstra. 2014. Assessing *Symbiodinium* diversity in scleractinian corals via next-generation sequencing-based genotyping of the ITS2 rDNA region. Mol. Ecol. **23**: 4418-4433. doi:10.1111/mec.12869

Baird, A. H., and others. 2018. A decline in bleaching suggests that depth can provide a refuge from global warming in most coral taxa. Marine Ecology Progress Series. **603**: 257-264. doi:10.3354/meps12732

Baker, A. C. 2003. Flexibility and specificity in coral-algal symbiosis: Diversity, ecology, and biogeography of *Symbiodinium*. Annual Review of Ecology, Evolution, and Systematics. **34**: 661-689. doi:10.1146/annurev.ecolsys.34.011802.132417

Baker, D. M., C. J. Freeman, J. C. Y. Wong, M. L. Fogel and N. Knowlton. 2018. Climate change promotes parasitism in a coral symbiosis. ISME J. **12**: 921-930. doi:10.1038/s41396-018-0046-8

Barott, K. L., A. A. Venn, S. O. Perez, S. Tambutte and M. Tresguerres. 2015. Coral host cells acidify symbiotic algal microenvironment to promote photosynthesis. Proc. Natl. Acad. Sci. U. S. A. **112**: 607-612. doi:10.1073/pnas.1413483112

Barshis, D. J., J. H. Stillman, R. D. Gates, R. J. Toonen, L. W. Smith and C. Birkeland. 2010. Protein expression and genetic structure of the coral *Porites lobata* in an environmentally extreme Samoan back reef: does host genotype limit phenotypic plasticity? Mol. Ecol. **19**: 1705-1720. doi:10.1111/j.1365-294X.2010.04574.x

Berges, J. A., D. J. Franklin and P. J. Harrison. 2001. Evolution of an artificial seawater medium: Improvements in enriched seawater, artificial water over the last two decades. Journal of Phycology. **37**: 1138-1145. doi:10.1046/j.1529-8817.2001.01052.x

Berkelmans, R. and M. J. van Oppen. 2006. The role of zooxanthellae in the thermal tolerance of corals: a "nugget of hope" for coral reefs in an era of climate change. Proc. Biol. Sci. **273**: 2305-2312. doi:10.1098/rspb.2006.3567

Boulotte, N. M., S. J. Dalton, A. G. Carroll, P. L. Harrison, H. M. Putnam, L. M. Peplow and M. J. van Oppen. 2016. Exploring the *Symbiodinium* rare biosphere provides evidence for symbiont switching in reef-building corals. ISME J. **10**: 2693-2701. doi:10.1038/ismej.2016.54

Brading, P., M. E. Warner, P. Davey, D. J. Smith, E. P. Achterberg and D. J. Suggett. 2011. Differential effects of ocean acidification on growth and photosynthesis among phylotypes of *Symbiodinium* (Dinophyceae). Limnology and Oceanography. **56**: 927-938. doi:10.4319/lo.2011.56.3.0927

Brading, P., M. E. Warner, D. J. Smith and D. J. Suggett. 2013. Contrasting modes of inorganic carbon acquisition amongst *Symbiodinium* (Dinophyceae) phylotypes. New Phytol. **200**: 432-442. doi:10.1111/nph.12379

Camacho, C., G. Coulouris, V. Avagyan, N. Ma, J. Papadopoulos, K. Bealer and T. L. Madden. 2009. BLAST+: architecture and applications. BMC Bioinformatics. **10**: 421. doi:10.1186/1471-2105-10-421

Camp, E. F., D. J. Smith, C. Evenhuis, I. Enochs, D. Manzello, S. Woodcock and D. J. Suggett. 2016. Acclimatization to high-variance habitats does not enhance physiological tolerance of two key Caribbean corals to future temperature and pH. Proc. Biol. Sci. **283**. doi:10.1098/rspb.2016.0442

Camp, E. F., M. R. Nitschke, R. Rodolfo-Metalpa, F. Houlbreque, S. G. Gardner, D. J. Smith, M. Zampighi and D. J. Suggett. 2017. Reef-building corals thrive within hot-acidified and deoxygenated waters. Sci. Rep. **7**: 2434. doi:10.1038/s41598-017-02383-y

Camp, E. F., V. Schoepf, P. J. Mumby, L. A. Hardtke, R. Rodolfo-Metalpa, D. J. Smith and D. J. Suggett. 2018. The future of coral reefs subject to rapid climate change: Lessons from natural extreme environments. Frontiers in Marine Science. **5**. doi:10.3389/fmars.2018.00004

Camp, E. F., J. Edmondson, A. Doheny, J. Rumney, A. J. Grima, A. Huete and D. J. Suggett. 2019. Mangrove lagoons of the Great Barrier Reef support coral populations persisting under extreme environmental conditions. Marine Ecology Progress Series. **625**: 1-14. doi:10.3354/meps13073

Camp, E. F., and others. 2020a. Revealing changes in the microbiome of Symbiodiniaceae under thermal stress. Environmental Microbiology.

Camp, E. F., and others. 2020b. Corals exhibit distinct patterns of microbial reorganisation to thrive in an extreme inshore environment. Coral Reefs. doi:10.1007/s00338-019-01889-3

Cooper, T. F., M. Lai, K. E. Ulstrup, S. M. Saunders, G. R. Flematti, B. Radford and M. J. van Oppen. 2011. *Symbiodinium* genotypic and environmental controls on lipids in reef building corals. PLoS One. **6**: e20434. doi:10.1371/journal.pone.0020434

Cunning, R., P. Gillette, T. Capo, K. Galvez and A. C. Baker. 2015. Growth trade-offs associated with thermo-tolerant symbionts in the coral *Pocillopora damicornis* are lost in warmer oceans. Coral Reefs. **34**: 155-160. doi:10.1007/s00338-014-1216-4

Cunning, R., E. B. Muller, R. D. Gates and R. M. Nisbet. 2017. A dynamic bioenergetic model for coral-*Symbiodinium* symbioses and coral bleaching as an alternate stable state. J. Theor. Biol. **431**: 49-62. doi:10.1016/j.jtbi.2017.08.003

Cunning, R., R. N. Silverstein and A. C. Baker. 2018. Symbiont shuffling linked to differential photochemical dynamics of *Symbiodinium* in three Caribbean reef corals. Coral Reefs. **37**: 145-152. doi:10.1007/s00338-017-1640-3

D'Angelo, C., B. C. Hume, J. Burt, E. G. Smith, E. P. Achterberg and J. Wiedenmann. 2015. Local adaptation constrains the distribution potential of heat-tolerant *Symbiodinium*

from the Persian/Arabian Gulf. The ISME journal, **9**: 2551-2560. doi: 10.1038/ismej.2015.80

Davy, S. K., D. Allemand and V. M. Weis. 2012. Cell biology of cnidarian-dinoflagellate symbiosis. Microbiol. Mol. Biol. Rev. **76**: 229-261. doi:10.1128/MMBR.05014-11

Doherty, M. 2009. Ocean acidification: Comparative impacts on the photophysiology of a temperate symbiotic sea anemone and a tropical coral.

Epstein, H. E., G. Torda and M. J. H. van Oppen. 2019. Relative stability of the *Pocillopora acuta* microbiome throughout a thermal stress event. Coral Reefs. **38**: 373-386. doi:10.1007/s00338-019-01783-y

Eren, A. M., H. G. Morrison, P. J. Lescault, J. Reveillaud, J. H. Vineis and M. L. Sogin. 2015. Minimum entropy decomposition: unsupervised oligotyping for sensitive partitioning of high-throughput marker gene sequences. ISME J. **9**: 968-979. doi:10.1038/ismej.2014.195

Flot, J. F. and S. Tillier. 2007. The mitochondrial genome of *Pocillopora* (Cnidaria: Scleractinia) contains two variable regions: the putative D-loop and a novel ORF of unknown function. Gene. **401**: 80-87. doi:10.1016/j.gene.2007.07.006

Gorbunov, M. Y., F. I. Kuzminov, V. V. Fadeev, J. D. Kim and P. G. Falkowski. 2011. A kinetic model of non-photochemical quenching in cyanobacteria. Biochim. Biophys. Acta. **1807**: 1591-1599. doi:10.1016/j.bbabio.2011.08.009

Gregg, A., and others. 2013. Biological oxygen demand optode analysis of coral reef-associated microbial communities exposed to algal exudates. PeerJ. **1**: e107. doi:10.7717/peerj.107

Guthrie, J. N., D. J. W. Moriarty and L. L. Blackall. 2000. DNA extraction from coral reef sediment bacteria for the polymerase chain reaction. Journal of Microbiological Methods. **43**: 73-80. doi:10.1016/s0167-7012(00)00207-4

Hennige, S. J., D. J. Smith, S.-J. Walsh, M. P. McGinley, M. E. Warner and D. J. Suggett. 2010. Acclimation and adaptation of scleractinian coral communities along environmental gradients within an Indonesian reef system. Journal of Experimental Marine Biology and Ecology. **391**: 143-152. doi:10.1016/j.jembe.2010.06.019

Hill, M. S. 2014. Production possibility frontiers in phototroph:heterotroph symbioses: trade-offs in allocating fixed carbon pools and the challenges these alternatives present for understanding the acquisition of intracellular habitats. Front. Microbiol. **5**: 357. doi:10.3389/fmicb.2014.00357

Hoegh-Guldberg, O., E. V. Kennedy, H. L. Beyer, C. McClennen and H. P. Possingham. 2018. Securing a long-term future for coral reefs. Trends Ecol. Evol. **33**: 936-944. doi:10.1016/j.tree.2018.09.006

Howells, E. J., V. H. Beltran, N. W. Larsen, L. K. Bay, B. L. Willis and M. J. H. van Oppen. 2011. Coral thermal tolerance shaped by local adaptation of photosymbionts. Nature Climate Change. **2**: 116-120. doi:10.1038/nclimate1330

Hume, B. C., D'Angelo, C., Smith, E. G., Stevens, J. R., Burt, J. and J. Wiedenmann. 2015. *Symbiodinium thermophilum* sp. nov., a thermotolerant symbiotic alga prevalent in

corals of the world's hottest sea, the Persian/Arabian Gulf. Scientific reports, 5(1), 1-8. doi: 10.1038/srep08562

Hume, B. C. C., E. G. Smith, M. Ziegler, H. J. M. Warrington, J. A. Burt, T. C. LaJeunesse, J. Wiedenmann and C. R. Voolstra. 2019. SymPortal: A novel analytical framework and platform for coral algal symbiont next-generation sequencing ITS2 profiling. Mol. Ecol. Resour. **19**: 1063-1080. doi:10.1111/1755-0998.13004

Kanazawa, A. and D. M. Kramer. 2002. In vivo modulation of nonphotochemical exciton quenching (NPQ) by regulation of the chloroplast ATP synthase. Proc. Natl. Acad. Sci. U. S. A. **99**: 12789-12794. doi:10.1073/pnas.182427499

Krueger, T., J. Bodin, N. Horwitz, C. Loussert-Fonta, A. Sakr, S. Escrig, M. Fine and A. Meibom. 2018. Temperature and feeding induce tissue level changes in autotrophic and heterotrophic nutrient allocation in the coral symbiosis - A NanoSIMS study. Sci. Rep. **8**: 12710. doi:10.1038/s41598-018-31094-1

LaJeunesse, T. C., J. E. Parkinson, P. W. Gabrielson, H. J. Jeong, J. D. Reimer, C. R. Voolstra and S. R. Santos. 2018. Systematic revision of Symbiodiniaceae highlights the antiquity and diversity of coral endosymbionts. Curr. Biol. **28**: 2570-2580 e2576. doi:10.1016/j.cub.2018.07.008

Matthews, J. L., and others. 2017. Optimal nutrient exchange and immune responses operate in partner specificity in the cnidarian-dinoflagellate symbiosis. Proceedings of the National Academy of Sciences. **114**: 13194-13199.

Matthews, J. L., J. B. Raina, T. Kahlke, J. R. Seymour, M. J. H. van Oppen and D. J. Suggett. 2020. Symbiodiniaceae-bacteria interactions: rethinking metabolite exchange in reef-building corals as multi-partner metabolic networks. Environ. Microbiol. doi:10.1111/1462-2920.14918

Mora, C., and others. 2013. Biotic and human vulnerability to projected changes in ocean biogeochemistry over the 21st century. PLoS Biol. **11**: e1001682. doi:10.1371/journal.pbio.1001682

Morikawa, M. K. and S. R. Palumbi. 2019. Using naturally occurring climate resilient corals to construct bleaching-resistant nurseries. Proc. Natl. Acad. Sci. U. S. A. **116**: 10586-10591. doi:10.1073/pnas.1721415116

Nitschke, M. R., S. G. Gardner, S. Goyen, L. Fujise, E. F. Camp, P. J. Ralph and D. J. Suggett. 2018. Utility of photochemical traits as diagnostics of thermal tolerance amongst Great Barrier Reef corals. Frontiers in Marine Science. **5**. doi:10.3389/fmars.2018.00045

Oakley, C. A., G. W. Schmidt and B. M. Hopkinson. 2014. Thermal responses of *Symbiodinium* photosynthetic carbon assimilation. Coral Reefs. **33**: 501-512. doi:10.1007/s00338-014-1130-9

Oliver, T. A. and S. R. Palumbi. 2011. Many corals host thermally resistant symbionts in high-temperature habitat. Coral Reefs. **30**: 241-250. doi:10.1007/s00338-010-0696-0

Palardy, J. E., L. J. Rodrigues and A. G. Grottoli. 2008. The importance of zooplankton to the daily metabolic carbon requirements of healthy and bleached corals at two depths.

Journal of Experimental Marine Biology and Ecology. **367**: 180-188. doi:10.1016/j.jembe.2008.09.015

Palumbi, S. R., D. J. Barshis, N. Traylor-Knowles and R. A. Bay. 2014. Mechanisms of reef coral resistance to future climate change. Science. **344**: 895-898. doi:10.1126/science.1251336

Parker, K. E., J. O. Ward, E. M. Eggleston, E. Fedorov, J. E. Parkinson, C. P. Dahlgren and R. Cunning. 2020. Characterization of a thermally tolerant *Orbicella faveolata* reef in Abaco, The Bahamas. Coral Reefs. **39**: 675–685. doi: 10.1007/s00338-020-01948-0

Pernice, M., and others. 2014. A nanoscale secondary ion mass spectrometry study of dinoflagellate functional diversity in reef-building corals. Environ. Microbiol. **17**: 3570-3580. doi:10.1111/1462-2920.12518

Platt, T., C. Gallegos and W. G. Harrison. 1981. Photoinhibition of photosynthesis in natural assemblages of marine phytoplankton.

Ros, M., M. Pernice, S. Le Guillou, M. A. Doblin, V. Schrameyer and O. Laczka. 2016. Colorimetric detection of caspase 3 activity and reactive oxygen derivatives: Potential early indicators of thermal stress in corals. Journal of Marine Biology. **2016**: 1-11. doi:10.1155/2016/6825949

Ros, M., E. F. Camp, D. J. Hughes, J. R. Crosswell, M. E. Warner, W. P. Leggat and D. J. Suggett. 2020. Unlocking the black-box of inorganic carbon-uptake and utilization strategies among coral endosymbionts (Symbiodiniaceae). Limnology and Oceanography. doi:10.1002/lno.11416

Roth, E., K. Jeon and G. Stacey. 1988. Homology in endosymbiotic systems: the term "symbiosome".

Schindelin, J., and others. 2012. Fiji: an open-source platform for biological-image analysis. Nat. Methods. **9**: 676-682. doi:10.1038/nmeth.2019

Schloss, P. D., and others. 2009. Introducing mothur: open-source, platform-independent, community-supported software for describing and comparing microbial communities. Appl. Environ. Microbiol. **75**: 7537-7541. doi:10.1128/AEM.01541-09

Schmidt-Roach, S., K. J. Miller, P. Lundgren and N. Andreakis. 2014. With eyes wide open: a revision of species within and closely related to the *Pocillopora damicornis* species complex (Scleractinia; Pocilloporidae) using morphology and genetics. Zoological Journal of the Linnean Society. **170**: 1-33. doi:10.1111/zoj.12092

Silveira, C. B., G. S. Cavalcanti, J. M. Walter, A. W. Silva-Lima, E. A. Dinsdale, D. G. Bourne, C. C. Thompson and F. L. Thompson. 2017. Microbial processes driving coral reef organic carbon flow. FEMS Microbiol. Rev. **41**: 575-595. doi:10.1093/femsre/fux018

Smith, G. and L. Muscatine. 1999. Cell cycle of symbiotic dinoflagellates: variation in G1 phase-duration with anemone nutritional status and macronutrient supply in the *Aiptasia pulchella–Symbiodinium pulchrorum* symbiosis. Marine Biology. **134**: 405-418.

Sproles, A. E., C. A. Oakley, J. L. Matthews, L. Peng, J. G. Owen, A. R. Grossman, V. M. Weis and S. K. Davy. 2019. Proteomics quantifies protein expression changes in a

model cnidarian colonised by a thermally tolerant but suboptimal symbiont. ISME J. **13**: 2334-2345. doi:10.1038/s41396-019-0437-5

Suggett, D. J., M. E. Warner, D. J. Smith, P. Davey, S. Hennige and N. R. Baker. 2008. Photosynthesis and production of hydrogen peroxide by *Symbiodinium* (Pyrrhophyta) phylotypes with different thermal tolerances. J. Phycol. **44**: 948-956. doi:10.1111/j.1529-8817.2008.00537.x

Suggett, D. J., R. K. P. Kikuchi, M. D. M. Oliveira, S. Spanó, R. Carvalho and D. J. Smith. 2012. Photobiology of corals from Brazil's near-shore marginal reefs of Abrolhos. Marine Biology. **159**: 1461-1473. doi:10.1007/s00227-012-1925-6

Suggett, D. J., S. Goyen, C. Evenhuis, M. Szabo, D. T. Pettay, M. E. Warner and P. J. Ralph. 2015. Functional diversity of photobiological traits within the genus *Symbiodinium* appears to be governed by the interaction of cell size with cladal designation. New Phytol. **208**: 370-381. doi:10.1111/nph.13483

Suggett, D. J., M. E. Warner and W. Leggat. 2017. Symbiotic dinoflagellate functional diversity mediates coral survival under ecological crisis. Trends Ecol. Evol. **32**: 735-745. doi:10.1016/j.tree.2017.07.013

Suggett, D. J. and D. J. Smith. 2020. Coral bleaching patterns are the outcome of complex biological and environmental networking. Glob. Chang. Biol. doi:10.1111/gcb.14871

Syahrir, M. R., T. Hanjoko, A. Adnan, M. Yasser, M. Efendi, A. A. Budiarsa and I. Suyatna. 2018. The existence of estuarine coral reef at eastern front of Mahakam Delta, East Kalimantan, Indonesia: a first record. Aquaculture, Aquarium, Conservation & Legislation. **11**: 362-378.

Torda, G., S. Schmidt-Roach, L. M. Peplow, P. Lundgren and M. J. van Oppen. 2013. A rapid genetic assay for the identification of the most common *Pocillopora damicornis* genetic lineages on the Great Barrier Reef. PLoS One. **8**: e58447. doi:10.1371/journal.pone.0058447

Towanda, T. and E. V. Thuesen. 2012. Prolonged exposure to elevated CO_2 promotes growth of the algal symbiont *Symbiodinium muscatinei* in the intertidal sea anemone *Anthopleura elegantissima*. Biol. Open. **1**: 615-621. doi:10.1242/bio.2012521

Treignier, C., R. Grover, C. Ferrier-Pages and I. Tolosa. 2008. Effect of light and feeding on the fatty acid and sterol composition of zooxanthellae and host tissue isolated from the scleractinian coral *Turbinaria reniformis*. Limnology and Oceanography. **53**: 2702-2710.

Zhang, Y. Y., and others. 2015. The diversity of coral associated bacteria and the environmental factors affect their community variation. Ecotoxicology. **24**: 1467-1477. doi:10.1007/s10646-015-1454-4

Ziegler, M., F. O. Seneca, L. K. Yum, S. R. Palumbi and C. R. Voolstra. 2017. Bacterial community dynamics are linked to patterns of coral heat tolerance. Nat. Commun. **8**: 14213. doi:10.1038/ncomms14213

Ziegler, M., A. Roik, T. Röthig, C. Wild, N. Rädecker, J. Bouwmeester and C. R. Voolstra 2019. Ecophysiology of reef-building corals in the Red Sea. Coral Reefs of the Red

Sea. C. R. Voolstra and M. L. Berumen. Cham, Springer International Publishing: 33-52.

4.8. Supplementary Information

4.8.1. Supplementary Methods – Extraction of coral host DNA

For genotyping of *Pocillopora* fragments, DNA was extracted using a modified phenol-chloroform protocol. The coral tissue was removed from frozen fragments by air blasting into zip-lock bags containing 5 mL of sterile ASW. The coral slurry was then centrifuged at 8,000 RCF for 10 minutes, the supernatant was discarded, and pellets were resuspended in 0.5 mL of buffer (0.75 M Sucrose, 40 mM EDTA, 50 mM Tris base pH 8.3) with the addition of 75 µL of lysozyme (100 mg mL^{-1} stock), incubated at 37°C for one hour and periodically shaken, followed by three freeze/thaw cycles in liquid N_2 and incubation at 70°C on a heat block. Sodium dodecyl sulphate (SDS; 100 µL of a 25% solution) was added to samples and then incubated at 70°C for 10 minutes. Samples were then cooled to room temperature before adding proteinase K (20 µL of 20 mg mL^{-1} stock) and a further incubation of one hour at 37°C, followed by three additional freeze/thaw cycles. Samples were then added to an equal volume of phenol:chloroform:isoamyl alcohol (25:24:1) buffered to pH 8, and inverted for 10 minutes, followed by centrifugation for 15 minutes at 13,000 RCF for separation of aqueous phases. Aqueous phases were removed into clean tubes with the addition of equal volumes of chloroform:isoamyl alcohol (24:1) and underwent a further 10 minutes of inversion, then samples were centrifuged for 10 minutes at 16,000 RCF. The aqueous layer was again removed and mixed with sodium acetate (50 µl of 3 M solution) and an equal volume of molecular-grade isopropanol to precipitate the extracted DNA. Precipitated DNA was then centrifuged at 20,000 RCF for 30 minutes at 4°C, and the supernatant was discarded. Pellets were washed with 500 µL of molecular-grade ethanol (70%) and centrifuged for 10 minutes at 20,000 RCF. Ethanol was removed, and samples were air-dried for 15 minutes in the dark prior to resuspension of DNA pellets in 30 µL of nuclease-free water.

4.8.2. Supplementary Figures

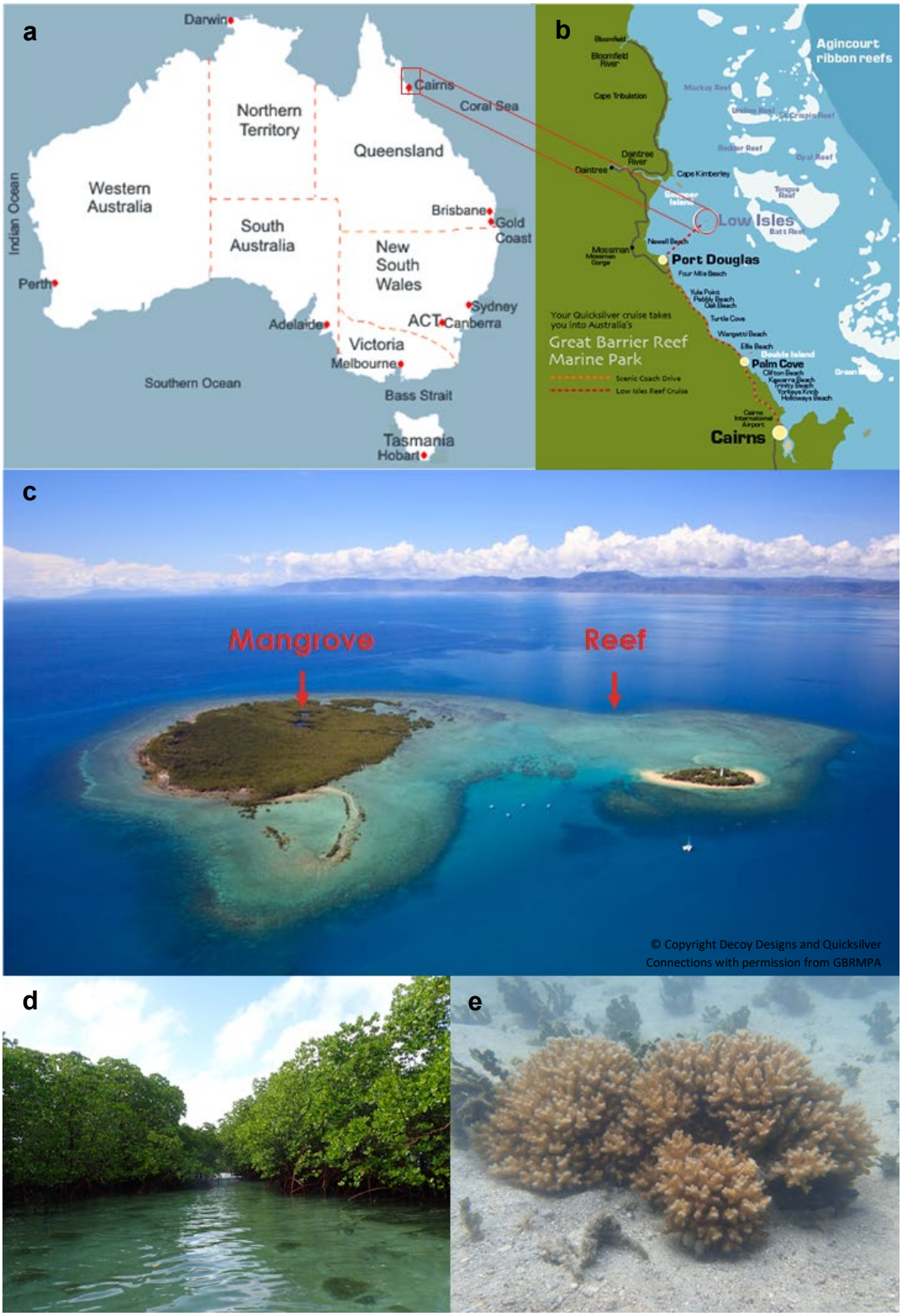

Supplementary Figure S4.1. Localisation of Low Isles on a map of Australia (**a**, denoted by a red rectangle) and relatively to Cairns (**b**, denoted by a red circle). Low Island reef (**c**) and Woody Island mangrove lagoon (**c**, **d**) were the collection sites of *Pocillopora acuta* colonies (**e**, in the mangrove).

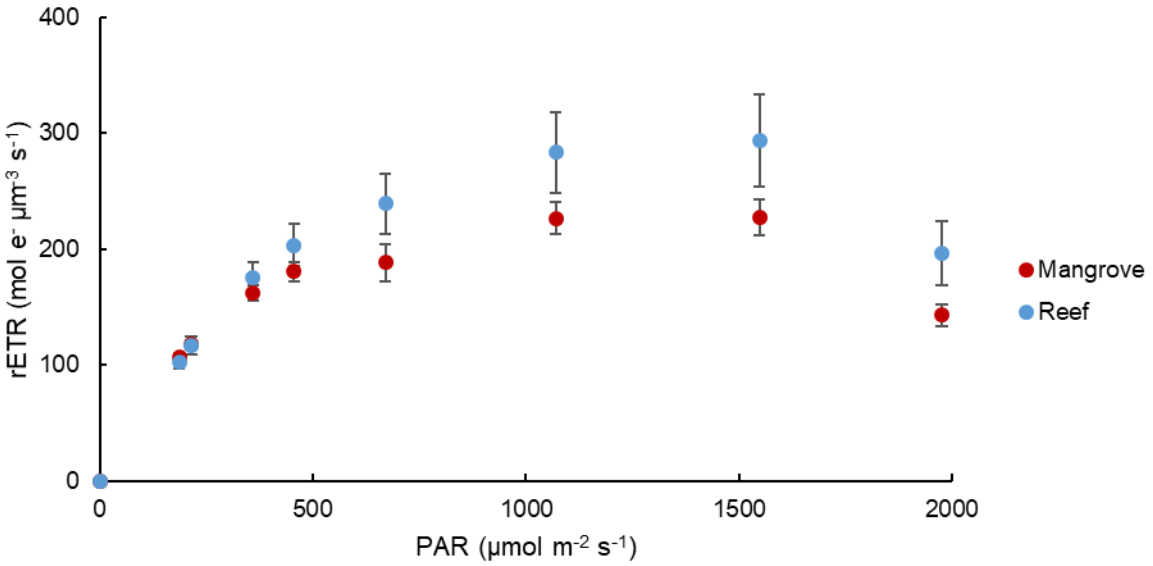

Supplementary Figure S4.2. Mean (± SE) relative electron transport rates (rETR, mol e^- μm^{-3} s^{-1}) obtained using rapid light curves (see Methods) for *Pocillopora acuta* (n = 4) across the Woody Isles mangrove lagoon (red) and Low Isles reef (blue).

Supplementary Figure S4.3. Image of the stable isotope incubations set-up, where FIS are incubated (small vials) close to their respective holobiont fraction (large vessels).

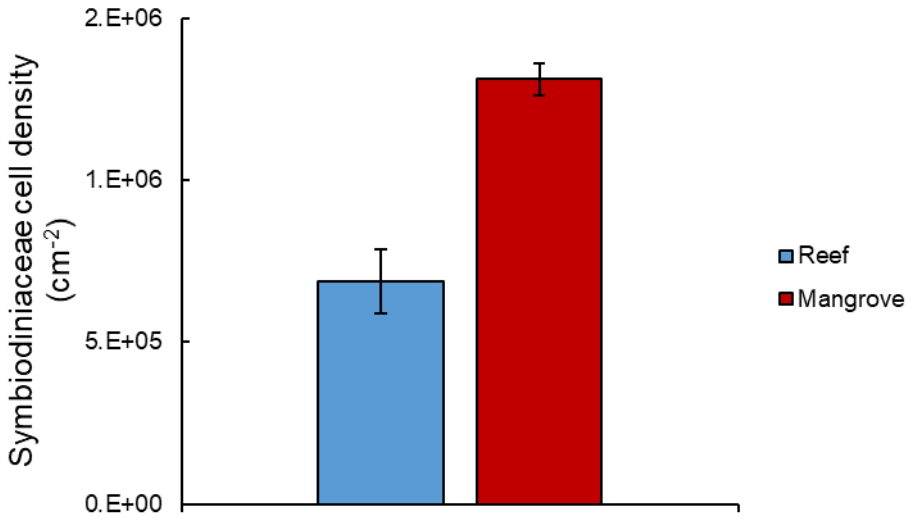

Supplementary Figure S4.4. Mean (± SE) Symbiodiniaceae cell density (cells cm^{-2}) for *Pocillopora acuta* (n = 4) across the Woody Isles mangrove lagoon (red) and Low Isles reef (blue).

4.8.3. Supplementary Table

Supplementary Table S4.1. Summary of the *Pocillopora acuta* samples taken from both Low Isles reef and Woody Isles mangrove and their subsamples (for stable isotope incubations and genomic analyses). Abbreviations: HB, holobiont; FIS, freshly isolated symbionts; H, host; S, symbiont; EA, enrichment analysis; NA, natural abundance; NS, NanoSIMS; CC, cell counts; PAM, pulse-amplified fluorometry.

		Reef								Mangrove							
		HB				FIS				HB				FIS			
Stable isotope labelling	Samples	7				7				5				5			
	Subsamples	EA		NA	NS	EA	NA	NS	CC	EA		NA	NS	EA	NA	NS	CC
		H	S							H	S						
		7	7	7	7	7	7	7	7	5	5	5	5	5	5	5	5
Genomic Analysis	Samples	4				N/A				4				N/A			
	Subsamples	H		S						H		S					
		4		4						4		4					
Respirometry	Samples	5				N/A				5				N/A			
	Subsamples	N/A								N/A							
PAM	Samples	4				N/A				4				N/A			
	Subsamples	N/A								N/A							
Total	**Samples**	**20**				**7**				**18**				**5**			

Chapter 5

General discussion: Synthesis, Perspectives and Conclusions

In this final chapter, I synthesise my findings from data Chapters 2-4 to highlight how my thesis addresses current gaps in knowledge in the role of Symbiodiniaceae dark reactions of photosynthesis in sustaining cellular fitness and survival. I identify still unresolved and novel unknowns stemming from these results and consider their relevance to understand the fate of carbon acquisition and transfer in corals. Finally, I examine how future research should address these gaps to improve our understanding of Symbiodiniaceae physiology, as their role is pivotal in explaining corals resistance to global environmental change.

5.1. Adaptive strategies of carbon transformation amongst coral symbionts

This thesis adopted a comprehensive array of approaches to examine the nature and variability of inorganic carbon (Ci) uptake and utilisation capacity amongst Symbiodiniaceae, a key metric necessary to explain the exchange of nutrients between corals and symbionts. Bridging this knowledge gap increased understanding of how Symbiodiniaceae (as a family) has evolved to sustain reef functioning across environmental conditions, including in response to climate change. Inorganic carbon uptake efficiency by Symbiodiniaceae was then determined for three different scenarios, i) *ex hospite* under steady-state and sub-optimal growth temperatures (**Chapter 2**) and ii) stressful heat conditions that drive cellular dysfunction and ultimately mortality (**Chapter 3**), as well as iii) *in hospite* across environmental gradients, including diverse thermal regimes (**Chapter 4**). The major outcome of this thesis is that dark reactions of photosynthesis, and more precisely carbon assimilation, are regulated by both the symbiont type, their growth environments and importantly by more functionally diverse – and presumably evolutionary less well conserved – upstream light reactions of photosynthesis such as light-harvesting and dynamic quenching.

5.1.1. Growth environments are the primary drivers of Ci uptake diversity

Results of **Chapters 2** and **3** suggested that sub-optimal and stressful conditions of growth are required to "trigger" Ci uptake diversity of Symbiodiniaceae, rather than being governed by their taxonomy only. As such, functional diversity in Ci uptake and excretion appears largely regulated by growth environment rather than genus diversity. The results of these two Chapters highlighted the relatively functionally conserved Ci assimilation strategies of Symbiodiniaceae across their broad genetic diversity. Such information may therefore be critical for resolving ecological patterns in Symbiodiniaceae physiological responses, where current taxonomic classification based on molecular markers alone will likely need to frame

categories of symbionts based on their responses to their surrounding environments, and particularly to stress. For example, populations of *P. acuta* living in contrasting growth environments (e.g. mangrove lagoons *versus* reef) uptake less Ci, but their symbionts are equally efficient as those of reef populations in translocating photosynthates to their host (**Chapter 4**.). Whilst my field data could not resolve how this functional shift was potentially driven by taxa (symbiont, host) *versus* environment, **Chapter 2** suggests that growth environment (either abiotic conditions or organic matter availability) – and specifically a change in optimum growth temperature that in turn selects for different species - is likely the most plausible explanation.

A key outcome from **Chapters 2-4**, and likely pivotal to explain free-living Symbiodiniaceae and coral-Symbiodiniaceae holobionts survival under sub-optimum conditions, was observations that more thermo-tolerant species fuel alternative electron flow (AEF; further detailed in section 5.1.2., including photorespiration) at a cost to – i.e. reduced – absolute Ci uptake, but in the case of symbiosis not proportion translocated (**Chapter 4**). This key symbiont property presumably is maintained whether the host has access to additional (or of a different nature) carbon supplements for "fuel" – although the latter needs further verification, as discussed in the following sections.

5.1.2. Light reactions regulate Ci uptake efficiency

The lack of obvious patterns in Ci uptake and translocation amongst 23 different isolates of Symbiodiniaceae (**Chapter 2**) suggests that differences in light-harvesting efficiency upstream of dark reactions (Warner and Suggett 2016; Suggett et al. 2015) is likely a strong effector on regulating the energy available for Ci fixation. This was confirmed by transcriptomics and physiological assessment in **Chapter 3** whereby heat stress had a strong impact on upstream light reactions of photosynthesis likely explaining declines in

"downstream" Ci uptake. Indeed, our *Breviolum minutum* isolate (most thermo-sensitive) exhibited strong down-regulations of genes involved in light reactions functioning, such as the primary units of PSI (psaA/psaB), and the D1 and D2 proteins of PSII, compared to the thermo-tolerant *Durusdinium trenchii* for which levels of expression remained unchanged. Interestingly, genes involved in dark reactions (carbonic anhydrase, Calvin-Benson cycle, and TCA cycle) were down-regulated in both isolates, where the *D. trenchii* isolate surprisingly exhibited the same trend, suggesting a response independent of Symbiodiniaceae thermal tolerance. Whilst these observations do not discount the hypothesis that light reactions dysfunction under heat stress may ultimately begin with an enzymatic slow-down in Ci uptake rates and electron "bottlenecking" that impact the light reactions (e.g. Jones et al. 1998), my results do demonstrate that cells have limited capacity to respond at the transcriptional level in compensating expression of key proteins needed to sustain maximum Ci uptake rates.

Importance of light reactions governing dark reactions was further demonstrated in the study of dynamic quenching patterns (**Chapter 4**) from natural coral-Symbiodiniaceae associations. We observed that for *Pocillopora acuta* populations from the mangrove, despite allocating more absorbed energy through [1-C] (photochemical quenching, qP), this did not translate to a higher measured P_G (O_2 production per cell, Figure 5.1). Reliance of corals on qP (compared to [1-Q] or non-photochemical quenching) as a "photosynthetic strategy" has already been proposed as a characteristic enabling enhanced tolerance by finely tuning the dissipation of excitation energy via NPQ pathways rather than major qP shifts (Nitschke et al. 2018). However, different species of corals (also harbouring different ITS types of symbionts) from the same mangrove lagoon (see Camp et al. 2019) exhibit the opposite quenching patterns, i.e. more reliant on [1-Q], than populations from the reef. Consequently, the mechanisms of survival in mangrove corals cannot be resolved yet by a universal response in dynamic

quenching (see Warner and Suggett 2016). My results from *P. acuta* are perhaps unsurprising since, in addition to linear electron transport which generates ATP and reductant required for Ci fixation in the Calvin Cycle, there are a range of AEF that flow to O_2 to generate ATP but not NADPH (Cardol et al. 2011; Hughes et al. 2018); and which may be activated when linear electron transport becomes saturated, or if there is increased cellular demand for ATP. Early work from Suggett et al. (2008) showed that a thermo-tolerant *Symbiodinium* sp. had increased light-driven respiration rates compared to a more sensitive isolate from the genus *Breviolum* – an outcome recently confirmed by Dang et al. (2019) for isolates from the same two genera. Even though my study comparing populations across the reef and mangrove habitat was accompanied by a flexibility in Symbiodiniaceae genera associations, the balance of oxygen consumption and reliance on AEF found in mangrove and reef corals highlight that in hospite Symbiodiniaceae physiology conforms to this observation from cultured Symbiodiniaceae with differences in thermal tolerance. As such, *Durusdinium* symbionts associating with mangrove *P. acuta* populations could have an increased energy demand for maintenance metabolism, requiring increased amounts of ATP to fuel pathways such as protein turnover (Quigg and Beardall 2003) – or may exhibit less capacity for linear electron capacity through limitations of one or more electron sinks (e.g. Ci fixation capacity).

Alternatively to AEF, the higher PSII electron flow yet lower P_G for mangrove corals, may reflect more pronounced rates of photorespiration whereby electrons flow linearly to ATP and NADPH, yet where O_2 is ultimately catalysed by RuBisCO instead of CO_2 (oxygenase activity; Lilley et al. 2010) – a phenomenon that could also reduce the ratio of P_G to PSII electron flow (Hughes et al. 2018). A previous study (Crawley et al. 2010) demonstrated that in response to elevated pCO_2 stress the coral *Acropora formosa* exhibited increased NPQ and reduced photorespiration. In *P. acuta* from the mangrove lagoons, I observed the opposite trend

(decreased NPQ but increased electron flow/reduced P_G signifying increased AEF or photorespiration). Mangrove coral populations are long-term adapted to elevated *p*CO2 conditions (Camp et al. 2018, 2019) and thus my contrasting observations are likely a photoprotective pathway by drawing excess of O_2 which could lead to the formation of ROS and oxidative damage (Suggett et al. 2008).

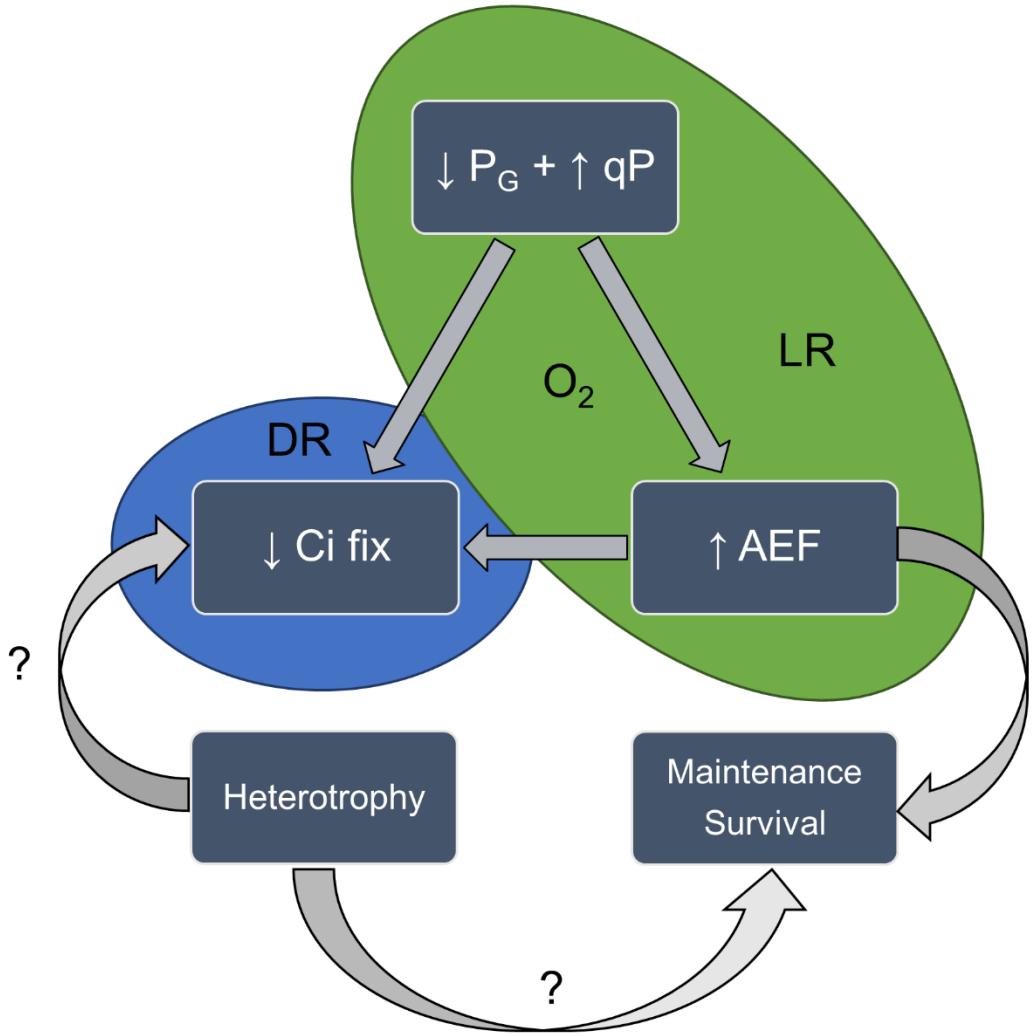

Figure 5.1. Summary of the interplay between light reactions and dark reactions of photosynthesis and how strategies promoting survival affects Ci fixation. LR: light reactions, DR: dark reactions, PG: gross photosynthesis, qP: photochemical quenching, AEF: alternative electron flows, Ci fix: inorganic carbon fixation. Question marks stand for pathways that have been suggested to play a role in coral-Symbiodiniaceae fitness but are to be quantified.

Importantly, as AEFs do not contribute to Ci fixation, upregulation of such pathways could ultimately reduce the amount of Ci fixed per unit of light absorbed (Hughes et al. 2018). Therefore, the plasticity with which dark reactions of photosynthesis potentially govern the trade-offs associated with harbouring multiple-stress tolerant symbionts, such as a decrease in calcification rates (Camp et al. 2019), need to be further investigated. Conversely, reef corals may be able to alleviate reliance upon AEF by employing dynamic non-photochemical quenching to divert excess excitation energy away as heat upstream of PSII (as evidenced by increased [1-Q] capacity of reef corals).

5.1.3. The use of cultures and holobionts in physiological studies

In this thesis, I have shown how nutritionally complex Symbiodiniaceae (as a family) cells appear to invest into alternative carbon pathways beyond dark reactions. Consequently, focusing on light or dark reactions alone may not be enough to "close the loop" on their ability to grow and survive. More integrated assessments are needed to explain the trade-offs for harbouring more stress-resistant symbionts, and clearly ones that can include the role of heterotrophic feeding (as on particulate or dissolved organic matter; Figure 5.1). Under sub-optimal conditions (here, decreased or elevated temperature), Symbiodiniaceae likely supplement their energetic requirement by feeding on bacteria (Jeong et al. 2012) and dissolved organic compounds (Steen 1987) when living *ex hospite* (**Chapter 2**; GPC:NPC ratios < 1). Similarly, the heavily reduced P_G:R observed for coral populations adapting from reef to mangrove habitats likely supplement carbon supply through feeding (Camp et al. 2017, 2019), although this has yet to be verified). For Symbiodiniaceae *in hospite*, a recent study by Wall et al. (2020) suggested that the coral *Montipora capitata* does not resort to increased heterotrophic feeding while harbouring *Durusdinium* spp. compared to *Cladocopium* spp. for populations in high *versus* low turbidity reef systems. However, the mangrove habitat I investigated on the

GBR is not considered to be a highly-turbid system, with minimal re-suspension of sediment or particulate organic matter as often observed for other mangrove systems (Camp et al. 2019). Instead, mangrove systems are characterised by increased dissolved organic matter compared to reefs (Watanabe and Nakamura 2019), suggesting that the corals I examined could still be able to benefit from dissolved organic sources without being impacted by resuspended particles reducing light incidence (Anthony 2006). Consequently, heterotrophic feeding extent and capacity could provide a common explanation for symbionts when both free-living and *in hospite* to sustain (and even govern) their health regulation under sub-optimal conditions.

This thesis considered two complementary perspectives in the study of Symbiodiniaceae physiology of dark reactions. **Chapters 2** and **3** focused on free-living cultures isolated from their host and maintained in culture conditions for >5 years, while **Chapter 4** examined the coral holobiont. While studies on holobionts are likely more ecologically relevant (in terms of symbiosis and the maintenance of reefs), there are still distinct advantages to working with laboratory cultures (Table 5.1), specifically in studies investigating mechanistic pathways that are critical to algal performance (Hallmann 2019) but also in the study of understanding symbiont fitness as free living cells (Jeong et al. 2012; Fujise et al. 2018; Bellantuono et al. 2019). This is especially the case when considering sufficient biological replication to overcome the immense natural variability found in environmental samples, and notably when the scope of research is to establish new techniques. In the case of this thesis, investigating the proportion of inorganic carbon used either for maintenance (GPC), or growth (NPC) could be difficult to resolve *in hospite* using stable isotopes, as longer incubations periods are needed, thus tending to confound the two processes inherent to long incubation periods (see section 1.5.2.). Alternatively, the SIMS technique could be used with radioactive isotopes (Hindie et al. 1992), but the still challenging nature of radiolabelled compounds renders their use limited, especially for *in situ* incubations. Finally, working with

optically-thin cultures permits use of single turnover active fluorometers such as FRRf (Hughes et al. 2018), which provide additional physiological information over more commonly used multiple turnover PAM-based approaches for example, but have rarely been optimised for use with corals (but see Gorbunov et al. 2001). Comparisons between free-living and *in hospite* photophysiology are challenged by reconciling different techniques optimised to different conditions and overcoming this limitation will be key moving forward. Even so, the two techniques used together provide important means to "fill in the gaps" that cannot be addressed by the technological limitations inherent to study free-living *versus in hospite*. In our case, the use of both lifestyles provided a robust way to study mechanisms of Ci assimilation and excretion/translocation.

Table 5.1. Summary of advantages and disadvantages of using Symbiodiniaceae in culture and in symbiosis with the holobiont. References: (**1**) Chapter 2; (**2**) Chapter 3; (**3**) Chapter 4; (**4**) Camp et al. 2019; (**5**) Hughes et al. 2018; (**6**) Gorbunov et al. 2001.

	Culture	**Holobiont**
Reproducibility (+ comparability)	Allows for direct comparison against previous (and future) studies (growth conditions can be adjusted accordingly).	Harder to standardise sample collection (e.g. depth, site, species). Species identification can be problematic (e.g. *Pocillopora* spp.).
Replication	Working with algal cultures allows for greater biological replication (short generation times).[1,2]	Generation times (years) constrains adaptive/evolutionary studies.
Growth environment	Full control over growth conditions (e.g. light, nutrients, and cell density). Cells can also be grown axenically, yet full manipulation of microbiome composition remains a step too far.	Growth environments are highly variable (e.g. site, location, and season). Intracellular conditions are also harder to quantify (nutritional status, light history, pH).
Ecological footprint	No research footprint on the reef itself. However, potential for environmental/carbon impacts through use of laboratory consumables (yet likely not as significant as carbon footprint incurred through fieldwork)	Collection of coral specimens from the field has inevitable impact on reef populations (although these can be minimised through best-practice scientific approaches).
Ecological significance	Algal cells are *ex hospite* so more difficult to interpret data in context of symbiosis. However, also permits for targeted study of cell physiology in absence of host factor.	Direct study of the coral holobiont provides data that can inform impacts of environmental variables to coral populations.

	Culture	**Holobiont**
Environment history (lifestyle adaptation)	Advantage of knowing full growth history of the cell line over multiple generations (e.g. months, years). However, for cells that are maintained long-term in culture conditions (years), genetic drift or adaptation could become more of a concern.	Environmental history is difficult to contextualise but does permit for working with material that is adapted/acclimated to specific environments. However, the study of corals in variable environments can serve as a natural lab setting for examining future climate scenarios (e.g. mangrove *versus* reef)[3,4]
Experiment acclimation	Acclimatory capacity (and speed) of algal cultures permits greater flexibility of environmental variable manipulation during research experimentation.[2]	Acclimation to experimental conditions are often short for holobionts (as a constraint of fieldwork). This is preferable however in some instances when examining corals in a short timeframe (e.g. such as at the end of summer), which may negate the need for lengthy experimental acclimation ahead of thermal stress experiments.
Methodology	Algal cultures allow for easy fractionation between dissolved and particulate fixed carbon.[1] Optically-thin microalgal cultures also permit use of single turnover active fluorometry which can provide additional useful photophysiological metrics[5]	Current advances (NanoSIMS) allow effectively tracking fate of carbon between host and symbiont[4] and metabolomics for identifying the nature of the compounds transferred. Most studies rely primarily on multiple turnover active fluorometry to assess holobiont photobiology[6] which yields less photophysiological data[5]

5.2. Perspectives for future research

5.2.1. Qualitative assessment of photosynthates

Throughout this thesis, I addressed the paradigm of "symbiotic efficiency" as the quantity of photosynthates translocated to the host. However, there is increasing evidence that the quality of translocated compounds, and ultimately their autotrophic or heterotrophic origin also have a role to play in coral fitness (Figure 5.1; Tremblay et al. 2014; Matthews et al. 2017; Hillyer et al. 2018). Metabolomics is the field studying cellular metabolites present in a cell or tissue in relation to their surrounding abiotic or biotic environment (Bundy et al. 2009). The recent implementation of metabolomics to Symbiodiniaceae studies is beginning to reshape much of our earlier knowledge of symbiotic efficiency. Of the few studies to date, assessment of the diversity of organic compounds secreted both by C3 type *Cladocopium* and its hard coral host *Acropora aspera* (Hillyer et al. 2016); and the fate of carbon from B1 type *Breviolum* to its sea anemone host *Aiptasia pulchella* (Hillyer et al. 2017) starts to emerge. By characterising the metabolite profiles of a wider array of Symbiodiniaceae genera and major ITS types, the gap in knowledge concerning the fate of inorganic carbon from the surrounding environment to its use by the symbiont or its host, either under the form of photosynthates involved in maintenance and growth, either to fuel the resistance to stressful environmental conditions could be addressed (Matthews et al. 2017). As such, investigating over a daily continuum the metabolic shifts involving trophic plasticity and determining the balance between hetero- and autotrophy in mangrove corals with the use of stable isotope labelled sources of carbon would be useful to link trophic strategies with resistance to "extreme" conditions. Moreover, unravelling metabolites differentially produced by the two main components of the symbiosis could orientate towards the measurement of standardised biomarkers, helpful in the monitoring of reef health (Figure 5.2).

5.2.2. Dark reactions "enzymatics"

This thesis revealed that light reactions of photosynthesis are important in explaining the differences in Ci assimilation, but the direct assessment of differences in dark reaction core constituents (CCM, RuBisCO) still need to be directly undertaken to determine what their roles in Ci assimilation efficiency are. To resolve fully the extent of diversity in dark reactions of photosynthesis, future studies should focus on enzyme kinetics to resolve dark reactions efficiencies amongst different Symbiodiniaceae taxa, increasing the resolution of our functional groups (**Chapter 2**). There is increasing evidence of differential activity of CCM in response to ocean acidification (Brading et al. 2013) and elevated temperatures (Oakley et al. 2014), but the full extent of diversity across the whole Symbiodiniaceae family is yet to be addressed. The other key enzyme regulating Ci fixation is RuBisCO, where activity can be independent of RuBisCO affinity and rate where CCMs have low affinity for CO_2. Lilley et al. (2010) proposed methods to study RuBisCO activity from symbiont extracts, and the inherent poor stability of this enzyme constitutes a challenge for future studies to overcome in the future years to come. While metabolomics (as suggested in previous section 5.2.1) can characterise the nature of translocated compounds to the host (Hillyer et al. 2018; Matthews et al. 2017, 2018), targeting the symbiont and characteristic intermediate metabolites (OAA for C4 and PGA for C3; Ludwig 2016) could help in resolving the large gap in knowledge regarding the type of photosynthesis Symbiodiniaceae ultimately employ (C3- or C4-photosynthesis, see section 1.2.4.). The flipside of these compounds is their short-life in the cell, due to their rapid conversion into CO_2 to sustain the CBC (Ludwig 2016). As such, capturing their presence in Symbiodiniaceae is still a major challenge to address even with the current metabolomics techniques. Another approach would be to study the presence or absence (and in the first case, activity) in Symbiodiniaceae of the NAD/NADP-malic decarboxylating enzyme, which converts malate from OAA into CO_2, and consequently act as a CCM specific of C4 plants

(Rao and Dixon 2016). Ultimately, resolving the photosynthesis type could help in establishing the metabolic pathway and productivity models (Figure 5.2) explaining how efficiently CO_2 is delivered to RuBisCO to maximise its carboxylase activity *versus* oxygenase (Beardall and Raven 2016). Resolving such knowledge gap is central to implementing Metabolic Pathways Analysis models (see Suggett and Smith 2020) needed to advance biological engineering of Symbiodiniaceae (Figure 5.2) to improve their performance and their rate of translocation to their host coral (Ortiz-Matamoros et al. 2015; Levin et al. 2017; Hallmann 2019).

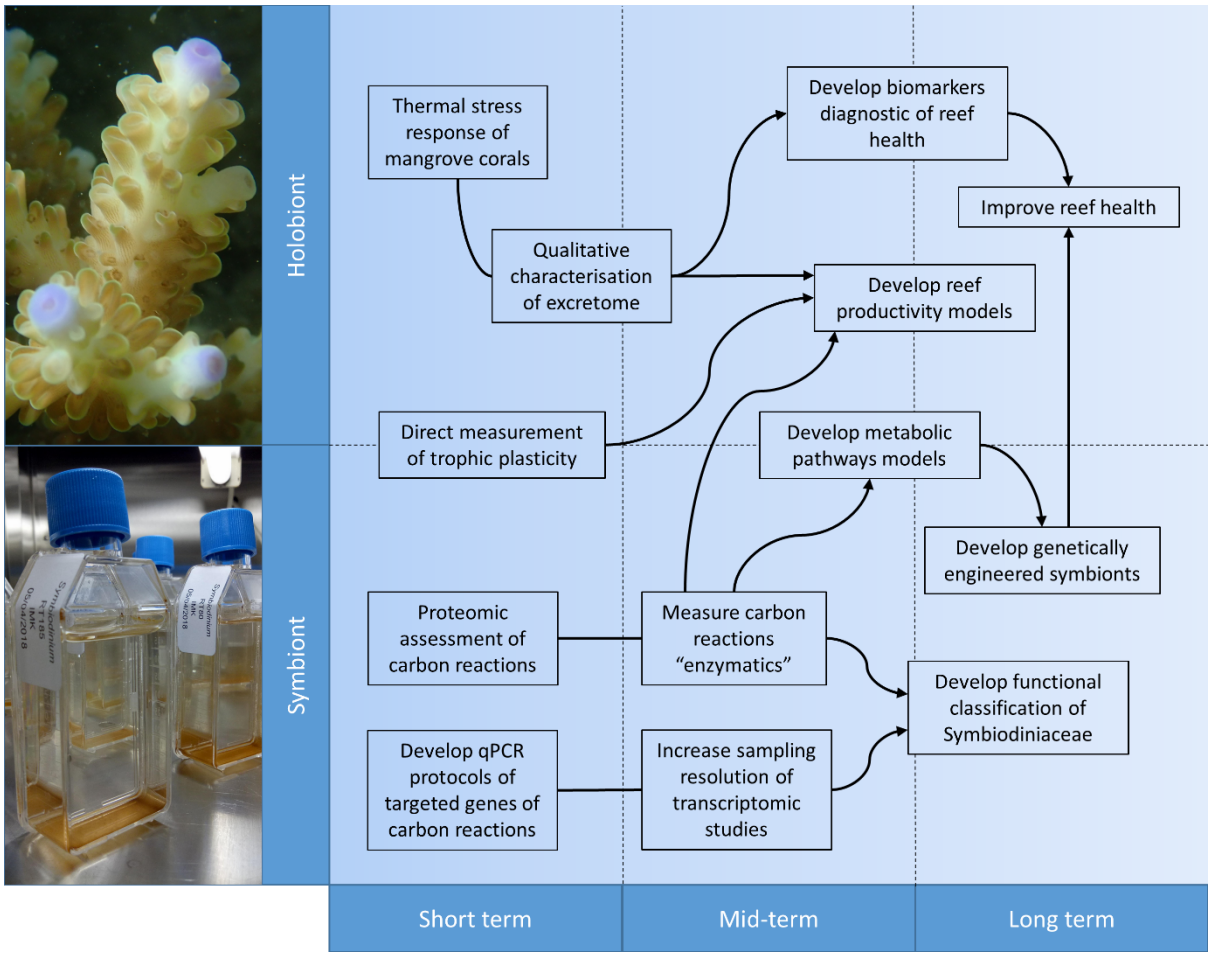

Figure 5.2. Proposed roadmap of future studies over the short and mid-terms leading on the long term to a better understanding of the Symbiodiniaceae and their holobiont physiologies.

5.2.3. Stress response of mangrove corals

For the past 30 years, there has been an increasing interest in understanding the physiology and the mechanisms of survival of corals in marginal and extreme environments (Camp et al. 2018). Such areas of the world are characterised by abiotic conditions that are representative of future conditions induced by climate change (Perry and Larcombe 2003; Camp et al. 2018). As such, mangrove coral populations, as reviewed in **Chapter 4**, constitute a nugget of hope for Australian reef systems (Camp et al. 2019), notably not only to unravel biological adaptation to extremes but as locations for genetic reservoirs of already stress hardened populations. It will be increasingly important to characterise the response of mangrove coral populations to future climate change and assess their survivability. The results in the **Chapter 4** of this thesis open three novel gaps in our knowledge of mangrove corals: (i) are environmental conditions or symbiont host identity driving Ci assimilation strategies? (ii) how would carbon transfer models shift when subjected to a wide range of stressors? (and hence will mangrove corals still fix less Ci than reef corals?); and finally (iii) what is the role of heterotrophic feeding for coral survival under future conditions? While resolving these questions is critical, addressing them may be further challenged with the increasing evidence of the microbiome as a significant stakeholder in holobiont survival. For example, a recent study (Motone et al. 2020) demonstrated that bacteria likely regulate ROS emissions and nutrient exchange for the symbiont (see also Matthews et al. 2020). Whilst photosynthesis is still the clear make-or-break for Symbiodiniaceae and coral survival – the paths as a "multi-partner" framework both in culture and *in hospite* need more focus.

5.2.4. Proteomics as high throughput resolution of metabolic function

The use of gene expression biomarkers (GEBs) by transcriptomics (i.e. the study of the cell transcriptome at a given time) has been already proposed as a proxy to study the response of either the host (Miller et al. 2011; Mayfield et al. 2014) or symbiont (Leggat et al. 2011b; Ladner et al. 2012; Levin et al. 2016) to thermal stress. In this thesis, transcriptomics proved useful to detect first-order trends in light reactions (only for a thermo-sensitive *Breviolum* isolate) but failed to match the dark reactions phenotype regardless of isolate thermal tolerance (**Chapter 3**). Moreover, transcripts are subject to significant variability of expression (Leggat et al. 2011a) and downstream processes as they are cleaved in the cell by RNAses and modified post-translationally, as suggested by low-levels of fold change within the genus *Cladocopium* (**Chapter 3**; Gierz et al. 2017). This decoupling between physiology and molecular responses highlights the necessity to monitor physiology in transcriptomic studies. However, this combination of techniques only allowed us to witness the end-result of thermal stress, and there are still questions that remain unanswered regarding the upstream pathways leading to the observed physiological responses. As such, the next step of stress response characterisation would be to investigate the nature and quantity of proteins successfully produced. Without coupled transcripts-protein studies to verify whether transcriptomics reflect functional expressions, this leaves GEBs as a poor biomarker of thermal stress (Feder and Walser 2005; Louis et al. 2017). Future transcriptomics studies should be complemented by proteomics targeting specifically key proteins of light and dark reactions (**Chapter 3**) to integrate the functional response of an organism in a systems biology approach (Gordon and Leggat, 2010) for potential coral restoration approaches (Parkinson et al. 2019).

5.3. Concluding remarks

In summary, by exploring the previously "hidden" world of the dark reactions, I have shown that Symbiodiniaceae have complex and still difficult-to-resolve carbon pathways that clearly play a role in overall fitness and capacity for survival. Knowledge gained from this thesis has begun to unlock this role by improving our understanding of Symbiodiniaceae functional evolution towards well-conserved Ci-uptake strategies, shaped by local environmental conditions and light utilisation strategies – and highlighting the importance of "carbon subsidies" needed to survive under sub-optimum (heat) conditions. In doing so, the thesis has raised questions regarding processes and pathways that will need more attention to close metabolism central to survival, such as the importance of non-autotrophic supplements, and the study of proteomics and metabolomics to build on our knowledge of metabolic differences in Ci uptake and translocation *versus* transcriptional expression. By answering these questions, we will move one-step forward to understand – and potentially better fast track through novel metabolic engineering approaches - adaptation of coral holobionts in sustaining their fitness under future climate pressures (Figure 5.2).

5.4. References

Anthony, K. R. 2006. Enhanced energy status of corals on coastal, high-turbidity reefs. Marine Ecology Progress Series. **319**: 111-116.

Beardall, J. and J. A. Raven. 2016. Carbon acquisition by microalgae. The physiology of microalgae, Springer: 89-99.

Bellantuono, A. J., K. E. Dougan, C. Granados-Cifuentes and M. Rodriguez-Lanetty. 2019. Free-living and symbiotic lifestyles of a thermotolerant coral endosymbiont display profoundly distinct transcriptomes under both stable and heat stress conditions. Mol. Ecol. **28**: 5265-5281. doi:10.1111/mec.15300

Brading, P., M. E. Warner, D. J. Smith and D. J. Suggett. 2013. Contrasting modes of inorganic carbon acquisition amongst *Symbiodinium* (Dinophyceae) phylotypes. New Phytol. **200**: 432-442. doi:10.1111/nph.12379

Bundy, J. G., M. P. Davey and M. R. Viant. 2009. Environmental metabolomics: a critical review and future perspectives. Metabolomics. **5**: 3-21. doi:10.1007/s11306-008-0152-0

Camp, E. F., M. R. Nitschke, R. Rodolfo-Metalpa, F. Houlbreque, S. G. Gardner, D. J. Smith, M. Zampighi and D. J. Suggett. 2017. Reef-building corals thrive within hot-acidified and deoxygenated waters. Sci Rep. **7**: 2434. doi:10.1038/s41598-017-02383-y

Camp, E. F., V. Schoepf, P. J. Mumby, L. A. Hardtke, R. Rodolfo-Metalpa, D. J. Smith and D. J. Suggett. 2018. The future of coral reefs subject to rapid climate change: Lessons from natural extreme environments. Frontiers in Marine Science. **5**. doi:10.3389/fmars.2018.00004

Camp, E. F., J. Edmondson, A. Doheny, J. Rumney, A. J. Grima, A. Huete and D. J. Suggett. 2019. Mangrove lagoons of the Great Barrier Reef support coral populations persisting under extreme environmental conditions. Marine Ecology Progress Series. **625**: 1-14. doi:10.3354/meps13073

Cardol, P., G. Forti and G. Finazzi. 2011. Regulation of electron transport in microalgae. Biochim. Biophys. Acta. **1807**: 912-918. doi:10.1016/j.bbabio.2010.12.004

Crawley, A., D. I. Kline, S. Dunn, K. E. N. Anthony and S. Dove. 2010. The effect of ocean acidification on symbiont photorespiration and productivity in *Acropora formosa*. Global Change Biology. **16**: 851-863. doi:10.1111/j.1365-2486.2009.01943.x

Dang, K. V., M. Pierangelini, S. Roberty and P. Cardol. 2019. Alternative photosynthetic electron transfers and bleaching phenotypes upon acute heat stress in *Symbiodinium* and *Breviolum* spp. (Symbiodiniaceae) in culture. Frontiers in Marine Science. **6**. doi:10.3389/fmars.2019.00656

Feder, M. E. and J. C. Walser. 2005. The biological limitations of transcriptomics in elucidating stress and stress responses. J. Evol. Biol. **18**: 901-910. doi:10.1111/j.1420-9101.2005.00921.x

Fujise, L., M. R. Nitschke, J. C. Frommlet, J. Serodio, S. Woodcock, P. J. Ralph and D. J. Suggett. 2018. Cell cycle dynamics of cultured coral endosymbiotic microalgae

(*Symbiodinium*) across different types (species) under alternate light and temperature conditions. J. Eukaryot. Microbiol. **65**: 505-517. doi:10.1111/jeu.12497

Gierz, S. L., S. Foret and W. Leggat. 2017. Transcriptomic analysis of thermally stressed Symbiodinium reveals differential expression of stress and metabolism genes. Front. Plant. Sci. **8**: 271. doi:10.3389/fpls.2017.00271

Gorbunov, M. Y., Z. S. Kolber, M. P. Lesser and P. G. Falkowski. 2001. Photosynthesis and photoprotection in symbiotic corals. Limnology and Oceanography. **46**: 75-85.

Gordon, B. R. and W. Leggat. 2010. *Symbiodinium*-invertebrate symbioses and the role of metabolomics. Mar. Drugs. **8**: 2546-2568. doi:10.3390/md8102546

Hallmann, A. (2019). Advances in genetic engineering of microalgae. Grand Challenges in Algae Biotechnology: 159-221.

Hillyer, K. E., S. Tumanov, S. Villas-Boas and S. K. Davy. 2016. Metabolite profiling of symbiont and host during thermal stress and bleaching in a model cnidarian-dinoflagellate symbiosis. J. Exp. Biol. **219**: 516-527. doi:10.1242/jeb.128660

Hillyer, K. E., D. A. Dias, A. Lutz, U. Roessner and S. K. Davy. 2017. Mapping carbon fate during bleaching in a model cnidarian symbiosis: the application of ^{13}C metabolomics. New Phytol. **214**: 1551-1562. doi:10.1111/nph.14515

Hillyer, K. E., D. Dias, A. Lutz, U. Roessner and S. K. Davy. 2018. ^{13}C metabolomics reveals widespread change in carbon fate during coral bleaching. Metabolomics. **14**: 12. doi:10.1007/s11306-017-1306-8

Hindie, E., B. Coulomb and P. Galle. 1992. SIMS microscopy: a tool to measure the intracellular concentration of carbon 14-labelled molecules. Biology of the Cell. **74**: 89-92.

Hughes, D. J., and others. 2018. Roadmaps and Detours: Active chlorophyll-a assessments of primary productivity across marine and freshwater systems. Environ. Sci. Technol. **52**: 12039-12054. doi:10.1021/acs.est.8b03488

Jeong, H. J., and others. 2012. Heterotrophic feeding as a newly identified survival strategy of the dinoflagellate *Symbiodinium*. Proc. Natl. Acad. Sci. U. S. A. **109**: 12604-12609. doi:10.1073/pnas.1204302109

Jones, R. J., O. Hoegh-Guldberg, A. W. Larkum and U. Schreiber. 1998. Temperature-induced bleaching of corals begins with impairment of the CO_2 fixation mechanism in zooxanthellae. Plant, Cell & Environment. **21**: 1219-1230.

Ladner, J. T., D. J. Barshis and S. R. Palumbi. 2012. Protein evolution in two co-occurring types of *Symbiodinium*: an exploration into the genetic basis of thermal tolerance in *Symbiodinium* clade D. BMC Evolutionary Biology. **12**: 217.

Leggat, W., D. Yellowlees and M. Medina. 2011a. Recent progress in *Symbiodinium* transcriptomics. Journal of Experimental Marine Biology and Ecology. **408**: 120-125. doi:10.1016/j.jembe.2011.07.032

Leggat, W., F. Seneca, K. Wasmund, L. Ukani, D. Yellowlees and T. D. Ainsworth. 2011b. Differential responses of the coral host and their algal symbiont to thermal stress. PLoS One. **6**: e26687. doi:10.1371/journal.pone.0026687

Levin, R. A., V. H. Beltran, R. Hill, S. Kjelleberg, D. McDougald, P. D. Steinberg and M. J. van Oppen. 2016. Sex, scavengers, and chaperones: Transcriptome secrets of divergent *Symbiodinium* thermal tolerances. Mol. Biol. Evol. **33**: 2201-2215. doi:10.1093/molbev/msw119

Levin, R. A., C. R. Voolstra, S. Agrawal, P. D. Steinberg, D. J. Suggett and M. J. H. van Oppen. 2017. Engineering strategies to decode and enhance the genomes of coral symbionts. Front. Microbiol. **8**: 1220. doi:10.3389/fmicb.2017.01220

Lilley, R. M., P. J. Ralph and A. W. Larkum. 2010. The determination of activity of the enzyme Rubisco in cell extracts of the dinoflagellate alga *Symbiodinium* sp. by manganese chemiluminescence and its response to short-term thermal stress of the alga. Plant Cell. Environ. **33**: 995-1004. doi:10.1111/j.1365-3040.2010.02121.x

Louis, Y. D., R. Bhagooli, C. D. Kenkel, A. C. Baker and S. D. Dyall. 2017. Gene expression biomarkers of heat stress in scleractinian corals: Promises and limitations. Comp. Biochem. Physiol. C. Toxicol. Pharmacol. **191**: 63-77. doi:10.1016/j.cbpc.2016.08.007

Ludwig, M. 2016. The roles of organic acids in C4 photosynthesis. Front. Plant. Sci. **7**: 647. doi:10.3389/fpls.2016.00647

Matthews, J. L., and others. 2017. Optimal nutrient exchange and immune responses operate in partner specificity in the cnidarian-dinoflagellate symbiosis. Proceedings of the National Academy of Sciences. **114**: 13194-13199.

Matthews, J. L., C. A. Oakley, A. Lutz, K. E. Hillyer, U. Roessner, A. R. Grossman, V. M. Weis and S. K. Davy. 2018. Partner switching and metabolic flux in a model cnidarian-dinoflagellate symbiosis. Proc. Biol. Sci. **285**. doi:10.1098/rspb.2018.2336

Matthews, J. L., J. B. Raina, T. Kahlke, J. R. Seymour, M. J. H. van Oppen and D. J. Suggett. 2020. Symbiodiniaceae-bacteria interactions: rethinking metabolite exchange in reef-building corals as multi-partner metabolic networks. Environ. Microbiol. doi:10.1111/1462-2920.14918

Mayfield, A. B., Y. B. Wang, C. S. Chen, C. Y. Lin and S. H. Chen. 2014. Compartment-specific transcriptomics in a reef-building coral exposed to elevated temperatures. Mol. Ecol. **23**: 5816-5830. doi:10.1111/mec.12982

Miller, D. J., E. E. Ball, S. Forêt and N. Satoh. 2011. Coral genomics and transcriptomics — Ushering in a new era in coral biology. Journal of Experimental Marine Biology and Ecology. **408**: 114-119. doi:10.1016/j.jembe.2011.07.031

Motone, K., T. Takagi, S. Aburaya, N. Miura, W. Aoki and M. Ueda. 2020. A zeaxanthin-producing bacterium isolated from the algal phycosphere protects coral endosymbionts from environmental stress. mBio. **11**. doi:10.1128/mBio.01019-19

Nitschke, M. R., S. G. Gardner, S. Goyen, L. Fujise, E. F. Camp, P. J. Ralph and D. J. Suggett. 2018. Utility of photochemical traits as diagnostics of thermal tolerance amongst Great Barrier Reef corals. Frontiers in Marine Science. **5**. doi:10.3389/fmars.2018.00045

Oakley, C. A., G. W. Schmidt and B. M. Hopkinson. 2014. Thermal responses of *Symbiodinium* photosynthetic carbon assimilation. Coral Reefs. **33**: 501-512. doi:10.1007/s00338-014-1130-9

Ortiz-Matamoros, M. F., T. Islas-Flores, B. Voigt, D. Menzel, F. Baluska and M. A. Villanueva. 2015. Heterologous DNA uptake in cultured *Symbiodinium* spp. aided by *Agrobacterium tumefaciens*. PLoS One. **10**: e0132693. doi:10.1371/journal.pone.0132693

Parkinson, J. E., A. C. Baker, I. B. Baums, S. W. Davies, A. G. Grottoli, S. A. Kitchen, M. V. Matz, M. W. Miller, A. A. Shantz and C. D. Kenkel. 2019. Molecular tools for coral reef restoration: beyond biomarker discovery. Conservation Letters. 13: e12687. doi: 10.1111/conl.12687

Perry, C. T. and P. Larcombe. 2003. Marginal and non-reef-building coral environments. Coral Reefs. **22**: 427-432. doi:10.1007/s00338-003-0330-5

Quigg, A. and J. Beardall. 2003. Protein turnover in relation to maintenance metabolism at low photon flux in two marine microalgae. Plant, Cell & Environment. **26**: 693-703.

Rao, X. and R. A. Dixon. 2016. The differences between NAD-ME and NADP-ME subtypes of C4 photosynthesis: More than decarboxylating enzymes. Front. Plant Sci. **7**: 1525. doi:10.3389/fpls.2016.01525

Steen, R. 1987. Evidence for facultative heterotrophy in cultured zooxanthellae. Marine Biology. **95**: 15-23.

Suggett, D. J., M. E. Warner, D. J. Smith, P. Davey, S. Hennige and N. R. Baker. 2008. Photosynthesis and production of hydrogen peroxide by *Symbiodinium* (Pyrrhophyta) phylotypes with different thermal tolerances. J. Phycol. **44**: 948-956. doi:10.1111/j.1529-8817.2008.00537.x

Suggett, D. J., S. Goyen, C. Evenhuis, M. Szabo, D. T. Pettay, M. E. Warner and P. J. Ralph. 2015. Functional diversity of photobiological traits within the genus *Symbiodinium* appears to be governed by the interaction of cell size with cladal designation. New Phytol. **208**: 370-381. doi:10.1111/nph.13483

Suggett, D. J. and D. J. Smith. 2020. Coral bleaching patterns are the outcome of complex biological and environmental networking. Global Change Biology. **26**: 68-79.

Tremblay, P., R. Grover, J. F. Maguer, M. Hoogenboom and C. Ferrier-Pagès. 2014. Carbon translocation from symbiont to host depends on irradiance and food availability in the tropical coral *Stylophora pistillata*. Coral Reefs. **33**: 1-13. doi:10.1007/s00338-013-1100-7

Wall, C. B., M. Kaluhiokalani, B. N. Popp, M. J. Donahue and R. D. Gates. 2020. Divergent symbiont communities determine the physiology and nutrition of a reef coral across a light-availability gradient. ISME J. doi:10.1038/s41396-019-0570-1

Warner, M. E. and D. J. Suggett. 2016. The photobiology of *Symbiodinium* spp.: Linking physiological diversity to the implications of stress and resilience. The Cnidaria, Past, Present and Future: 489-509.

Watanabe, A. and T. Nakamura. 2019. Carbon dynamics in coral reefs. Blue Carbon in Shallow Coastal Ecosystems, Springer: 273-293.

Appendix

Supplementary Table S3.1 Full list of proteins and their associated genes and cellular functions used to target and refine the transcripts analysis in all the studied Symbiodiniaceae (*Breviolum minutum*, *Cladocopium goreaui,* and *Durusdinium trenchii*). Colours of cells represent the functional grouping proteins were associated with green: light reactions; blue: dark reactions; yellow: metabolism; orange: stress response; grey: transport. Information of protein function was retrieved from the UniProt knowledgebase (UniProtKB). "N/A" denotes a protein for which a gene name has not been identified.

Protein	*Gene*	Function	Functional group
Cytochrome b2, mitochondrial	*CYB2*	Catalyses lactate in pyruvate.	Electron transport
Cytochrome b5, ER	*Cyt-b5*	Cytochrome b5 is a membrane-bound hemoprotein which functions as an electron carrier for several membrane-bound oxygenases.	
Cytochrome b6	*petB*	Component of the cytochrome b6-f complex, which mediates electron transfer between photosystem II (PSII) and photosystem I (PSI), cyclic electron flow around PSI, and state transitions.	
Cytochrome b6-f complex iron-sulphur subunit, chloroplastic	*petC*		
Cytochrome b6-f complex subunit 4	*petD*		
Cytochrome b6-f complex subunit 5	*petG*	Required for either the stability or assembly of the cytochrome b6-f complex.	
Cytochrome b6-f complex subunit 6	*petL*	Important for photoautotrophic growth as well as for electron transfer efficiency and stability of the cytochrome b6-f complex.	
Cytochrome c oxidase subunit 1	*ctaD*	Component of the respiratory chain that catalyses the reduction of oxygen to water. Subunits 1-3 form the functional core of the enzyme complex.	
Cytochrome c oxidase subunit 2	*COX2*		
Cytochrome c oxidase subunit 3	*ctaE*		
Cytochrome c1, mitochondrial	*Cyc1*	Heme-containing component of the cytochrome b-c1 complex, which accepts electrons from Rieske protein and transfers electrons to cytochrome c in the mitochondrial respiratory chain.	
Cytochrome c1-2, heme protein, mitochondrial	*CYCL*		
Cytochrome c6, chloroplastic	*petJ*	Functions as an electron carrier between membrane-bound cytochrome b6-f and photosystem I in oxygenic photosynthesis.	

Cytochrome f	*petA*	Component of the cytochrome b6-f complex, which mediates electron transfer between photosystem II (PSII) and photosystem I (PSI), cyclic electron flow around PSI, and state transitions.	Electron transport
Ferredoxin-1	*petF*	Ferredoxins are iron-sulphur proteins that transfer electrons in a wide variety of metabolic reactions.	
Ferredoxin--NADP reductase, chloroplastic	*petH*	May play a key role in regulating the relative amounts of cyclic and non-cyclic electron flow to meet the demands of the plant for ATP and reducing power.	
Plastocyanin	*petE*	Participates in electron transfer between P700 and the cytochrome b6-f complex in photosystem I.	
Succinate dehydrogenase [ubiquinone] flavoprotein subunit, mitochondrial	*SDH1*	Catalytic subunit of succinate dehydrogenase (SDH) that is involved in complex II of the mitochondrial electron transport chain and is responsible for transferring electrons from succinate to ubiquinone (coenzyme Q). SDH1 and SDH2 form the catalytic dimer. Electrons flow from succinate to the FAD bound to SDH1, and sequentially through the iron-sulphur clusters bound to SDH2 and enter the membrane dimer formed by SDH3 and SDH4.	
Caroteno-chlorophyll a-c-binding protein	N/A	The light-harvesting complex (LHC) functions as a light receptor, it captures and delivers excitation energy to photosystems with which it is closely associated. Energy is transferred from the carotenoid and chlorophyll-c (or b) to chlorophyll-a and the photosynthetic reaction centres where it is used to synthesize ATP and reducing power.	Light harvesting
Chlorophyll a-b binding protein 1B-20, chloroplastic	*LHC Ib-20*		
Chlorophyll a-b binding protein 1B-21, chloroplastic	*LHC Ib-21*		
Chlorophyll a-b binding protein 4, chloroplastic	*LHCA4*		
Chlorophyll a-b binding protein L1818, chloroplastic	*L1818*		
Fucoxanthin-chlorophyll a-c binding protein A, chloroplastic	*FCPA*		
Fucoxanthin-chlorophyll a-c binding protein B, chloroplastic	*FCPB*		
Fucoxanthin-chlorophyll a-c binding protein C, chloroplastic	*FCPC*		
Fucoxanthin-chlorophyll a-c binding protein D, chloroplastic	*FCPD*		

Fucoxanthin-chlorophyll a-c binding protein E, chloroplastic	*FCPE*		Light harvesting
Fucoxanthin-chlorophyll a-c binding protein F, chloroplastic	*FCPF*		
Peridinin-chlorophyll a-binding protein, chloroplastic	N/A	Water-soluble antenna for capture of solar energy in the blue-green range. Peridinin is an asymmetric carotenoid.	
Photosystem I assembly protein Ycf3	*ycf3*	Essential for the assembly of the photosystem I (PSI) complex. May act as a chaperone-like factor to guide the assembly of the PSI subunits.	PSI - Biogenesis
Photosystem I iron-sulphur centre	*psaC*	Apoprotein for the two 4Fe-4S centres FA and FB of photosystem I (PSI); essential for photochemical activity. FB is the terminal electron acceptor of PSI, donating electrons to ferredoxin. The C-terminus interacts with PsaA/B/D and helps assemble the protein into the PSI complex. Required for binding of PsaD and PsaE to PSI. PSI is a plastocyanin/cytochrome c6-ferredoxin oxidoreductase, converting photonic excitation into a charge separation, which transfers an electron from the donor P700 chlorophyll pair to the spectroscopically characterized acceptors A0, A1, FX, FA and FB in turn.	PSI - Electron transport
Photosystem I P700 chlorophyll a apoprotein A1	*psaA*	PsaA and PsaB bind P700, the primary electron donor of photosystem I (PSI), as well as the electron acceptors A0, A1 and FX. PSI is a plastocyanin/cytochrome c6-ferredoxin oxidoreductase, converting photonic excitation into a charge separation, which transfers an electron from the donor P700 chlorophyll pair to the spectroscopically characterized acceptors A0, A1, FX, FA and FB in turn. Oxidised P700 is reduced on the lumenal side of the thylakoid membrane by plastocyanin or cytochrome c6. Both potential cofactor branches in PSI seem to be active; however, electron transfer seems to proceed preferentially down the path including the phylloquinone bound by PsaA.	PSI - Photosynthesis
Photosystem I P700 chlorophyll a apoprotein A2	*psaB*		
Photosystem I reaction centre subunit II, chloroplastic	*psaD*	PsaD can form complexes with ferredoxin and ferredoxin-oxidoreductase in photosystem I (PSI) reaction centre. *psaD* may encode the ferredoxin-docking protein.	

Photosystem I reaction center subunit III, chloroplastic	*psaF*	Probably participates in efficiency of electron transfer from plastocyanin to P700 (or cytochrome c553 in algae and cyanobacteria). This plastocyanin-docking protein contributes to the specific association of plastocyanin to PSI.	PSI - Photosynthesis
Photosystem I reaction center subunit IV, chloroplastic	*psaE*	Stabilizes the interaction between PsaC and the PSI core, assists the docking of the ferredoxin to PSI and interacts with ferredoxin-NADP oxidoreductase.	
Photosystem biogenesis factor 1	*psbN*	May play a role in photosystem I and II biogenesis.	PSII - Biogenesis
Photosystem II stability/assembly factor HCF136, chloroplastic	*HCF136*	Essential for photosystem II (PSII) biogenesis; required for assembly of an early intermediate in PSII assembly that includes D2 (PsbD) and cytochrome b559. Has been suggested (PubMed: 11826309) to be required for chlorophyll a binding.	
Cytochrome b559 subunit alpha	*psbE*	With its partner (PsbF) binds heme. PSII binds additional chlorophylls, carotenoids and specific lipids.	PSII - Photosynthesis
Cytochrome b559 subunit beta	*psbF*	With its partner (PsbE) binds heme. PSII binds additional chlorophylls, carotenoids and specific lipids.	
Cytochrome c-550	*psbV*	Low-potential cytochrome c that plays a role in the oxygen-evolving complex of photosystem II (PSII). Required for normal function or stabilization of PSII. Extrinsic protein associated with PSII that enhances oxygen evolution.	
Oxygen-evolving enhancer protein 1, chloroplastic	*psbO*	Stabilizes the manganese cluster which is the primary site of water splitting.	
Oxygen-evolving enhancer protein 2-1, chloroplastic	*psbP*	May be involved in the regulation of photosystem II.	
Oxygen-evolving enhancer protein 3-1, chloroplastic	*psbQ*	Required for photosystem II assembly/stability and photoautotrophic growth under low light conditions.	
Photosystem II 10 kDa polypeptide, chloroplastic	*psbR*	Associated with the oxygen-evolving complex of photosystem II.	
Photosystem II 12 kDa extrinsic protein, chloroplastic	*psbU*	Stabilizes the structure of photosystem II oxygen-evolving complex (OEC), the ion environment of oxygen evolution and protects the OEC against heat-induced inactivation.	

Photosystem II 22 kDa protein, chloroplastic	*psbS*	Plays an important role in non-photochemical quenching, a process maintains the balance between dissipation and utilization of light energy to minimize generation of oxidizing molecules, thereby protecting the plant against photo-oxidative damage. Is not necessary for efficient light harvesting and photosynthesis.	PSII - Photosynthesis
Photosystem II core complex proteins psbY, chloroplastic	*psbY*	PSBY-1 and -2 are manganese-binding polypeptides with L-arginine metabolizing enzyme activity. They are a component of the core of photosystem II. They have also a minor catalase-like activity since they cause evolution of oxygen from hydrogen peroxide in a reaction stimulated by manganese.	
Photosystem II CP43 reaction center protein	*psbC*	Binds chlorophyll and helps catalyse the primary light-induced photochemical processes of PSII.	
Photosystem II CP47 reaction center protein	*psbB*		
Photosystem II D1 protein	*psbA*	The D1/D2 heterodimer binds P680, chlorophylls that are the primary electron donor of PSII, and subsequent electron acceptors. It shares a non-heme iron and each subunit binds pheophytin, quinone, additional chlorophylls, carotenoids and lipids. D1 provides most of the ligands for the Mn4-Ca-O5 cluster of the oxygen-evolving complex (OEC).	
Photosystem II D2 protein	*psbD*	The D1/D2 (PsbA/PsbD) reaction centre heterodimer binds P680, the primary electron donor of PSII as well as several subsequent electron acceptors (PubMed: 19433803, PubMed: 23426624). D2 is needed for assembly of a stable PSII complex.	
Photosystem II reaction center protein H	*psbH*	Required for PSII stability and/or assembly.	
Photosystem II reaction center protein I	*psbI*	May be required for formation of PSII dimers but not their subsequent stability (PubMed: 21195048).	
Photosystem II reaction center protein J	*psbJ*	One of the components of the core complex of photosystem II (PSII). PSII is a light-driven water:plastoquinone oxidoreductase that uses light energy to abstract electrons from H_2O, generating O_2 and a proton gradient subsequently used for ATP formation. It consists of a core antenna complex that captures photons, and an electron transfer chain that converts photonic excitation into a charge separation.	

Photosystem II reaction center protein K	*psbK*	Required for association of PsbZ and Ycf12 with PSII (PubMed: 20194360).	PSII - Photosynthesis
Photosystem II reaction center protein L	*psbL*	Found at the monomer-monomer interface and is required for correct PSII assembly and/or dimerization (By similarity). Required for PSII activity, at least in part due to its effects on PSII assembly. May make specific contact(s) with lipids.	
Photosystem II reaction center protein M	*psbM*	Found at the monomer-monomer interface. Probably involved in dimerization of PSII; at the monomer-monomer interface the only protein-protein contacts observed are between the 2 PsbM subunits. Lipids, chlorophylls and carotenoids contribute strongly to PSII dimerization.	
Photosystem II reaction center protein T	*psbT*	Seems to play a role in the dimerization of PSII.	
Photosystem II reaction center protein Z	*psbZ*	Controls the interaction of photosystem II (PSII) cores with the light-harvesting antenna. May also aid in binding of PsbK, Ycf12 and the oxygen-evolving complex to PSII, at least in vitro.	
Photosystem II reaction center W protein, chloroplastic	*psbW*	Stabilizes dimeric photosystem II (PSII). In its absence, no dimeric PSII accumulates and there is a reduction of monomeric PSII (By similarity).	
Photosystem II reaction center X protein	*psbX*	Involved in the binding and/or turnover of quinones at the Q(B) site of Photosystem II.	
Fructose-1,6-bisphosphatase, chloroplastic	*FBP*	Involved in the pathway Calvin cycle, which is part of Carbohydrate biosynthesis.	Calvin cycle
Fructose-bisphosphate aldolase	*fba*	Catalyses the aldol condensation of dihydroxyacetone phosphate (DHAP or glycerone-phosphate) with glyceraldehyde 3-phosphate (G3P) to form fructose 1,6-bisphosphate (FBP) in gluconeogenesis and the reverse reaction in glycolysis.	
Glyceraldehyde-3-phosphate dehydrogenase	*gapA*	Catalyses the oxidative phosphorylation of glyceraldehyde 3-phosphate (G3P) to 1,3-bisphosphoglycerate (BPG) using the cofactor NAD.	
Phosphoglycerate kinase	*pgk*	Catalyses the phosphorylation of 3-PG, producing 1,3-BPG and ADP, as part of the reactions that regenerate ribulose-1,5-bisphosphate.	
Phosphoribulokinase	*prkB*	Involved in the pathway Calvin cycle, which is part of Carbohydrate biosynthesis.	

Ribose-5-phosphate isomerase A	*rpiA*	Involved in the first step of the non-oxidative branch of the pentose phosphate pathway. It catalyses the reversible conversion of ribose-5-phosphate to ribulose 5-phosphate.	Calvin cycle
Ribulose bisphosphate carboxylase	*rbcL*	Catalyses two reactions: the carboxylation of D-ribulose 1,5-bisphosphate, the primary event in carbon dioxide fixation, as well as the oxidative fragmentation of the pentose substrate. Both reactions occur simultaneously and in competition at the same active site.	
Ribulose-phosphate 3-epimerase, chloroplastic	*rpe*	Catalyses the reversible epimerization of D-ribulose 5-phosphate to D-xylulose 5-phosphate.	
Sedoheptulose-1,7-bisphosphatase, chloroplastic	*CSBP*	Involved in the pathway Calvin cycle, which is part of Carbohydrate biosynthesis.	
Transketolase	*tkt*	Catalyses the reverse reaction, the conversion of sedoheptulose-7-P and glyceraldehyde-3-P to pentoses, the aldose D-ribose-5-P and the ketose D-xylulose-5-P.	
Triose phosphate isomerase	*tpiA*	Involved in the gluconeogenesis. Catalyses stereospecifically the conversion of dihydroxyacetone phosphate (DHAP) to D-glyceraldehyde-3-phosphate (G3P).	
alpha-Carbonic anhydrase 1, periplasm	*CAH1*	Catalyses the reversible dehydration of bicarbonate to form carbon dioxide	Carbon assimilation
alpha-Carbonic anhydrase 2, periplasm	*CAH2*		
alpha-Carbonic anhydrase 3, thylakoid lumen	*CAH3*		
Beta carbonic anhydrase 5, chloroplastic	*BCA5*		
Bicarbonate transport ATP-binding protein CmpD	*cmpD*	Part of the ABC transporter complex CmpABCD involved in bicarbonate transport. Responsible for energy coupling to the transport system.	
Carbonic anhydrase	*AN1805*	Catalyses the reversible hydration of CO_2 to H_2CO_3. The main role may be to provide inorganic carbon for the bicarbonate-dependent carboxylation reactions catalysed by pyruvate carboxylase, acetyl-CoA carboxylase and carbamoyl-phosphate synthetase (By similarity). Involved in osmoadaptation.	

6-phosphogluconate dehydrogenase, decarboxylating	*gnd*	Catalyses the oxidative decarboxylation of 6-phosphogluconate to ribulose 5-phosphate and CO_2, with concomitant reduction of NADP to NADPH.	Pentose-phosphate pathway
Glucose-6-phosphate 1-dehydrogenase	*zwf*	Catalyses the oxidation of glucose 6-phosphate to 6-phosphogluconolactone.	
Glucose-6-phosphate isomerase	*pgi*	Involved in the pathway gluconeogenesis, which is part of Carbohydrate biosynthesis.	
Transaldolase	*tal*	Important for the balance of metabolites in the pentose-phosphate pathway.	
Phosphoglycolate phosphatase	*gph*	Specifically catalyses the dephosphorylation of 2-phosphoglycolate. Is involved in the dissimilation of the intracellular 2-phosphoglycolate formed during the DNA repair of 3'-phosphoglycolate ends, a major class of DNA lesions induced by oxidative stress.	Metabolism - Carbohydrate
Chlorophyll synthase, chloroplastic	*CHLG*	Involved in one of the last steps of the biosynthesis of chlorophyll a. Catalyses the esterification of chlorophillide-a with either geranylgeranyldiphosphate (GGPP) or phytyldiphosphate (PhyPP). May also use with a lower efficiency the monophosphates GGMP and PhyMP, but not the non-phosphorylated alcohols geranylgeraniol and phytol. The tetraprenyl diphosphate must bind to the enzyme as the first substrate and esterification occurs when this pre-loaded enzyme meets the second substrate, chlorophyllide.	Metabolism - Chlorophyll
Chlorophyllide a oxygenase, chloroplastic	*CAO*	Catalyses a two-step oxygenase reaction involved in the synthesis of chlorophyll b. Acts specifically on the non-esterified chlorophyllide a and not on chlorophyll a.	
Divinyl chlorophyllide a 8-vinyl-reductase, chloroplastic	*DVR*	Catalyses the conversion of divinyl chlorophyllide to monovinyl chlorophyllide. Reduces the 8-vinyl group of the tetrapyrrole to an ethyl group using NADPH as the reductant. Can use (3,8-divinyl)-chlorophyllide a (DV-Chlidea) > (3,8-divinyl)-chlorophyll a (DV-Chla) > (3,8-divinyl)-protochlorophyllide a (DV-Pchlidea) > (3,8-divinyl)-magnesium-protoporphyrin IX monomethyl ester (DV-MPE) > (3,8-divinyl)-magnesium-protoporphyrin IX (DV-Mg-Proto) as substrates.	

7-hydroxymethyl chlorophyll a reductase, chloroplastic	*HCAR*	Probable iron-sulphur flavoprotein that converts 7-hydroxymethyl chlorophyll a to chlorophyll a using ferredoxin as a reducing equivalent. Catalyses the reduction of a hydroxymethyl group to a methyl group. Belongs to the chlorophyll catabolic enzymes (CCEs).	Metabolism - Chlorophyll
Protochlorophyllide reductase A, chloroplastic	*PORA*	Phototransformation of protochlorophyllide (Pchlide) to chlorophyllide (Chlide). PORA may also function as a photoprotectant during the transitory stage from dark to light. Functions in skotomorphogenesis, photomorphogenesis and throughout the plant life under specific light conditions.	Metabolism - Chlorophyll - Photosynthesis
Protochlorophyllide reductase B, chloroplastic	*PORB*	Phototransformation of protochlorophyllide (Pchlide) to chlorophyllide (Chlide).	
Fumarate reductase	*osm1*	Irreversibly catalyses the reduction of fumarate to succinate. Involved in maintaining redox balance during oxygen deficiency conditions.	Metabolism - FAD process
Ferredoxin-dependent glutamate synthase	*gltB*	Involved in step 1 of the subpathway that synthesizes L-glutamate from 2-oxoglutarate and L-glutamine (ferredoxin route).	Metabolism - Glutamate
Glycerol-3-phosphate dehydrogenase [NAD(P)+]	*gpsA*	Involved in the biosynthesis of the sn-glycerol 3-phosphate required for phospholipid synthesis.	Metabolism - Glycerophospholipid
1-acyl-sn-glycerol-3-phosphate acyltransferase	*plsC*	Converts lysophosphatidic acid (LPA) into phosphatidic acid (PA) by incorporating an acyl moiety at the 2 position. This enzyme utilizes acyl-ACP as fatty acyl donor, but not acyl-CoA.	Metabolism - Lipid
ATP-citrate synthase	*Acly*	Primary enzyme responsible for the synthesis of cytosolic acetyl-CoA in many tissues. Has a central role in de novo lipid synthesis.	
Glycerol-3-phosphate acyltransferase	*plsY*	Catalyses the transfer of an acyl group from acyl-phosphate (acyl-PO4) to glycerol-3-phosphate (G3P) to form lysophosphatidic acid (LPA). This enzyme utilizes acyl-phosphate as fatty acyl donor, but not acyl-CoA or acyl-ACP.	

NADH-cytochrome b5 reductase 2	*cyb5r2*	The outer membrane form may mediate the reduction of outer membrane cytochrome b5, and the soluble inter-membrane space form may transfer electrons from external NADH to cytochrome c, thereby mediating an antimycin-insensitive, energy-coupled oxidation of external NADH by yeast mitochondria. Involved in the reduction of D-erythroascorbyl free radicals.	Metabolism - Lipid
Phthiocerol/phenolphthiocerol synthesis polyketide synthase type I	*ppsB*	Involved in the elongation of either C22-24 fatty acids or p-hydroxyphenylalkanoic acids by the addition of malonyl-CoA and methylmalonyl-CoA extender units to yield phthiocerol and phenolphthiocerol derivatives, respectively.	
Outer membrane lipoprotein Blc	*blc*	Involved in the storage or transport of lipids necessary for membrane maintenance under stressful conditions. Displays a binding preference for lysophospholipids.	Metabolism - Lipid - Stress response
3-isopropylmalate dehydratase	*leuA*	Catalyses the isomerization between 2-isopropylmalate and 3-isopropylmalate, via the formation of 2-isopropylmaleate.	Metabolism - L-leucine
3-isopropylmalate dehydratase large subunit 1	*leuC1*		
3-isopropylmalate dehydratase large subunit 2	*leuC2*		
3-isopropylmalate dehydratase small subunit 1	*leuD1*		
3-isopropylmalate dehydratase small subunit 2	*leuD2*		
3-isopropylmalate dehydrogenase	*leuB*	Catalyses the oxidation of 3-carboxy-2-hydroxy-4-methylpentanoate (3-isopropylmalate) to 3-carboxy-4-methyl-2-oxopentanoate. The product decarboxylates to 4-methyl-2 oxopentanoate.	
2-methyl-6-phytyl-1,4-hydroquinone methyltransferase, chloroplastic	*VTE3*	Involved in a key methylation step in both tocopherols (vitamin E) and plastoquinone synthesis. Catalyses the conversion of 2-methyl-6-phytyl-1,4-hydroquinone (MPBQ) to 2,3-dimethyl-6-phytyl-1,4-hydroquinone (DMPQ, a substrate for tocopherol cyclase), and 2-methyl-6-solanyl-1,4-benzoquinone (MSBQ) to plastoquinone.	Metabolism - Plastoquinone
4-hydroxyphenylpyruvate dioxygenase	*lly*	Catalyses the transformation of p-hydroxyphenylpyruvate into HGA. Has haemolytic and brown pigment production activity.	

Homogentisate solanesyltransferase, chloroplastic	*HST*	Involved in the synthesis of plastoquinone-9. Can use both homogentisic acid and 2,5-dihydroxyphenylacetic acid gamma-lactone as prenyl acceptors, and solanesyl diphosphate > farnesyl diphosphate > geranylgeranyl diphosphate >> phytyl diphosphate as prenyl donors. Do not catalyse the decarboxylation of homogentisate uncoupled from prenylation.	Metabolism - Plastoquinone
Alanine aminotransferase 1, mitochondrial	*ALAAT1*	This protein is involved in the pathway C4 acid pathway, which is part of Photosynthesis.	Photorespiration
Alanine aminotransferase 2, mitochondrial	*ALAAT2*		
Alanine--glyoxylate aminotransferase 2 homolog 1, mitochondrial	*AGT2*	Catalyses the glyoxylate + L-alanine = glycine + pyruvate reaction	
D-glycerate 3-kinase, chloroplastic	*GLYK*	Catalyses the concluding reaction of the photorespiratory C2 cycle, an indispensable ancillary metabolic pathway to the photosynthetic C3 cycle that enables land plants to grow in an oxygen-containing atmosphere.	
Dihydrolipoyl dehydrogenase 1, mitochondrial	*LPD1*	Lipoamide dehydrogenase is a component of the glycine decarboxylase (GDC) or glycine cleavage system as well as of the alpha-ketoacid dehydrogenase complexes. LPD1 is probably the protein most often associated with the glycine decarboxylase complex while LPD2 is probably incorporated into alpha-ketoacid dehydrogenase complexes.	
Gamma carbonic anhydrase 2, mitochondrial	*GAMMACA2*	Involved in the catabolism of H_2CO_3 but that does not mediates the reversible hydration of carbon dioxide.	
Glutamate--glyoxylate aminotransferase 1	*GGAT1*	Catalyses the glutamate:glyoxylate (GGT or GGAT), alanine:glyoxylate (AGT), alanine:2-oxoglutarate (AKT) and glutamate:pyruvate (GPT) aminotransferase reactions in peroxisomes. Required for abscisic acid (ABA) and stress-mediated responses in an H_2O_2-dependent manner. Function as a photorespiratory aminotransferase that modulates amino acid content during photorespiration (GGAT activity); promotes serine, glycine and citrulline metabolism in response to light.	

Glutamate--glyoxylate aminotransferase 2	*GGAT2*	Catalyses the glutamate:glyoxylate aminotransferase (GGT), alanine:glyoxylate aminotransferase (AGT), alanine:2-oxoglutarate aminotransferase (AKT) and glutamate:pyruvate aminotransferase (GPT) reactions in peroxisomes.	Photorespiration
Glycerol-3-phosphate phosphatase	*PGP*	Hydrolyses glycerol-3-phosphate into glycerol. Thereby, regulates the cellular levels of glycerol-3-phosphate a metabolic intermediate of glucose, lipid and energy metabolism.	
Glycine cleavage system H protein 1, mitochondrial	*GDH1*	The glycine decarboxylase (GDC) or glycine cleavage system catalyses the degradation of glycine. The H protein shuttles the methylamine group of glycine from the P protein to the T protein.	
Glycine dehydrogenase (decarboxylating) 1, mitochondrial	*GLDP1*	The glycine decarboxylase (GDC) or glycine cleavage system catalyses the degradation of glycine. The P protein binds the alpha-amino group of glycine through its pyridoxal phosphate cofactor; CO_2 is released and the remaining methylamine moiety is then transferred to the lipoamide cofactor of the H protein (By similarity).	
Glycine dehydrogenase (decarboxylating) 2, mitochondrial	*GLDP2*		
Glycolate dehydrogenase	*GYD1*	Catalyses the reduction of glycolate in glyoxylate.	
Glyoxylate/hydroxypyruvate reductase A	*HPR2*	Catalyses the NADPH-dependent reduction of glyoxylate and hydroxypyruvate (HP) into glycolate and glycerate in the cytoplasm, thus providing a cytosolic bypass to the photorespiratory core cycle. Mostly active in the presence of NADPH and hydroxypyruvate.	
Serine hydroxymethyltransferase 1, mitochondrial	*SHM1*	Functions in the photorespiratory pathway in catalysing the interconversion of serine and glycine. Involved in controlling cell damage caused by abiotic stress, such as high light and salt and the hypersensitive defence response of plants.	
Serine hydroxymethyltransferase 2, mitochondrial	*SHM2*	Functions outside the photorespiratory pathway in catalysing the interconversion of serine and glycine.	
Serine hydroxymethyltransferase 3, chloroplastic	*SHM3*	Catalyses the interconversion of serine and glycine and directs the hydroxymethyl moiety of serine into the metabolic network of H4PteGlu(n)-bound one-carbon units.	
Serine--glyoxylate aminotransferase	*AGT1*	Photorespiratory enzyme that catalyses transamination reactions with multiple substrates, including asparagine. Function exclusively as a catabolic enzyme in Asn metabolism.	

Citrate synthase	*gltA*	Citrate synthase is found in nearly all cells capable of oxidative metabolism.	TCA cycle
Malate dehydrogenase, mitochondrial	*MDH2*	Involved in the tricarboxylic acid cycle, a series of metabolic reactions in aerobic cellular respiration, which occurs in the mitochondria of animals and plants and in which acetyl-CoA, formed from pyruvate produced during glycolysis, is completely oxidized to CO_2 via the interconversion of various carboxylic acids. It results in the reduction of NAD and FAD to NADH and FADH2, whose reducing power is then used indirectly in the synthesis of ATP by oxidative phosphorylation.	
Catalase-peroxidase	*katG*	Bifunctional enzyme with both catalase and broad-spectrum peroxidase activity.	Stress response
Cytochrome P450	*CYP-1*	Cell detoxification and protection from oxidative stress.	
Cytochrome P450 3A13	*Cyp3a13*		
Cytochrome P450 704C1	*CYP704C1*		
Glutaredoxin 2	*grxB*	Involved in reducing some disulphide bonds in a coupled system with glutathione reductase. Does not act as hydrogen donor for ribonucleotide reductase.	
Glutathione peroxidase 1, mitochondrial	*GPX*	May constitute a glutathione peroxidase-like protective system against oxidative stresses. Hydrogen peroxide, tert-butyl hydroperoxide and cumene, but not phosphatidylcholine hydroperoxide, can act as acceptors.	
Heat shock 70 kDa protein 1A	*Hspa1a*	Molecular chaperone implicated in a wide variety of cellular processes, including protection of the proteome from stress, folding and transport of newly synthesized polypeptides, activation of proteolysis of misfolded proteins and the formation and dissociation of protein complexes.	
Heat shock 70 kDa protein 1B	*Hspa1b*		
Heat shock protein 90	*HSP90*	Molecular chaperone that promotes the maturation, structural maintenance and proper regulation of specific target proteins involved for instance in cell cycle control and signal transduction.	
L-ascorbate peroxidase 3	*APX3*	Plays a key role in hydrogen peroxide removal.	

Peroxiredoxin Q, chloroplastic	*PRXQ*	Thiol-specific peroxidase that catalyses the reduction of hydrogen peroxide and organic hydroperoxides to water and alcohols, respectively. Plays a role in cell protection against oxidative stress by detoxifying peroxides. Involved in the photosystem II protection against hydrogen peroxide.	Stress response
Peroxiredoxin-6	*PRDX6*	Catalyses the reduction of hydrogen peroxide and organic hydroperoxides to water and alcohols, respectively. Can reduce H_2O_2 and short chain organic, fatty acid, and phospholipid hydroperoxides. Also has phospholipase activity, and can therefore either reduce the oxidized sn-2 fatty acyl group of phospholipids (peroxidase activity) or hydrolyse the sn-2 ester bond of phospholipids (phospholipase activity). These activities are dependent on binding to phospholipids at acidic pH and to oxidized phospholipids at cytosolic pH. Plays a role in cell protection against oxidative stress by detoxifying peroxides and in phospholipid homeostasis.	
Peroxiredoxin-B	*PMPB*	Catalyses the reduction of hydrogen peroxide and organic hydroperoxides to water and alcohols, respectively. Plays a role in cell protection against oxidative stress by detoxifying peroxides and as sensor of hydrogen peroxide-mediated signalling events.	
Photosystem II repair protein PSB27-H1, chloroplastic	*psb27-1*	Probably involved in repair of photodamaged photosystem II (PSII).	
Superoxide dismutase [Cu-Zn]	*sodC*	Destroys superoxide anion radicals which are normally produced within the cells and which are toxic to biological systems.	
Superoxide dismutase [Fe]	*sodB*		
Superoxide dismutase [Mn]	*sodA*		
Superoxide-generating NADPH oxidase heavy chain subunit A	*noxA*	Critical component of the membrane-bound oxidase that generates superoxide. It is the terminal component of a respiratory chain that transfers single electrons from cytoplasmic NADPH across the plasma membrane to molecular oxygen on the exterior.	
Thioredoxin 1	*trxA*	Participates in various redox reactions through the reversible oxidation of its active centre dithiol to a disulphide and catalyses dithiol-disulphide exchange reactions.	

GDP-fucose transporter 1	*GFT1*	Acts as the major nucleotide-sugar transporter for the import of GDP-Fucose into the Golgi lumen. Transports GDP-Fucose in a strict counter-exchange mode.	Transport - Carbohydrates
GDP-mannose transporter 5	*GONST5*	GDP-mannose transporter that may be involved in the import of GDP-mannose from the cytoplasm into the Golgi lumen.	
sn-glycerol-3-phosphate import ATP-binding protein UgpC	*ugpC*	Part of the ABC transporter complex UgpABCE involved in sn-glycerol-3-phosphate import. Responsible for energy coupling to the transport system.	
Solute carrier family 2, facilitated glucose transporter member 2	*Slc2a2*	Facilitative hexose transporter that mediates the transport of glucose and fructose. Also able to mediate the transport of dehydroascorbate.	
Trehalose/maltose import ATP-binding protein MalK	*malK*	Part of the ABC transporter complex MalEFGK involved in trehalose/maltose import. Responsible for energy coupling to the transport system.	
Trehalose/maltose transport system permease protein MalG	*malG*	Part of the ABC transporter complex MalEFGK involved in trehalose/maltose import. Responsible for the translocation of the substrate across the membrane.	
sn-glycerol-3-phosphate transport system permease protein UgpE	*ugpE*	Part of the binding-protein-dependent transport system for sn-glycerol-3-phosphate; probably responsible for the translocation of the substrate across the membrane.	Transport - Glycerol
Vesicle-fusing ATPase	*NSF*	Involved in vesicle-mediated transport. The ATPase activity of NSF serves to disassemble the SNARE complex, freeing the components for subsequent pairing and fusion events.	Transport - Proteins